Competitive Hydroconversion of Decalin and n-Decane on Noble-Metal Catalysts and the Evaluation of Molybdenum Carbide as Ring-Opening Catalyst

von der Fakultät Chemie der Universität Stuttgart
zur Erlangung der Würde eines
Doktors der Naturwissenschaften (Dr. rer. nat.)
genehmigte Abhandlung

vorgelegt von
Tobias Holl
aus Göppingen

Hauptberichter: Prof. Dr.-Ing. Jens Weitkamp
Mitberichter: Prof. Dr. Thomas Schleid

Tag der mündlichen Prüfung: 21.03.2014

Institut für Technische Chemie
der Universität Stuttgart
2014

Litera scripta manet.

Die vorliegende Arbeit entstand in der Zeit von April 2009 bis April 2013 am Institut für Technische Chemie der Universität Stuttgart.

Mein allererster und tief empfundener Dank gebührt Herrn Prof. Dr.-Ing. Jens Weitkamp für die Überlassung des hochaktuellen Themas, die sehr gute Betreuung und ebenso für die Möglichkeit zur Konstruktion und zum Aufbau einer eigenen Hochdruckapparatur.

Für die guten Rahmenbedingungen am Institut danke ich Herrn Prof. Dr.-Ing. Elias Klemm.

Herrn Prof. Dr. Thomas Schleid danke ich für die freundliche Übernahme des Koreferats.

Weiterhin danke ich den Herren Dr. Vincenzo Calemma und Dr. Marco Ferrari von Eni S.p.A. für die gute Zusammenarbeit im Rahmen des Industrie-projektes.

Ein ganz besonderer Dank gebührt meinen Kollegen aus dem Arbeitskreis Sandra Rabl, Andreas Haas, Dominic Santi und Frank Salzbauer für die freundschaftliche und inspirierende Zusammenarbeit. Sie waren gemeinsam mit allen anderen Kollegen, namentlich seien hier Matthias Aimer, Thomas Montsch, Gregor Näfe und Matthias Rupp genannt, für das sehr gute Betriebsklima verantwortlich.

Dank gebührt auch Daniel Barunović, Felix Neher und Alexis Schmidt, die im Rahmen von Diplomarbeit, Bachelorarbeit oder Forschungspraktikum zum Gelingen dieser Arbeit beigetragen haben.

Für diverse Charakterisierungen, Analysen sowie die Anfertigung von Metallteilen und Glasgeräten danke ich Herrn Prof. Dr. Michael Hunger, Michael Dyballa, Heike Fingerle, Barbara Gehring, Daniel Geiß, Ines Kley, Christian Lieder, Matthias Scheibe, Dennis Wan Hussin, sowie Ingo Nägele, Andreas Stieber, Werner Hopf und Walter Röhm.

Den größten Dank verdient aber meine Familie und besonders meine Lebensgefährtin Ines, die mich während der Zeit der Promotion und der Anfertigung dieser Arbeit immer unterstützt und an mich geglaubt haben.

I Table of Contents

II Symbols, Indices and Abbreviations

Symbols

Symbol	Unit	Designation
A	$A \cdot s$	Peak area in the chromatogram
A_{BET}	$m^2 \cdot g^{-1}$	Specific surface area according to Brunauer, Emmett and Teller [1]
c	$mol \cdot m^{-3}$	Concentration
CN	-	Cetane number
d	m	Diameter
f	Hz	Frequency
I	A	Current intensity
k	-	Compound-specific correction factor of the flame-ionization detector
$LHSV$	h^{-1}	Liquid hourly space velocity
m	kg	Mass
M	$kg \cdot mol^{-1}$	Molar mass
$\dot{m}$	$kg \cdot s^{-1}$	Mass flux
MP	°C	Melting point
n	mol	Molar amount
$\dot{n}$	$mol \cdot s^{-1}$	Molar flux
p	Pa	Pressure

s	$kg \cdot A^{-1} \cdot s^{-1}$	Instrument-specific factor of the gas chromatograph
S	-	Selectivity
S^*	-	Modified hydrocracking selectivity
t	s	Time
T	K or °C	Temperature
U	V	Voltage
$\dot{V}$	$m^3 \cdot s^{-1}$	Volumetric flow rate
$WHSV$	h^{-1}	Weight hourly space velocity
x	-	Mole fraction
X	-	Conversion
Y	-	Yield
δ	-	Chemical shift
Θ	°	Angle
λ	m	Wavelength
v	-	Stoichiometric factor

Indices

amorph.	Amorphous
cat.	Catalyst
i	Reactant in the stoichiometric equation

j	Product in the stoichiometric equation
max.	Maximum
mix	Mixture
naphth.	Naphthene, naphthenic
r	Reaction
ret	Retention
synth.	Synthetic

Abbreviations

ALD	Atomic layer deposition
a.u.	Arbitrary units
BEA	Zeolite Beta
C_9-	Hydrocarbons with less than 10 carbon atoms (hydrocracked products)
D	Vessel
DHP(s)	Dehydrogenated product(s)
dROP(s)	Direct ring opening product(s)
EMC	Elf (or Ecole Supérieure) Mulhouse Chimie
EMT	Elf (or Ecole Supérieure) Mulhouse Chimie - two
Eq(s).	Equation(s)
EU	European Union

EXAFS	Extended X-ray absorption fine structure
FAU	Faujasite
fcc	face-centered cubic
FCC	Fluid catalytic cracking
FI	Flow indicator
FIC	Flow indication and controller
FID	Flame ionization detector
FT	Fourier transform
GC	Gas chromatograph(y)
GC/MS	Gas chromatograph(y) coupled with mass spectrometry (-meter)
GSL	Gas sampling loop
hcp	hexagonal close-packed
ICP-OES	Inductively coupled plasma - optical emission spectrometry (-meter)
IR	Infrared
ITQ	Instituto de Tecnología Química Valencia
IZA	International Zeolite Association
LCO	Light cycle oil
LTL	Linde Type L
M	Metal

MAS	Magic angle spinning
MCM	Mobil Composition of Matter
MFI	Mobile five
MIX	Mixture
MOR	Mordenite
N	Needle valve
NMR	Nuclear magnetic resonance
OCD(s)	Open-chain decane(s)
PAH(s)	Polycyclic aromatic hydrocarbon(s)
PC	Personal computer
PI	Pressure indicator
PID	Proportional, integral and differential
R	Reactor
Ref(s).	Reference(s)
ROP(s)	Ring-opening products
S	Saturator
SEM	Scanning electron microscope/microscopy
SG	Special gas
sk-Iso(s)	Skeletal isomer(s)
TCD	Thermal conductivity detector

TEM	Transmission electron microscopy
TGA	Thermogravimetric analyzer
TI	Temperature indicator
TIC	Temperature indicator and controller
TPD	Temperature programmed desorption
US	United States of America
USY	Ultrastable Y zeolite
V	Valve
vol.	Volume
VW	4/2 Valve
wt.	Weight
XRD	X-ray diffractometer (-gram)
ZSM	Zeolite Socony Mobil

Abbreviations of Hydrocarbons

B-	Butyl-
Bu	Butane
Bz	Benzene
c-Dec	cis-Decalin
CDe	Cyclodecane

CHx	Cyclohexane
CPn	Cyclopentane
De	Decane
DE-	Diethyl-
Dec	Decalin (cis- and trans-)
DM-	Dimethyl-
E-	Ethyl-
Hp	Heptane
Hx	Hexane
M-	Methyl-
Me	Methane
Nap	Naphthalene
No	Nonane
Oc	Octane
P-	Propyl-
Pr	Propane
TM-	Trimethyl-
tr-Dec	trans-Decalin
Ttr	Tetralin

Nomenclature of the Catalysts

The aim of the catalysts nomenclature is to comprise the relevant information about a catalyst in a short designation. Due to the fact that three absolutely different classes of catalysts were prepared within this work, each class has its own nomenclature which is designated as follows:

Supported noble metal catalysts:
The base for the nomenclature of these catalysts is the zeolite type. In front of the zeolite type, and separated from it by a hyphen, are the element symbols of the charge compensating cations arranged by their abundance in decreasing order and separated from each other by a comma. The subscripts after the cations denote the mole fractions of the respective cations. If the n_{Si}/n_{Al} ratio of a catalyst is given, it appears behind the zeolite type from which it is separated by a hyphen. When a noble metal is loaded onto the zeolite, its amount in wt.-% related to the mass of the dry zeolite is put in front of the cations and separated from them by a slash. As an example, 3.0Ir/$Na_{0.96}$,$H_{0.04}$-Y-2.4 stands for a zeolite Y catalyst which contains 96 % of sodium and 4 % of protons as charge compensating cations and has an n_{Si}/n_{Al} ratio of 2.4. Additionally, the catalyst is loaded with 3.0 wt.-% of iridium.

Bulk molybdenum carbide catalysts:
The designation of a bulk molybdenum carbide catalyst consists of three parts: (i) the phase of the molybdenum carbide, (ii) the carburization temperature in °C at which the carbide was obtained out of MoO_3 and (iii) the carburization agent. Beginning with the phase of the molybdenum carbide, the carburization temperature and the carburization agent are separated from each other by a hyphen. Hence, β-Mo_2C-700-Me is a bulk molybdenum carbide in its beta phase which was obtained by carburization of MoO_3 with methane at 700 °C.

Supported molybdenum carbide catalysts:
An extensive nomenclature was applied for the supported molybdenum carbide catalysts which comprises the amount of molybdenum, impregnation salt used, the zeolitic support and its charge compensating cations as well as its n_{Si}/n_{Al} ratio. This information was arranged as follows: It begins with the amount of molybdenum, symbolized by Mo_2C when it is carburized, which is followed by Na or NH_4 in square brackets. Na or NH_4 stand for Na_2MoO_4 or $(NH_4)_6Mo_7O_{24}$, the molybdenum salt which was used for the impregnation of the respective zeolitic support. Separated from the molybdenum carbide by a

slash are the charge compensating cations of the zeolite arranged in the order of decreasing abundance. The subscripts after the cations denote their mole fractions. After the cations, the type of the zeolite is given followed by its n_{Si}/n_{Al} ratio, which is separated by a hyphen. 8.2Mo_2C[Na]/$Na_{0.96}$,$H_{0.04}$-Y-2.4, for example, is zeolite Y with an n_{Si}/n_{Al} ratio of 2.4 of which 96 % sodium ions and 4 % of protons are the charge compensating cations. Carburized on the zeolite is 8.2 wt.-% of molybdenum which was impregnated onto the zeolite with an aqueous solution of Na_2MoO_4.

1 Zusammenfassung

Der europäische Kraftstoffmarkt ist seit mehr als einem Jahrzehnt im Wandel begriffen. Während der Konsum von Benzin beständig abnimmt, steigt die Nachfrage nach Dieselkraftstoff. Zugleich sinkt die Qualität des Rohöls, d.h. das Rohöl ist wasserstoffärmer und enthält einen höheren Anteil an mehrkernigen Aromaten (PAHs). Das stellt die Raffinerien vor ein doppeltes Problem. Zum einen lässt sich so aus einer definierten Menge an Rohöl weniger Dieselkraftstoff herstellen und zum anderen ist der darin enthaltene Anteil an PAHs in der Europäischen Union auf 8 % per Gesetz beschränkt. Die Beschränkung ist auf einige unerwünschte Eigenschaften der PAHs im Kraftstoff, wie z.B. schlechte Zündwilligkeit und Kältefließeigenschaften sowie auch die Neigung zur Rußbildung, zurückzuführen.

Als eine mögliche Lösung des Problems wird die Hydrierung der Aromaten zu Naphthenen und die anschließende Ringöffnung von diesen zu offenkettigen Alkanen angesehen. Über diesen Weg ist es möglich aromatenreiche Raffinerieströme in einen qualitativ hochwertigen Dieselkraftstoff zu überführen. Weiterhin könnte durch geschickte Prozessänderungen in der Raffinerie, z.B. beim „Fluid Catalytic Cracking“, der Anteil an PAH-reichem „Light Cycle Oil“ auf Kosten von Benzin erhöht werden. Mit einer nachgeschalteten Ringöffnung könnte somit dem Wandel im Kraftstoffmarkt in doppelter Hinsicht Rechnung getragen werden.

In der gegenwärtigen Literatur zur hydrierenden Ringöffnung von Mehrring-Naphthenen wurde meist Decalin als Modellkohlenwasserstoff eingesetzt. Allerdings bestehen reale Eduktströme aus aromatischen, naphthenischen und aliphatischen Kohlenwasserstoffen mit komplett unterschiedlichen Strukturen. Deshalb wurde in der vorliegenden Arbeit untersucht, wie sich Produktselektivitäten verhalten, wenn an einem Katalysator eine äquimolare Mischung von Decalin und n-Decan umgesetzt wird. Diese Mischung dient als Modell sowohl für naphthenische als auch aliphatische Komponenten in einem realen Einsatzöl, aber auch für gebildete offenkettige Decane und deren Edukt.

Bislang haben sich geträgertes Iridium und Platin als besonders effektiv in der Ringöffnung von reinem Decalin erwiesen. Deshalb wurde in einem ersten Schritt eine äquimolare Mischung von Decalin und n-Decan an Iridium bzw. Platin geträgert auf nichtsaurem Silica umgesetzt, um die katalytischen

Eigenschaften der Edelmetalle allein zu untersuchen. n-Decan stellte sich im Vergleich mit Decalin als deutlich reaktiver heraus, wenn es als Reinkomponente umgesetzt wurde. Im Gegensatz dazu waren die Reaktivitäten der beiden Kohlenwasserstoffe, insbesondere die von n-Decan, bei der konkurrierenden Umsetzung vermindert, so dass dort beide Einsatzkohlenwasserstoffe einen nahezu identischen Umsatzverlauf mit der Temperatur zeigten.

Primäre Produkte bei der konkurrierenden Umsetzung von Decalin und n-Decan an 2.6Ir/Silica waren direkte Ringöffnungsprodukte (dROPs) und Crackprodukte (C_9-). Durch den Vergleich der so erhaltenen Produktselektivitäten mit den Selektivitäten aus der Umsetzung der reinen Kohlenwasserstoffe konnte die Bildung der Crackprodukte auf die Umsetzung von n-Decan zurückgeführt werden. Weiterhin ließen sich die Produktselektivitäten der Decalin-Gerüstisomere (sk-Isos), der Ringöffnungsprodukte (ROPs), der offenkettigen Decane (OCDs) und der Crackprodukte in der Gemischumsetzung direkt aus den erzielten Produktselektivitäten bei der Umsetzung der Reinkomponenten berechnen. Dadurch ließ sich zeigen, dass die Produktselektivitäten an 2.6Ir/Silica durch die Anwesenheit des jeweils anderen Kohlenwasserstoffs nicht beeinflusst werden.

Im Gegensatz zu Iridium erwies sich Platin als deutlich inaktiver in der Umsetzung von Decalin, was sich in stark erhöhten Reaktionstemperaturen zeigte, die für dessen Umsetzung notwendig waren. Die primären Produkte der Umsetzung einer äquimolaren Decalin/n-Decan-Mischung waren sk-Isos, wobei Spiro[4.5]decan hervorstach, und Crackprodukte. Die Zusammensetzung der direkten Ringöffnungsprodukte von Decalin (dROPs) zeigte keine Veränderung bei gleichzeitiger Umsetzung von n-Decan. Es wurde jeweils bevorzugt die substituierte C-C Bindung von Decalin zu Butylcyclohexan geöffnet.

Die Bildung von Isomerisierungsprodukten an 2.7Pt/Silica lässt sich auf die literaturbekannte Fähigkeit von Platin zur Isomerisierung von Kohlenwasserstoffen zurückführen. Gleichzeitig bestand ein höherer Anteil der Crackprodukte aus verzweigten Alkanen. Bei der Umsetzung des äquimolaren Decalin/n-Decan Gemischs wurden deutlich höhere Selektivitäten an OCDs gefunden, als von der Umsetzung der einzelnen Einsatzkohlenwasserstoffe zu erwarten war. Dies wurde auf die Isomerisierung von n-Decan zu iso-Decanen

zurückgeführt, welche anschließend durch Decalin oder n-Decan vom Katalysator verdrängt werden.

Es wurden in der Folge zeolithische Katalysatoren bestehend aus 3 Massen-% Iridium oder Platin geträgert auf Zeolith Y mit unterschiedlichen Konzentrationen an Brønsted Säurezentren hergestellt und in der hydrierenden Umsetzung von Decalin und n-Decan getestet. Dabei zeigte sich eine erhöhte Katalysatoraktivität mit zunehmender Konzentration an Brønsted-Säurezentren. Wie schon an den nichtsauren Katalysatoren war auch hier n-Decan deutlich reaktiver als Decalin im direkten Vergleich bei der Umsetzung der jeweiligen reinen Kohlenwasserstoffe. Allerdings wird der Reaktivitätsunterschied zwischen n-Decan und Decalin mit zunehmender Konzentration an Brønsted Säurezentren des Katalysators geringer. Wenn eine äquimolare Mischung aus Decalin und n-Decan umgesetzt wurde, zeigte sich eine invertierte Reaktivität der beiden Einsatzkohlenwasserstoffe – in diesen Fällen reagierte Decalin bevorzugt. Eine Erklärung für dieses Verhalten konnte mit Durchbruchsmessungen von Decalin/n-Decan-Gemischen an einer Reihe von Ir/Na,H-Y-Zeolithen als Adsorbenzien gefunden werden. Decalin wurde jeweils deutlich bevorzugt adsorbiert. Dadurch bildet sich eine höhere Konzentration an Decalin an den katalytisch aktiven Zentren heraus, was in der Folge zu einer bevorzugten Umsetzung von Decalin führt.

Mit zunehmender Konzentration der Brønsted Säurezentren der vier Ir/Na,H-Y-Katalysatoren sank der Anteil der Hydrogenolyse an der Bindungsspaltung in der Umsetzung von Decalin. Das zeigte sich in der Änderung der Verteilungskurve der Spaltprodukte von einer „Hängemattenkurve“ (hammock-type curve), wie sie für Hydrogenolyse von Decalin an Iridium typisch ist, zu einer „M-Kurve“ (M-shaped curve), die für bifunktionelles Hydrocracken von Decalin gefunden wird.

Die vier Pt/Na,H-Y-Katalysatoren zeichneten sich allesamt durch eine sehr hohe Isomerisierungsaktivität aus. Die gemeinsame Umsetzung von Decalin und n-Decan führte zu keinen Änderungen der Selektivitäten der dROPs von Decalin, genau wie an den Ir/Na,H-Y-Katalysatoren. Es wurden ebenso in der Umsetzung der äquimolaren Decalin/n-Decan-Mischung höhere Selektivitäten an OCDs und niedrigere Selektivitäten zu Spaltprodukten gefunden als durch Berechnung der erhaltenen Selektivitäten bei der Umsetzung der reinen Einsatzkohlenwasserstoffe zu erwarten war. Die höchsten Ausbeuten an OCDs bei der Umsetzung von Decalin wurden an den beiden HIPEROCs

(High-Performance Ring-Opening Catalysts) 2.8Pt/$Na_{0.59}$,$H_{0.41}$-Y-2.4 ($Y_{OCDs,max.}$ = 37.3 %) und 3.3Ir/$Na_{0.72}$,$H_{0.28}$-Y-2.4 ($Y_{OCDs,max.}$ = 33.9 %) gefunden. Was beide HIPEROCs auszeichnet, sind die niedrigen Konzentrationen an Brønsted-Säurezentren.

Als weitere Träger wurden neben Zeolith Y auch die Zeolithe Beta, EMC-2, L, Mordenit und ZSM-5 untersucht. Diese Zeolithe unterscheiden sich in ihrer Dimensionalität und den Abmessungen des Porensystems, was sich in ihren „Spaciousness Indices“ (*SI*) zwischen 21 und 1 zeigt. Alle Zeolithe wurden mit *ca.* 3 Massen-% an Iridium beladen. Die Aktivitäten der Beta- und EMC-2-Katalysatoren (*SI* von 18 bzw. 21) waren vergleichbar mit der von 3.3Ir/$Na_{0.72}$,$H_{0.28}$-Y-2.4, was sich insbesondere auch auf die Reaktivität der einzelnen Kohlenwasserstoffe und deren invertierte Reaktivitäten in der Gemischumsetzung bezog. An allen diesen Katalysatoren wurden sehr hohe Ausbeuten an OCDs erhalten, wobei am HIPEROC 3.3Ir/$H_{0.58}$,$Cs_{0.42}$-Beta-14 die in dieser Arbeit höchsten Ausbeuten an OCDs ($Y_{OCDs,max.}$ = 41.1 %) gefunden wurden.

Eine detaillierte Untersuchung der Zusammensetzung der Produkte der n-Decanumsetzung am HIPEROC 3.3Ir/$H_{0.58}$,$Cs_{0.42}$-Beta-14 ergab, dass (i) sämtliche Spaltprodukte ausschließlich aus n-Alkanen bestehen und (ii) die gleichzeitig gebildeten iso-Decane den sehr charakteristischen Gehalt an Methylnonanen und Ethyloctanen aufweisen, wie er in der Isomerisierung von n-Alkanen an bifunktionellen Katalysatoren gefunden wird. Diese Befunden wurden als starke Hinweise darauf gewertet, dass die hydrogenolytische C-C Bindungsspaltung am Iridium und die Isomerisierung an Brønsted-Säurezentren unabhängig voneinander ablaufen. Diese Tatsache stellt unabhängige Evidenz für den früher postulierten Mechanismus für die Umsetzung von Decalin an HIPEROCs dar.

Mit abnehmendem Spaciousness Index der zeolithischen Träger (von Zeolith L über Mordenit zu ZSM-5) steigt die Selektivität zu Gerüstisomeren des Decalins und gleichzeitig sinken die Selektivitäten zu ROPs und in der Folge auch die zu OCDs in der Umsetzung von Decalin. Darüber hinaus ändert sich auch die Reaktivität der beiden Einsatzkohlenwasserstoffe. Mit niedrigerem *SI* wird bevorzugt n-Decan umgesetzt. Diese Reaktivitätsabfolge besteht dann auch bei der konkurrierenden Umsetzung von Decalin und n-Decan (im Gegensatz zu den Reaktivitäten an den HIPEROCs). Damit kommt an diesen Katalysatoren der für die Bildung von OCDs wichtige Effekt der Verdrängung

von n-Decan und seinen Isomeren durch Adsorption von Decalin nicht zum Tragen. Dies zeigt sich auch auf anschauliche Weise darin, dass die experimentell ermittelten OCD-Selektivitäten bei der konkurrierenden Umsetzung von Decalin und n-Decan niedriger sind als man auf der Grundlage der entsprechenden Selektivitäten bei Einsatz der reinen Komponenten Decalin und n-Decan berechnet.

Molybdäncarbid wurde als mögliche preiswerte Alternative zu Edelmetallen in Ringöffnungskatalysatoren getestet. Als Modellkohlenwasserstoff wurde in diesen Experimenten Decalin eingesetzt. Es wurde gezeigt, dass sich β-Mo_2C durch Carbidisierung von MoO_3 sowohl mit einem Methan/Wasserstoff- als auch mit einem n-Octan/Wasserstoffgemisch synthetisieren ließ. Der so hergestellte Vollkatalysator besaß jedoch nur eine geringe spezifische Oberfläche von 30 $m^2 \cdot g^{-1}$ und war äußerst inaktiv in der Ringöffnung von Decalin. Erhaltene Primärprodukte waren Gerüstisomere, insbesondere Spiro[4.5]decan. Offenkettige Decane wurden nur mit niedriger Selektivität ($S_{OCDs,max.} \approx 4$ % bei $X_{Dec} = 45$ %) aus Decalin gebildet. Hauptprodukte waren kurzkettige Spaltprodukte, insbesondere Methan. Damit erwies sich β-Mo_2C in seinen katalytischen Eigenschaften als dem Edelmetall Platin ähnlich.

Mit dem Ziel höhere Aktivitäten zu erzielen, wurden Katalysatoren mit auf Zeolith Y geträgertem Molybdäncarbid präpariert. Dazu wurde Zeolith Y mit einer wässrigen Lösung an $(NH_4)_6Mo_7O_{24}$ oder Na_2MoO_4 imprägniert, und diese Katalysatorvorläufer wurden anschließend mit Methan/Wasserstoff oder n-Octan/Wasserstoff carbidisiert. Auf nichtsaurem Zeolith Y erwies sich β-Mo_2C als sehr inaktiv und glich in seinen katalytischen Eigenschaften dem β-Mo_2C-Vollkatalysator. Mit Erhöhung der Brønsted-Säurezentren-konzentration des Trägers erhöhten sich sowohl die Katalysatoraktivität als auch die Produktselektivitäten zu ROPs und OCDs. Gleichzeitig stiegen aber auch die Selektivitäten von unerwünschtem Isobutan und Methylcyclopentan durch die „Paring Reaktion“.

Zur Optimierung der geträgerten Molybdäncarbidkatalysatoren wurden das n_{Si}/n_{Al}-Verhältnis zwischen 2.4 und 105 und die Molybdänbeladung zwischen 5 und 20 Massen-% variiert. Die höchsten Selektivitäten zu OCDs ($S_{OCDs,max.} = 18$ % bei $X_{Dec} = 90$ %) wurden an Katalysator $9.8Mo_2C/H_{0.99},Na_{0.01}$-Y-7 erzielt. Im Allgemeinen zeigten sich Molybdänbeladungen von *ca.* 10 Massen-% und ein n_{Si}/n_{Al}-Verhältnis von 7 bei Zeolith Y als vorteilhaft für die Ringöffnung von Decalin an diesen

alternativen Katalysatoren. Wenn man jedoch die maximal erzielten Ausbeuten an OCDs als Gütekriterium für Ringöffnungskatalysatoren nimmt, dann kommt kein auf Zeolith Y geträgerter Molybdäncarbidkatalysator auch nur in die Nähe der geträgerten Edelmetall-HIPEROCs.

2 Summary

The aim of this work was an understanding of the behavior of ring-opening catalysts concerning their activity and product selectivities in the hydroconversion of decalin when n-decane as a representative for aliphatic hydrocarbons is present. This is a first step towards the approximation of conditions which occur in the hydroconversion of real refinery streams, since these consist of paraffins, naphthenes and aromatics possessing similar boiling points. In addition, as currently investigated ring-opening catalysts use noble metals, a possible substitute for these expensive noble metals was investigated, *viz.* molybdenum carbide.

As known from the literature, iridium and platinum have been both proved and often used as ring-opening catalysts in the hydroconversion of model naphthenic hydrocarbons. Therefore, the focus was put on catalysts containing these two noble metals. In a first step it was investigated how iridium and platinum on non-acidic silica behave as catalysts in the ring opening of decalin alone and in the hydroconversion of an equimolar mixture of decalin with n-decane. It was found that decalin is much less reactive than n-decane when the hydrocarbons are converted alone on 2.6Ir/silica or 2.7Pt/silica. In the competitive hydroconversion of the equimolar mixture, the reactivity of both feed hydrocarbons was reduced, especially the one of n-decane. It was concluded that the two-ring naphthene decalin is preferentially adsorbed and converted on the catalytically active sites.

Primary products in the conversion of an equimolar decalin/n-decane mixture on 2.6Ir/silica were hydrocracked products with less than 10 carbon atoms and direct ring-opening products of decalin (dROPs). From a comparison with the results of the pure feed experiments it was possible to attribute the formation of hydrocracked products to the conversion of n-decane. Moreover, it was shown that the product selectivities of skeletal isomers (sk-Isos), ring-opening products (ROPs), open-chain decanes (OCDs) and hydrocracked products (C_9-) in the mixed feed experiments can be calculated directly out of the product selectivities obtained in the conversion of the pure hydrocarbons. This was also found for the distribution of the dROPs and the composition of the hydrocracked products. Hence, it can be stated that the product selectivities of decalin and n-decane are not influenced by the presence of the respective other hydrocarbon on this non-acidic iridium catalyst.

Platinum supported on non-acidic silica was found to be much less active than iridium as catalyst in the hydroconversion of decalin. Primary products of the conversion of the equimolar decalin and n-decane mixture were skeletal isomers of decalin, especially spiro[4.5]decane, and hydrocracked products. These findings indicate an isomerization ability of platinum, which was also reflected in the high degree of branching of the hydrocracked products. It was found that much higher selectivities of OCDs were obtained in the mixed feed experiment than one would expect from the results of each pure feed hydrocarbon. This is best explained by an isomerization of n-decane on platinum and displacement of the iso-decanes by decalin before they can be hydrocracked, leading to high amounts of branched decanes in the product mixture. Additionally, a detailed look at the composition of the direct ring-opening products indicated a preferred hydrogenolysis of substituted carbon-carbon bonds in decalin which was not influenced by the presence of n-decane.

Catalysts containing 3 wt.-% iridium or platinum supported on zeolite Y with different concentrations of Brønsted acid sites were prepared. An increased catalyst activity in the hydroconversion of equimolar decalin/n-decane mixtures was found with increasing concentration of Brønsted acid sites for iridium and platinum catalysts. When decalin and n-decane were converted solely on the iridium catalysts, n-decane was significantly more reactive than decalin. But, with increasing Brønsted acid site concentration of the catalyst, the reactivity difference gets smaller. It is striking, that the reactivity of decalin and n-decane was inverted when both hydrocarbons were converted competitively. An explanation for this finding was obtained by breakthrough measurements. Decalin was found to be preferentially adsorbed on the Ir/Na,H-Y catalysts. Hence, decalin gets preferred access to the catalytically active sites and is consequently hydroconverted preferentially.

With increasing Brønsted acid sites concentrations of the catalysts, their hydrogenolytic bond-scission activity was lowered. This was indicated by a change in the distribution of the hydrocracked products from hammock-type to M-shape curves. In addition, with increasing concentration of Brønsted acid sites, these catalysts were prone to isomerize the feed hydrocarbons in a primary reaction.

The selectivities of methylcyclohexane and butylcyclohexane were taken as indicators for the participation of hydrogenolysis in the ring opening of decalin,

as both products were preferentially formed on 2.6Ir/silica. It was found that the selectivities of the previously mentioned products were reduced with increasing concentration of Brønsted acid sites of the catalysts. However, when an equimolar mixture of decalin and n-decane was converted, the selectivities of butylcyclohexane and methylcyclohexane increased when using the HIPEROC (High-Performance Ring-Opening Catalysts). Thus, the fraction of bond-scission of decalin due to hydrogenolysis increased with the presence of n-decane. This finding may explain the increased selectivities of OCDs and lowered selectivities of C_9- products on Ir/Na,H-Y when decalin/n-decane mixtures were converted, compared to calculated selectivities based on the pure-feed experiments.

On the platinum counterparts to the four Ir/Na,H-Y catalysts, a very high isomerization activity was found in the hydroconversion of decalin. In addition, the presence of n-decane did not cause a change in the product selectivities, but as on the Ir/Na,H-Y catalysts, the formation of OCDs was favored and the formation of C_9- products was slightly suppressed in the competitive hydroconversion of decalin/n-decane. The highest yields of OCDs among the platinum and iridium catalysts were obtained on the HIPEROCs 2.8Pt/$Na_{0.59}$,$H_{0.41}$-Y-2.4 ($Y_{OCDs,max.}$ = 37.3 %) and 3.3Ir/$Na_{0.72}$,$H_{0.28}$-Y-2.4 ($Y_{OCDs,max.}$ = 33.9 %) with very moderate concentrations of Brønsted acid sites.

Besides zeolite Y, also zeolites Beta, EMC-2, L, MOR and ZSM-5 with different pore systems were loaded with *ca.* 3 wt.-% iridium. On all these catalysts with Spaciousness Indices (*SI*) between 21 and 1, pure n-decane was found to be more reactive than pure decalin. However, the reactivity was inverted when an equimolar mixture of decalin and n-decane was used as feed on the Beta and EMC-2 catalysts. Those were the catalysts with the highest selectivities of OCDs, among them was 3.3Ir/$H_{0.58}$,$Cs_{0.42}$-Beta-14, the catalyst on which the highest yields of OCDs ($Y_{OCDs,max.}$ = 41.1 %) were obtained within this work. Decalin was converted preferably on these HIPEROCs in the competitive hydroconversion of decalin and n-decane.

Moreover, it was found that the hydrocracked products from the n-decane hydroconversion on the HIPEROC 3.3Ir/$H_{0.58}$,$Cs_{0.42}$-Beta-14 consist exclusively of n-alkanes indicating a purely hydrogenolytic carbon-carbon bond scission. At the same time, iso-decanes were formed which possess a distribution of methylnonanes and ethyloctanes which was reported for the isomerization of n-decane on bifunctional isomerization catalysts. It was concluded that both

mechanisms proceed simultaneously in the hydroconversion of n-decane on HIPEROCs. This finding supports and gives independent evidence for a mechanism advanced recently for the hydroconversion of decalin on HIPEROCs.

With decreasing *SI* of the support the relative reactivities of the hydrocarbons changed in the mixture, leading to a preferred hydroconversion of n-decane on zeolite L, MOR and ZSM-5 catalysts. Moreover, a decreasing *SI* led to an increased selectivity of skeletal isomers and a decreased selectivity of ROPs. Thus, the pore size of the zeolite is an important parameter for converting decalin into ROPs.

Subsequently, it was found for HIPEROCs that the selectivity of OCDs is increased and that of C_9- lowered in the product mixtures from the competitive hydroconversion of decalin and n-decane compared to the selectivities calculated from the results of the experiments with pure feeds. It was concluded that OCDs, once they are formed, are displaced from the active sites by decalin and thus prevented from being hydrocracked. If the *SI* of the support was below 16, this positive effect was not found. On such catalysts n-decane is hydrocracked preferentially, and the same is true for its isomers. Additionally, it was found that the experimental selectivities of OCDs in the hydroconversion of the mixed feed are significantly lower than the ones calculated from the selectivities achieved with the pure feed hydrocarbons.

Molybdenum carbide was tested as a possible cheaper substitute for noble metals in the ring opening catalysts. In these tests, decalin was used as the model hydrocarbon. It was shown that β-Mo_2C can be synthesized from MoO_3 *via* carburization with either methane/hydrogen or n-octane/hydrogen mixtures. Bulk molybdenum carbide made in this manner had a low specific surface area around 30 $m^2 \cdot g^{-1}$ and turned out to be hardly active in the ring opening of decalin. The primary products were skeletal isomers of decalin, especially spiro[4.5]decane. With bulk molybdenum carbide as catalyst, open-chain decanes were formed with low selectivities only ($S_{OCDs,max.}$ ≈ 4 % at X_{Dec} = 45 %), whereas hydrocracked products, especially methane, were predominantly made. Overall, the catalytic behavior of bulk molybdenum carbide was found to resemble that of the 2.7Pt/silica catalyst.

Catalysts consisting of β-Mo_2C supported on zeolite Y were also prepared. The zeolite was first impregnated with an aqueous solution of either Na_2MoO_4

or $(NH_4)_6Mo_7O_{24}$, and the resulting samples were carburized with methane/hydrogen or n-octane/hydrogen. β-Mo_2C supported on non-acidic zeolite Y turned out to have a very poor activity in the hydroconversion of decalin. The product selectivities were similar as those observed on bulk molybdenum carbide. Upon increasing the concentration of Brønsted acid sites in the zeolite, both the catalytic activity and the selectivities of ROPs and OCDs increased. However, these catalysts showed a considerable contribution of the paring reaction leading to the undesired products iso-butane and methylcyclopentane, as indicated by M-shaped carbon number distribution curves of the hydrocracked products.

In an attempt to optimize the β-Mo_2C/zeolite Y catalysts, the n_{Si}/n_{Al} ratio of the zeolite was varied between 2.4 and 105 and the molybdenum loading between 5 and 20 wt.-%. The best selectivities of OCDs ($S_{OCDs,max.}$ = 18 % at X_{Dec} = 90 %) were achieved with the catalyst 9.8Mo_2C/$H_{0.99}$,$Na_{0.01}$-Y-7. More generally speaking, intermediate molybdenum loadings around 10 wt.-% and an n_{Si}/n_{Al} ratio of zeolite Y around 7 appear to be favorable for these alternative ring-opening catalysts. However, if the capability to produce OCDs from decalin is used as the criterion, none of the β-Mo_2C/zeolite Y catalysts comes close to the noble metal/zeolite HIPEROCs.

3 Introduction and Objectives

Over the last decade, there has been an ongoing tremendous change in the consumption of transportation fuels in Europe. Less gasoline and much more diesel fuel will be consumed [2]. Depicted in Figure 3.1 are the consumed amounts of the main products from petroleum in Germany. While the amount of consumed gasoline decreased within the last twelve years, an opposite trend is visible for diesel fuel. The increase in diesel fuel consumption will confront refineries in Europe with serious problems, since the quality of crude oils decreases with a trend to heavier feedstocks leading to a reduced possible yield of diesel fuel by the use of conventional refinery processes.

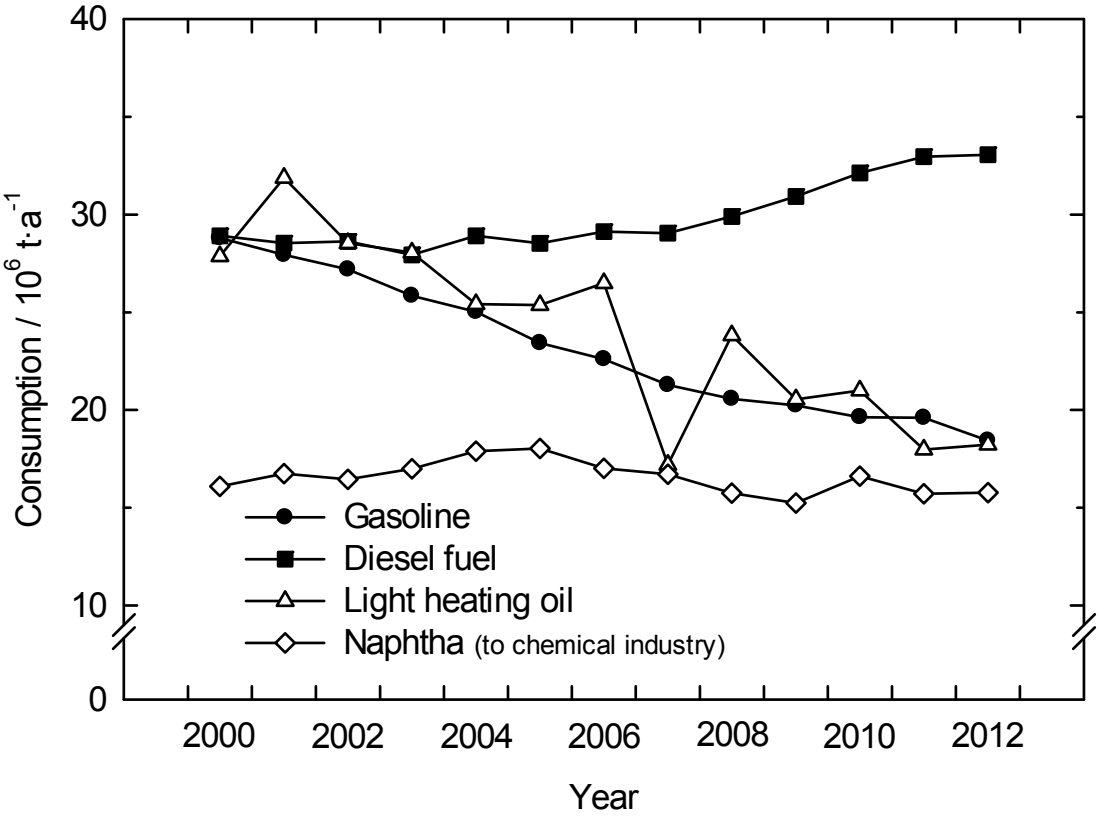

Figure 3.1: Consumption of the main products from petroleum in Germany [3].

Heavy feedstocks contain high amounts of polycyclic aromatic hydrocarbons (PAHs). These PAHs possess several highly undesired properties, such as low cetane numbers, high melting points and poor cold-flow properties. But, and more important from an environmental point of view, PAHs have low n_H/n_C ratios, which lead to a relatively high emissions of CO_2 during the combustion, and they possess a high propensity for soot formation. Thus, the content of PAHs in diesel fuel is limited by EU legislation, currently to 8 wt.-% [4]. A

discussion about a further reduction of the content of PAHs in diesel fuel is in progress.

Nowadays, diesel fuel is blended together from different refinery streams having the same boiling range (200 - 350 °C), *e.g.* light cycle oil (LCO) from the fluid catalytic cracking (FCC) unit which is rich in PAHs. A starting point for a solution of the twofold dilemma of the undesired PAHs together with an increased demand of diesel fuel might be the conversion of PAHs into a high quality diesel fuel. The first step of such an upgrading would be the complete hydrogenation of the polycyclic aromatics into multi-ring naphthenes, followed by a selective opening of the naphthenic rings without a loss of carbon atoms into open-chain alkanes [5]. Such an approach is depicted in Figure 3.2 for the ring opening of decalin.

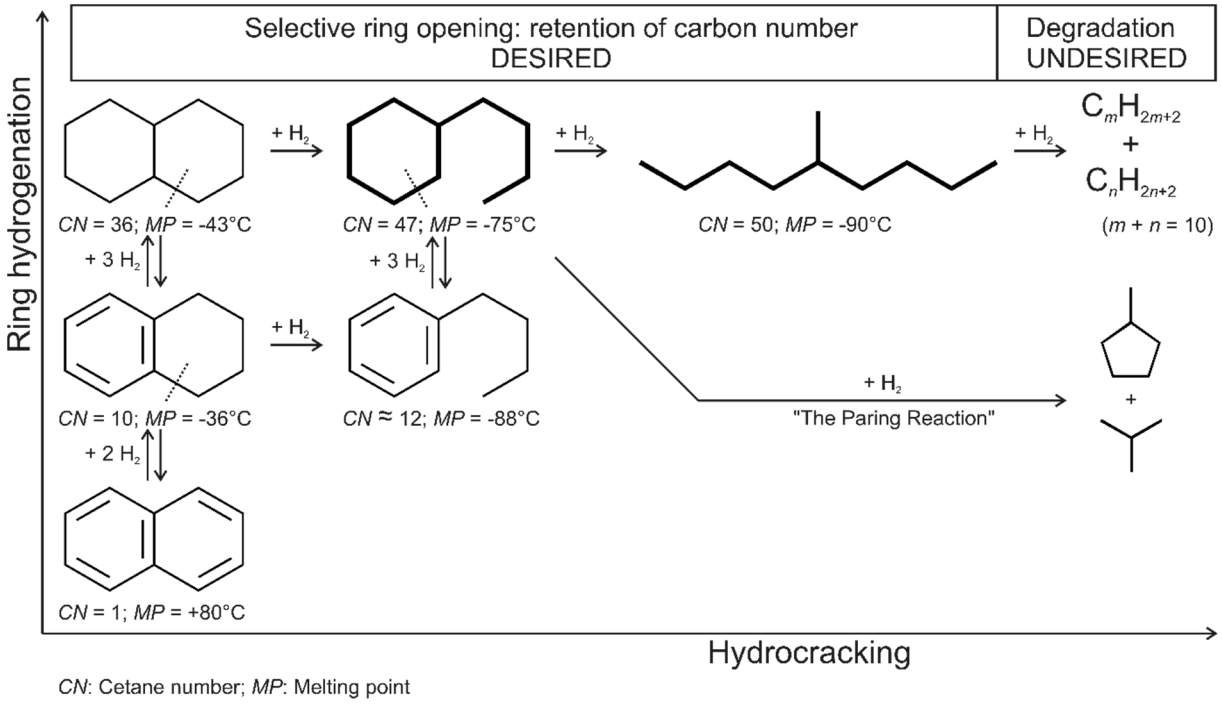

Figure 3.2: Reaction network for the complete ring hydrogenation of the PAH naphthalene into the naphthene decalin, followed by selective ring opening to an alkane. After Ref. [5].

As depicted in Figure 3.2 for decalin, opening of the naphthenic rings lowers the melting point and increases the cetane number significantly. Hence, this technique could be envisaged to upgrade the present diesel fuel. Moreover, it could help to satisfy the increasing demand of diesel fuel.

Today, the FCC units run for maximum yields of gasoline. If the processes were modified towards higher LCO yields, selective ring opening could increase the production of high-quality diesel fuel while simultaneously reducing the production of gasoline. In addition, if the heavy cycle oils from the FCC process were treated in a similar manner, still higher yields of diesel fuel could be produced out of a given crude oil [6].

The objectives of this work are twofold: There exists already a considerable body of literature on catalytic ring opening of multi-ring naphthenic hydrocarbons, typically decalin. Our own group, for example, spent much effort to identify new catalysts that enable one to convert decalin, with as high as possible yields, into alkanes with the same number of carbon atoms, *i.e.*, decane isomers. The outcome of these prior studies with a single feed hydrocarbon will be reviewed in Section 4.2.2.3 of the present thesis. Bearing in mind that refinery feedstocks are almost always complex mixtures of hydrocarbons, we now go one step further and study the catalytic hydroconversion of an equimolar mixture of the model feeds decalin and n-decane. To the best of our knowledge, no such investigations have been described in the existing literature.

As the second aim of this study, the potential of substituting the expensive noble metals in most ring-opening catalysts described so far by a much cheaper non-noble metal were explored. Molybdenum carbide was chosen because of hints in the literature that it may possess a hydrogenation and hydrogenolysis activity. Both bulk and supported molybdenum carbide catalysts were tested. These ring opening experiments were conducted with the model hydrocarbon decalin.

4 Literature Review

4.1 Zeolites and their Properties as Catalyst Carriers

In the middle of the 18th century it was found that some “stones” possess the ability to evolve water when they are heated up. One could have the impression of a boiling stone, and this was why such stones were named “zeolites” by Cronstedt [7] (Greek: zeo: to boil, lithos: stone).

A concise definition of zeolites was given more than 200 years later by Coombs *et al.* [8]: “A zeolite mineral is a crystalline substance with a structure characterized by a framework of linked tetrahedra, each consisting of four O atoms surrounding a cation. This framework contains open cavities in the form of channels and cages. These are usually occupied by H_2O molecules and extra-framework cations that are commonly exchangeable. The channels are large enough to allow the passage of guest species. In the hydrated phases, dehydration occurs at temperatures mostly below about 400 °C and is largely reversible. The framework may be interrupted by (OH, F) groups; these occupy a tetrahedron apex that is not shared with adjacent tetrahedra.”

Hence, zeolites are crystalline, inorganic macromolecules following the molecular formula [9]:

$M_{x/n}[(AlO_2)_x(SiO_2)_y]\cdot m\ H_2O$ n = charge of the cation M

As displayed in the molecular formula, all zeolites are built up by $SiO_{4/2}$- and $AlO^-_{4/2}$-tetrahedra. According to Loewenstein’s rule [10], there cannot be more aluminum than silicon tetrahedra within a zeolite, resulting in a minimum n_{Si}/n_{Al} ratio of 1. Aluminum or silicon are referred to as T atoms. The structures of all zeolites used in this work are depicted in Figure 4.1. It can be seen that the primary building units, *viz.* the tetrahedra, may be connected *via* their vertices to composite building units [11]. In Figure 4.1, all T atoms are located on the vertices, and the lines connecting them symbolize T-O-T bonds. For each zeolite structure certain composite building units have to be connected to get a three dimensional zeolite framework. For example, sodalite units and hexagonal prisms can be arranged to form zeolite Y, but also EMC-2 can be formed by connecting these building units in a different way.

The classification of zeolites is done by the Structure Commission of the International Zeolite Association (IZA). As of today, 213 zeolite structures were approved by the IZA Structure Commission [12]. Each structure represents a framework type, independent of the chemical composition, for which a three-letter code is assigned (*e.g.* FAU for zeolite Y or MFI for zeolite ZSM-5).

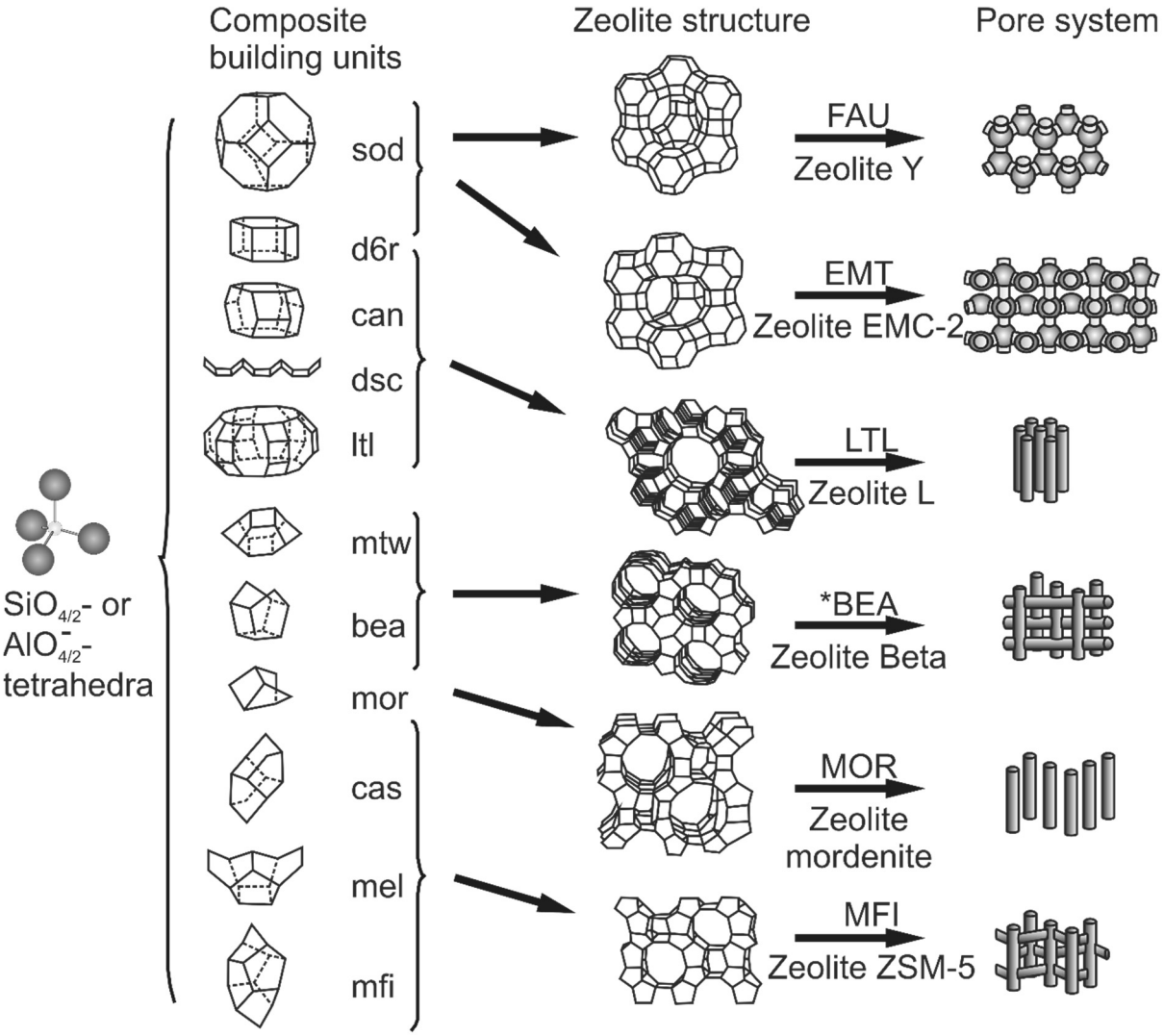

Figure 4.1: Composite building units and structures of all zeolites used in this work and schemes of their pore systems [13-16]. The asterisk before *BEA is to indicate the existence of an intergrowth of two distinct structures termed Polymorphs A and B.

One characteristic property of zeolites is their porosity. Each zeolite possesses a pore system which can be one (1d), two (2d) or three dimensional (3d) in which the pores of the latter two can be interconnected. The pores can be linear or zig-zag-shaped and can even form supercages as in zeolite Y (see Figure 4.1). Usually, the pore systems are discriminated by the number of tetrahedra forming their cross section. Small-pore, medium-pore and large-

pore zeolites consist of eight-, ten- and twelve-membered ring pores, respectively (see Table 4.1).

Table 4.1: Pore systems and dimensions of all zeolites used in this work [14].

Zeolite	Pore system	Pore dimensions / nm
Y (FAU)	12-ring channels, 3d	0.74 x 0.74
EMC-2 (EMT)	12-ring channels, 3d	0.73 x 0.73; 0.62 x 0.75
L (LTL)	12-ring channels, 1d	0.71 x 0.71
Beta (*BEA)	12-ring channels, 3d	0.66 x 0.67; 0.56 x 0.56
Mordenite (MOR)	12-ring channels (1d) with interconnecting 8-ring channels	0.65 x 0.70; 0.26 x 0.57
ZSM-5 (MFI)	10-ring channels, 3d	0.51 x 0.55; 0.53 x 0.56

Due to their systems of micropores, zeolites possess very high specific surface areas of several hundreds of square meters per gram. The high specific surface area and their thermal stability make zeolites ideal as supports for catalysts. Additionally, in some catalytic reactions, *e.g.* the production of p-ethyltoluene from toluene and ethene, zeolites can favorably influence the product selectivities due to their shape selective properties [17]. The effect can occur if the pore dimensions and the size of the reactant or product molecules are similar.

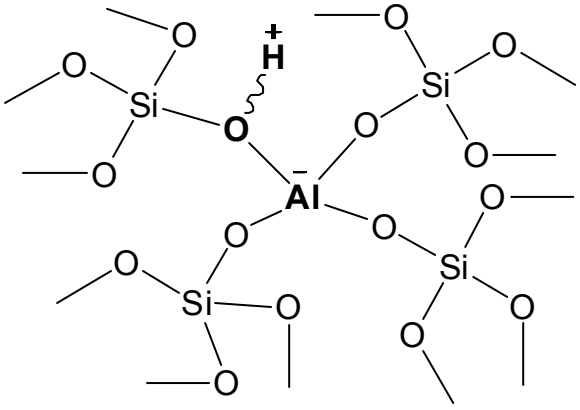

Figure 4.2: Scheme of a Brønsted acid site in the zeolite framework.

When silicon T atoms in the zeolite framework are replaced by aluminum atoms, one negative charge is added per aluminum atom to the framework. This is not surprising, since aluminum is incorporated as $AlO^-_{4/2}$ unit into the zeolitic framework. The negative charges thereby generated have to be compensated by cations. Usually, protons (see Figure 4.2), small alkali or

alkaline earth cations take over that role. A very important feature of zeolites is their ability to exchange those cations, *i.e.* they can act as ion exchangers.

For the synthesis of zeolites, usually by hydrothermal synthesis, a silicon and an aluminum source are mixed in aqueous phase together with a structure directing organic template and a base like sodium hydroxide to form a gel which is then transferred into an autoclave. After several hours or days of crystallization at elevated temperatures, the zeolite is filtered off from the mother liquor and calcined. Hence, the resulting zeolite will often contain alkali cations for compensation of the negative framework charge.

Zeolites can act as catalysts in acid catalyzed reactions. To achieve this, the alkali cations have to be replaced by protons. This is best done by an aqueous ion exchange of the zeolite with ammonium ions, followed by a calcination of the zeolite which results in deammoniation and leaves behind a proton inside the zeolite (see Eq. 4.1) [18].

$$NH_4^+ + Na^+Z^- \xrightarrow[-\,Na^+]{} NH_4^+Z^- \xrightarrow[-\,NH_3]{T > 573\ K} H^+Z^- \qquad (4.1)$$

In many cases, catalysts are needed which contain both Brønsted acid sites and hydrogenation/dehydrogenation sites, for example noble metals. To produce such bifunctional catalysts, the metal can be loaded onto the zeolite by ion exchange or impregnation. A simple aqueous ion exchange can be applied, as long as water-soluble salts or cationic complexes of the metal are available. If this is not the case, solid-state ion exchange is often an alternative: Introduction of the metal by ion exchange usually leads to catalysts with higher metal dispersion than impregnation.

Metals on a catalyst are mostly required in the oxidation state 0. If a metal has been introduced as a cation, its reduction is necessary. For noble metals this reduction is readily achieved with hydrogen. It has to be borne in mind that such a reduction is inevitably accompanied by the formation of Brønsted acid sites, according to Eq. 4.2. In this equation, Z^- denotes the negatively loaded zeolite framework.

$$0.5n\ H_2 + M^{n+}(Z^-)_n \longrightarrow M^0 + (H^+)_n(Z^-)_n \qquad (4.2)$$

The term “acidity” of a solid catalyst requires some clarification, as it embraces at least three different physico-chemical quantities, *viz.* the chemical nature, the density (or concentration) and the strength of the acid sites [19]. Both Brønsted and Lewis acid sites occur in zeolites. The Brønsted acid sites are generally considered to consist of bridging OH groups residing on the framework (*cf*. Figure 4.2). According to Kühl [20] and Jacobs and Beyer [21], aluminum on extra-framework positions is responsible for Lewis acidity. Experimentally, the discrimination between Brønsted and Lewis acid sites is usually achieved by IR spectroscopy with pyridine as a probe molecule. The most widely used method for measuring the density of Brønsted and Lewis acid sites is again IR spectroscopy with pyridine as probe performed in a quantitative manner, but ^{1}H-MAS-NMR spectroscopy is a popular tool as well, especially for Brønsted acid sites. The most difficult to determine quantity is the strength of the acid sites. Various techniques have been proposed for this purpose, including microcalorimetry and temperature-programmed desorption of bases, such as ammonia or pyridine. Perhaps the most widely employed method for collecting semi-quantitative information concerning the strength of acid sites is based on a proposal by Liengme and Hall [22]: Pyridine is adsorbed on a sample of the zeolite which is placed in the cell of an IR spectrometer and can be heated in a temperature-programmed manner. The decrease of the amount of pyridine adsorbed on both the Brønsted and Lewis sites with increasing temperature is quantitatively measured, and the effect is exploited that pyridine is released from weak acid sites at relatively low temperatures, whereas high temperatures are required for desorption of the base from strong acid sites.

For a given zeolite framework type, *e.g.* faujasite, the amount of aluminum in the framework which is often expressed in terms of the n_{Si}/n_{Al} ratio, can be varied within certain limits. Obviously, with increasing aluminum content of the framework, its n_{Si}/n_{Al} ratio decreases and the density of Brønsted acid sites increases. It has furthermore been found that the strength of the Brønsted acid sites decreases with increasing aluminum content [23]. This has been rationalized in terms of an increasing negative charge density of the zeolitic framework which results in a stronger interaction of the hydroxyl groups with the framework and hampers the deprotonation. It has been shown that Sanderson’s electronegativity model can be used to quantitatively correlate the acid strength with the electronegativity of the framework [24,25]. The latter can be readily calculated as the arithmetic means of the electronegativity of the elements forming the framework.

Sanderson's electronegativity model was also used to explain the influence of the nature of the charge-compensating cations on the strength of the Brønsted acid sites [26]. For example, the model predicted a strong decrease in the acid strength of faujasites exchanged with the alkali cations from lithium to cesium, in complete agreement with the experimentally measured acid strengths of these materials.

4.2 Ring Opening of Multi-Ring Aromatics and Naphthenes

4.2.1 Four Mechanisms of C-C Bond Breaking

In addition to non-catalytic thermal cracking, three distinctly different mechanisms of catalytic C-C bond breaking are usually discerned which proceed on different types of catalysts [5]: The so-called "catalytic cracking" of hydrocarbons occurs on monofunctional, Brønsted acidic catalysts. C-C bond cleavage on metallic catalysts (mostly noble metals) is generally referred to as "hydrogenolysis". Finally, "hydrocracking" is the generic term for cleavage of hydrocarbons on bifunctional catalysts containing both acidic and metallic sites.

4.2.1.1 Thermal (Hydro-)Cracking

Thermal (hydro-)cracking is the easiest way of C-C bond breaking. No catalyst is necessary, the C-C bonds are simply broken by homolytic scission at reaction temperatures above 500 °C. Cracking at these high temperatures proceeds *via* radicals as reactive intermediates and leads to mainly small hydrocarbons and coke [27]. Industrial use of thermal cracking is made in the steam cracking process, in which mainly naphtha (EU) or ethane/propane (US) are used as reactants. The reactants are diluted with steam to lower their partial pressures which results in higher yields of olefins and a suppressed coke formation. Steam cracking is the major industrial source of ethene and propene.

4.2.1.2 Acid-Catalyzed Cracking and Hydrocracking

For the acid-catalyzed hydrocracking of hydrocarbons on monofunctional acidic catalysts two different mechanisms are known, *viz.* the classical (or bimolecular) and the non-classical (or monomolecular or Haag-Dessau) cracking. Depending on the reaction conditions and the type of hydrocarbon, one of these two mechanisms prevails. Both mechanisms start with the formation of a carbocationic species as the first reaction step [28].

The first step in the classical bimolecular cracking (Figure 4.3, top), which is demonstrated for an n-alkane, is the formation of a carbenium ion. This can be achieved by protonation of an olefinic hydrocarbon or by protonation of an alkane followed by abstraction of dihydrogen (dotted arrow of Figure 4.3, bottom). Olefins may be present in the feed as an impurity.

Once formed, the alkylcarbenium ion can undergo skeletal isomerizations *via* type A or type B rearrangements [29] (step A1 in Figure 4.3). While the number of branching keeps constant in type A rearrangements it increases or decreases in type B rearrangements. Type A rearrangements proceed *via* classical intramolecular hydride and alkyl shift, whereas type B rearrangements are slower and proceed *via* a transition state of protonated cyclopropanes [29]. The tertiary alkyl carbenium ion thereby formed is in equilibrium with the secondary alkyl carbenium ion where the positive charge is in β-position to the branching (step B1 in Figure 4.3). This alkyl carbenium ion can undergo a so-called β-scission, in which the C-C bond in β-position to the positively charged carbon atom is cleaved (step C1 in Figure 4.3).

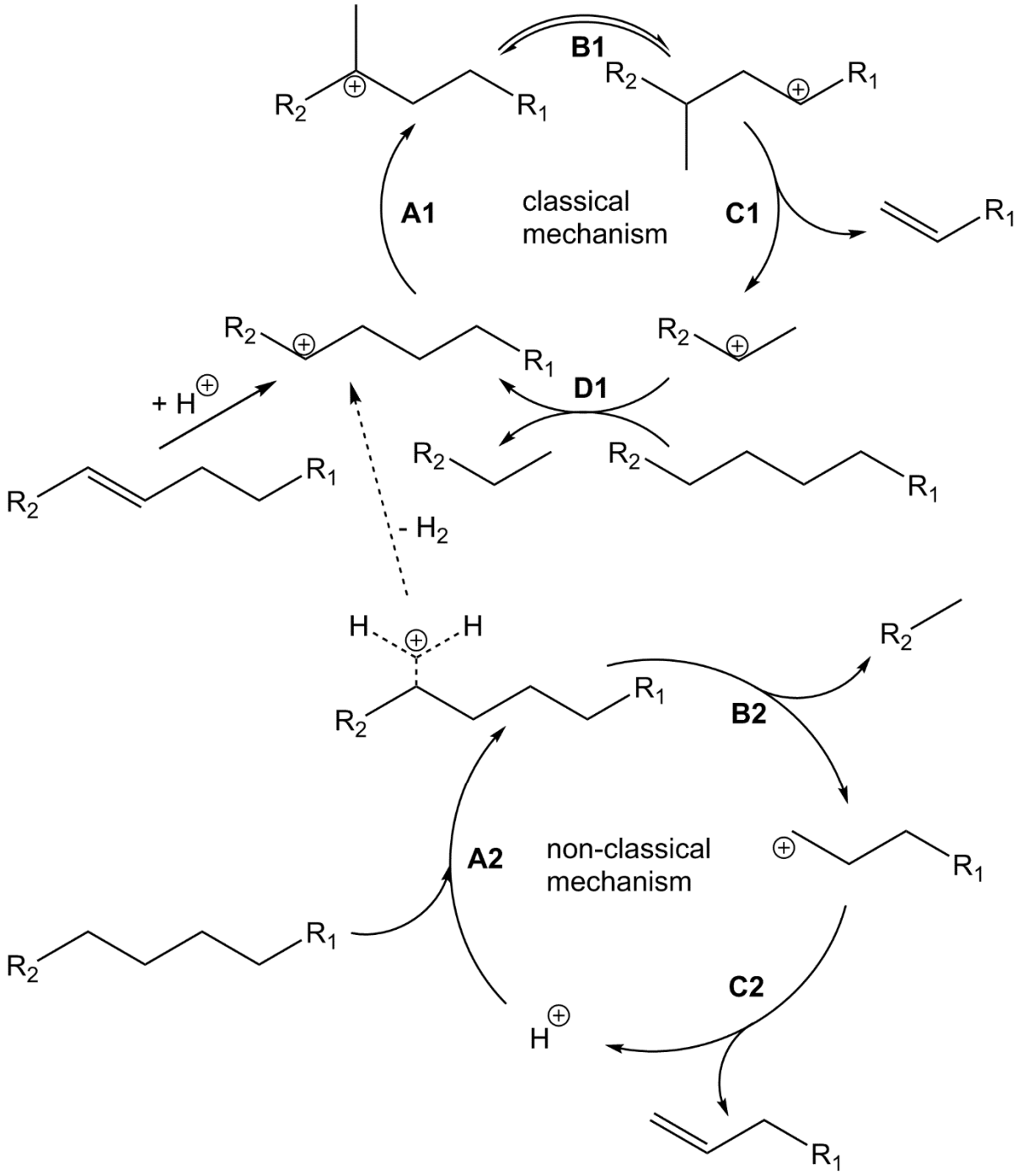

Figure 4.3: Classical (top) and non-classical (bottom) mechanism of Brønsted acid catalyzed cracking of an alkane after Ref. [28].

Since this reaction pathway proceeds *via* carbocations it is easily understandable that the stability of the carbocationic species plays a major role in the kinetics of the C-C bond scission. The stability of the cations decreases from tertiary to primary carbenium ions. Hence, one can conclude that β-scissions starting from a tertiary carbocation and resulting in a branched alkene and a tertiary carbocation proceed the fastest. The β-scissions of alkylcarbenium ions were classified by Weitkamp *et al.* [30] (see Figure 4.4)

according to the kinetics of their bond scission from very fast (Type A) to very slow (Type C) or even forbidden (Type D).

The carbocation in Figure 4.3 undergoes a β-scission of type C (step C1) and forms both a non-branched olefin and a non-branched secondary alkyl carbenium ion. The catalytic cycle is closed by an intermolecular hydride transfer from a feed alkane molecule to the alkyl carbenium ion (step D1 in Figure 4.3). This last step is the rate limiting step, and since two molecules are involved, this mechanism is named “bimolecular cracking”.

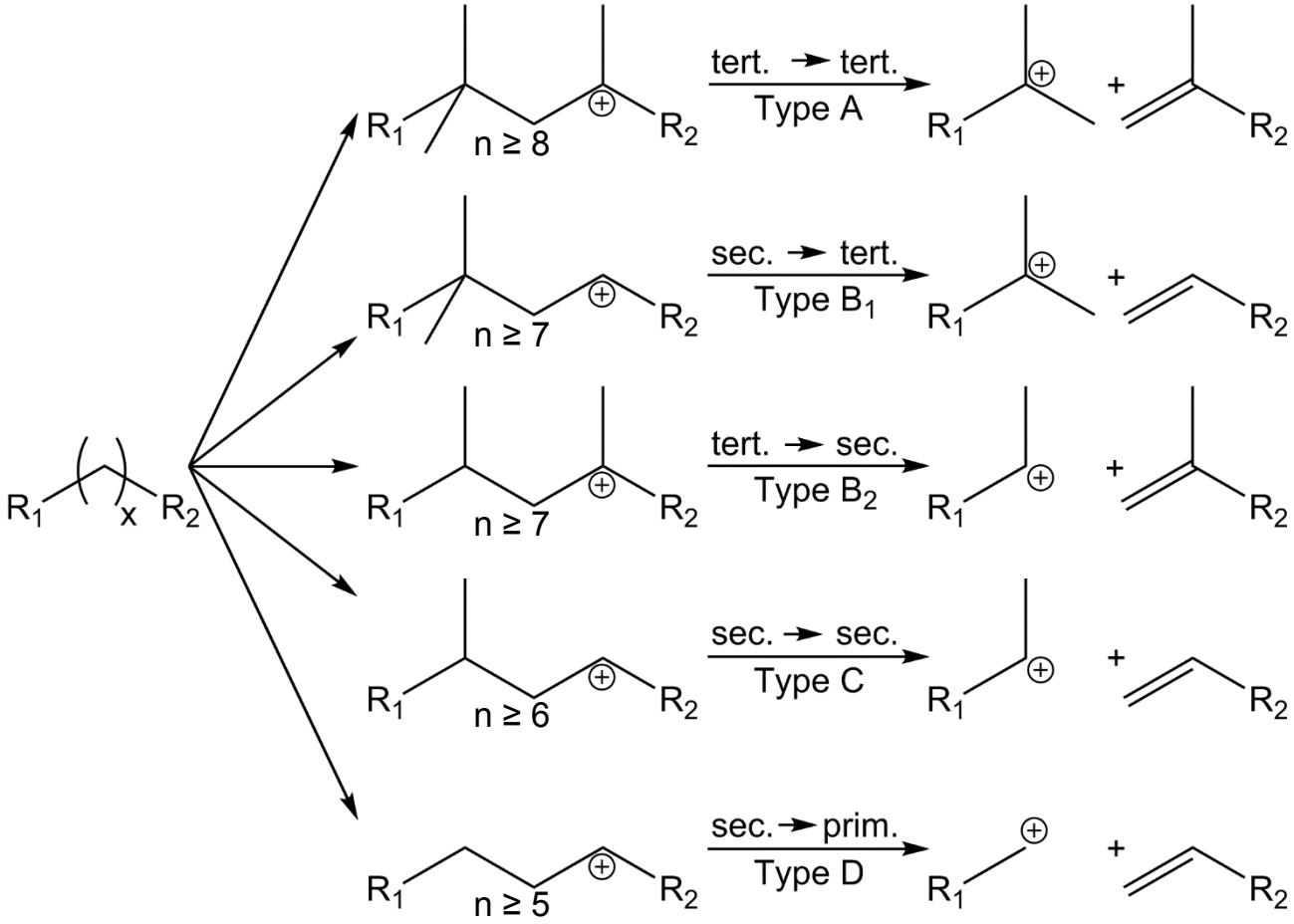

Figure 4.4: Modes of β-scission after Ref. [30]. R stands for alkyl groups and n is the number of carbon atoms of the respective carbenium ion.

Catalytic bimolecular cracking is usually looked upon as the dominating mechanism in the process of fluid catalytic cracking (FCC). Vacuum gasoil is converted on an acidic ultra-stable Y zeolite mainly into gasoline. Most of the world’s gasoline is produced by this process. By adding a medium pore zeolite, *viz.* H-ZSM-5, to the main faujasitic cracking catalyst, the yield of

propene is increased. Today, FCC is the second most important source of propene besides steam cracking.

Beside the classical bimolecular cracking mechanism, a monomolecular mechanism is known which is depicted in the bottom half of Figure 4.3 for the cracking of an alkane. This mechanism is also named Haag-Dessau cracking after the two scientists who first proposed this mechanism [31]. In the non-classical mechanism, the first step is the protonation of the feed alkane to form an alkyl carbonium ion (step A2 in Figure 4.3). In the carbonium ion, either dihydrogen can be abstracted, which is a starting reaction for the classical mechanism resulting in an alkyl carbenium ion (dashed arrow in Figure 4.3). Alternatively, carbon-carbon bond scission can happen resulting in the formation of an alkane and an alkyl carbenium ion (step B2). The catalytic cycle is closed by the decomposition of the alkyl carbenium ion into an alkene and a proton (step C2).

Both mechanisms, *i.e.*, the classical and the non-classical, proceed in parallel, with typically a strong preponderance of one mechanism, and cannot be strictly separated in acid-catalyzed reactions. In general, the non-classical mechanism is favored at higher reaction temperatures and with short chain alkanes which cannot be isomerized. Moreover, low partial pressures of the feed hydrocarbon and steric hindrance, *e.g.* inside a zeolite with narrow pores, can hamper the bimolecular step in the classical mechanism while the non-classical monomolecular mechanism is not affected. Strong evidence for Haag-Dessau cracking is the occurrence of methane and/or ethane in the product mixture, since the formation of these products is negligible in the classical mechanism, due to the formation of a primary carbenium ion in the transition state.

4.2.1.3 Metal-Catalyzed Hydrocracking (Hydrogenolysis)

C-C bond cleavage can be catalyzed by monofunctional noble metal catalysts without any participation of acid sites. Hydrocracking of carbon-carbon bonds by means of metals is called hydrogenolysis. The first reaction step is the chemisorption of the hydrocarbon on the metal atom(s). Depending on the nature of the noble metal (and in some instances on its dispersion), different product distributions in the hydrogenolysis of alkanes can be obtained. Based on this finding, several mechanisms for hydrogenolytic carbon-carbon bond

cleavage have been advanced. A good overview was given by Gault [32], and selected mechanisms are depicted in Figure 4.5.

The major reaction occurring on palladium is demethylation [33]. Since metallocarbenes are assumed to be the main intermediates and demethylation is also the major reaction in the hydroconversion of neopentane, mechanism A in Figure 4.5 was postulated which involves a 1,3-diadsorbed species. After C-C bond cleavage and subsequent hydrogenation of the π-adsorbed iso-butene and the metallocarbene species, methane and iso-butane are evolved.

An analysis of the products from hydrocracking of monobranched hydrocarbons on platinum reveals that the carbon-carbon bond in α,β-position to the branching is cleaved preferentially [34]. To account for this, mechanism B in Figure 4.5 was postulated, and it is shown here exemplarily for 2-methylpentane. 2-Methylpentane is adsorbed on the metal and forms a 1,1,3-triadsorbed species. The bridging carbon chain between the adsorbed C-atoms will then be cleaved next to the diadsorbed carbon atom, leading to the formation of a π-adsorbed iso-butene and a metallocarbyne. After complete hydrogenation, iso-butane and ethane are released.

The product composition obtained in the conversion of a branched alkane on iridium reveals a preferred cleavage of secondary-secondary or secondary-primary carbon-carbon bonds. Due to this finding a mechanism was proposed which is depicted exemplarily in Figure 4.5C for the conversion of n-butane. In a first step, n-butane is adsorbed on iridium as 1,2-diadsorbed dicarbene species. This step is followed by a cleavage of the carbon-carbon bond between the two adsorbed carbon atoms. The thereby formed metallocarbynes are hydrogenated to ethane and desorbed from the metal.

It was found that metals of the 4th period of the periodic table of the elements like Co and Ni lead to large amounts of methane or even a total degradation of hydrocarbons to methane in a hydroconversion. In Figure 4.5D, a mechanism is depicted exemplarily for the hydrogenolysis of n-hexane. On nickel and cobalt, multiple adsorption of the hydrocarbon to the metal is proposed, followed by several consecutive carbon-carbon bond cleavages before desorption. This leads to small fragments of the hydrocarbons which are hydrogenated and desorbed as methane.

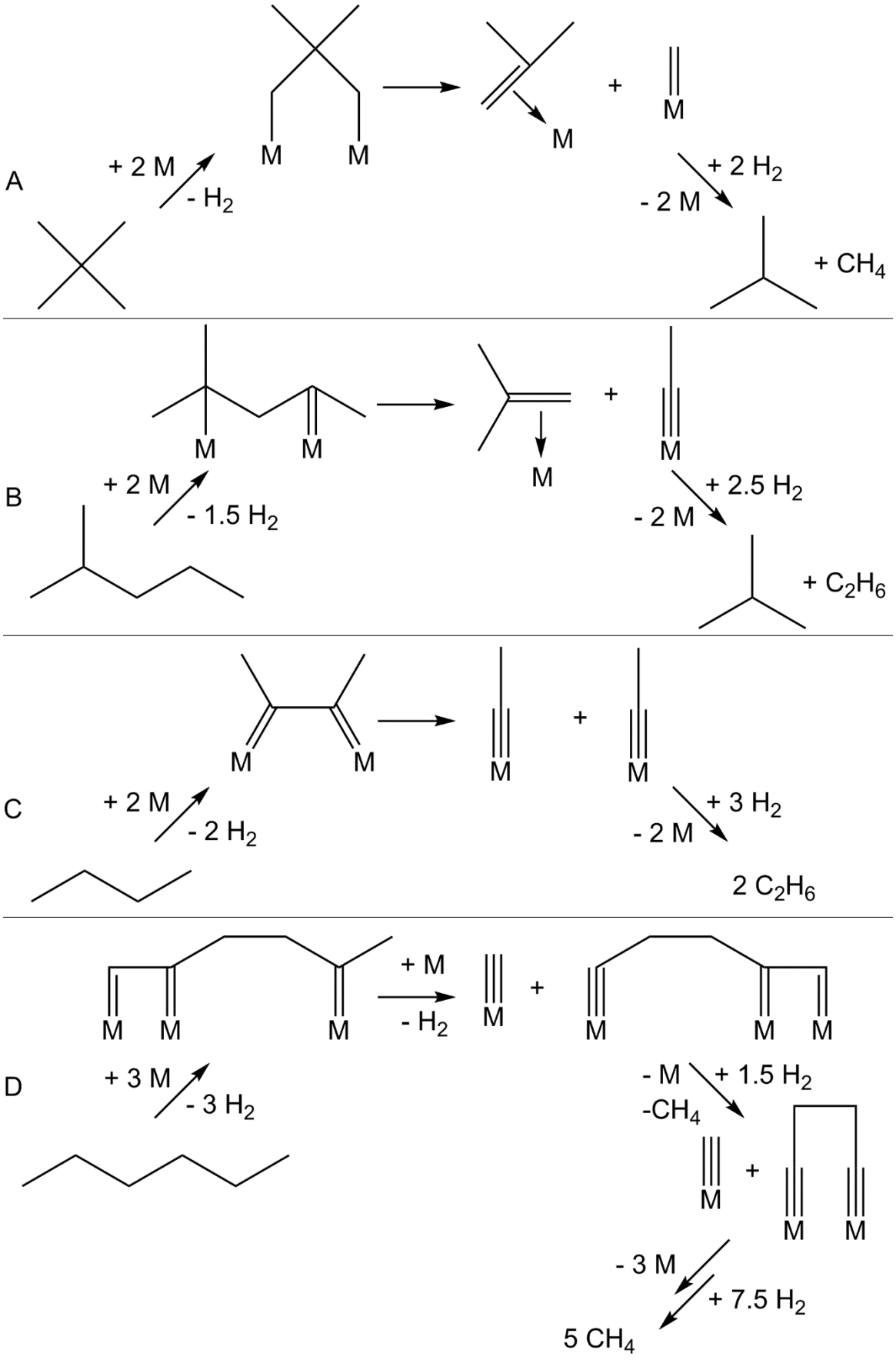

Figure 4.5: Postulated mechanisms for hydrogenolytic carbon-carbon bond cleavage on A) palladium, B) platinum, C) iridium and D) nickel or cobalt. After Ref. [32].

4.2.1.4 Bifunctional Hydrocracking

Bifunctional catalysts contain Brønsted acid sites as well as metal sites. Therefore, the hydrocracking mechanism on bifunctional catalysts combines reaction steps of the classical bimolecular cracking on Brønsted acid sites, hydrogenation/dehydrogenation reactions on the metal sites and hydrogenolysis on noble metals.

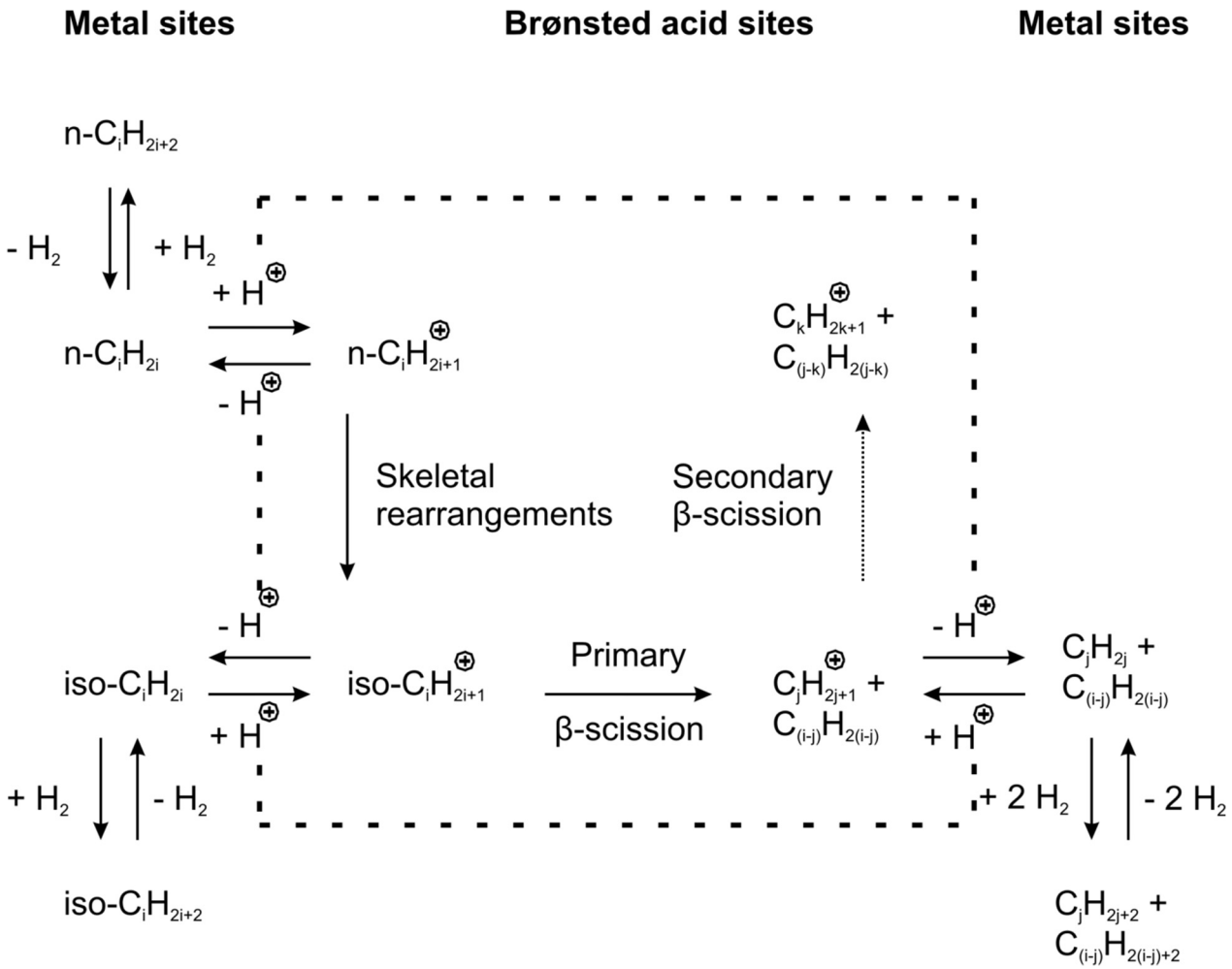

Figure 4.6: Mechanism of isomerization and hydrocracking of an n-alkane on a bifunctional catalyst [35].

The mechanism for the bifunctional hydrocracking of an n-alkane is depicted in Figure 4.6. At first, the n-alkane is dehydrogenated on a dehydrogenation/ hydrogenation site, typically a noble metal like platinum or palladium. The n-alkenes thereby formed can diffuse to a Brønsted acid site where they are easily protonated to form an alkylcarbenium ion. As depicted in Figure 4.3 for the classical bimolecular cracking, n-alkylcarbenium ions can undergo skeletal rearrangements to form branched alkylcarbenium ions. At this point, the isomerized alkanes can react into different directions: they can be

deprotonated, hydrogenated and then desorbed as iso-alkanes or they can be cracked into smaller fragments. Carbon-carbon bonds of the branched alkylcarbenium ions can be cleaved by β-scissions (see Figure 4.4) into an alkene and an alkylcarbenium ion. After deprotonation of the ion and a subsequent hydrogenation of both fragments, they are desorbed from the catalyst as alkanes.

It was found by Coonradt and Garwood [36] that secondary cracking of hydrocarbons can be inhibited to a certain extent by the use of a highly dehydrogenation/hydrogenation active metal or by increasing the amount of metal. They concluded that the rate-controlling step, the skeletal rearrangements and the β-scissions on the acid sites, might be hampered due to competitive adsorption of alkenes. The alkenes formed on metal sites by dehydrogenation can displace alkylcarbenium ions from the acid sites and keep them away from secondary cracking reactions.

Later, Weitkamp and Schulz [37] investigated the hydroconversion of n-dodecane on a Pd/Ca-Y zeolite. At low hydrocarbon conversions, they found surprisingly high concentrations of alkenes, which were orders of magnitude higher than those calculated for thermodynamic equilibrium. This was new and independent evidence for the mechanism proposed for bifunctional hydrocracking (see Figure 4.6).

4.2.2 Mechanisms of Ring Opening of Cyclic Hydrocarbons

This section will focus on the mechanisms of catalytic ring opening of multi-ring naphthenes. The most frequently used model hydrocarbons for such studies are naphthalene, tetralin and decalin, and the catalysts can be classified as monofunctional acidic, classical bifunctional and monofunctional metallic. Thermal hydrocracking is not appropriate for selective ring opening of naphthenes because it inevitably leads to a degradation of the carbon number and to coke and will therefore not be reviewed.

4.2.2.1 Classical Bifunctional and Acid-Catalyzed Naphthene Hydroconversion

For the acid-catalyzed cracking of naphthenes the same principles as for alkanes (see Section 4.2.1.2, page 21) can be applied. However, β-scission of endocyclic carbon-carbon bonds is surprisingly slow. A good explanation for this finding was given by Brouwer and Hogeveen [38]. They proposed that the free rotation around the α-bond in an alkylcarbenium ion allows a coplanar grouping of the vacant p-orbital and the β-bond to be broken. Hence, a good orbital overlap can be realized supporting a fast carbon-carbon bond β-scission (see Figure 4.7). In contrast, if the β-bond is part of a naphthenic ring, a rotation around the α-bond is impossible, and the empty p-orbital of the cycloalkylcarbenium ion is nearly perpendicular to the β-bond. Hence, an orbital overlap is hardly possible in the transition state of β-scission which hampers the kinetics of the β-scission.

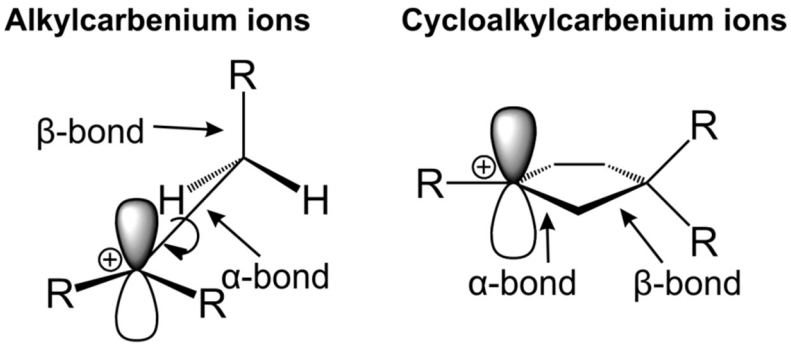

Figure 4.7: Role of orbital orientation in the β-scission of aliphatic and cyclic carbenium ions [38,39].

The resistance of naphthenic rings against cationic endocyclic carbon-carbon bond scission leads to a special reaction pathway, the so-called paring reaction. A scheme of the paring reaction, a term coined by Egan *et al.* 50 years ago [40], is depicted in Figure 4.8. The paring reaction is best shown by ring opening of C_{10} naphthenes with one ring. Independent of the structure of the C_{10} naphthene used as reactant three cyclopentyl structures can be obtained by fast skeletal rearrangements resulting in carbocations that are capable to undergo the very fast β-scission of type A. This reaction pathway leads to high amounts of methylcyclopentane and iso-butane in the hydrocracked products from the acidic hydroconversion of C_{10} naphthenes. These saturated products are formed if a hydrogenation-active metal is present on the catalyst, otherwise the respective olefinic products will be obtained.

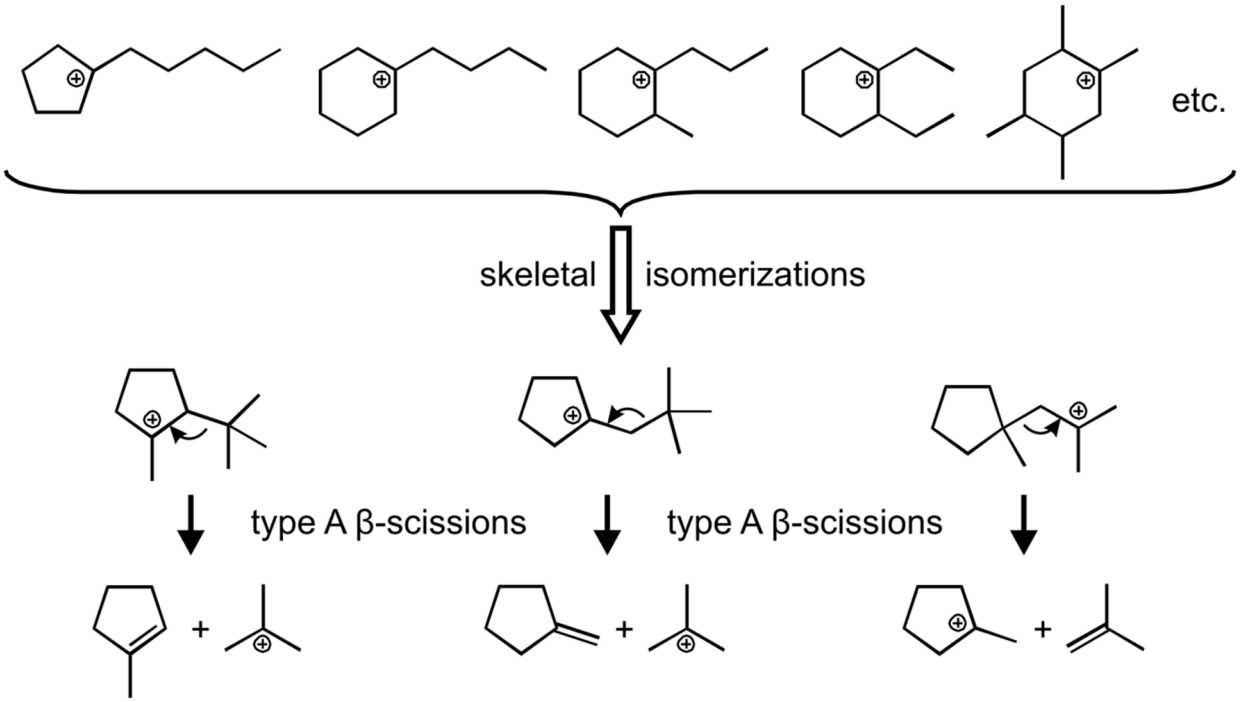

Figure 4.8: Scheme of the paring reaction. After Ref. [35].

Modified hydrocracking selectivities (S_j*, for calculation see Section 5.5.3.1, page 91) from n-decane and butylcyclohexane on conventional bifunctional catalysts are depicted in Figure 4.9. The term “conventional bifunctional catalysts” refers to catalysts with a relatively low content (up to *ca.* 1 wt.-%) of a noble metal on a support with a high concentration and strength of Brønsted acid sites. In Figure 4.9, the modified selectivity of hydrocracked products (S_j*) are shown in dependence of their number of carbon atoms. The calculation of modified hydrocracking selectivities is given in Section 5.5.3.1, page 91. Although no protons were included in the short designation of 0.5Pt/Ca-Y, this catalyst does contain Brønsted acid sites which are formed on catalysts with multivalent cations. The formation of protons occurs during a thermal treatment where water molecules dissociate into hydroxyl groups and protons as postulated by Hirschler and Plank [41,42]. Since both curves are symmetrical around C_5, which is half the carbon number of the feed, it can be stated that both curves indicate a pure primary hydrocracking which means that one feed molecule is cracked into two product molecules. C_1, C_2, C_8 and C_9 products were neither obtained from n-decane nor from butylcyclohexane on these conventional bifunctional catalysts. This is due to the fact that a formation of methane or ethane as hydrocracking products can only occur *via* the formation of primary carbenium ions in the β-scission of the respective carbon-carbon bond (see Figure 4.3 top).

The curves shown in Figure 4.9 differ sharply from each other in the range of C_4 to C_6. A bell-shaped curve with a maximum at C_5 is obtained in the hydrocracking of n-decane. By contrast, an M-shaped carbon number distribution with a pronounced minimum at C_5 results in the hydrocracking of the naphthenic hydrocarbon butylcyclohexane. In the latter case, the strongly dominating products in the C_4 and C_6 fraction are iso-butane and methyl-cyclopentane, respectively [43,44]. The M-shaped distribution curve is a fingerprint of the occurrence of the paring reaction.

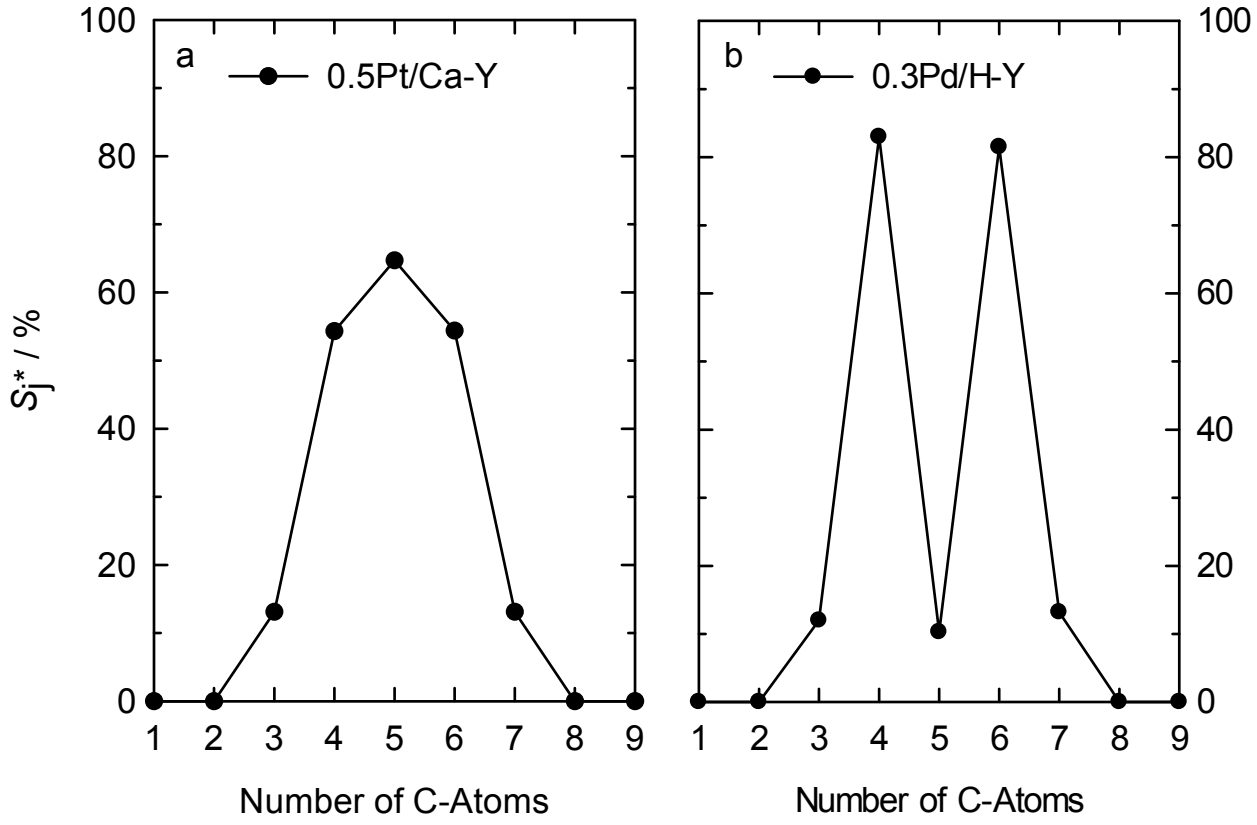

Figure 4.9: Carbon number distributions of the hydrocracked products from a) n-decane and b) butylcyclohexane on conventional bifunctional catalysts [43,44] at similar yields of hydrocracked products Y_{C_9-}.
Reaction conditions:
a) T_r = 270 °C Y_{C_9-} = 40 %
b) T_r = 270 °C Y_{C_9-} = 25 %

The paring reaction was introduced by Weitkamp *et al.* [45,46] as catalytic test reaction for probing of the pore width of zeolites. This was based on the finding, that the formation of iso-butane is hampered in medium pore zeolites when converting butylcyclohexane. An explanation for the lowered iso-butane formation is the bulky transition state of type A β-scissions (see Figure 4.8).

Hence, the yield ratio of iso-butane and n-butane in the hydrocracking of butylcyclohexane was introduced as a quantitative measure of the pore width of large pore zeolites. Since $Y_{\text{iso-butane}}/Y_{\text{n-butane}}$ increases with increasing space inside the pores, this yield ratio was named the “Spaciousness Index” (*SI*) [46-48].

The ring opening of cis-decalin (c-Dec) or mixtures of cis- and trans-decalin (Dec) on monofunctional acidic catalysts was investigated by Mostad *et al.* [49], Kubička *et al.* [50], Corma *et al.* [51], Santikunaporn *et al.* [52] and others. A broad range of reaction temperatures from 260 to more than 480 °C were applied at hydrogen pressures of 2.0 MPa or less. The reaction conditions and relevant results in terms of maximal yields or selectivities of ring-opening products are summarized in Table 4.2.

Table 4.2: Maximum yields or initial selectivities of ring-opening products (ROPs) obtained from decalin on several monofunctional acidic catalysts.

Catalyst	T_r / °C	p_{H_2} / MPa	$Y_{ROPs,max.}$ / %	S_{ROPs} / %	**Ref.**
H-Y	482 °C	-	5.1[1]	6.5	[49]
H-USY	482 °C	-	9.0[1]	9.3	[49]
H-Beta-12.5	280 °C	1.7 MPa	11.0[1]	12.9	[50]
H-Beta-37.5	280 °C	1.7 MPa	9.9[1]	12.7	[50]
H-Y-6	270 °C	1.7 MPa	3.8[1]	7.9	[50]
H-MOR-10	300 °C	1.7 MPa	3.7[1]	9.5	[50]
H-ZSM-5-15	450 °C	0.1 MPa	-	2.2[2]	[51]
H-MCM-22-15	450 °C	0.1 MPa	-	3.9[2]	[51]
H-ITQ-2-15	450 °C	0.1 MPa	-	2.6[2]	[51]
H-Beta-16	450 °C	0.1 MPa	-	3.3[2]	[51]
H-USY-15	450 °C	0.1 MPa	-	3.5[2]	[51]
H-UTD-1-80	450 °C	0.1 MPa	-	3.8[2]	[51]
H-[Al]MCM-41-17	450 °C	0.1 MPa	-	2.0[2]	[51]
H-Y-5.3	260 °C	2.0 MPa	19.1	46.8	[52]

[1]in the liquid products

[2]values are $S_{ROPs,max.}$ at very low conversions

Only small yields of ROPs were obtained on the investigated monofunctional acidic catalysts (see Table 4.2). If harsh reaction temperatures of 450 °C or more are applied, the selectivities of ROPs remain below 10 %. Hence, ROPs are only minor products on such catalysts. One exception was the catalyst H-Y-5.3, on which clearly higher yields of ROPs ($Y_{ROPs,max.}$ = 19.1 %) were

obtained compared to the other catalysts listed in Table 4.2. This finding might be a result of the lowered reaction temperature and increased hydrogen pressure, which prevented the decalin from being converted into short-chain hydrocracked products.

It was found by Corma *et al.* [51] that the rate of decalin cracking depends on the pore structure of the H-zeolites used as catalysts. The rate decreased in the order: H-USY > H-UTD-1 > H-Beta > H-ZSM-5 > H-MCM-22 > H-ITQ-2 > H-[Al]MCM-41. However, Kubička *et al.* [50] found H-Beta more active than H-Y and H-MOR. In general, one can conclude that the initial catalyst activity depends directly on the concentration of Brønsted acid sites. All catalysts showed a fast deactivation due to coke formation. Two factors seem to be decisive for the deactivation rate, *viz.* the concentration of Brønsted acid sites and the pore structure of the zeolite. For the same pore structure, the rate of deactivation increased with increasing concentration of Brønsted acid sites, as demonstrated by Kubička *et al.* with H-Beta-12.5 and H-Beta-37.5. The same authors showed that H-Y-6 deactivated faster than H-Beta-12.5 which contained almost the same concentration of Brønsted acid sites, as determined by FT-IR spectroscopy of adsorbed pyridine. The fast deactivation of H-Y-6 was explained by the larger cavities of zeolite Y which allow the formation of bulky organic coke molecules which block the pores for the reactant molecules.

Interestingly, H-MOR, which had the highest concentration of Brønsted acid sites of all catalysts tested by Kubička *et al.* [50], was very inactive in the hydroconversion of decalin. This was interpreted in terms of a fast blockage of the outer surface and the pore mouths of the zeolite which also led to a strong loss of specific surface area measured by N_2 physisorption.

It has been reported in Refs. [49-51] that C_4 and C_6 hydrocarbons are prevailing in the hydrocracked products from decalin hydroconversion on monofunctional acidic catalysts. This can be looked upon as a clear hint for the occurrence of the paring reaction, even though the term was not explicitly used in Refs. [49-51], and no reference to the work by Egan *et al.* [40] was made.

In the study by Santikunaporn *et al.* [52] three H-Y catalysts with different concentrations of Brønsted acid sites were tested in the hydroconversion of decalin. The highest selectivity of ROPs was obtained on the catalyst with the lowest concentration of Brønsted acid sites. With this catalyst, only small

amounts of hydrocracked products were formed. With increasing acid site concentration of the catalyst, higher decalin conversions were obtained with yields of ROPs up to 19.1 % and a simultaneous increase of the yields of hydrocracked products.

To overcome the problem of the fast catalyst deactivation, many groups [52-60] used conventional bifunctional catalysts in their studies of decalin hydroconversion. Conventional catalysts from the literature that were used in the ring opening of decalin and the reaction conditions applied together with the obtained maximal yields of ROPs are summarized in Table 4.3.

Such catalysts generally show a much lower tendency of deactivation and the build-up of carbonaceous deposits. The direct comparison between a monofunctional H-Y and a bifunctional Pt/H-Y catalyst was made by Santikunaporn *et al.* [52]. They demonstrated that the incorporation of platinum does not only bring about a significant reduction of the rate of catalyst deactivation, but also a diminution of the concentration of Brønsted acid sites. This was interpreted by an “anchoring on proton sites” of the noble metal.

The hydroconversion of decalin on platinum-loaded zeolite catalysts was also investigated by Kubička *et al.* [53]. A batch-type reactor was used by these authors. They found that H-zeolites loaded with 2 wt.-% of platinum gave higher conversions of decalin and a lower deactivation compared to their monofunctional acidic counterparts. The initial activities followed the order 2.0Pt/H-Beta-12.5 > 2.0Pt/H-Y-6 > 2.0Pt/H-MOR-10. The carbon content of the used catalysts decreased in the order 2.0Pt/H-Y-6 ≈ 2.0Pt/H-Beta-12.5 > 2.0Pt/H-MOR-10. The reduction of the specific surface area measured after catalysis was 39 % for the Beta and Y catalysts and 57 % for 2.0Pt/H-MOR-10. This finding was interpreted in terms of different locations of the carbonaceous deposits with a favored position at the pore mouths for 2.0Pt/H-MOR-10. The hydrogen pressure was varied between 0.7 and 3.7 MPa, but it did not influence the initial activity of the Pt/H-Beta catalyst. Increasing the hydrogen pressure just led to a reduced formation of heavy dehydrogenation products.

Table 4.3: Maximum yields or initial selectivities of ROPs obtained from decalin on several conventional bifunctional catalysts.

Catalyst	**Conditions** T_r **/ °C,** p_{H_2} **/ MPa**	$Y_{ROPs,max.}$ **/ %**	**Ref.**
1.0Pt/H-Y	260 °C, 2.0 MPa	11.8	[52]
2.0Pt/H-MOR-10	270 °C, 2.0 MPa	8.8[1]	[53]
2.0Pt/H-Y-6	250 °C, 2.0 MPa	27.2[1]	[53]
2.0Pt/H-Beta-12.5	250 °C, 2.0 MPa	30.2[1]	[53]
1.0Ir/H-Y-6	250 °C, 2.0 MPa	23.8[1]	[54]
1.0Ir/H-Beta-12.5	250 °C, 2.0 MPa	22.1[1]	[54]
1.0Ir/H-Beta-12.5(ALD)	270 °C, 6.0 MPa	62.0[1]	[54]
2.0Pt/H-Y-6	250 °C, 2.0 MPa	15.6[1]	[54]
2.0Pt/H-Beta-12.5	250 °C, 2.0 MPa	28.6[1]	[54]
1.5Ir/0.75Pt/H-Zr-MCM-41	400 °C, 5.0 MPa	14.0[1]	[55]
1.5Ir,0.75Pt/H-Y-7	220 °C, 5.0 MPa	31.7[1]	[56]
2.0Ir/H-Beta-12.5	325 °C, 6.0 MPa	53.0[1]	[57]
2.0Ir/H-Beta-150	350 °C, 3.0 MPa	18.0[1]	[57]
2Pd/H-Y-15	350 °C, 3.0 MPa	28.0[1]	[57]
Pd/H-Y	300 °C, 3.0 MPa	92.0[1]	[58]
1.0Ir/H-Y-3.2	350 °C, 3.0 MPa	38.4[1]	[59]
1.0Ir,0.5Pt/H-Y-3.2	350 °C, 3.0 MPa	35.4[1]	[59]
1.0Ir,1.0Pt/H-Y-3.2	350 °C, 3.0 MPa	49.5[1]	[59]
1.5Pt,1.0Ir/H-Y-3.2	350 °C, 3.0 MPa	36.9[1]	[59]
1.0Pt/H-Y-3.2	350 °C, 3.0 MPa	41.6[1]	[59]
1.5Ir/H-Y-3.2	350 °C, 3.0 MPa	37.8[1]	[59]
1.5Ir,0.5Pt/H-Y-3.2	350 °C, 3.0 MPa	32.5[1]	[59]
1.5Ir,1.0Pt/H-Y-3.2	350 °C, 3.0 MPa	42.5[1]	[59]
1.5Ir,1.5Pt/H-Y-3.2	350 °C, 3.0 MPa	44.4[1]	[59]
1.5Pt/H-Y-3.2	350 °C, 3.0 MPa	43.9[1]	[59]
1.0Pt/H-Y-3.2	350 °C, 3.0 MPa	37.4[1]	[60]
1.0Pt,0.1Ir/ H-Y-3.2	350 °C, 3.0 MPa	35.3[1]	[60]
1.0Pt,0.3Ir/ H-Y-3.2	350 °C, 3.0 MPa	41.6[1]	[60]
1.0Pt,0.6Ir/ H-Y-3.2	350 °C, 3.0 MPa	48.3[1]	[60]
0.6Ir/ H-Y-3.2	350 °C, 3.0 MPa	43.6[1]	[60]
1.2Ir/[W]Al_2O_3	250-350 °C, 5.0 MPa	48.8	[61]

[1]in the liquid products

For the hydroconversion of decalin on 2.0Pt/H-Beta-12.5, Kubička *et al.* [53] established a plot of product concentration *vs.* the reaction time. The concentration of skeletal isomers of decalin went through a maximum at short reaction times, whereas the concentration of ring-opening products increased monotonously. For comparison, the authors undertook the same catalytic experiment using a non-acidic platinum catalyst. Now, no formation of skeletal isomers occurred, and no ring opening took place, only decalin dehydrogenation was observed. From these findings the authors concluded that skeletal isomerization of decalin is essential for and precedes ring opening.

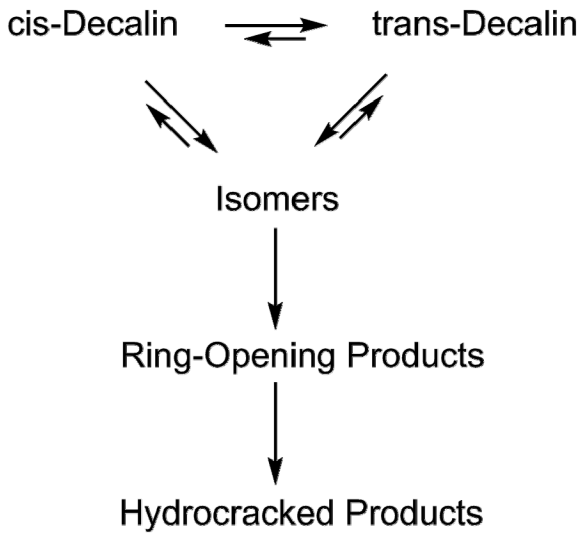

Figure 4.10: Reaction scheme of decalin hydroconversion after Kubička *et al.* [54].

In a later study [54], the same group compared catalysts containing iridium or platinum supported on the zeolites H-Y or H-Beta in the hydroconversion of decalin. The iridium catalysts were generally found to be more active. The pore system of the two large-pore zeolites had no influence on their catalytic activity, as long as the concentration of Brønsted acid sites was the same. The highest selectivities and yields of ring-opening products were found on catalyst 1.0/H-Beta-12.5 which contained the lowest concentration and strength of Brønsted acid sites. The authors arrived at the general conclusion that a mildly acidic support in combination with the noble metal iridium are beneficial for high selectivities to the desired ring-opening products. They proposed the reaction scheme depicted in Figure 4.10. By far the fastest reaction is stereoisomerization between cis- and trans-decalin. At more severe reaction conditions, skeletal isomerization of decalin occurs, *inter alia* to isomers with one or two five-membered rings. The latter are opened much more readily

than the six-membered rings in the reactant decalin. The ring-opening products can be hydrocracked further into hydrocarbons with less than ten carbon atoms.

Mouli *et al.* [55] prepared bimetallic catalysts consisting of iridium and platinum supported on Zr-MCM-41. The content of the two metals was varied between 0 and 1.5 wt.-%. All catalysts showed a relatively low activity in the hydroconversion of decalin, the yield of ring-opening products (ROPs) was 14 % at best. The yield of ROPs increased with an increasing iridium content. It was qualitatively reported that open-chain decanes (OCDs) occurred in the product, and one particular isomer, *viz.* 3,5-dimethyloctane, was claimed to be formed, but no effort was undertaken to rationalize such a peculiar selectivity. In a later study, Mouli *et al.* [56] studied the hydroconversion of decalin on bimetallic catalysts such as 1.5Pt,0.75Ir/H-Y-7 and 1.5Pt,0.75Ir/H-Beta-14. Again, open-chain decanes, such as n-decane, were claimed to be formed and, for the first time, quantitative yield data for OCDs were given. The maximum yield of OCDs was reported to be 4 %.

The formation of ROPs in the hydroconversion of decalin was also investigated in a very recent paper by Alzaid and Smith [57]. They used 2.0Ir/H-Beta-12.5, 2.0Ir/H-Beta-150, and 2.0Pd/H-Y-15 as catalysts. At an identical decalin conversion of 60 %, the yield of ROPs was said to decrease from 33 to 25 % in the order 2.0Ir/H-Beta-12.5 > 2.0Ir/H-Beta-150 > 2.0Pd/H-Y-15. In another study by the same group [58] a commercial Pd/H-Y catalyst was used and claimed to be extraordinarily active in the ring-opening reaction: At decalin conversions of > 90 %, selectivities of ROPs of nearly 100 % were claimed to be reached. However, catalyst deactivation had occurred after 10 h time-on-stream.

In two very recent studies by D'Ippolito *et al.* [59,60], a series of mono- and bimetallic iridium and platinum catalysts with zeolite H-Y-3.2 as carrier was tested in the hydroconversion of decalin. It was found as a main result that the hydrogenolytic activity of the catalysts was enhanced by increasing their iridium content. Deactivation was absent for catalysts with an iridium content of 1.5 wt.-%.

Very recently, Moraes *et al.* [61] reported on the hydroconversion of decalin on bifunctional catalysts prepared in a special manner: Alumina was impregnated with aqueous solutions of ammonium metatungstate. Upon calcination, this

gave carriers with Brønsted acid sites in a controllable concentration. In a second impregnation step, these were loaded with an aqueous solution of hydrogen hexachloroiridate (IV) hexahydrate, such as to arrive at bifunctional catalysts with 1.2 wt.-% of iridium after calcination and reduction. It was found that catalysts with a low tungsten loading and, hence, with a low concentration of Brønsted acid sites gave ring-opening selectivities of 100 % at nearly zero decalin conversion indicating that ring-opening products (ROPs) seemed to be primary products. Upon increasing the concentration of Brønsted acid sites, the initial selectivities of ROPs decreased, while the selectivities of skeletal isomers increased. Furthermore, an increased concentration of strong Brønsted acid sites led to a lower selectivity of hydrocracked products. It was also shown in this paper that the main ring-opening products are different on Ir/Al_2O_3 without Brønsted acid sites and catalysts made acidic by impregnation with the tungsten compound. It was suggested that skeletal isomerization occurred through a classical bifunctional mechanism *via* carbocations, though hydrogenolytic ring opening on iridium could not be ruled out. Finally, open-chain decanes were reported to be formed in small amounts ($S_{OCDs,max.}$ = 6 %, $Y_{OCDs,max.}$ = 2.4 %) on some of the bifunctional catalysts.

4.2.2.2 Metal-Catalyzed Bicyclic Naphthene Hydroconversion

Many groups studied the ring opening of small monocyclic molecules, such as methylcyclopentane or methylcyclohexane, on metal catalysts without Brønsted acid sites [62-66]. The use of such model hydrocarbons restricts the number of possible ring-opening products to less than ten, which makes the product analysis relatively easy. However, the usage of such small hydrocarbons can also limit the possible reaction pathways and hence provide limited information on ring opening of larger bicyclic naphthenic hydrocarbons. Hence, this section will focus on results which have a bearing on ring opening of decalin.

The hydroconversion of pentylcyclopentane, among other naphthenic hydrocarbons, on non-acidic iridium or platinum catalysts was investigated by McVicker *et al.* [67]. They found that the product distributions from pentyl-cyclopentane were highly dependent on the nature of the metal. The products which can be obtained by endocyclic carbon-carbon bond scission of pentylcyclopentane are depicted in Figure 4.11. Bond a connects a secondary

and a tertiary carbon atom, whereas bonds b and c connect two secondary carbon atoms.

It is evident from Figure 4.11 that, if all endocyclic bonds were cleaved with the same rate, one would expect a product distribution of 40 % n-decane, 40 % 4-methylnonane, and 20 % 3-ethyloctane. Using $0.9Pt/Al_2O_3$ with a high platinum dispersion as a catalyst, McVicker *et al.* found a distribution of 55 % n-decane, 31 % 4-methylnonane, and 15 % 3-ethyloctane [67]. This is not identical with the purely statistical distribution (see above), but the deviations are small. According to Gault [32], the occurrence of a statistical distribution can be rationalized in terms of the so-called multiplet mechanism with a flat adsorption of the naphthenic ring on the metal.

Using $0.9Ir/Al_2O_3$ as catalyst the distribution of ring-opening products was 3 % n-decane, 64 % 4-methylnonane, and 33 % 3-ethyloctane [67]. Obviously, iridium strongly prefers the hydrogenolysis of the bisecondary bonds b and c between two secondary carbon atoms. Following again Gault's earlier work [32] such a selectivity of ring opening is indicative of the so-called dicarbene mechanism and an adsorption of the naphthenic ring *via* two adjacent secondary carbon atoms in a direction perpendicular to the metal surface.

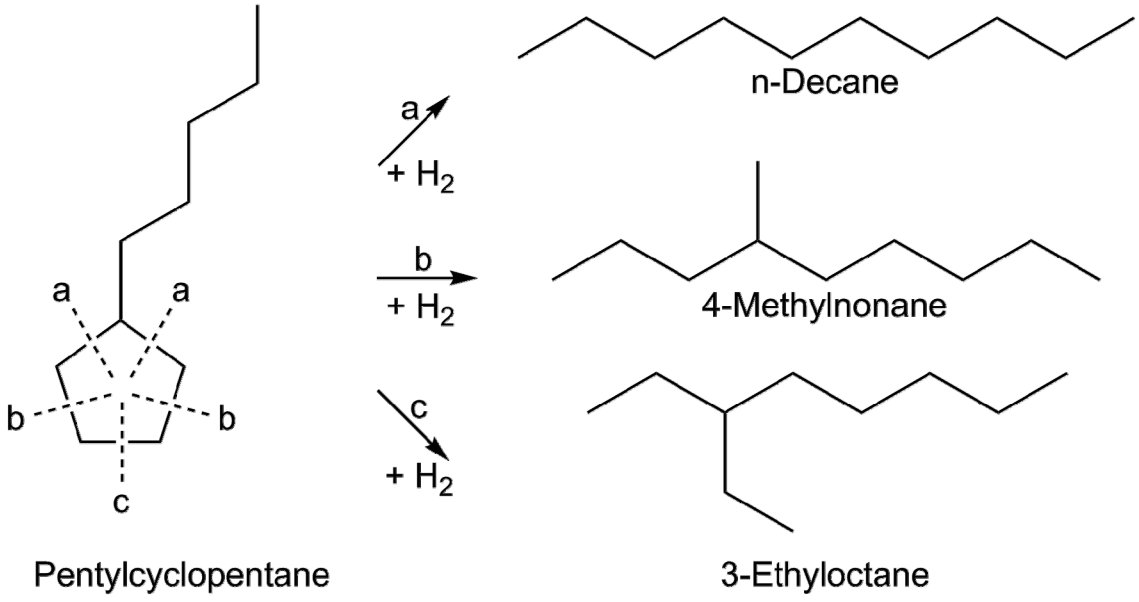

Figure 4.11: Predicted products of hydrogenolysis of endocyclic carbon-carbon bonds in pentylcyclopentane.

McVicker *et al.* furthermore investigated the hydrogenolytic ring opening of substituted cyclohexanes [67]. Their reactivity was generally found to be significantly lower than the one of alkylcyclopentanes, especially on platinum

catalysts. Higher reaction temperatures are therefore needed for reaching the same ring-opening conversions as with substituted cyclopentanes.

Figure 4.12 shows that the expected products of hydrogenolytic ring opening of methylcyclohexane are n-heptane, 2-methylhexane, and 3-methylhexane. For the case of a purely statistical ring opening, these products would be predicted to be formed in equal amounts. The experimental product distributions obtained from methylcyclohexane on 0.6Pt/SiO_2 was 65 % n-heptane, 35 % 2-methylhexane, and traces of 3-methylhexane [67] indicating a preferred hydrogenolysis of the bond involving the alkyl-substituted carbon atom. A completely different ring-opening selectivity was observed in the hydrogenolysis of methylcyclohexane on 0.9Ir/Al_2O_3, *viz.* 5 % n-heptane, 37 % 2-methylhexane, and 58 % 3-methylhexane [67]. The dicarbene mechanism is hence prevailing on iridium, in much the same manner as with alkylcyclopentanes as reactants. However, the reactivity of alkylcyclohexanes is much lower than that of alkylcyclopentanes.

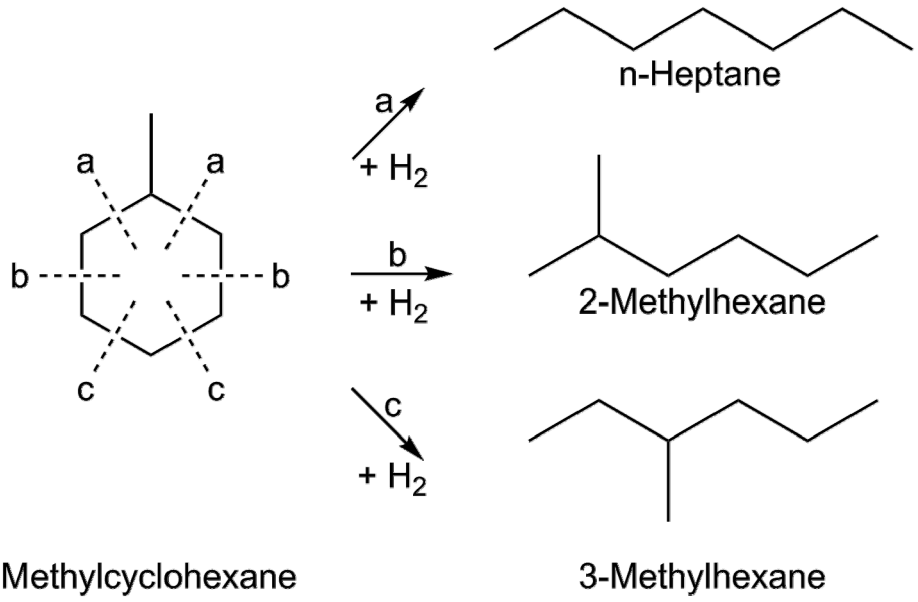

Figure 4.12: Predicted products of hydrogenolysis of endocyclic carbon-carbon bonds in methylcyclohexane.

The much higher rate of hydrogenolysis of five-membered compared to six-membered naphthenic rings has also been nicely demonstrated using perhydroindan as model hydrocarbon [67,68]. For example, Bellussi *et al.* [68] studied the hydroconversion of perhydroindan on 0.77Ir/SiO_2 and 0.93Pt/SiO_2. The iridium catalyst was found to be much more active than the platinum one in the ring opening of perhydroindan. Moreover, almost exclusively the five-membered ring of perhydroindan was opened on 0.77Ir/SiO_2. More than 96 %

of the direct ring opening products were 1-ethyl-2-methylcyclohexane (see Figure 4.13), which can be explained by a carbon-carbon bond cleavage according to the dicarbene mechanism. In contrast, on 0.93Pt/SiO_2 *ca*. 10 % of the perhydroindan was opened to ring-opening products by cleavage of the six-membered ring. However, higher yields of open-chain nonanes were obtained on the iridium catalyst.

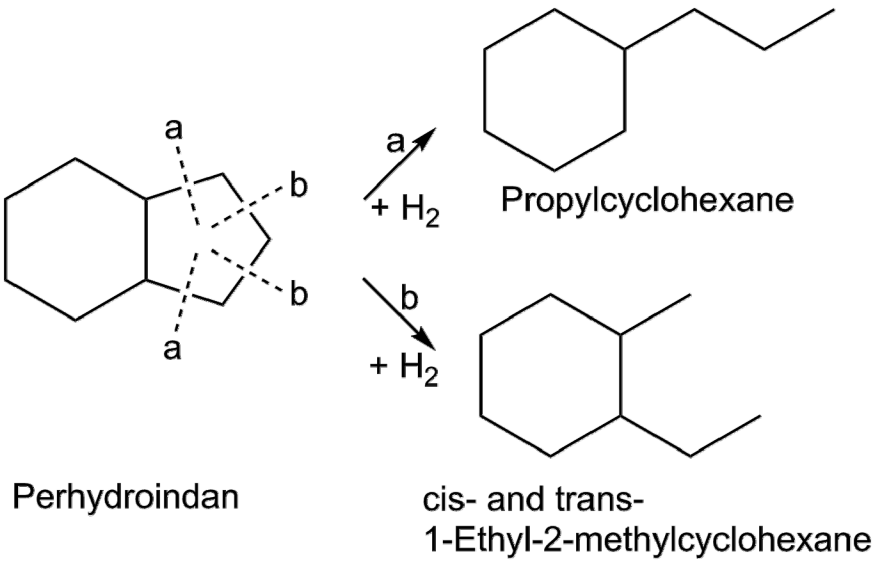

Figure 4.13: Predicted products of hydrogenolysis of endocyclic carbon-carbon bonds in perhydroindan.

Very recently, two groups published detailed reports on the hydrogenolytic ring opening of decalin on Ir/Al_2O_3 [69] and Ir/SiO_2 [70] catalysts lacking Brønsted acid sites. On such catalysts, no skeletal isomerization of decalin can take place, because neither the noble metal nor the carrier possess an activity for isomerization. In particular, there is no ring contraction into perhydroindan-like structures. Completely in-line with the known recalcitrance of six-membered rings to undergo hydrogenolytic cleavage, the hydroconversion of decalin requires much more severe conditions, *e.g.*, by 50 to 100 °C higher temperatures around 300 °C, than that of, *e.g.*, perhydroindan.

At these high temperatures, direct hydrogenolytic opening of one six-membered ring occurs leading to the primary products butylcyclohexane, cis- and trans-1-methyl-2-propylcyclohexane, and cis- and trans-1,2-diethylcyclohexane (Figure 4.14). At low decalin conversions the selectivities of butylcyclohexane, trans-1-methyl-2-propylcyclohexane (cis- and trans-), and 1,2-diethylcyclohexane (cis- and trans-) were 10 %, 60 %, and 30 %, respectively, which shows again the pronounced preference of iridium to

cleave bonds between bisecondary carbon atoms according to the dicarbene mechanism.

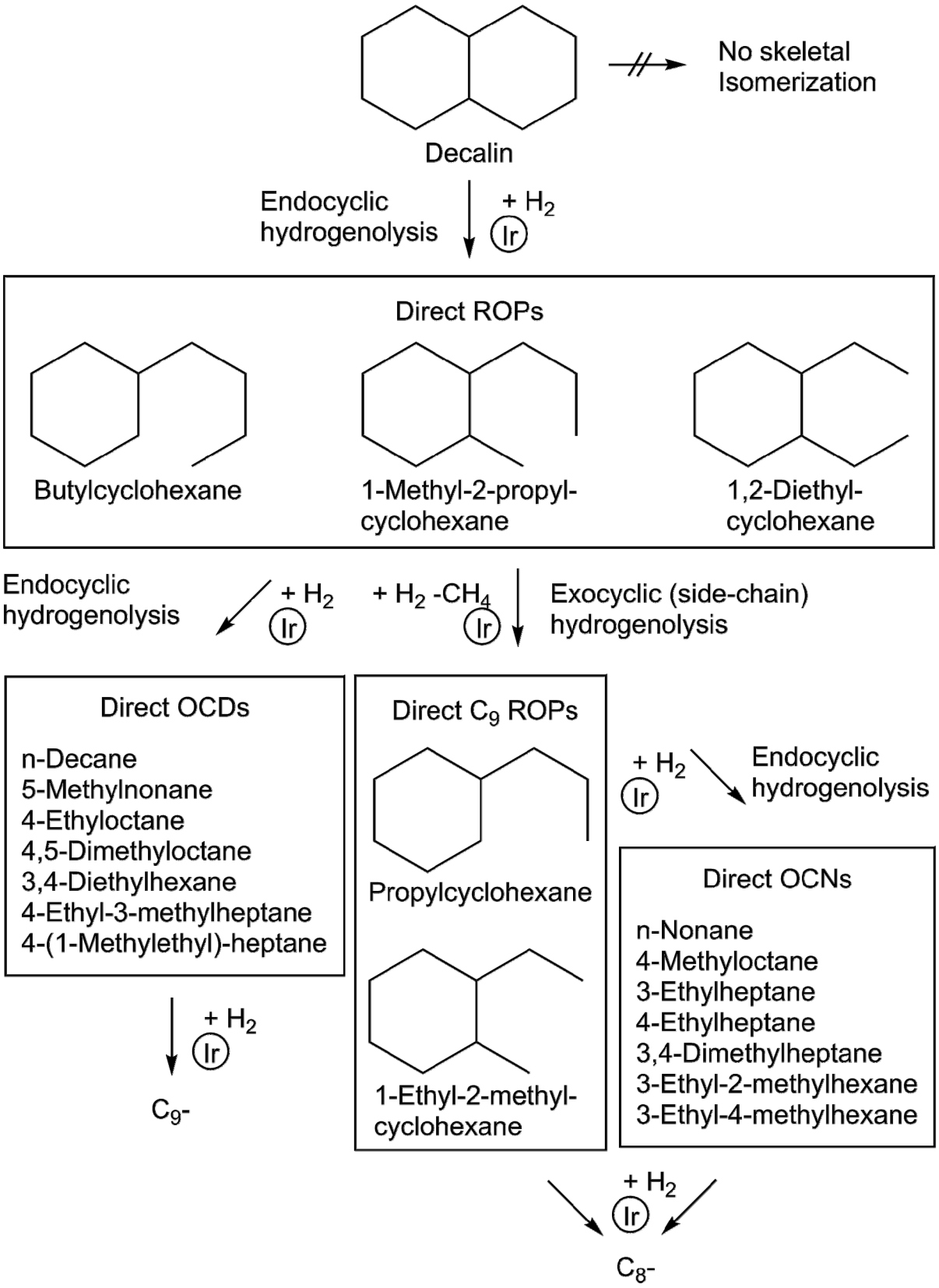

Figure 4.14: Direct hydrogenolytic ring-opening of decalin and consecutive hydrogenolysis reactions over iridium on non-acidic silica. After Ref. [70].

As also shown in Figure 4.14, the primary ring-opening products (ROPs) underwent consecutive reactions, namely an endocyclic hydrogenolysis to the direct open-chain decanes (OCDs) and an exocyclic hydrogenolysis to methane and the direct C_9 ring opening products propylcyclohexane or 1-ethyl-2-methylcyclohexane. Finally, these two latter C_9 naphthenes showed again endocyclic hydrogenolysis to give seven nonane isomers referred to as direct open-chain nonanes (OCNs). It is particularly noteworthy that the seven direct OCD isomers and the seven direct OCN isomers listed in Figure 4.14 in the respective boxes were formed out of many more theoretically possible decane and nonane isomers.

With iridium on non-acidic alumina as catalyst in the hydroconversion of decalin Moraes *et al.* [69] arrived at essentially the same results. In particular, it was found that no skeletal isomerization occurs and that the direct ROPs shown in Figure 4.14 are primary products.

The large selectivity differences in the hydrogenolysis of decalin on the metals iridium and platinum are also reflected by the molar carbon number distributions of the hydrocracked products with less than ten carbon atoms (Figure 4.15). On iridium, by far the predominant products are methane and C_9 hydrocarbons with a strongly declining selectivity for (C_2 + C_8), (C_3 + C_7), (C_4 + C_6), and (C_5 + C_5). In fact, the distribution curve observed on Ir/silica strongly reminds one the shape of a hammock, and this is why the term “hammock-type distribution curves” was coined for such curves [71]. Note that the curve for Ir/silica is nearly symmetrical around C_5 which indicates an almost pure primary hydrocracking, *i.e.*, a C_{10} specie is hydrocracked, and the moieties are desorbed from the active sites before they can undergo a second carbon-carbon bond cleavage step.

It has been reported in Ref. [70] that open-chain decanes are formed on Ir/silica (*cf*. Figure 4.14), but the maximum yields of these highly desired products are around 20 %, at best.

The distribution curve of the hydrocracked products observed on Pt/silica differs substantially from the one on Ir/silica (Figure 4.15). Light hydrocarbons in the range C_1 to C_3 strongly dominate, even though the yield of hydrocracked products is modest. This indicated a substantial occurrence of secondary hydrocracking which may, in part, be due to the much higher reaction temperature needed for achieving the desired severity on platinum.

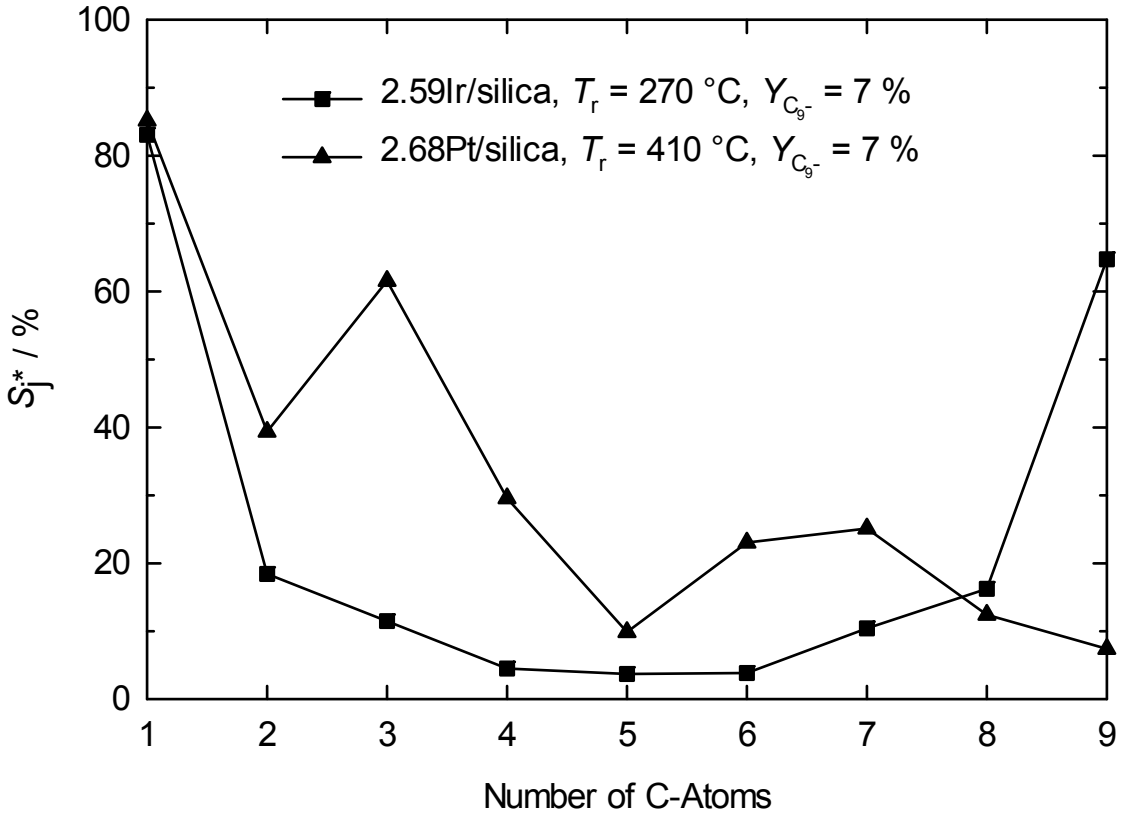

Figure 4.15: Modified hydrocracking selectivities S_j* in the hydroconversion of decalin on iridium and platinum on a non-acidic support at equal yields of hydrocracked products. After Ref. [70].

Another fundamental difference between the hydroconversion of decalin on Ir/silica and Pt/silica pertains to the finding [70] that the latter metal possesses some activity for skeletal isomerization of decalin. This was inferred from the finding that, at low conversions, spiro[4.5]decane is formed from decalin on Pt/silica in appreciable selectivities. Skeletal isomerization of decalin on Pt/silica was envisaged to occur *via* the so-called bond-shift mechanism which is well established in the literature for skeletal isomerization of light alkanes on platinum [72,73]. At last, it should be mentioned that Pt/silica turned out to be a very poor catalyst for making open-chain decanes from decalin. The maximum yields of OCDs on Pt/silica amounted to 2 % [70].

4.2.2.3 High-Performance Ring-Opening Catalysts (HIPEROCs)

Approximately since the year 2000, a substantial body of literature appeared dealing with the catalytic hydrodecyclization of multi-ring naphthenes, typically decalin [49-61,69,70]. It is usually stated in these papers that the rationale of

such studies consists of developing advanced catalysts which enable one to improve the quality of diesel fuels, *inter alia* their cetane numbers. Deeper analyses of the issue revealed that a substantial gain in the cetane number can only be attained, if the model hydrocarbon decalin is hydroconverted into alkanes with the same carbon numbers, *i.e.* decane isomers, with as high as possible yields [56,69,74].

Given this importance of alkanes as products of a possible ring-opening process, it is particularly remarkable that the vast majority of papers on ring opening of decalin fail to give any information concerning the yields or selectivities of open-chain decanes. Among the very few exceptions are Refs. [56,69]. In these papers the maximal yields of open-chain decanes (OCDs) in the hydroconversion of decalin were reported to be 4 % for a 1.5Pt,0.75Ir/H-Y-7 catalyst [56] and 8 % for 1.8Ir/Al_2O_3 [69].

An inspection of the reasons for this lack of information on the yields of OCDs in the catalytic hydroconversion of decalin revealed that analytical difficulties were at the origin of the problem: The hydroconversion of decalin leads to a large number (typically 100 to 200) of product hydrocarbons, and inadequate gas chromatographic methods were used in the majority of prior investigations.

It turned out, in particular, that these oversimplified methods for product analysis were not capable to reliably distinguish between C_{10} hydrocarbons still containing one naphthenic ring (called “ring-opening products” or “ROPs” in this thesis) and open-chain decanes (OCDs). In most publications on the hydroconversion of decalin, ROPs and OCDs are therefore lumped, and these combined groups of C_{10} hydrocarbons are referred to as “ring-opening products”.

Our group spent much effort to enhance the analytical situation, especially with respect to the C_{10} hydrocarbons. Both the separation of these hydrocarbons in the gas chromatographic column and the assignment of the peaks were significantly improved, mostly by

- use of a Supelco Petrocol DH 150 capillary column [78]
- co-injection of pure hydrocarbons [78]
- co-injection of a mixture of decane isomers [78]
- ancillary GC/MS analyses of the liquid product samples [78]

At the end of this methodological work, a reasonably safe separation between ring-opening products and open-chain decanes could be achieved. Applying these improved analytical techniques to the products of decalin hydroconversion led to the following rough estimation for the maximum attainable yields of open-chain decanes:

- monofunctional acidic catalysts: $Y_{OCDs,max.} \approx 10$ %
- monofunctional metallic catalysts: $Y_{OCDs,max.} \approx 20$ %
- conventional bifunctional catalysts: $Y_{OCDs,max.} \approx 10$ %

The term “conventional bifunctional catalysts” refers to materials with a relatively low content (up to *ca*. 1 wt.-%) of a noble metal like platinum or palladium and a relatively high concentration and strength of Brønsted acid sites. Such catalysts are typically used in industrial hydrocrackers for the conversion of heavy gas oils [75,76] or in the isomerization of light gasoline [77].

A systematic search for principally improved ring-opening catalysts was successful [78-84]. In view of the limitations experienced with the three conventional classes of catalysts (*vide supra*), the target criterion for the new catalysts was set at

$$Y_{OCDs,max.} \geq 25\ \%$$

in the hydroconversion of the model hydrocarbon decalin. For catalysts that fulfill this criterion, the label “*HI*gh-*PE*rformance *R*ing-*O*pening *C*atalysts” (HIPEROCs) was introduced [79]. In Figure 4.16 the performance of three typical HIPEROCs in the hydroconversion of decalin is shown. It is clearly seen that, with these catalysts, the maximum selectivities of OCDs are passing through maxima of about 40 %, and since this happens at decalin conversions of nearly 100 %, the maximum yields of OCDs are not much smaller, *viz.* 31 %, 39 %, and 44 % for the zeolites 2.9Ir/$Na_{0.90}$,$H_{0.10}$-Y, 3.0Pt/$Na_{0.88}$,$H_{0.12}$-Y, and 3.4Ir/$H_{0.58}$,$Cs_{0.42}$-Beta, respectively.

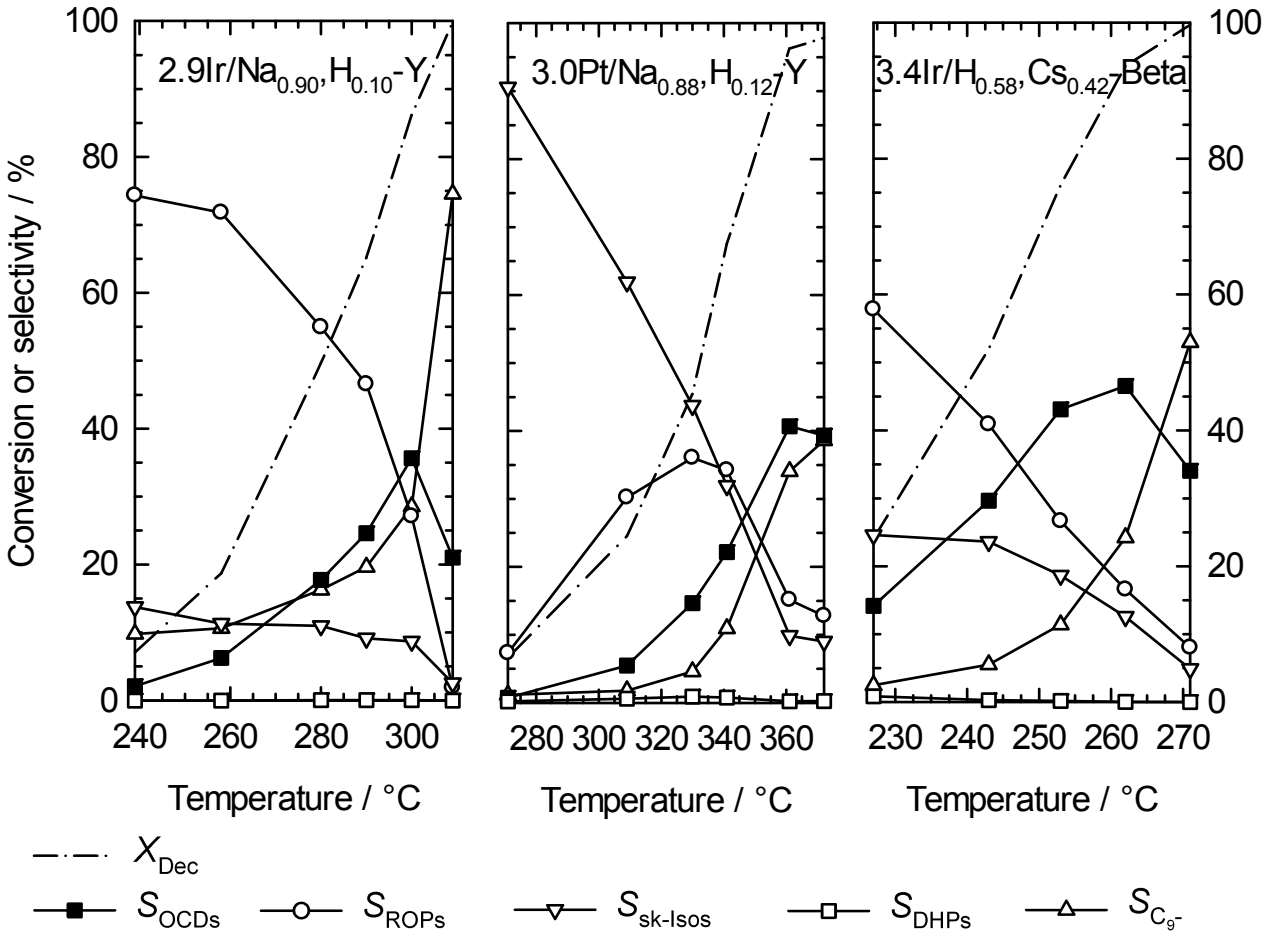

Figure 4.16: Conversion of decalin and selectivities of the different products obtained on HIPEROCs. After Refs. [79,81].

The currently known HIPEROCs have in common that they consist of a large-pore (12-membered ring) zeolite onto which relatively large amounts (often around 3 wt.-%) of a hydrogenolytically active noble metal, such as iridium or platinum, were loaded, *e.g.* by ion exchange with a cationic complex of the metal followed by its thermal decomposition and reduction by hydrogen. Furthermore, HIPEROCs contain Brønsted acid sites in a relatively low concentration (often just those co-produced by reduction of the noble metal with hydrogen). Usually, the catalytic performance of HIPEROCs can be further improved by carefully tuning their hydrogenolytic activity and the strength of their Brønsted acid sites, for example by varying the nature of the residual alkali cations in the zeolite [79,81]. HIPEROCs are bifunctional, but in view of all features described above, they represent a family of novel catalysts which principally differ from conventional bifunctional hydrocracking and isomerization catalysts: On the latter, skeletal isomerization and carbon-carbon bond cleavage occur on the acid sites, and the selectivities are governed by carbocation chemistry. On HIPEROCs, by contrast, carbon-carbon bond rupture occurs by hydrogenolysis on the noble metal, and this

appears to be much more favorable for making OCDs from decalin than hydrocracking over conventional bifunctional catalysts.

It was shown that the product distribution of the hydrocracked products can give a valuable information about the mechanism of hydrocracking. Modified hydrocracking selectivities of the C_9- products observed in the hydroconversion of decalin on the three HIPEROCs are depicted in Figure 4.17.

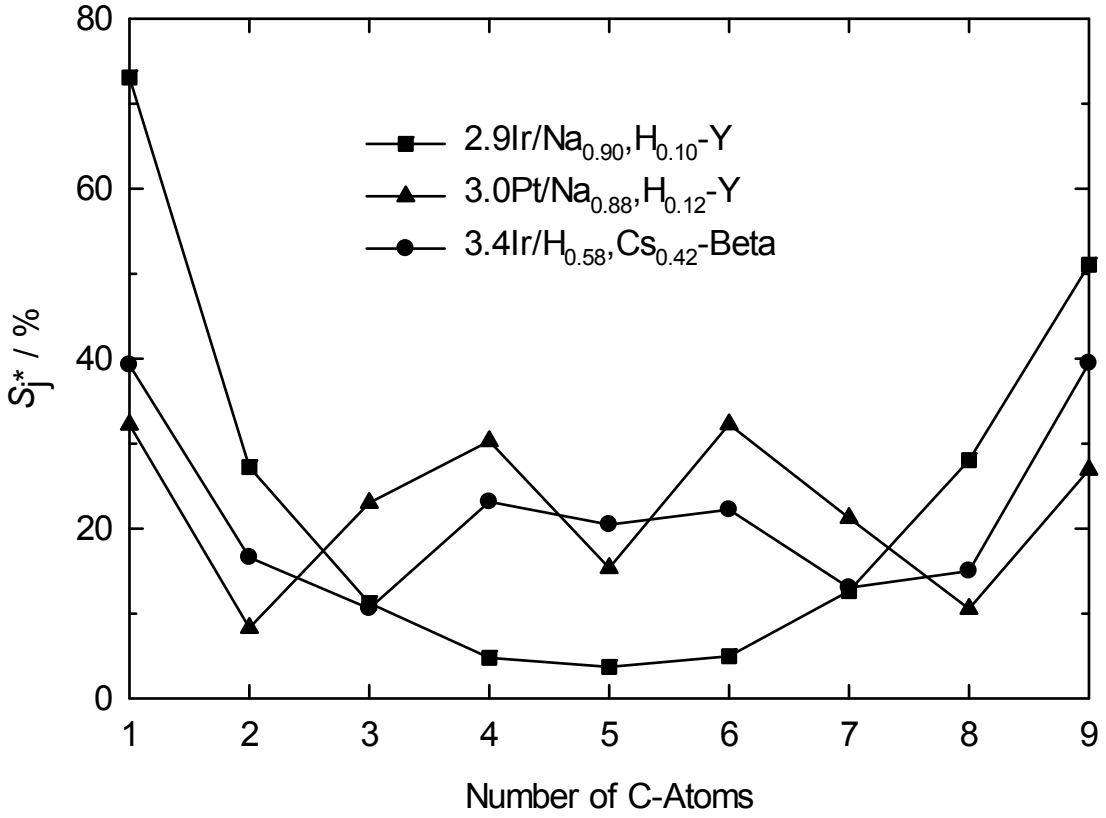

Figure 4.17: Modified hydrocracking selectivities of the hydrocracked products obtained on three HIPEROCs. After Refs. [79,81].

The interpretation of the selectivities of hydrocracked products obtained on 3.0Pt/$Na_{0.88}$,$H_{0.12}$-Y was difficult. The formation of methane is a strong hint for hydrogenolysis on this catalyst. However, it was mentioned that due to the high reaction temperatures, bifunctional hydrocracking could be superimposed by hydrogenolysis on the platinum catalyst. In addition, the ability of isomerization of hydrocarbons on platinum, together with its preference for a cleavage of substituted carbon-carbon bonds, can lead to this pattern of hydrocracked products [81]. In contrast, the curve obtained from the decalin hydroconversion on 2.9Ir/$Na_{0.90}$,$H_{0.10}$-Y revealed a clear hammock shape (as

found for 2.59Ir/silica), indicating unambiguously that the ring opening occurs *via* hydrogenolysis on the metal sites. For 3.4Ir/$H_{0.58}$,$Cs_{0.42}$-Beta, nearly a plateau at the carbon numbers C_4 to C_6 appears. It was speculated that the origin of this plateau arises from hydrocracking of OCDs, either *via* hydrogenolysis or conventional bifunctional hydrocracking. Hence, the S_j* curve could be regarded as a combination of a hammock-type and a bell-shape curve [79].

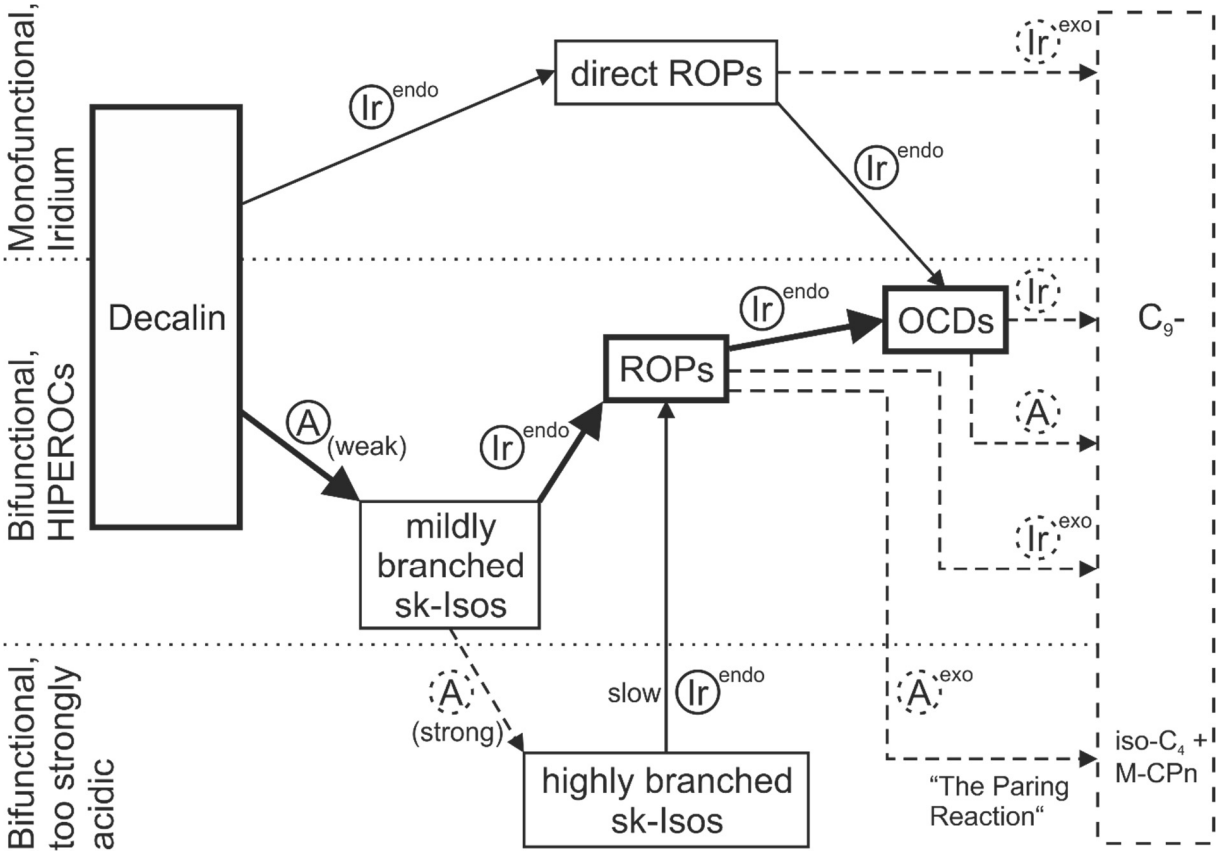

Figure 4.18: Proposed reaction scheme for the hydroconversion of decalin on iridium-containing HIPEROCs. A: Brønsted acid sites. Endo and exo denote hydrocracking of endocyclic and exocyclic carbon-carbon bonds, respectively. The bold arrows show the desired reaction path. After Ref. [79].

The current mechanistic view on the hydroconversion of decalin on iridium-containing HIPEROCs is sketched in the middle section of Figure 4.18. Decalin first undergoes a mild skeletal isomerization on the acid sites, whereby one six-membered ring is contracted to a five-membered ring. Such acid-catalyzed isomerizations, in which the number of branchings does not change, are known to be fast even on weakly acidic sites. Once isomers of decalin with a five-membered naphthenic ring are formed, these are readily opened by endocyclic hydrogenolysis on the noble metal. The resulting ring-opening

products (ROPs) can undergo a number of competing reactions. The desired one is endocyclic hydrogenolytic cleavage of the remaining ring which directly leads to open-chain decanes. At this stage of the reaction network, it becomes evident that a very active (high concentration and/or strength of the Brønsted acid sites) acid catalyst component is deleterious, because it will bring about the direct hydrocracking of ROPs into undesired C_9- hydrocarbons.

Also undesired is the exocyclic hydrogenolysis of ROPs in the alkyl side chain(s). At high severities, the formed OCDs show consecutive hydrocracking reactions, either *via* carbocations on acidic sites or on the metal by hydrogenolysis which are both equally undesired.

The scheme also shows the likely reaction paths on iridium catalysts lacking Brønsted acid sites and, conversely, on catalysts with a too active acid component. On the latter catalysts, multiple skeletal isomerization of decalin occurs, and the highly branched isomers formed were shown to undergo hydrogenolytic ring opening only reluctantly [79]. Also, a strongly acidic catalyst component favors the paring reaction of ROPs to iso-butane and methylcyclopentane which has often been overlooked in prior work.

4.3 Competitive Catalytic Conversion of Hydrocarbons

In many catalytic refinery processes, the feedstock is an oil fraction consisting of numerous individual hydrocarbons rather than a pure compound. For studying the catalytic chemistry of such processes, it is customary to simulate the oil by a suitably selected model hydrocarbon. The main advantage of doing so is a much easier follow-up of the chemical reaction paths from the single-compound model feed to the experimentally determined products. However, this approach may have disadvantages as well. For example, a frequently encountered effect in the conversion of feed mixtures on solid catalysts is a preferential adsorption of one reactant (or class of reactants) over another. If this effect is operative, the relative rates of reaction measured with pure reactants may not be representative for those of the same reactants offered to the catalyst in admixture. In the limiting case the more strongly adsorbed reactant may completely prevent the less strongly adsorbed one from reaching the catalyst surface and hence from being catalytically converted.

In the literature, the effect of competitive adsorption on the catalytic conversion of hydrocarbons has mostly been described for mixtures of n-alkanes of different chain lengths. For example, n-dodecane and n-decane were isomerized and hydrocracked in the gas phase on a Pd/La-Y zeolite catalyst at temperatures around 250 °C [85]. When converted separately, n-dodecane with its somewhat larger number of CH_2 groups was found to be more reactive than n-decane. When both n-alkanes were converted together as an equimolar mixture, the same qualitative order of reactivities was observed, but now the difference in the reactivities was much more pronounced. This was interpreted in terms of a competitive adsorption of n-dodecane on the zeolite catalyst. Essentially the same effect was later found by Denayer *et al.* [86] for the hydroconversion of an equimolar n-nonane/n-heptane mixture on a Pt/H-Y catalyst at *ca.* 250 °C in the gas phase. The preferred adsorption of n-alkanes with longer chains has also been demonstrated in the liquid phase at room temperature without any catalytic reaction [87].

Equimolar mixtures of toluene/n-pentane, toluene/n-heptane, and toluene/n-tetradecane were adsorbed on silica at room temperature, and the adsorbate phase was directly analyzed using IR/visible sum frequency generation vibrational spectroscopy. The surface coverage of the alkane increased markedly from ca. 40 % to 80 % from n-pentane to n-tetradecane [88].

In the present work, the competitive hydroconversion of an equimolar mixture of decalin/n-decane on several attractive ring opening catalysts was studied in an attempt to qualitatively investigate the possible role of competitive adsorption effects in the manufacture of alkanes from multi-ring naphthenes.

4.4 Molybdenum Carbides as Catalysts for the Selective Ring Opening of Naphthenes

As shown in Section 4.2, selective ring opening, especially on high-performance ring-opening catalysts, encompasses as essential steps the contraction of six-membered into five-membered rings *via* carbocations and cleavage of endocyclic bonds in the five-membered ring naphthenes *via* hydrogenolysis. Due to their well known hydrogenolysis activities, noble metals such as Pt, Ir, Rh, Ru or Pd, or alloys of these, are typically used in ring-opening catalysts. It must be borne in mind, however, that these noble metals are expensive and tend to be very sensitive to catalyst poisons, such as sulfur and nitrogen compounds which occur in all petroleum fractions. Certain

transition metal sulfides, *e.g.*, those of molybdenum, tungsten, or nickel, have a significantly higher resistance towards sulfur and nitrogen compounds and are hence used industrially for the hydrodesulfurization and hydrodenitrogenation of petroleum fractions. Their hydrogenolysis activity is, however, low, and they are hence less suitable for ring opening.

As another option, the use of carbides or nitrides of the above-mentioned transition metals, in particular of molybdenum carbide, as hydrogenolysis catalysts has been envisaged [89,90]. In some reactions, for example the isomerization of alkanes [91] or the hydrogenation of carbon monoxide (Fischer-Tropsch reaction) [92], their catalytic behavior has been found to resemble that of noble metals. In particular, it has been envisaged to use molybdenum carbide as a much cheaper, relatively sulfur- and nitrogen-tolerant substitute for noble-metal catalysts. As a second objective of this work, molybdenum carbide was tested with decalin as model hydrocarbon as a catalyst for hydrodecyclization of multi-ring naphthenes.

4.4.1 Phases of Molybdenum Carbide

Molybdenum carbide was discovered by Moissan in 1893 [93]. In succession, the molybdenum-carbon system was investigated for a long time by several groups, leading to a considerable amount of literature dealing with this system. However, there seem to persist discrepancies concerning the number, crystal structures and most appropriate nomenclature of molybdenum-carbide phases. Most authors are discerning between four and six molybdenum-carbon phases [94 - 106] of which four are generally accepted, *viz.* β-Mo_2C, α-Mo_2C, η-$MoC_{1-x.}$ and α-MoC_{1-x}. In addition, the two phases denoted as γ- and γ'-MoC_{1-x} are considered as metastable high-temperature phases. Unfortunately, the nomenclature is not uniform in the literature, and the designations MoC or Mo_3C_2 are being used synonymously for the MoC_{1-x} phases. Table 4.4 gives an overview of the six molybdenum-carbon phases that are usually discerned in the literature.

Table 4.4: Phases of molybdenum carbide [99].

Phase	**Crystal system**	**Space group**	**Type**	**Molybdenum packing sequence**	**Carbon coordination**
β-Mo_2C	hcp	$P6_3/mmc$	ε-Fe_2N	AB,AB	octahedr.
α-Mo_2C	o'rhombic	Pbcn	ζ-Fe_2N	AB,AB	octahedr.
α-MoC_{1-x}	fcc	$Fm\bar{3}m$	NaCl	ABC,ABC	octahedr.
γ-MoC_{1-x}	hexagonal	$P\bar{6}m2$	WC	A,A	trig. prism.
γ'-MoC_{1-x}	hexagonal	$P6_3/mmc$	TiAs	AABB,AABB	octahedr. and trig. prism.
η-MoC_{1-x}	hcp	$P6_3/mmc$	Mo_3C_2	ABCACB, ABCACB	octahedr.

Dependent on the preparation conditions, molybdenum carbides with different crystal structures can be formed [107]. These structures of molybdenum carbides are characterized by a different packing sequence of the repeating molybdenum layers as shown in Table 4.4. Because of its small atomic radius, carbon can nest in the octahedral or trigonal-prismatic interstices of the lattice. These interstitial carbides show strong resistance against oxidation [102]. Since β-Mo_2C is mostly used in catalysis, its crystallographic structure is represented in Figure 4.19.

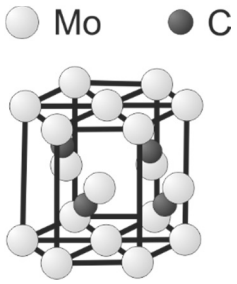

Figure 4.19: Crystallographic structure of hexagonal close-packed β-Mo_2C. [104,105].

The molybdenum-carbon phase diagram in Figure 4.20 gives information about the formation temperature of the different phases and of their stoichiometric composition. However, some phases of molybdenum carbides, *e.g.* α-MoC_{1-x}, are accessible at lower temperatures than expected from the carbon-molybdenum phase diagram, *via* topotactic solid-state transformations

[100,108]. These reactions allow the formation of metastable molybdenum carbides at less severe temperature conditions.

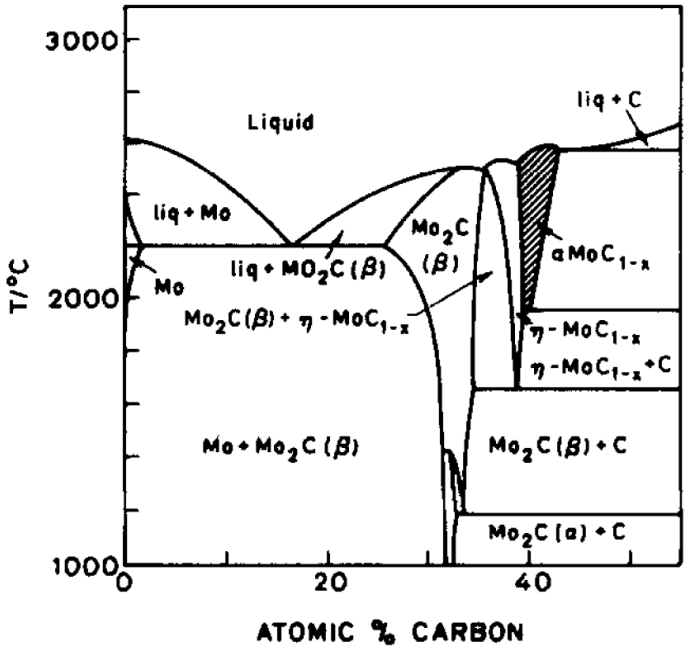

Figure 4.20: Molybdenum-carbon phase diagram [100].

4.4.2 Preparation and Characterization of Molybdenum Carbide Catalysts

4.4.2.1 Bulk Molybdenum Carbide Catalysts

The first reports about the preparation of molybdenum carbides with high specific surface areas were published by Volpe and Boudart [100]. They prepared these materials at atmospheric pressure by purging pure methane through packed beds of Mo_2N. The samples were heated up within 10 h from 400 to 700 °C. They received α-MoC_{1-x} with a specific surface area of 150 $m^2 \cdot g^{-1}$. To determine the nature of the molybdenum carbides they treated them in *aqua regia*. According to Samsonov and Vinitskii [109], molybdenum carbide should completely dissolve in *aqua regia*. However, free carbon was found by Volpe and Boudart [100] as a residue, which led to the conclusion that surplus carbon deposits were obtained during the carburization with pure methane. To overcome the formation of carbon deposits, they passed a H_2 flow at 600 °C through the α-MoC_{1-x} samples. This treatment increased the specific surface area to 185 $m^2 \cdot g^{-1}$. In a separate experiment, it was found that α-MoC_{1-x} with high specific surface area can be obtained by using a mixture of methane and hydrogen ($\dot{n}_{CH_4}/\dot{n}_{H_2} = 0.25$) instead of pure methane which makes the subsequent treatment with hydrogen superfluous. Because of

possible pyrophoric properties of transition metal carbides, all samples were passivated in a flow of 1 vol.-% O_2 in helium before they were exposed to air.

Hanif *et al.* [110] studied the influence of the carburizing agent (methane or ethane) on the formation mechanism of molybdenum carbides in more detail. They passed mixtures ($\dot{V}$ = 100 to 120 $cm^3 \cdot min^{-1}$) of 20 vol.-% methane in hydrogen or 10 vol.-% ethane in hydrogen over MoO_3. The carburization was investigated from 250 to 1100 °C. Passivation of the samples occurred in a flow of 1 vol.-% oxygen in nitrogen at room temperature. During the reaction the exhaust gases were monitored by using a gas chromatograph equipped with a mass spectrometer. With methane/hydrogen as carburizing agent mixture, it was observed that water was formed between 400 °C and 430 °C, while the methane concentration remained constant. This showed that only hydrogen was involved in this early stage of reduction. At about 600 °C the concentration of methane in the off-gas decreased, and simultaneously peaks of CO, CO_2 and water appeared which indicated that methane acted as carbon source and also as reducing agent. When ethane/hydrogen was used as the carburizing agent mixture, the first water peak appeared at almost the same temperature as with methane/hydrogen. This could be expected, as hydrogen should behave similarly in both systems. For ethane/hydrogen at a temperature of about 470 °C hydrogenolysis occurred to produce methane. Reduction and carburization occurred at 525 °C and 625 °C, respectively, which was indicated by the appearance of CO, CO_2 and water peaks. So ethane was found to be more active in the reduction process than methane. Observation of the reaction products from 250 °C to 1100 °C by XRD showed reflexes from MoO_2 (400 °C), MoO_xC_y (550 °C) and hexagonal close-packed β-Mo_2C (700 °C). The specific surface area of β-Mo_2C obtained was in the range from 49 to 76 $m^2 \cdot g^{-1}$ for the preparation method with methane. For ethane, the specific surface area was higher, *viz.* 73 to 108 $m^2 \cdot g^{-1}$.

A similar method for the preparation of Mo_2C bulk catalysts was described by Ardakani *et al.* [90]. They also treated MoO_3 in a quartz tubular reactor at 700 °C in a flow of methane and hydrogen with $\dot{V}_{CH_4}/\dot{V}_{H_2}$ = 1 for 3 h. After rapid cooling in a H_2 flow the resulting solid was passivated by exposing it to a slightly oxidative gas flow (2 vol.-% O_2 in He). The X-ray diffractograms show the presence of crystalline β-Mo_2C with BET surface areas between 1.9 and 8.5 $m^2 \cdot g^{-1}$. Ardakani *et al.* [90] suggested that about 0.02 % of the Mo were available at the surface, which was measured by CO adsorption. This value should be taken with care. It can only be true if the formula of the

catalyst is Mo_2C without any amorphous fraction and if one Mo atom adsorbs precisely one CO molecule. Another uncertainty is the small amount of CO adsorbed per mass of catalyst. The value of around 1 $\mu mol \cdot g^{-1}$ is close to the detection limit of the method.

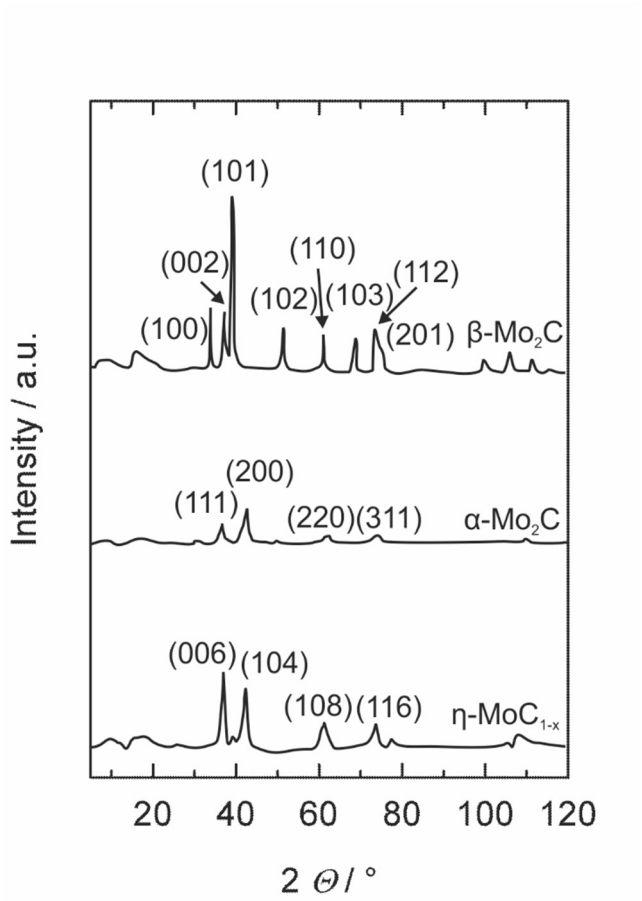

Figure 4.21: X-ray diffraction patterns of different molybdenum carbides [107] (CuKα radiation).

The differences between the specific surface areas of the prepared molybdenum carbide catalysts were investigated by Miyao *et al.* [107]. They reported, that carburization of MoO_3 in a methane-containing hydrogen flow led to materials with low specific surface areas of about 7 $m^2 \cdot g^{-1}$ of the resulting molybdenum carbide. This molybdenum carbide was identified as β-Mo_2C. The previous transformation of MoO_3 with ammonia at 500 °C into molybdenum nitride offered the possibility to achieve different molybdenum carbide structures only by changing the temperature of the sample during the carburization step. Carburization at 700 °C led to α-Mo_2C, while carburization at 900 °C led to η-MoC_{1-x}. The carbide partially kept the structure of the nitride. This is called topotactic solid-state transformation and means a crystallographic orientation dependency between the parent material and the product. This method allows the preparation of molybdenum carbide with a high

specific surface area, *e.g.* α-Mo_2C or η-MoC_{1-x}. The corresponding XRD patterns are shown in Figure 4.21. The specific surface areas of these molybdenum carbides were about 200 $m^2 \cdot g^{-1}$.

Other starting materials for Mo_2C bulk catalysts with a high specific surface are powdery MoO_3 and charcoal (d = 0.2 – 0.5 mm, $A_{BET} \approx 1150$ $m^2 \cdot g^{-1}$). A mixture of these compounds was heated up in a graphite reactor under vacuum (p = 130 Pa) for 4 h to more than 1120 °C. Dependent on the n_C/n_{Mo} ratio, Ledoux *et al.* [111] measured specific surface areas in the range from 2 to 261 $m^2 \cdot g^{-1}$. The main product formed by reaction (4.3) is hexagonal β-Mo_2C with traces of cubic α-MoC_{1-x}, γ-MoC_{1-x} or elemental molybdenum.

$$2\ MoO_{3(g)} + 7\ C_{(s)} \longrightarrow Mo_2C_{(s)} + 6\ CO_{(g)} \qquad (4.3)$$

4.4.2.2 Supported Molybdenum Carbide Catalysts

Ardakani *et al.* [90] prepared supported Mo_2C catalysts by wet impregnation of zeolites in their acid form with an aqueous ammonium heptamolybdate tetrahydrate solution containing the desired amount of Mo. After impregnation, the catalysts were dried and calcined before placing them in a quartz tubular reactor. The samples were heated up to 700 °C in a flow of $\dot{V}_{CH_4}/\dot{V}_{H_2} = 1$. Subsequently, the solid was exposed to a slightly oxidative gas flow (2 vol.-% O_2 in He) for passivation. Before their use as catalysts, the materials were activated in a hydrogen flow at 400 °C for 1 h. Catalysts were obtained with BET surface areas in the range of 344 to 658 $m^2 \cdot g^{-1}$ for Mo_2C on H-Y [89]. In a later publication [112], the authors added an aging step (70 °C for 2 h) after the impregnation and changed the flow composition to $\dot{V}_{CH_4}/\dot{V}_{H_2} = 0.2$. The oxygen content of the gas mixture for the passivation was reduced to 1 vol.-% O_2 in He. Similar conditions were reported earlier by Da Costa *et al.* [113].

The characterization of the supported catalysts by X-ray diffraction is difficult, especially for small loadings of the zeolite. Ardakani *et al.* [90] reported that there were no reflexes of Mo_2C visible in the diffractogram of Mo_2C supported on zeolite H-Y. This was true for Mo_2C loadings of less than 10 wt.-% on H-Y and explained by a very good dispersion of the carbide. This was additionally confirmed by TEM measurements. From a later publication by the same group [112] it can be seen that for higher Mo_2C loadings characteristic reflexes occur

in the diffractogram. For these catalysts they calculated a particle size of 19 ± 4 nm for the distributed Mo_2C from X-ray line broadening.

Ding *et al.* [114] prepared a supported Mo_2C catalyst by solid-state ion exchange of MoO_3 with OH-groups of H-ZSM-5. Under preparation conditions, the MoO_3 species migrated into the zeolite channels and exchanged with OH-groups in H-ZSM-5 to form $(Mo_2O_5)^{2+}$ dimers (see Figure 4.22), when physical mixtures of MoO_3 and the zeolite were heated in dry air. This was confirmed by *in situ* Raman and X-ray absorption spectroscopy [115].

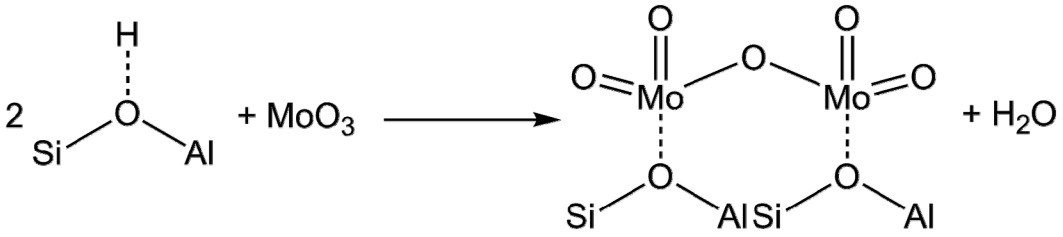

Figure 4.22: Solid-state ion exchange of MoO_3 with OH-groups of H-ZSM-5 [114].

Mixtures of MoO_3 and zeolite H-ZSM-5 (n_{Si}/n_{Al} = 15) were heated up to 700 °C in a quartz cell under an oxidizing atmosphere (20 vol.-% O_2 in He). This led to the molybdenum dimer formation as shown in Figure 4.22. After cooling the samples to 675 °C the gas flow was switched to a mixture of 20 vol.-% CH_4, 20 vol.-% argon and 60 vol.-% helium. Methane conversion occurred under these conditions. Subsequently, the gas flow was switched to helium to desorb any reaction intermediates present on the surface of the catalyst. After some further treatment in hydrogen- or oxygen-containing atmospheres the catalysts were ready for use.

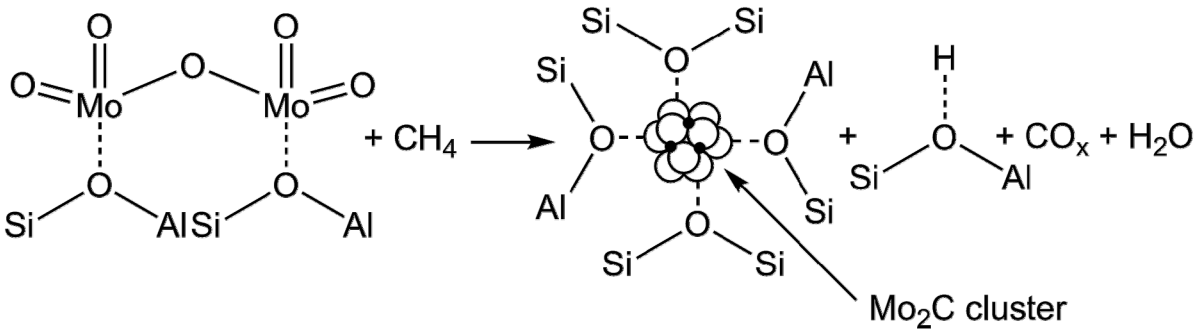

Figure 4.23: Creation of Mo_2C clusters in H-ZSM-5. After Ref. [114].

The structure of Mo_2C on H-ZSM-5 was investigated by Ding *et al.* [114]. After preparation (*v.s.*), the interatomic Mo-C and Mo-Mo distances in a supported Mo_2C catalyst were determined by EXAFS. The distances were very similar to those in bulk Mo_2C implying that the local structures of Mo atoms in Mo_2C and MoC_x/H-ZSM-5 were the same. The coordination number was found to be close to 3, suggesting that isolated Mo precursors formed very small Mo_2C clusters as shown in Figure 4.23.

Ding *et al.* [114] explained the resistance of the clusters to migration and external agglomeration at even higher temperatures with the high melting point of molybdenum carbides, the high initial dispersion of the MoO_x precursors and the possible complexation of the clusters by framework oxygens.

4.4.3 Molybdenum Carbides as Potential Catalysts in Ring Opening of Naphthenes

4.4.3.1 Catalytic Properties of Molybdenum Carbide Bulk Catalysts

Naphthalene was chosen as model reactant for hydrogenation and ring opening by Ardakani *et al.* [90]. The reaction was carried out at temperatures from 280 to 340 °C in H_2 at a total pressure of 3.0 MPa with a feed composition of 10 wt.-% naphthalene in n-heptane. 160 $\mu l \cdot min^{-1}$ of the feed were totally vaporized and mixed with 58 $cm^3 \cdot min^{-1}$ of H_2 before it was passed through the fixed-bed reactor. However, none of the bulk catalysts showed high selectivities of ROPs or OCDs. This was explained in terms of being due to the low concentration of acid sites, which was measured by TPD of n-propylamine. The same group confirmed the good hydrogenation activity of bulk Mo_2C, but the yield of ring opening products remained at 0.6 % with a selectivity of 0.8 % [112].

4.4.3.2 Catalytic Properties of Molybdenum Carbide Catalysts Supported on Zeolites

The Mo_2C/H-Y catalysts described by Ardakani *et al.* [90] showed conversions of naphthalene (10 wt.-% naphthalene in n-heptane as feed) between 50 % and 97 %. Their results are presented in Figure 4.24a and b. It can be seen that for partly dealuminated zeolite H-Y (n_{Si}/n_{Al} = 6) the addition of Mo_2C up to

a content of 7 wt.-% to the zeolite increased the naphthalene conversion. At higher loadings the conversion decreased. $7Mo_2C$/H-Y-6 was the most selective catalyst for ROPs formation (see Figure 4.24a), but this situation changed with a higher n_{Si}/n_{Al} ratio of the support. For H-Y with $n_{Si}/n_{Al} = 15$ (Figure 4.24b) the optimal catalyst was $5Mo_2C$/H-Y-15 which showed an initial naphthalene conversion of 97 % and a selectivity of ROPs of 40 %. For all catalysts fast deactivation occurred, which seems to be dependent on the Al content of the support. Ardakani *et al.* [90] concluded that these catalysts were bifunctional with a hydrogenation/hydrogenolysis activity provided by Mo_2C and isomerization, ring opening, cracking and polymerization occurring on acid sites, associated with the H-Y zeolite. A special property of these catalysts is their resistance to sulfur. This was investigated by adding 0.1 wt.-% dibenzothiophene to the reaction mixture.

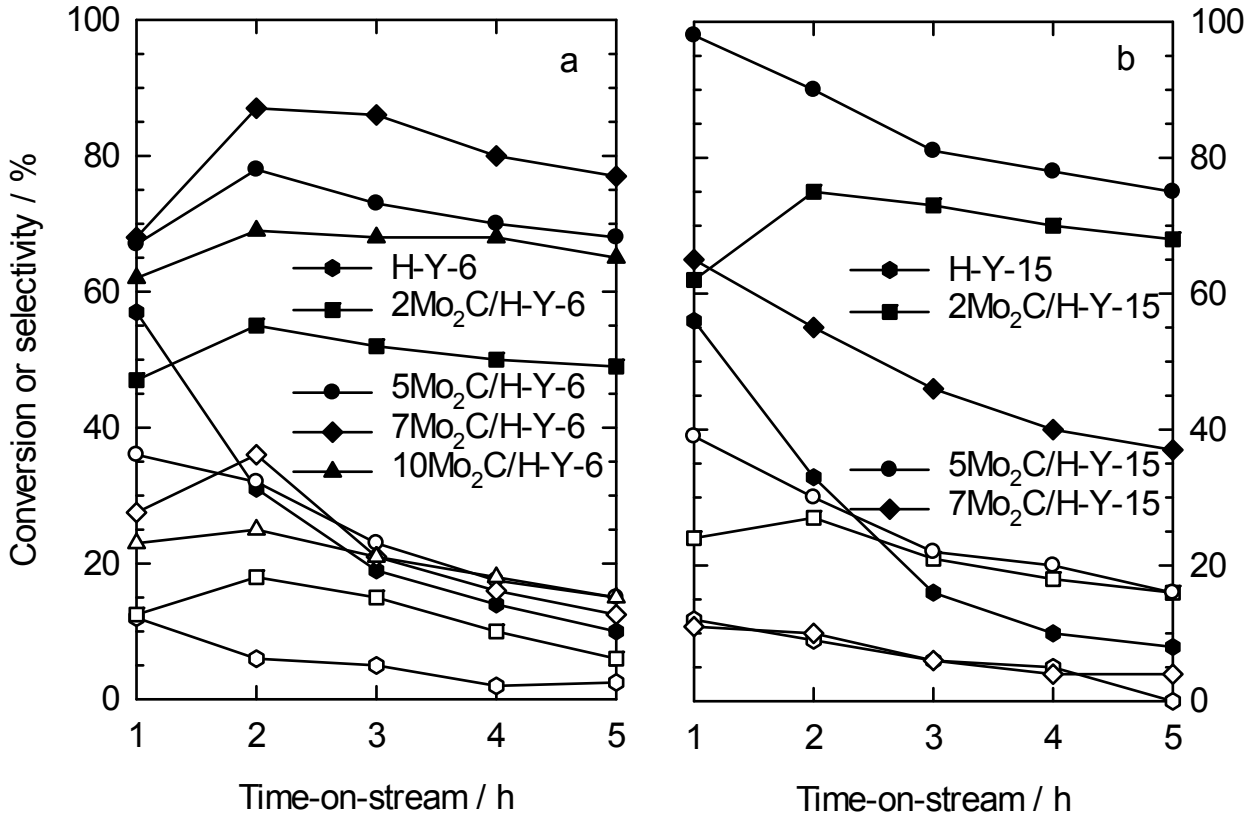

Figure 4.24: Naphthalene conversion (filled symbols) and selectivity of ROPs (open symbols) in dependence of time-on-stream at $T_r = 300$ °C and $p_{H_2} = 3.0$ MPa.

Later, the same group reported about supported Mo_2C/H-Y catalysts with loadings of 7 to 27 wt.-% Mo_2C [112]. The maximum conversion of naphthalene (5 wt.-% in n-heptane) was 91 % for the Mo_2C loading of

20 wt.-%. For $\dot{n}_{H_2}/\dot{n}_{naphthalene}$= 20 the selectivities of ROPs reached 22 %. A further increase of Mo_2C lowered the conversion of naphthalene. A ratio of $\dot{n}_{H_2}/\dot{n}_{naphthalene}$= 30 together with 20$Mo_2C$/H-Y showed S_{ROPs} = 33 % at a conversion of 92 %. According to Liu and Smith [112], this is due to hydrogen spillover which facilitates hydrogenation on metal and acidic sites. All supported catalysts that were investigated showed significant selectivities to polymerization products which are responsible for coking, and catalyst deactivation.

In 2011, the same group changed the reactant from naphthalene to decalin and tested the properties of their molybdenum carbide catalysts with this feed [116]. As previously, the reactant was diluted (5 wt.-% in n-heptane) and fed to the catalysts which were placed in a fixed-bed reactor. On the catalysts 7Mo_2C/H-Y and 20Mo_2C/H-Y they report selectivities of ROPs up to 100 % at decalin conversions of *ca.* 60 to 70 %, but their definition of the term “ROPs” is different from the one in the present thesis and includes, besides C_{10} one-ring naphthenes, all kinds of alkylcyclohexanes, alkylbenzenes, and alkylindenes, regardless of their carbon numbers.

5 Experimental Section

All chemicals and zeolites used in this work are listed in Table 5.1.

Table 5.1: Chemicals and zeolites used within this work.

Chemical	Producer, Purity/Composition
Ammonium acetate	Aldrich, 98 wt.-%
Ammonium hexafluorosilicate	Ventron, > 99 wt.-%
Ammonium molybdate tetrahydrate	Fluka, p.a. ≥ 99.0 wt.-%
Ammonium nitrate	Merck, p.a. ≥ 99 wt.-%
Calcium nitrate tetrahydrate	Merck, ≥ 98 wt.-%
cis-Decalin	Merck, 97.4 wt.-%
n-Decane	Sigma Aldrich, 99.7 wt.-%
Hydrofluoric acid	Merck, 40 wt.-%
Hydrogen 5.0	Westfalen AG, 99.999 vol.-%
Methane 5.5/Hydrogen 5.0	Westfalen AG, 20 vol.-% CH_4 in H_2, 99.999 vol.-%
Nitrogen 5.0	Westfalen AG, 99.999 vol.-%
n-Octane	Fluka, 99.3 wt.-%
Pentaamminechloroiridium(III) chloride	Colonial Metals, 49.9 wt.-% Ir
Pyridine	Aldrich, ≥ 99 wt.-%
Sodium molybdate dihydrate	Fluka, ≥ 99.0 wt.-%
Tetraammineplatinum(II) chloride hydrate	ChemPur, 55.63 wt.-% Pt
Zeolite Na-Y-2.4	Strem Chemicals, lot No. 148 960, n_{Si}/n_{Al} = 2.4
Zeolite H-Y-14	Alfa Aesar, lot No. A05X039, n_{Si}/n_{Al} = 14
Zeolite H-Y-105	Degussa-Hüls, lot No. 001 48/43320160, n_{Si}/n_{Al} = 105

5.1 Preparation of the Catalysts

The preparation of some molybdenum carbide catalysts was conducted by Dipl.-Chem. Daniel Barunović, Dipl.-Chem. Felix Neher and B.Sc. Alexis Schmidt.

5.1.1 Starting Materials and Modification of the Zeolites

Prior to any treatment, it was made sure that all exchangeable cations of the zeolite Na-Y-2.4 were sodium ions. For that purpose the following ion exchange procedure was applied: The zeolite was suspended in 40 cm^3 of a 1 $mol \cdot dm^{-3}$ aqueous solution of $NaNO_3$ per gram of dry zeolite. After stirring for 4 h at 80 °C, the zeolite was filtered and washed with demineralized water until no nitrate ions could be detected by means of a nitrate test strip. This whole procedure was done twice to ensure a full exchange of all cations. The composition of this zeolite was determined by ICP-OES and revealed an n_{Na}/n_{Al} ratio of 0.96 ($Na_{0.96}$,$H_{0.04}$-Y-2.4). A methodically identical treatment was applied with the zeolites H-Y-14 and H-Y-105, but with the aim to achieve a quantitative ammonium exchange. Thus, the ion exchange was applied with ammonium nitrate. The washed and filtered zeolites were dried in an oven for at least 12 h before they were stored in a desiccator over a saturated $Ca(NO_3)_2$ solution to reach a constant water content.

5.1.2 Ion Exchange with Ammonium Ions

$Na_{0.72}$,$H_{0.28}$-Y-2.4

1 g of zeolite Na-Y-2.4 (on a dry basis) was slurried under stirring in 15 g demineralized water. A solution of 98.9 mg NH_4NO_3 in 12.5 g demineralized water was added dropwise to the suspension. The suspension was stirred at 80 °C for 4 h. After filtration, washing with demineralized water and drying at 80 °C for 18 h, the n_{Na}/n_{Al} ratio determined by ICP-OES amounted to 0.72.

$Na_{0.67}$,$H_{0.33}$-Y-2.4

Zeolite Na-Y-2.4 (1 g, on a dry basis) was slurried under stirring in 22 g demineralized water. A solution of 101.2 mg NH_4NO_3 in 13.0 g demineralized water was added dropwise to the suspension. The suspension was stirred at 80 °C for 22 h. After filtration, washing with demineralized water and drying at 80 °C for more than 12 h, the n_{Na}/n_{Al} ratio determined by ICP-OES amounted to 0.67.

$H_{0.57}$,$Na_{0.43}$-Y-2.4

1 g of zeolite Na-Y-2.4 (on a dry basis) was slurried under stirring in 15 g demineralized water. A solution of 197.8 mg NH_4NO_3 in 12.5 g demineralized water was added dropwise to the suspension. After stirring for 4 h at 80 °C, the suspension was filtered, washed with demineralized water and dried at 80 °C for 18 h. The n_{Na}/n_{Al} ratio determined by ICP-OES amounted to 0.60.

To achieve a higher degree of ammonium exchange, a second ion exchange was necessary. 1 g (on a dry basis) of the zeolite (*v.s.*) was slurried in 25 g of demineralized water. Subsequently, 149.2 mg of NH_4NO_3 were dissolved in 6 g demineralized water and added dropwise to the suspension. After stirring at 80 °C for 14 h, the suspension was filtered, washed with demineralized water and dried at 80 °C for 6 h. The final n_{Na}/n_{Al} ratio determined by ICP-OES amounted to 0.43.

$H_{0.62}$,$Na_{0.38}$-Y-2.4

Zeolite Na-Y-2.4 (1 g, on a dry basis) was slurried under stirring in 40 g demineralized water. A solution of 748.7 mg NH_4NO_3 in 9.0 g demineralized water was added dropwise to the suspension. The suspension was stirred at 80 °C for 4 h. After filtration, washing with demineralized water and drying at 80 °C for more than 12 h, the n_{Na}/n_{Al} ratio determined by ICP-OES amounted to 0.38.

$H_{0.88}$,$Na_{0.12}$-Y-2.4

Zeolite Na-Y-2.4 (1 g, on a dry basis) was slurried under stirring in 20.5 g of a 1.0 $mol \cdot dm^{-3}$ solution of NH_4NO_3. The suspension was stirred at 80 °C for 4 h. After filtration and washing with demineralized water, the procedure was repeated a second time before the zeolite was dried at 80 °C for more than 12 h. The n_{Na}/n_{Al} ratio determined by ICP-OES amounted to 0.12.

$H_{0.90}$,$Na_{0.10}$-Y-2.4

1 g of zeolite Na-Y-2.4 (on a dry basis) was slurried under stirring in 65 g of a 1.0 mol·dm^{-3} solution of NH_4NO_3. The suspension was stirred for 4 h at 80 °C and filtered, and the solid was washed with demineralized water and slurried again under stirring in the same amount of a 1.0 M solution of NH_4NO_3 as in the first step. After stirring the suspension for 120 h at 70 °C, it was filtered, washed with demineralized water and dried for 4 h at 80 °C. The n_{Na}/n_{Al} ratio determined by ICP-OES amounted to 0.10.

5.1.3 Dealumination of $H_{0.88}$,$Na_{0.12}$-Y-2.4

Following a procedure described by Kühl [117], 1.0 g (on a dry basis) zeolite $H_{0.88}$,$Na_{0.12}$-Y-2.4 was suspended in 10.4 g of a 10 mol·dm^{-3} aqueous solution of ammonium acetate. The suspension was heated to 75 °C. Afterwards, 0.5 g of a 1 M aqueous solution of $(NH_4)_2SiF_6$ was added dropwise. The resulting suspension was heated to 90 °C under stirring and kept for 3 h under these conditions. The zeolite was filtered and suspended again five times in 45 cm^3 of hot water (95 °C). The zeolite was calcined, and the chemical composition determined by ICP-OES yielded $H_{0.99}$,$Na_{0.01}$-Y-7.

5.1.4 Ion Exchange with $[Pt(NH_3)_4]Cl_2$ or $[Ir(NH_3)_5Cl]Cl_2$

The introduction of iridium or platinum into the catalyst precursors was done by means of ion exchange. The zeolites were suspended in a 25-fold excess of demineralized water relative to their dry weight. An aqueous solution of $[Pt(NH_3)_4]Cl_2$ or $[Ir(NH_3)_5Cl]Cl_2$ in a 200-fold excess of demineralized water was slowly added to the suspension within 30 min under vigorous stirring. For the calculation of the necessary amount of noble metal complex two assumptions were made: all dissolved platinum and only 80 wt.-% of iridium will be introduced into the zeolite. The resulting suspension was stirred for 4 h at 80 °C before the zeolite was filtered off, washed thoroughly with demineralized water and dried at 80 °C in an oven for at least 12 h. All noble metal catalysts thus prepared are listed in Table 5.2.

Table 5.2: All prepared noble metal catalysts and their corresponding supports.

Zeolitic Support	**Iridium Catalyst**	**Platinum Catalyst**
$Na_{0.96},H_{0.04}$-Y-2.4	3.0Ir/$Na_{0.96},H_{0.04}$-Y-2.4	3.3Pt/$Na_{0.85},H_{0.15}$-Y-2.4
$Na_{0.72},H_{0.28}$-Y-2.4	3.3Ir/$Na_{0.72},H_{0.28}$-Y-2.4	2.8Pt/$Na_{0.59},H_{0.41}$-Y-2.4
$H_{0.57},Na_{0.43}$-Y-2.4	2.9Ir/$H_{0.57},Na_{0.43}$-Y-2.4	2.7Pt/$H_{0.63},Na_{0.37}$-Y-2.4
$H_{0.90},Na_{0.10}$-Y-2.4	3.1Ir/$H_{0.90},Na_{0.10}$-Y-2.4	2.6Pt/$H_{0.88},Na_{0.12}$-Y-2.4

5.1.5 Forming of the Catalyst Powder

For the catalytic experiments the catalyst size fraction of 200 µm < $d_{cat.}$ < 315 µm was used. For the preparation of these particles, the catalyst powder was pressed at 127 MPa for more than 10 min to a compact disc. Afterwards, it was crushed and sieved into the correct fraction.

5.1.6 Decomposition of the Complex

All catalyst precursors, which were ion-exchanged with noble metals, were treated thermally under oxidative conditions to destroy the noble-metal complexes. For this purpose, the catalyst precursors where heated up to 300 °C in a fixed-bed reactor (see Figure 5.3, page 76) with a heating rate of 0.5 °C·min^{-1} in a flow of synthetic air ($\dot{V}_{synth.\ air}$ = 130 cm^3·min^{-1}) and held for 2 h at these conditions.

5.1.7 Reduction of the Noble Metals

To activate the noble metal, the catalyst precursors were placed into a fixed-bed reactor depicted in Figure 5.3 (page 76). The catalyst precursors were reduced under a hydrogen pressure of 5 MPa (high-pressure experiments) or 0.1 MPa (atmospheric-pressure experiments) and a hydrogen flow of 130 cm^3·min^{-1} (referenced to ambient pressure and temperature) while heating with a rate of 2 °C·min^{-1} from room temperature to 360 °C. The final temperature of 360 °C was held for 2 h before the catalyst was cooled down to the first reaction temperature. Note that, during the reduction, Brønsted acid sites are formed (see Section 4.1).

The catalysts 2.9Ir/$Na_{0.90}$,$H_{0.10}$-MOR-5.8, 2.9Ir/$K_{0.68}$,$Na_{0.21}$,$H_{0.11}$-L-2.9, 3.0Ir/$Na_{0.80}$,$H_{0.20}$-EMC-2-4.3, 0.52Ir/$H_{0.59}$,$Na_{0.41}$-ZSM-5-18, 3.5Ir/$Rb_{0.52}$,$H_{0.48}$-Beta-14 and 3.3Ir/$H_{0.58}$,$Cs_{0.42}$-Beta-14 were kindly provided by Dr. Dominic Santi [118]. The catalysts 2.6Ir/silica and 2.7Pt/silica were kindly provided by Dr. Andreas Haas [119].

5.1.8 Impregnation with $(NH_4)_6Mo_7O_{24} \cdot 4\ H_2O$ or $Na_2MoO_4 \cdot 2\ H_2O$

For the incipient wetness impregnation of the carriers, a determination of the water adsorption capacity was made prior to the impregnation. Water was dropped onto a known amount of the zeolite powder until saturation. In the next step the added water was weighted. Then, the calculated amount of $(NH_4)_6Mo_7O_{24} \cdot 4\ H_2O$ or $Na_2MoO_4 \cdot 2\ H_2O$ for the desired zeolite loading was dissolved in the respective amount of water. Afterwards, the solution was dropped onto the support and the water was evaporated under vacuum (2.5 kPa) at 35 °C. The resulting catalyst precursors were stored in a desiccator for 24 h over a saturated $Ca(NO_3)_2$ solution.

5.1.9 Carburization of the Catalyst Precursors and Bulk MoO_3

An amount of *ca.* 500 mg of the pressed and sieved molybdenum-containing catalyst precursor was introduced into a fixed-bed quartz glass reactor (see Figure 5.3, page 76). A scheme of the atmospheric-pressure apparatus can be seen in Figure 5.4 (page 78). The samples were heated up to 150 °C with a heating rate of 2 °C·min^{-1} in a nitrogen flow ($\dot{V}_{N_2}$ = 120 cm^3·min^{-1}). Subsequently, a gas flow of 330 cm^3·min^{-1} of hydrogen and methane or octane vapor with a ratio of gas volumes of 5:1 or 40:1 was applied. The catalyst precursor was heated up to 700 °C with a heating rate of 5 °C·min^{-1} and kept for 3 h at this temperature. Afterwards, the carburized sample was cooled down to room temperature in a hydrogen flow of 300 cm^3·min^{-1} within 30 min.

5.2 Characterization of the Starting Materials and Catalysts

5.2.1 X-Ray Diffraction

The crystallinity and the phase purity of the zeolite samples was investigated by powder X-ray diffractometry (XRD). For this purpose a Bruker D8 Advance diffractometer with CuKα radiation (λ = 0.154 nm) was used. The excitation voltage and the current intensity were 35 kV and 40 mA, respectively. The range of 2Θ values was from 5 to 50° with a step size of 0.016° and a step time of 0.2 s.

5.2.2 Thermogravimetric Analysis

Since the metal content of all catalysts is expressed as the mass of the respective metal per mass of the dry catalyst, it is necessary to determine the water content of the samples. To obtain a constant water content, the zeolite samples were stored for more than 12 h in a desiccator over a saturated aqueous solution of calcium nitrate. Afterwards, the samples were heated up with a heating rate of 20 °C·min^{-1} in a Setaram Thermogravimetric Analyzer (TGA) Setsys TG-16/18 under a nitrogen atmosphere from room temperature to 600 °C. The loss of weight of the sample is measured during the whole procedure which allows the precise calculation of the water content. All water content determinations were conducted by Mrs. Barbara Gehring, Dr. Ines Kley, Dipl.-Chem. Dennis Wan Hussin and Dr. Frank Salzbauer.

5.2.3 Chemical Analysis

5.2.3.1 ICP-OES

The chemical composition of the samples was analyzed by means of a Varian Vista-MPX CCD optical emission spectrometer with an inductively coupled plasma (ICP-OES). The elements silicon, aluminum, sodium, potassium, rubidium, cesium, molybdenum, iridium and platinum were determined. The method requires dissolved samples. Thus, *ca.* 100 mg of the sample were dissolved in 3 cm^3 of diluted hydrofluoric acid (10 wt.-% HF in doubly distilled water) and 6 cm^3 of *aqua regia*. The resulting solution was filled up to 250 cm^3 with doubly distilled water. Usually, all zeolite samples were analyzed directly

after the loading with metals and prior to any further oxidative/reductive treatment, because some of the samples could not be dissolved with the above mentioned procedure after such a treatment. The measurements were conducted by Mrs. Heike Fingerle.

5.2.3.2 CHN Analysis

The carbon content of the molybdenum carbide catalysts was measured with an elemental analyzer Elementar Vario EL. The samples were decomposed at 950 °C, and evolving gases were passed through an oxidation-active CuO catalyst. Water, carbon dioxide and nitrogen were adsorbed in different adsorption columns. The gases were desorbed successively and detected with a TCD. The quantification of the TCD signals revealed the amounts of C,H and N contained in the respective sample. The determinations were conducted by Mrs. Barbara Gehring.

5.2.4 MAS NMR Spectroscopy

^{27}Al and ^{29}Si MAS NMR spectra were measured on a Bruker MSL 400 spectrometer. In Table 5.3 the conditions for the acquisition of the MAS NMR spectra are summarized. The aluminum spectra give information concerning the position of the aluminum inside the zeolite, since the signals for tetrahedrally and octahedrally coordinated framework or extra-framework aluminum occur at different chemical shifts. Combined with the ^{29}Si MAS NMR spectra, the ^{27}Al MAS NMR spectra enable a calculation of the framework n_{Si}/n_{Al} ratio according to equation (5.1) [120]. In the ^{29}Si MAS NMR spectra different signals were obtained which can be attributed to Si species with zero to four Al atoms in their neighborhood. In equation (5.1), F is the relative fraction of the respective signal and a stands for the number of corresponding neighboring Al atoms.

$$n_{Si}/n_{Al} = \frac{\sum_{a=0}^{4} F_{Si(a\ Al)}}{\sum_{a=0}^{4} 0.25 \cdot a \cdot F_{Si(a\ Al)}} \qquad (5.1)$$

The measurements were conducted by Dipl.-Chem. Michael Dyballa and Prof. Michael Hunger.

Table 5.3: Parameters of the ^{27}Al and ^{29}Si MAS NMR measurements.

Nucleus	**^{27}Al**	**^{29}Si**
Rotor diameter	4 mm	7 mm
Resonance frequency	104.3 MHz	79.5 MHz
Spinning rate	8 kHz	3.5 kHz
Pulse length	0.61 µs	5 µs
Repetition time	0.5 s	10 s
Number of accumulations	1000-2000	300-400
Internal standard	Aluminum nitrate	Tetramethylsilane

5.2.5 Scanning Electron Microscopy

A scanning electron microscope (SEM) Cam Scan 44 was used for the determination of the crystallite size and the morphology of the zeolites. For this kind of microscopy a conductivity of the samples is necessary. Since zeolites possess no conductivity, the samples were sputtered with gold by a sputter coating equipment K550 of Emitech. Layers of gold up to 200 nm were formed on the zeolites with this procedure. The high-resolution images were achieved with an excitation voltage of 5 kV. The images were taken by Dipl.-Chem. Daniel Geiß, Dr. Ines Kley, Dipl.-Chem. Christian Lieder and Dipl.-Chem. Dennis Wan Hussin.

5.2.6 FT-Infrared Spectroscopy

The acidic properties of some zeolite samples were determined by means of Fourier transform infrared (FT-IR) spectroscopy with a Vector 22 spectrometer from Bruker. The setting of the apparatus can be found in Ref. [121]. A self-supporting thin wafer of the sample was pressed and placed in an IR cell with CaF_2 windows. The IR cell was equipped with a vacuum system and a separated oven. The activation of the zeolitic sample was performed by heating it to 300 °C within 9.5 h in an air flow of 200 $cm^3 \cdot min^{-1}$. This temperature was held for 2 h before the sample was cooled to 50 °C and the whole cell was flushed with nitrogen. Subsequently, the sample was heated up to 500 °C with 2 $°C \cdot min^{-1}$ in a hydrogen flow of 100 $cm^3 \cdot min^{-1}$. The final temperature was held for 2 h before the sample was cooled down to 200 °C. Then the IR cell was evacuated for 12 h at 200 °C under a vacuum of

$2 \cdot 10^{-4}$ Pa. Subsequently, pyridine vapor ($p_{pyridine}$ = 330 Pa) was introduced into the cell for 30 min. To remove physically adsorbed pyridine the cell was evacuated at 200 °C for 1 h. After that, the wafer was placed into the measurement cell, which was kept at 80 °C. Subsequently, the wafer was brought back into the oven, and the temperature was raised in steps of 50 °C from 200 to 500 °C. At each temperature a spectrum was recorded from which the band at 1544 cm^{-1}, which is assigned to Brønsted acid sites, was integrated. The concentration of Brønsted acid sites was calculated by using the following equation [122]:

$$c_{pyridine} = \frac{\overline{A} \cdot l_1 \cdot l_2}{m \cdot \varepsilon} \tag{5.2}$$

$\overline{A}$ stands for the integral absorption (in cm^{-1}), l_1 and l_2 are the edge lengths and m is the mass of the dry wafer. The value for the extinction coefficient ε is 1.67 $cm \cdot \mu mol^{-1}$ and was taken from Ref. [123]. Some spectra were recorded by Dr. Dominic Santi.

5.2.7 N_2 Physisorption

A Quantachrome Autosorb-1-C instrument was used for the measurement of the porous properties of the catalyst samples. The samples were first evacuated at 350 °C for 16 h. Then they were cooled to -196 °C, and the nitrogen physisorption experiments were started. The specific surface area A_{BET} was calculated according to Brunauer, Emmett and Teller (BET) [1]. Values of p/p_0 between 0.003 and 0.3 were chosen for the BET plot. An average diameter of the N_2 molecule of 0.3 nm was assumed. The measurements were conducted by Dr. Andreas Haas, Dipl.-Chem. Thomas Montsch and Mr. Matthias Scheibe.

5.2.8 H_2 Chemisorption

The dispersion of the noble metal on the zeolites was determined by means of a Quantachrome Autosorb-1-C instrument. Prior to the measurement, the samples were heated up with 0.5 $°C \cdot min^{-1}$ from room temperature to 300 °C in a flow of synthetic air and held at this temperature for 2 h before they were cooled to room temperature. Subsequently, the gas was switched to hydrogen, and the samples were reduced by heating them with 2 $°C \cdot min^{-1}$ to 360 °C and held for 2 h at this temperature. Two hydrogen adsorption isotherms at

T = 40 °C were measured, of which the first one was considered to be a combination of physisorption and chemisorption, whereas the second isotherm was associated to physisorption only. The difference between the two isotherms stems from irreversibly adsorbed hydrogen. This data was used for the calculation of the noble-metal dispersion with the assumption of an adsorption stoichiometry of $n_H/n_{noble\ metal}$ = 1. Dispersions greater than unity were found for several Ir samples which may be due to an adsorption stoichiometry of n_H/n_{Ir} > 1, in agreement with literature reports [124,125]. The measurements were conducted by Dr. Andreas Haas and Mr. Matthias Scheibe.

5.3 Catalytic Ring-Opening Experiments

Some of the catalytic experiments with molybdenum carbide catalysts were performed by Dipl.-Chem. Daniel Barunović and B.Sc. Alexis Schmidt.

5.3.1 Experimental Set-Up of the Apparatuses

5.3.1.1 One-Component Saturator

A scheme of the one-component saturator is depicted in Figure 5.1. Generally, the one-component saturator consists of a tube made from glass for atmospheric-pressure or stainless steel for high-pressure applications. The tube is filled with a chemically inert porous adsorbent (Chromosorb) which is loaded with the feed hydrocarbon. The saturator is surrounded by a thermoliquid (atmospheric pressure) or mounted in an oven (high pressure), it can be held at a constant temperature. When a carrier gas, say hydrogen, is passed through the saturator, it is in intimate contact with the hydrocarbon. The carrier gas is saturated with vapors of the hydrocarbon according to its vapor pressure at the chosen temperature and the hydrogen pressure in the saturator. According to Dalton's law (see Eq. (5.3)), the composition of the gas which leaves the saturator is given by the partial pressures of the pure hydrocarbon (= vapor pressure) and the carrier gas.

$$p_{total} = \sum_{i=1}^{n} p_i = p_{hydrocarbon} + p_{carrier\ gas} \qquad (5.3)$$

The saturator temperature needed to obtain the required partial pressure can be derived from tables as Ref. [126].

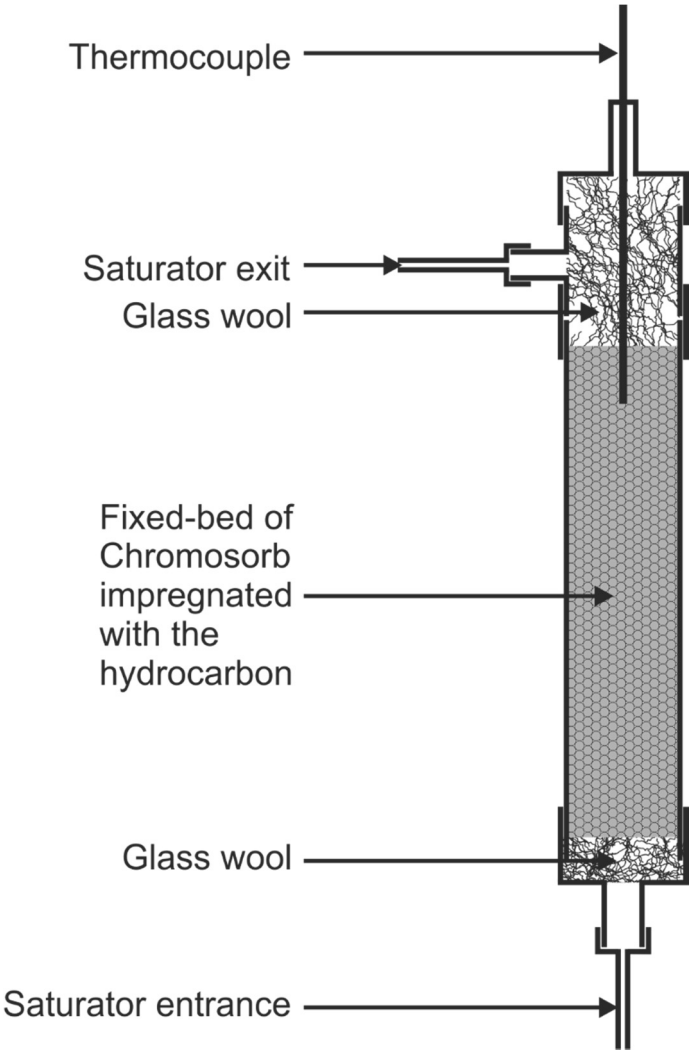

Figure 5.1: Scheme of the one-component saturator.

When elevated pressures of the carrier gas are applied, the chemical potential of the liquid phase of the hydrocarbon is increased. In phase equilibrium the chemical potential of the liquid phase is equal to the one of the vapor phase, the vapor pressure of the hydrocarbon increases with increasing pressure of the carrier gas. The increased vapor pressure of the hydrocarbon ($p^*_{\text{hydrocarbon}}$) can be accounted for by the Poynting correction (Eq. (5.4)) [127]:

$$p^*_{\text{hydrocarbon}} = p_{\text{hydrocarbon}} \cdot e^{\frac{\bar{V}_{\text{hydrocarbon}} \cdot (p_{\text{total}} - p_{\text{hydrocarbon}})}{R \cdot T}} \qquad (5.4)$$

$\bar{V}_{\text{hydrocarbon}}$, p_{total}, $p_{\text{hydrocarbon}}$, R and T denote the molar volume of the liquid hydrocarbon, the total pressure, the partial pressure of the pure hydrocarbon and the gas constant at the temperature T, respectively.

5.3.1.2 Multi-Component Saturator

For the generation of gas mixtures containing more than one hydrocarbon and the carrier gas, a saturator as described in Section 5.3.1.1 is inappropriate. If such a saturator contains two or more hydrocarbons, the more volatile one will be enriched in the gas phase, leading to a depletion of this component in the liquid phase. This, in turn, would lead to a non-stationary composition of the effluent gas mixture.

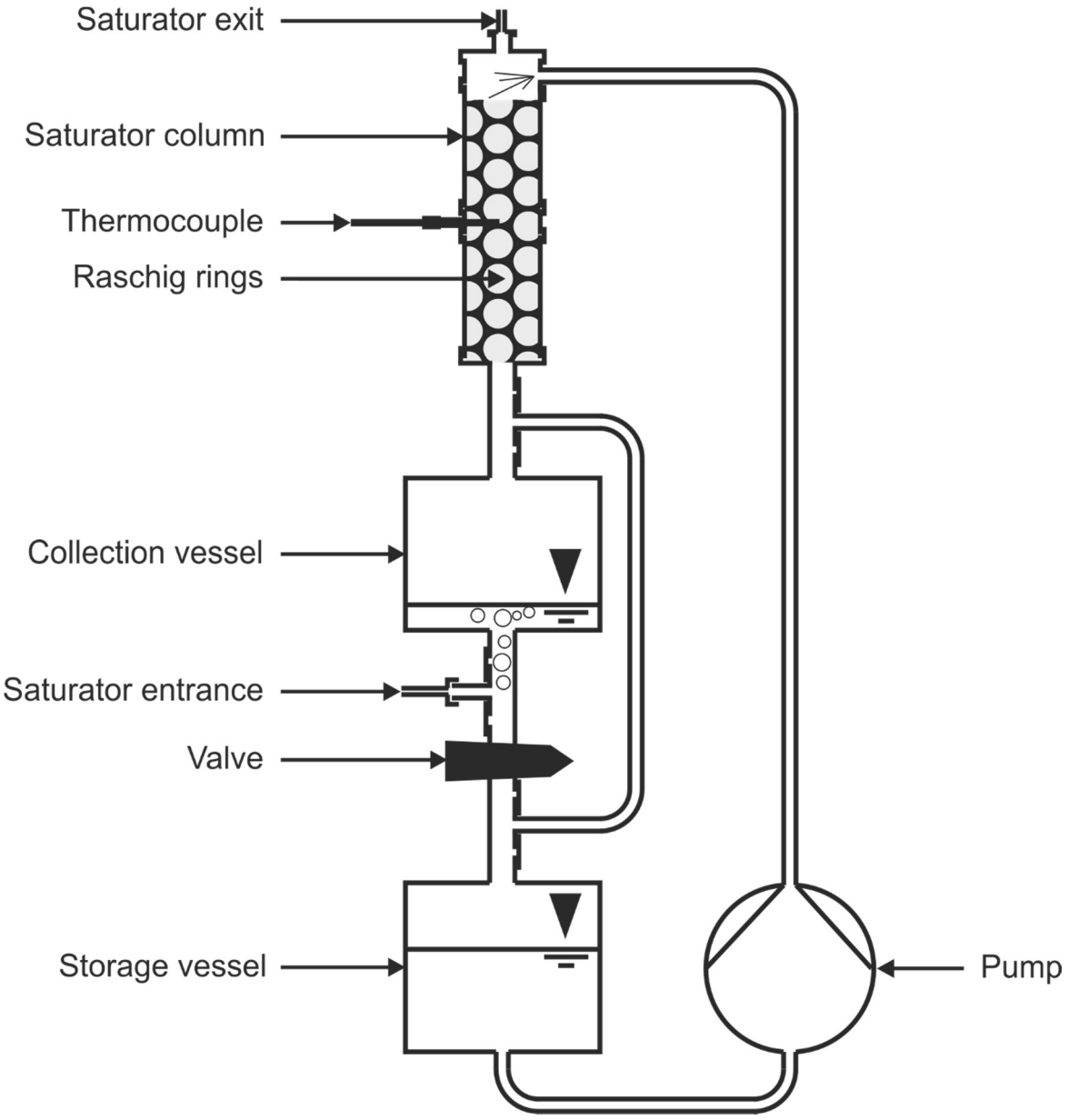

Figure 5.2: Scheme of the multi-component saturator.

These problems can be overcome by a multi-component saturator sketched in Figure 5.2 [128-130]. Such a saturator for high-pressure experiments was

constructed in the present work from stainless steel for generating well-defined hydrogen/decalin/n-decane gas mixtures at elevated pressures. It consists of four main parts, *viz.* the saturator column filled with Raschig rings, a collection vessel at the bottom of the saturator column, a storage vessel, and a micro-annular gear pump.

The characteristic feature of this saturator is a moving liquid phase. The liquid mixture of hydrocarbons is pumped from the storage vessel to the top of the saturator column which is held at a constant temperature by means of an oven. The liquid hydrocarbon mixture trickles down the saturator column, countercurrent to the carrier gas flow, before it is collected in the collection vessel. On its way upwards from the saturator entrance to the saturator exit, hydrogen is saturated with the vapors of the hydrocarbons contained in the downwards-trickling liquid. At the last contact point between the gas phase and the liquid phase, *i.e.*, at the top of the saturator column, the composition of the liquid phase is strictly stationary, and hence the composition of the gas leaving the saturator is strictly stationary as well (though different from the composition of the liquid phase).

Assuming that decalin and n-decane form ideal liquid mixtures, Raoult's law can be applied (Eq. (5.5)).

$$p_{\text{hydrocarbon,mix}} = p_{\text{hydrocarbon}} \cdot x_{\text{hydrocarbon}} \tag{5.5}$$

Where $p_{\text{hydrocarbon}}$, $x_{\text{hydrocarbon}}$ and $p_{\text{hydrocarbon,mix}}$ denote the vapor pressure of the pure hydrocarbon, its mole fraction in the liquid mixture, and its vapor pressure above the liquid mixture, respectively. At high-pressure conditions, $p_{\text{hydrocarbon}}$ can be replaced by $p^{*}_{\text{hydrocarbon}}$ from Eq. (5.4), thereby introducing Poynting's correction. For a binary liquid mixture and neglecting the solubility of hydrogen in the liquid hydrocarbon mixture, Eq. (5.6) holds:

$$x_{\text{hydrocarbon,1}} + x_{\text{hydrocarbon,2}} = 1 \tag{5.6}$$

Rearrangement of Eq. (5.5) and substituting into Eq. (5.6) results in Eq. (5.7).

$$\frac{p_{\text{hydrocarbon,mix,1}}}{p_{\text{hydrocarbon,1}}} + \frac{p_{\text{hydrocarbon,mix,2}}}{p_{\text{hydrocarbon,2}}} = 1 \tag{5.7}$$

For high-pressure experiments $p_{hydrocarbon,1}$ and $p_{hydrocarbon,2}$ can be replaced by $p^*_{hydrocarbon,1}$ and $p^*_{hydrocarbon,2}$, respectively. Eq. (5.4) is then introduced into Eq. (5.7) which can now be solved for the saturator temperature iteratively by spreadsheet processing. When the temperature is known, the corresponding partial pressure $p_{hydrocarbon}$ can be derived from the tables [126]. As $p_{hydrocarbon}$ is calculated and $p_{hydrocarbon,mix}$ was defined previously, the composition of the liquid hydrocarbon mixture can be obtained from Eq. (5.5).

5.3.1.3 Fixed-Bed Reactor and Adsorber

Fixed-bed reactors made from quartz glass (atmospheric pressure) or stainless steel (high pressure) were used in this work. They are identical in construction, a scheme of these reactors is depicted in Figure 5.3 (left).

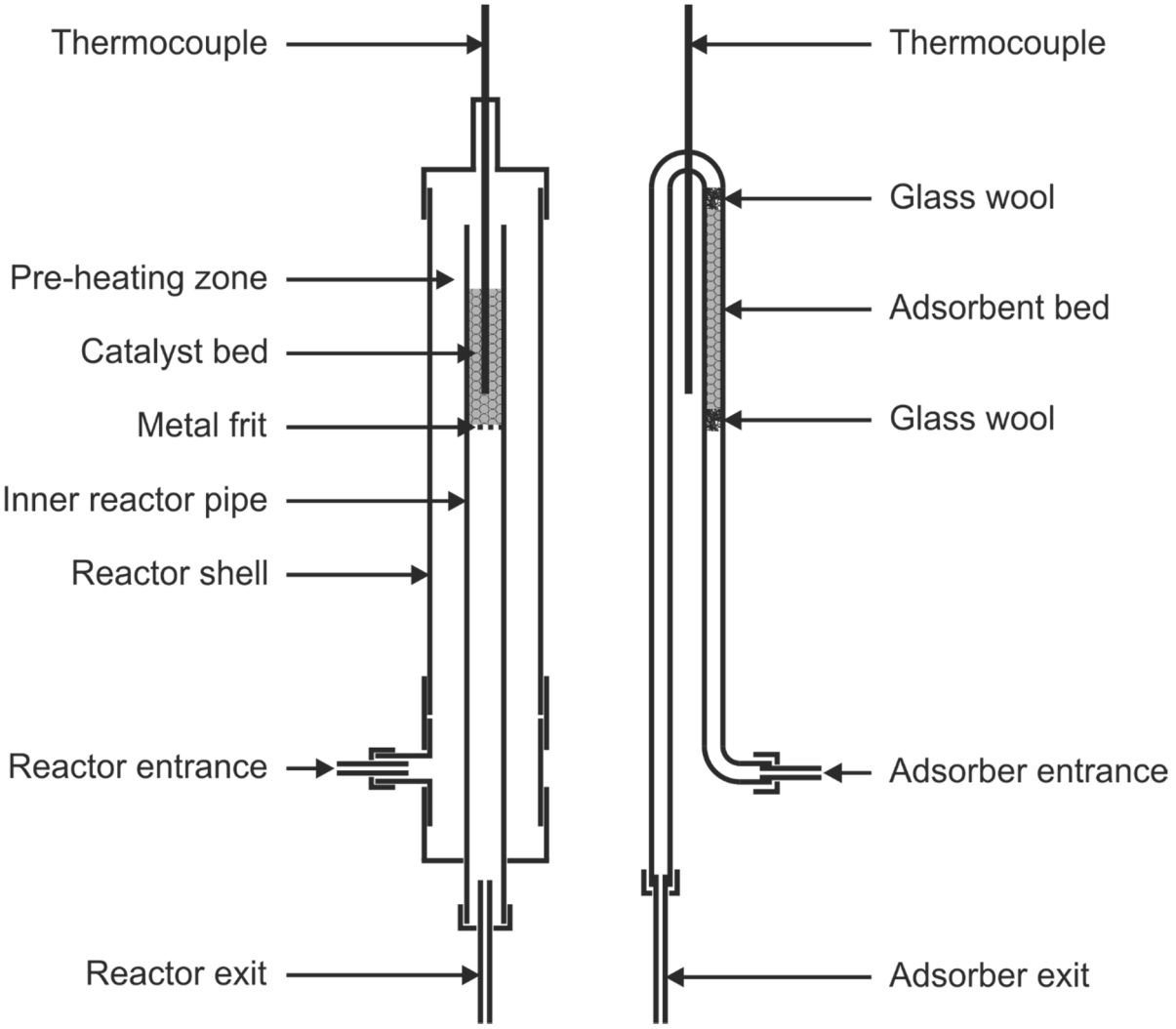

Figure 5.3: Scheme of the fixed-bed reactors (left) and the adsorber (right).

In the case of the apparatus from quartz glass, the reactor was placed in a tube furnace, whereas the high-pressure reactor was wrapped with heating wires and insulated with fiberglass cloth. This was necessary to achieve isothermal conditions inside the reactor.

The reactant gas flow entered the reactor at the entrance (see Figure 5.3) and was directed from bottom to top for preheating. At the highest point, the flow direction was changed and the feed passed into the inner reactor pipe and through the catalyst bed held in place by a metal frit. The product gas flow left the reactor on the bottom side.

For the adsorption experiments, the reactor of the atmospheric-pressure apparatus was exchanged by an adsorber made from quartz glass (see Figure 5.3, right). It consisted of a tube which was shaped in such a manner that it could be placed into the tube furnace. Inside the adsorber, the adsorbent was fixed between two plugs of glass wool. As the gas flow with the adsorptives passed through the adsorbent bed from the entrance to the exit, parts of the adsorptive molecules were adsorbed.

5.3.1.4 Experimental Set-Up of the Atmospheric-Pressure Flow-Type Apparatus

An atmospheric-pressure apparatus was designed and constructed for several purposes, such as the carburization of the molybdenum carbide precursors, the measurement of breakthrough curves for the competitive adsorption of decalin/n-decane mixtures or the generation of iso-decane mixtures by catalytic isomerization of n-decane. A piping and instrumentation diagram of this apparatus is shown in Figure 5.4.

The main parts of the apparatus are the reactor (R) and the saturator (S) which are connected by two 4/2 valves (VW) to the activation and reaction gases. A detailed description of the reactor and saturator can be found in Sections 5.3.1.1 and 5.3.1.3, respectively. All valves and tubes inside the dotted frame were heated electrically to 140 °C to avoid condensation of the reactants or products. The controlling and regulation of the temperatures was realized by means of LabVIEW programmed PID controllers. Valves, which are not mentioned in the description, are normally closed and do not serve a specific purpose in the following procedure descriptions.

For the oxidation, reduction or carburization treatment of the catalyst precursors, according to Sections 5.1.6, 5.1.7 and 5.1.9, the following procedure was applied: (i) before each treatment, the reactor was flushed with nitrogen. To do so, valve V3 was opened, and the 4/2 valves VW1 and VW2 were set to direct the flow through the reactor, the gas sampling loop (GSL) and the cooling trap. (ii) Air, hydrogen or a methane/hydrogen mixture was chosen according to the requirements by closing V3 and turning V4 and V6 in the way to allow the flowing of the necessary gas. The flow rate was set with the needle valve N4.

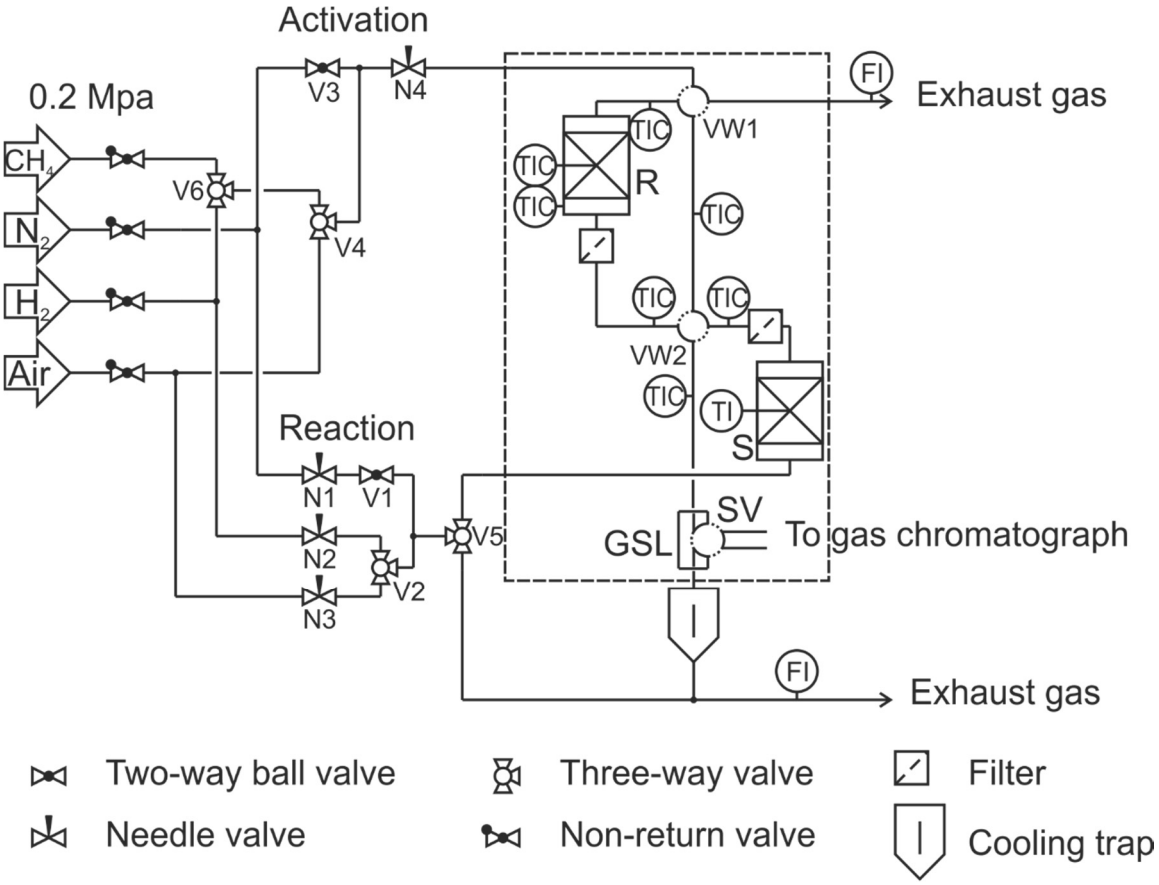

Figure 5.4: Scheme of the atmospheric-pressure apparatus (FI: flow indicator; GSL: gas sampling loop; N: needle valve; R: reactor; S: saturator; SV: 6/2 sampling valve; TI: temperature indicator; TIC: temperature indicator and controller; V: valve; VW: 4/2 valve).

Before each reaction, the complete apparatus was flushed with nitrogen and all valves were closed. Then the 4/2 valve VW1 was turned. The carrier gas was chosen by opening V1 or V2 and turning V5 to direct it to the saturator. The needle valves N1, N2 or N3 were used to regulate the flow rate. At first on its way through the apparatus, the carrier gas was loaded with the reactant hydrocarbon when passing the saturator (for more information see Section

5.3.1.1). Subsequently, the reactant gas passed the reactor. The product gas which left the reactor flowed through the gas sampling loop, where samples were taken for capillary gas chromatographic analysis, before all liquid products were condensed in the cooling trap which was held at 0 °C.

In the case of the breakthrough experiments, the reactor was substituted by the adsorber (see Section 5.3.1.3). The concentration of the adsorptiv in the gas mixture leaving the adsorber was investigated by capillary gas chromatographic analysis. For that purpose, the gases inside the gas sampling loop were periodically injected into the gas chromatograph.

5.3.1.5 Experimental Set-Up of the High-Pressure Flow-Type Apparatus

A special high-pressure flow-type apparatus was designed and constructed which allows both the catalytic hydroconversion of one single hydrocarbon and of well-defined mixtures of two or more model hydrocarbons. Main parts of the apparatus were the one-component (S2) and multi-component (S1) saturator and the reactor (R) (for details see Sections 5.3.1.1, 5.3.1.2 and 5.3.1.3). The arrangement of the main parts, tubes and valves is depicted in Figure 5.5. The saturators are located in an oven to ensure isothermal operation. The reactor and all lines are heated electrically, temperature control is accomplished with in-house LabVIEW programmed PID controllers. All parts downstream of the saturator are kept at temperatures $T > 180$ °C to avoid condensation of hydrocarbons. The heated parts of the apparatus are shown inside the dotted frame of the flow scheme in Figure 5.5. To achieve a nearly homogeneous temperature, the valves V5 to V8 and V13 were arranged inside aluminum blocks.

Starting with closed valves for the activation of a catalyst the following procedures were applied: (i) the catalyst was placed in the reactor; (ii) valve V2 was turned to high-pressure nitrogen and valve V5 was opened to pressurize the reactor with 5.0 MPa of nitrogen; (iii) V2 was closed and the pressure course was traced with a pressure indicator in order to confirm leak tightness of the reactor. Then, the nitrogen was released into the exhaust by opening valve V8 and the throttle valve V9.

When an oxidation treatment was applied to the catalyst according to Section 5.1.6, valve V4 was turned to synthetic air, and valves V5, V8 and V9 were

opened to direct the gas flow through the apparatus. The flow rate was set with the needle valve N1. After the thermal treatment of the catalyst, the whole apparatus was flushed with nitrogen, simply by closing valve V4 and opening valve V3.

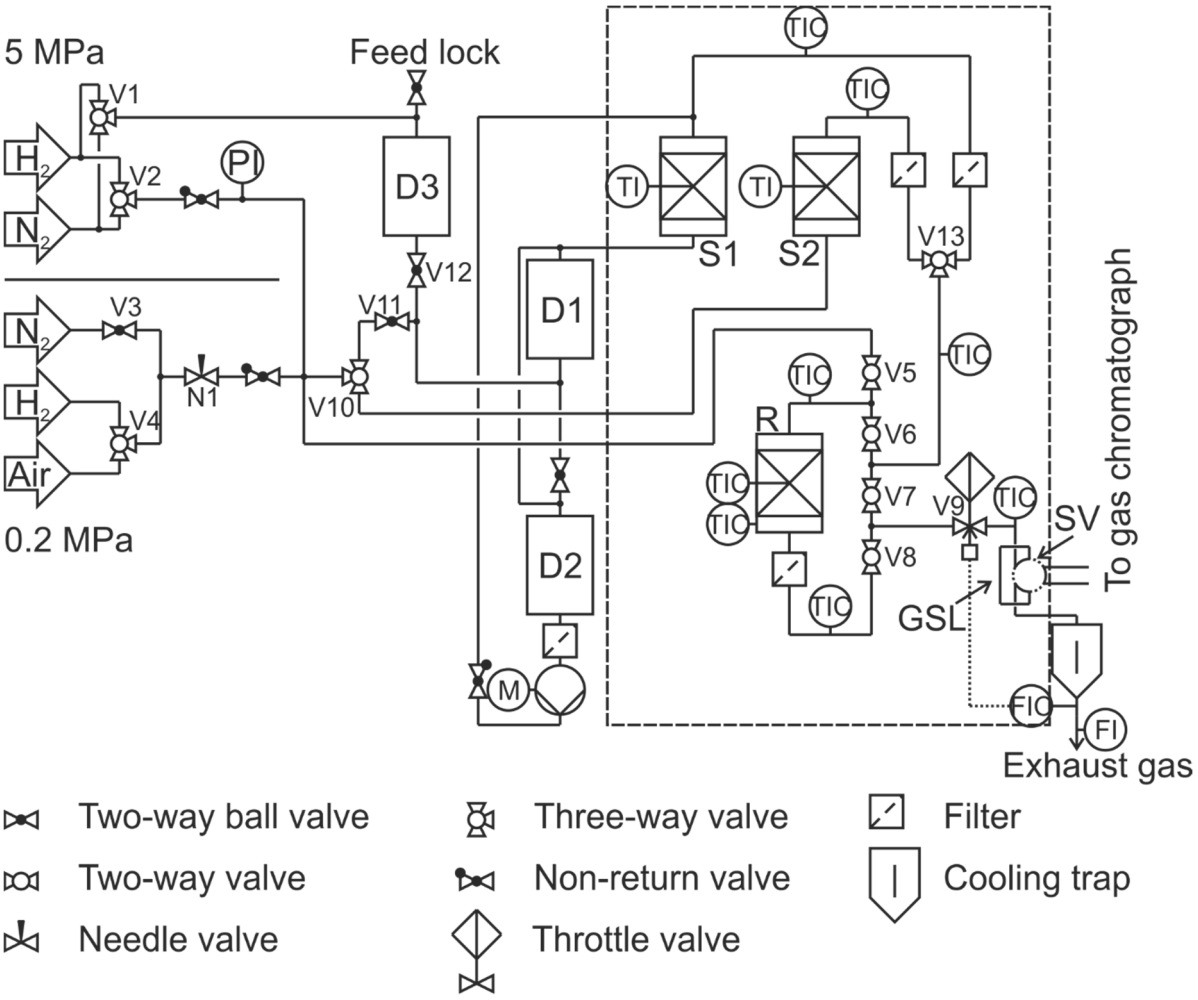

Figure 5.5: Scheme of the high-pressure flow-type apparatus used for the catalytic hydroconversion of cis-decalin and n-decane (D: vessel; FI: flow indicator; FIC: flow indicator and controller; GSL: gas sampling loop; M: motor; N: needle valve; PI: pressure indicator; R: reactor; S: saturator; SV: 6/2 sampling valve; TI: temperature indicator; TIC: temperature indicator and controller; V: valve).

The reduction of the catalysts was performed under pressurized conditions. For that purpose, hydrogen (5.0 MPa) was directed through the reactor by turning V2 to hydrogen and opening the valves V5 and V8. The flow rate of hydrogen was controlled with the pneumatic throttle valve V9 which was linked to a flow indicator. Hence, with such a setting it was possible to keep the hydrogen flow constant during the thermal treatment of the catalyst.

For the catalytic experiments, high-pressure hydrogen (5.0 MPa) was used by turning V2 to hydrogen and directing the flow through one of both saturators. The choice was made by turning valve V10 into the proper position. In addition, the three-way valve V13 was turned to the same saturator. The reactant gas flow, which was generated by passing the carrier gas through one of the saturators, was subsequently directed into the reactor by opening valve V6. The product gas flow left the reactor *via* valve V8 and was depressurized by the throttle valve V9. After V9, the product gas flow was at atmospheric pressure and passed through the gas sampling loop of the on-line gas chromatograph. A sample of the products was taken after more than 2 h at each reaction temperature to be quantitatively analyzed by means of capillary gas chromatography. Before leaving the apparatus through the exhaust gas line, liquid products were condensed in the cooling trap at 0 °C. These products were collected and analyzed additionally by GC/MS.

5.3.2 Catalytic Hydroconversion of cis-Decalin and n-Decane

5.3.2.1 Conditions in the Catalytic Hydroconversion of cis-Decalin

In all experiments with pure cis-decalin as feed hydrocarbon (purity 97.4 wt.-%; impurities: trans-decalin 0.9 wt.-%; unknown compounds 1.7 wt.-%), the mass of dry catalyst was between 0.16 and 0.21 g. The reaction temperature was varied between 220 and 440 °C. Throughout the experiments, the total pressure was 5.0 MPa, while the cis-decalin partial pressure at the reactor entrance was 19 kPa corresponding to a saturator temperature of 125 °C. The *LHSV* (Liquid Hourly Space Velocity) assumed values between 0.3 and 0.4 h^{-1}.

5.3.2.2 Conditions in the Catalytic Hydroconversion of n-Decane

In the experiments with pure n-decane as feed hydrocarbon (purity 99.7 wt.-%; impurities: unknown compounds 0.3 wt.-%), the mass of dry catalyst was between 0.18 and 0.21 g. The reaction temperature was varied between 220 and 360 °C. A total pressure of 5.0 MPa was applied throughout, while the n-decane partial pressure at the reactor entrance was 19 kPa corresponding to a saturator temperature of 109 °C. The *LHSV* (Liquid Hourly Space Velocity) assumed values between 0.3 and 0.4 h^{-1}.

5.3.2.3 Conditions in the Competitive Hydroconversion of cis-Decalin and n-Decane

An equimolar mixture of cis-decalin (49 to 50 mol-% plus *ca.* 1 mol-% trans-decalin) and n-decane (49 to 50 mol-%) was used as feed in the competitive hydroconversion experiments. The purity of the feed mixture [($\dot{m}_{\text{c-Dec}} + \dot{m}_{\text{tr-Dec}} + \dot{m}_{\text{n-De}}$)/ $\dot{m}_{\text{total hydrocarbons}}$] was 99.5 wt.-%. The mass of dry catalyst was between 0.18 and 0.21 g. The reaction temperature was varied between 200 and 440 °C. The total pressure was 5.0 MPa, while the partial pressure of cis-decalin and n-decane at the reactor entrance amounted to 19 kPa each. The saturator was held at a temperature of 137 °C. The volumetric flow rate of hydrogen (referenced to 25 °C and 0.10 MPa) and the *LHSV* were, respectively, 130 $cm^3 \cdot min^{-1}$ and between 0.3 and 0.4 h^{-1} for each feed hydrocarbon. The composition of the liquid phase pumped through the multicomponent saturator was 63.1 mol-% decalin (cis and trans) and 36.9 mol-% n-decane. This composition was reached by experimental fine-tuning of the values calculated using Raoult's law for the cis-decalin/n-decane system and Poynting's correction for the elevated hydrogen pressures (for more information about the calculation see Section 5.3.1.2, page 74).

5.3.2.4 Conditions in the Competitive Adsorption of cis-Decalin and n-Decane

For the competitive adsorption of cis-decalin and n-decane, an equimolar mixture of the two hydrocarbons was generated in the gas phase, according to the procedure described in the previous section. The following parameters were applied: total pressure of 0.1 MPa, an adsorber temperature of 100 °C, a saturator temperature of 62 °C, a liquid composition of 63.2 mol-% decalin (cis and trans) and 36.8 mol-% n-decane, a hydrogen flow rate of 400 $cm^3 \cdot min^{-1}$ and a mass of dry adsorbent of 400 to 410 mg. Under these conditions each hydrocarbon possesses a partial pressure of 0.60 kPa. The particle size of the adsorbents were between 215 and 320 µm. The adsorbent was exposed to the H_2/cis-decalin/n-decane gas stream for 25 min, and samples of the gas stream leaving the adsorber were injected every 77 s into an on-line gas chromatograph for analysis.

5.3.3 Generation of a Mixture of iso-Decanes

A mixture of iso-decanes was generated by isomerization of n-decane at 0.1 MPa on the bifunctional catalyst 0.49Pt/$H_{0.55}$,$Na_{0.45}$-Y which was provided by Dr. Sandra Rabl. 0.4 g of dry catalyst were activated in the reactor of the atmospheric-pressure apparatus depicted in Figure 5.4 by heating it up in a hydrogen flow of 100 $cm^3 \cdot min^{-1}$ from room temperature to 400 °C with 5 °C·min^{-1}. The final temperature was held for 2 h before the reactor was cooled down to the reaction temperature of 292 °C. The conditions in the catalytic experiments were as follows: hydrogen flow of 130 $cm^3 \cdot min^{-1}$, saturator temperature 52 °C, mass flow of n-decane of 109 mg·h^{-1}. The *LHSV* amounted to 0.19 h^{-1}. The liquid products were collected in a cooling trap which was held at 0 °C.

5.4 Product Analysis by Capillary Gas Chromatography

5.4.1 On-line Gas Chromatography

The quantitative composition of the reaction products was determined by means of an Agilent 7890A capillary gas chromatograph which was controlled by a PC with an Agilent Chemstation software which executed the signal recording and analysis. The detailed analytical conditions are listed in Table 5.4. By switching a gas sampling valve, the samples were flushed from a sample loop into the gas chromatograph.

Table 5.4: Properties of the gas chromatograph for the on-line sample analyses.

Column	Petrocol DH 150
Stationary phase	Dimethyl polysiloxane
Length	150 m
Internal diameter	0.25 mm
Film thickness	1.0 µm
Temperature program	10 min at 35 °C; heating with 1 °C·min^{-1} to 100 °C; heating with 0.5 °C·min^{-1} to 140 °C; hold for 1 min
Carrier gas	Hydrogen
Constant flow through column	1.5 cm^3·min^{-1}
Injection	*via* gas sampling loop
Volume of sampling loop	250 µl
Split ratio	5 : 1
Injector temperature	250 °C
Detector	Flame ionization detector (FID)
Temperature	250 °C
$\dot{V}_{H_2}$ to FID	35 cm^3·min^{-1}
$\dot{V}_{air}$ to FID	350 cm^3·min^{-1}

5.4.2 Off-line Gas Chromatography / Mass Spectrometry

The liquid product samples which were collected in the cooling trap were analyzed qualitatively by means of an Agilent 6890N capillary gas chromatograph which was coupled with an Agilent 5975B mass spectrometer.

With the information about the molar mass of the products thereby gained, it was possible to attribute most of them to the distinct product groups.

Table 5.5: Properties of the gas chromatograph for the off-line sample analyses.

Column	Petrocol DH 150
Stationary phase	Dimethyl polysiloxane
Length	150 m
Internal diameter	0.25 mm
Film thickness	1.0 µm
Temperature program	10 min at 35 °C; heating with 1 °C·min^{-1} to 100 °C; heating with 0.5 °C·min^{-1} to 160 °C; hold for 1 min
Carrier gas	Hydrogen
Constant flow through column	1.3 cm^3·min^{-1}
Injection	*via* syringe
Volume of injection	0.1 µl
Split ratio	5 : 1
Injector temperature	250 °C
Detector	Flame ionization detector (FID)
Temperature	250 °C
$\dot{V}_{H_2}$ to FID	35 cm^3·min^{-1}
$\dot{V}_{air}$ to FID	350 cm^3·min^{-1}
Mass spectrometer	Electron ionization
Acceleration voltage	70 eV
Temperature of ion source	230 °C
Temperature of quadrupole analyzer	150 °C
Mode	Total ion

5.5 Evaluation of the Catalytic Experiments

5.5.1 Terminology of the Reactions and Products

The product mixtures obtained in the hydroconversion of hydrocarbons become more and more complex with increasing number of carbon atoms of

the feed. For the evaluation of the results of the catalytic conversion, it is convenient to classify the individual hydrocarbons formed into product groups, as shown in the subsequent Tables 5.6 to 5.8.

5.5.1.1 Hydroconversion of n-Decane

In the n-decane hydroconversion three groups of products were observed. In Table 5.6, these product groups and the reactions leading to them are listed along with their molecular formulae, molar masses, and short designations.

Table 5.6: Reactions and product groups in the catalytic hydroconversion of n-decane (n-De).

Reaction	**Products**	**Formula**	**Molar mass / g·mol^{-1}**	**Short designation**
Isomerization	Skeletal isomers	$C_{10}H_{22}$	142	sk-Isos
Dehydrocyclization	Ring-closure products/one-ring naphthenes	$C_{10}H_{20}$	140	RCPs
Hydrocracking	Hydrocarbons with less than 10 carbon atoms	C_nH_{2n+2} ($n \leq 9$)	≤ 128	C_9-

5.5.1.2 Hydroconversion of cis-Decalin

In the cis-decalin hydroconversion under the conditions used in this work, five groups of products were formed. In Table 5.7 these product groups and the reactions leading to them are listed together with their molecular formulae, molar masses, and short designations.

Table 5.7: Reactions and product groups in the catalytic hydroconversion of cis-decalin (c-Dec).

Reaction	**Products**	**Formula**	**Molar mass / g·mol^{-1}**	**Short designation**
Isomerization	trans-Decalin	$C_{10}H_{18}$	138	tr-Dec
	Skeletal isomers			sk-Isos
Ring opening	Ring-opening products	$C_{10}H_{20}$	140	ROPs
	Alkylcyclohexanes			
	Alkylcyclopentanes			
Double ring opening	Open-chain decanes	$C_{10}H_{22}$	142	OCDs
Dehydrogenation	Dehydrogenated products			DHPs
	Tetralin	$C_{10}H_{12}$	132	
	Naphthalene	$C_{10}H_{8}$	128	
Hydrocracking	Hydrocarbons with less than 10 carbon atoms	C_nH_{2n+a} [1)] ($n \leq 9$)	≤ 128	C_9-

[1)] a = 0 for naphthenic cracked products and a = 2 for aliphatic cracked products

5.5.1.3 Hydroconversion of Decalin/n-Decane Mixtures

The product hydrocarbons observed in the hydroconversion of decalin/n-decane mixtures were classified in the same manner as those of the hydroconversion of cis-decalin (Table 5.7) with one exception: n-decane was not classified as an open-chain decane, since it is a reactant. The complete classification of products in the hydroconversion of decalin/n-decane mixtures is listed in Table 5.8.

Table 5.8: Reactions and product groups in the catalytic hydroconversion of decalin/n-decane mixtures.

Reaction	**Products**	**Formula**	**Molar mass / g·mol^{-1}**	**Short designation**
Isomerization	trans-Decalin Skeletal isomers	$C_{10}H_{18}$	138	tr-Dec sk-Isos
Ring opening	Ring-opening products Alkylcyclohexanes Alkylcyclopentanes	$C_{10}H_{20}$	140	ROPs
Double ring opening	Open-chain decanes except n-decane	$C_{10}H_{22}$	142	OCDs
Dehydrogenation	Dehydrogenated products			DHPs
	Tetralin	$C_{10}H_{12}$	132	
	Naphthalene	$C_{10}H_8$	128	
Hydrocracking	Hydrocarbons with less than 10 carbon atoms	C_nH_{2n+a} [1)] ($n \leq 9$)	≤ 128	C_9-

[1)] a = 0 for naphthenic cracked products and a = 2 for aliphatic cracked products

5.5.2 Assignment of the GC Signals

It is a salient feature of n-decane hydroconversion and, especially, of cis-decalin hydroconversion that a large number of individual product hydrocarbons can be formed. Under certain reaction conditions, the number of products may exceed 200. The Petrocol DH 150 capillary column used in this work turned out to be particularly suitable for the separation of such complex hydrocarbon mixtures. Usually, adjacent peaks were well resolved, even in the critical region of ring-opening products, *i.e.*, C_{10} hydrocarbons with a single naphthenic ring, and open-chain decanes. For assignment of the peaks thus separated, coupling of capillary gas chromatography and mass spectrometry of the liquid product samples was routinely used. This method furnished, *inter alia*, the molar mass of the hydrocarbon generating the peak, and hence its

classification into one of the product groups. To verify these classifications and in an attempt to identify the precise molecular structure of the C_{10} hydrocarbon, the following ancillary methods were used:

- Relevant hydrocarbons were purchased whenever they were commercially available and co-injected into the gas chromatograph together with the liquid product sample;
- Based on earlier work in the group on catalytic isomerization of n-decane and methylnonanes [29,131], mixtures of iso-decanes *of known compositions* were prepared and co-injected into the gas chromatograph together with the liquid product sample. This method turned out to be very valuable for the safe assignment of peaks originating from open-chain decanes, the most desirable products of a possible ring-opening process.

5.5.3 Conversion, Yield and Selectivity

5.5.3.1 Calculation of Conversion, Yield, Selectivity and Modified Hydrocracking Selectivity in the Single-Feed Experiments

Conversions X_{feed}, yields Y_j and selectivities S_j in the fixed-bed reactors were calculated according to the general Eqs. (5.8) to (5.10) for hydroconversion of the pure feeds decalin and n-decane.

$$X_{feed} = \frac{(\dot{n}_{feed})_{in} - (\dot{n}_{feed})_{out}}{(\dot{n}_{feed})_{in}} \tag{5.8}$$

$$Y_j = \frac{(\dot{n}_j)_{out} - (\dot{n}_j)_{in}}{(\dot{n}_{feed})_{in}} \cdot \frac{|v_{feed}|}{v_j} \tag{5.9}$$

$$S_j = \frac{(\dot{n}_j)_{out} - (\dot{n}_j)_{in}}{(\dot{n}_{feed})_{in} - (\dot{n}_{feed})_{out}} \cdot \frac{|v_{feed}|}{v_j} \tag{5.10}$$

In these equations v is the stoichiometric factor in the following reaction:

$$v_{feed} \cdot \dot{n}_{C,\,feed} \rightarrow v_j \cdot \dot{n}_{C,\,j}$$

The above equations (5.8) to (5.10) had to be adapted to the on-line analysis of the reaction products contained in the gas sampling loop (GSL) [132] of the

gas chromatograph (see Figure 5.5). The molar amount of a product j $(n_j)_{GSL}$ in the gas sampling loop at the time of sampling was calculated by Eq. (5.11)

$$(n_j)_{GSL} = \frac{(m_j)_{GSL}}{M_j} = \frac{s \cdot k_j \cdot A_j}{M_j} \tag{5.11}$$

Where A_j denotes the area of the peak generated by the product j and M_j is its molar mass. s and k_j are, respectively, an instrument-specific factor expressing the absolute sensitivity of the detector and the compound-specific correction factor (dimensionless) for hydrocarbon j. For hydrocarbons, the numeric values of k_j are usually referenced to benzene ($k_{Bz} \equiv 1$) [132]. The value of k_j for any other hydrocarbon can be calculated [132] by using Eq. (5.12).

$$k_j = \frac{\frac{M_j}{M_{C,j}}}{\frac{M_{Bz}}{M_{C,Bz}}} = \frac{\frac{M_j}{M_{C,j}}}{1.083} \tag{5.12}$$

Here, M_j is the molar mass of hydrocarbon j and $M_{C,j}$ is the molar mass of the contained carbon atoms of hydrocarbon j.

For solving Eqs. (5.8) to (5.10), a method for the calculation of the molar amount of the feed entering the reactor is necessary, since a direct measurement of this quantity is not possible. The method was based on a retroactive accounting: the feed originally entering the reactor $(n_{feed})_{GSL\ at\ X\ =\ 0}$ was calculated by addition of the measurable amount of non-converted feed $(n_{feed})_{GSL}$ and the amount of feed needed for making the reaction products (see Eq. (5.13)).

$$(n_{feed})_{GSL\ at\ X\ =\ 0} = (n_{feed})_{GSL} + s \cdot \sum_j \frac{k_j \cdot A_j}{M_j} \cdot \frac{|v_{feed}|}{v_j} \tag{5.13}$$

Substituting in Eqs. (5.8) to (5.10) $(\dot{n}_{feed})_{in}$ by $(n_{feed})_{GSL\ at\ X\ =\ 0}$ and $(\dot{n}_{feed})_{out}$ by $(n_{feed})_{GSL}$ results in Eqs. (5.14) to (5.16). Substitution of the molar flow by the molar amount in the gas sampling loop is allowed in the case of stationary behavior. Note that for evaluating the yields and selectivities (Eqs. (5.9) and (5.10), respectively) $(\dot{n}_j)_{in}$ was set zero, because no product hydrocarbons were entering the reactor.

$$X_{feed} = \frac{(n_{feed})_{GSL\ at\ X=0} - (n_{feed})_{GSL}}{(n_{feed})_{GSL\ at\ X=0}} = \frac{\sum_j \frac{k_j \cdot A_j}{M_j} \cdot \frac{|v_{feed}|}{v_j}}{\frac{k_{feed} \cdot A_{feed}}{M_{feed}} + \sum_j \frac{k_j \cdot A_j}{M_j} \cdot \frac{|v_{feed}|}{v_j}} \quad (5.14)$$

$$Y_j = \frac{(n_j)_{GSL}}{(n_{feed})_{GSL\ at\ X=0}} \cdot \frac{|v_{feed}|}{v_j} = \frac{\frac{k_j \cdot A_j}{M_j}}{\frac{k_{feed} \cdot A_{feed}}{M_{feed}} + \sum_j \frac{k_j \cdot A_j}{M_j} \cdot \frac{|v_{feed}|}{v_j}} \cdot \frac{|v_{feed}|}{v_j} \quad (5.15)$$

$$S_j = \frac{(n_j)_{GSL}}{(n_{feed})_{GSL\ at\ X=0} - (n_{feed})_{GSL}} \cdot \frac{|v_{feed}|}{v_j} = \frac{\frac{k_j \cdot A_j}{M_j}}{\sum_j \frac{k_j \cdot A_j}{M_j} \cdot \frac{|v_{feed}|}{v_j}} \cdot \frac{|v_{feed}|}{v_j} \quad (5.16)$$

In the catalytic hydroconversion of decalin or n-decane, not only hydrocarbons with 10 carbon atoms are formed, but also hydrocracked products with 1 to 9 carbon atoms (*cf.* Tables 5.6 and 5.7). Often, valuable information about the reaction mechanism can be deduced from their distribution in terms of carbon numbers. The modified hydrocracking selectivity S_j^* will be used for that purpose. It is defined as the molar amounts of hydrocarbons with a given carbon number formed (C_1 to C_9) divided by the molar amount of feed (decalin or n-decane) converted into hydrocracked products with less than 10 carbon atoms (see Eq. 5.17).

$$S_j^* = \frac{(\dot{n}_j)_{out}}{(\dot{n}_{feed})_{converted\ to\ C_9-}} = \frac{(n_j)_{GSL}}{(n_{feed})_{GSL,\ converted\ to\ C_9-}} = \frac{\frac{k_j \cdot A_j}{M_j}}{\sum_j \frac{k_j \cdot A_j}{M_j} \cdot \frac{|v_{feed}|}{v_j}} \quad (5.17)$$

5.5.3.2 Calculation of Conversion, Yield and Selectivity in the Competitive Hydroconversion of cis-Decalin and n-Decane

The calculation of conversions, yields and selectivities of the multi-component feed experiments are closely related to the ones described in Section 5.5.3.1, page 89. Following the same principle, the mass balance equations (Eq. (5.18)) are based on the identical retroactive accounting method described in the previous section.

$$(n_{Dec} + n_{n\text{-}De})_{GSL\ at\ X\,=\,0} = (n_{Dec} + n_{n\text{-}De})_{GSL} + s \cdot \sum_j \frac{k_j \cdot A_j}{M_j} \cdot \frac{|v_{feed}|}{v_j} \qquad (5.18)$$

Starting from the general Eq. (5.19), a calculation of the total conversion X_{Total}, which is the conversion related to both reactants, is possible by substitution of the molar flows by the measured and calculated feed amounts in the gas sampling loop (see Eq. (5.20)).

$$X_{Total} = \frac{(\dot{n}_{Dec} + \dot{n}_{n\text{-}De})_{in} - (\dot{n}_{Dec} + \dot{n}_{n\text{-}De})_{out}}{(\dot{n}_{Dec} + \dot{n}_{n\text{-}De})_{in}} \qquad (5.19)$$

$$X_{Total} = \frac{(n_{Dec} + n_{n\text{-}De})_{GSL\ at\ X\,=\,0} - (n_{Dec} + n_{n\text{-}De})_{GSL}}{(n_{Dec} + n_{n\text{-}De})_{GSL\ at\ X\,=\,0}} \qquad (5.20)$$

The yields can be calculated by using Eq. (5.21) which was adapted to the multi-component feed mixture. The molar fluxes had to be substituted by the amounts of reactants and products in the gas sampling loop before and after the reaction.

$$Y_j = \frac{(\dot{n}_j)_{out} - (\dot{n}_j)_{in}}{(\dot{n}_{Dec} + \dot{n}_{n\text{-}De})_{in}} \cdot \frac{|v_{feed}|}{v_j} \qquad (5.21)$$

Setting $(\dot{n}_j)_{in} = 0$ since no component j enters the reactor and substituting $(\dot{n}_{Dec} + \dot{n}_{n\text{-}De})_{in}$ by $(n_{Dec} + n_{n\text{-}De})_{GSL\ at\ X\,=\,0}$ leads to Eq. (5.22).

$$Y_j = \frac{(n_j)_{GSL}}{(n_{Dec} + n_{n\text{-}De})_{GSL\ at\ X\,=\,0}} \cdot \frac{|v_{feed}|}{v_j} \qquad (5.22)$$

Analogously, the product selectivities are calculated using Eqs. (5.23) and (5.24).

$$S_j = \frac{(\dot{n}_j)_{out} - (\dot{n}_j)_{in}}{(\dot{n}_{Dec} + \dot{n}_{n\text{-}De})_{in} - (\dot{n}_{Dec} + \dot{n}_{n\text{-}De})_{out}} \cdot \frac{|v_{feed}|}{v_j} \qquad (5.23)$$

$$S_j = \frac{(n_j)_{GSL}}{(n_{Dec} + n_{n\text{-}De})_{GSL\ at\ X\,=\,0} - (n_{Dec} + n_{n\text{-}De})_{GSL}} \cdot \frac{|v_{feed}|}{v_j} \qquad (5.24)$$

It is, *a priori*, unknown from which of the two reactants (decalin or n-decane) a given product j has been formed. In all these cases, the yields and selectivities can only be calculated related to the total conversion.

By contrast, partial conversions of the two reactants can be calculated: First, the molar amounts of cis-decalin and n-decane in the gas sampling loop at zero conversion are calculated according to Eq. (5.18). Since the composition of the reactant mixture is known, the total molar amount at zero conversion can be broken down into the partial molar amounts of each feed hydrocarbon. For the special case of an equimolar mixture of cis-decalin and n-decane Eq. (5.25) holds:

$$(n_{Dec})_{GSL\ at\ X\ =\ 0} = (n_{n\text{-}De})_{GSL\ at\ X\ =\ 0} = (0.5n)_{GSL\ at\ X\ =\ 0} \tag{5.25}$$

Based on the above equation, partial conversions for each feed hydrocarbon can be calculated as described in Eq. (5.8) in Section 5.5.3.1 on page 89.

5.5.4 Calculation of Theoretical Selectivities in the Mixed-Feed Experiments

For the investigation of the influence of a second hydrocarbon on the product selectivities, theoretical selectivities were calculated. The selectivity of a product j in the mixed-feed experiments is defined as its yield divided by the total conversion (see Eq. (5.26)).

$$S_{j,mix} = \frac{Y_{j,mix}}{X_{Total}} \tag{5.26}$$

When two hydrocarbons, *viz.* decalin and n-decane, are used as feed, the total conversion X_{Total} can be calculated from the partial conversions $X_{Dec,mix}$ and $X_{n\text{-}De,mix}$ as shown in Eq. (5.27). The ratio of the molar flows of the feeds entering the reactor is necessary for the weighing of the respective conversion.

$$X_{Total} = \frac{(\dot{n}_{Dec})_{in}}{(\dot{n}_{Dec})_{in} + (\dot{n}_{n\text{-}De})_{in}} \cdot X_{Dec,mix} + \frac{(\dot{n}_{n\text{-}De})_{in}}{(\dot{n}_{Dec})_{in} + (\dot{n}_{n\text{-}De})_{in}} \cdot X_{n\text{-}De,mix} \tag{5.27}$$

Theoretically, product yields $Y_{j,mix}$ can be calculated if their selectivities are known and if it is possible to attribute them directly to the feed from which they originate. This would allow the calculation of $Y_{j,mix}$ according to Eq. (5.28). In this equation $S_{j,Dec,mix}$ and $S_{j,n\text{-}De,mix}$ stand for the product selectivity of the

product j obtained from the hydroconversion of decalin or n-decane, respectively.

$$Y_{j,mix} = \frac{(\dot{n}_{Dec})_{in}}{(\dot{n}_{Dec})_{in} + (\dot{n}_{n\text{-}De})_{in}} \cdot X_{Dec,mix} \cdot S_{j,Dec,mix} + \frac{(\dot{n}_{n\text{-}De})_{in}}{(\dot{n}_{Dec})_{in} + (\dot{n}_{n\text{-}De})_{in}} \cdot X_{n\text{-}De,mix} \cdot S_{j,n\text{-}De,mix} \tag{5.28}$$

The substitution of Eqs. (5.27) and (5.28) into Eq. (5.26) results in Eq. (5.29).

$$S_{j,mix} = \frac{\frac{(\dot{n}_{Dec})_{in}}{(\dot{n}_{Dec})_{in} + (\dot{n}_{n\text{-}De})_{in}} \cdot X_{Dec,mix} \cdot S_{j,Dec,mix} + \frac{(\dot{n}_{n\text{-}De})_{in}}{(\dot{n}_{Dec})_{in} + (\dot{n}_{n\text{-}De})_{in}} \cdot X_{n\text{-}De,mix} \cdot S_{j,n\text{-}De,mix}}{\frac{(\dot{n}_{Dec})_{in}}{(\dot{n}_{Dec})_{in} + (\dot{n}_{n\text{-}De})_{in}} \cdot X_{Dec,mix} + \frac{(\dot{n}_{n\text{-}De})_{in}}{(\dot{n}_{Dec})_{in} + (\dot{n}_{n\text{-}De})_{in}} \cdot X_{n\text{-}De,mix}} \tag{5.29}$$

For an equimolar feed stream Eq. (5.30) holds. This allows the elimination of the molar flows in Eq. (5.29). Hence, Eq. (5.31) can be directly obtained from Eq. (5.29).

$$(\dot{n}_{Dec})_{in} = (\dot{n}_{n\text{-}De})_{in} \tag{5.30}$$

$$S_{j,mix} = \frac{X_{Dec,mix} \cdot S_{j,Dec,mix} + X_{n\text{-}De,mix} \cdot S_{j,n\text{-}De,mix}}{X_{Dec,mix} + X_{n\text{-}De,mix}} \tag{5.31}$$

If product selectivities are assumed to be only depending on the degree of conversion of the reactant, Eq. (5.31) can be modified for the calculation of theoretical mixed-feed selectivities. In the first step, partial conversions of decalin and n-decane are determined at all reaction temperatures for each of the two hydrocarbons in the mixed feed experiments. Then, for these partial conversion values, product selectivities for the same value in the respective pure-feed conversions are taken. Subsequently, the calculated mixed-feed product selectivities are obtained by replacing $S_{j,Dec,mix}$ and $S_{j,n\text{-}De,mix}$ by the respective product selectivities $S_{j,Dec}$ and $S_{j,n\text{-}De}$ from the pure feed experiments (see Eq. (5.32)).

$$S_{j,mix} = \frac{X_{Dec} \cdot S_{j,Dec} + X_{n\text{-}De} \cdot S_{j,n\text{-}De}}{X_{Dec} + X_{n\text{-}De}} \tag{5.32}$$

5.5.5 Liquid Hourly Space Velocity

Among the key parameters in heterogeneously catalyzed reactions and processes with a fixed-bed reactor is the liquid hourly space velocity (*LHSV*). It is defined as the volumetric flow rate of the reactant referenced to the liquid state at ambient temperature (see Eq. (5.33)) divided by the bulk catalyst volume.

$$LHSV = \frac{\dot{V}_{\text{reactant,liquid at ambient temperature}}}{V_{\text{bulk,cat.}}} \tag{5.33}$$

The *LHSV* was determined by weighing the content of the cooling trap (see Figure 5.5) accumulated within one hour and dividing this value by the density of the liquid feed mixture and the bulk catalyst volume. The latter amounted to 0.40 cm^3. The mass flow rates of the two hydrocarbons in the experiments with the mixed feeds were approximately 0.14 $g \cdot h^{-1}$ each or 0.28 $g \cdot h^{-1}$ for the overall mass flux, or 0.35 $cm^3 \cdot h^{-1}$ for the overall volumetric flux. The overall *LHSV* was hence *ca.* 0.88 h^{-1}.

6 Characterization of the Catalysts and their Precursors

The chemical composition of the catalysts was determined by an optical emission spectrometer with inductively coupled plasma (ICP-OES; see Section 5.2.3, page 68). A deeper insight into the carrier structure was obtained by means of MAS NMR spectroscopy (see Section 5.2.4, page 69). The ^{29}Si MAS NMR technique allows the determination of the n_{Si}/n_{Al} ratio of the zeolite framework, whereas ^{27}Al MAS NMR provides information about the coordination sphere of aluminum atoms. The strength of Brønsted acid sites was investigated by FT-IR measurements (see Section 5.2.6, page 70) with desorption of pyridine at increasing temperatures (step size 50 °C between 200 and 500 °C). By means of X-ray powder diffraction, the phase purity and crystallinity of the zeolitic carrier were investigated (see Section 5.2.1, page 68).

6.1 Characterization of the Zeolite Y Supports

It can be seen from Table 6.1 that the concentration of Brønsted acid sites was varied among the upper four carriers. The variation was obtained by ion exchange of $Na_{0.96}H_{0.04}$-Y-2.4 with ammonium nitrate as described in Section 5.1.2, page 63. By careful washing of the exchanged zeolites with water, it was ensured that no excess ions remained on the carrier. Hence, the molar amount of sodium plus ammonium ($n_{Na} + n_{NH_4} = n_{Al}$) can be assumed to equal the molar amount of aluminum in the zeolite. Ammonium ions were not detectable by ICP-OES, and therefore the composition of the charge-compensating cations have to be calculated as the molar amount of aluminum minus the molar amount of sodium. The difference to unity was assumed to represent the number of protons, since ammonium ions decompose to ammonia and protons (deammoniation) during the thermal treatment [18].

Table 6.1: Chemical composition of all zeolite carriers of the molybdenum carbide catalysts as determined by ICP-OES.

n_{Si}/n_{Al} (ICP-OES)	n_{Na}/n_{Al} (ICP-OES)	Zeolite Y Composition
2.4	0.96	$Na_{0.96},H_{0.04}$-Y-2.4
2.4	0.67	$Na_{0.67},H_{0.33}$-Y-2.4
2.4	0.38	$H_{0.62},Na_{0.38}$-Y-2.4
2.4	0.12	$H_{0.88},Na_{0.12}$-Y-2.4
6.9	0.01	$H_{0.99},Na_{0.01}$-Y-7
14.4	0.01	$H_{0.99},Na_{0.01}$-Y-14
105.3	0.08	$H_{0.92},Na_{0.08}$-Y-105

The phase purity and crystallinity of the modified Y zeolites were determined by XRD. The diffractograms of all supports are depicted in Figure 6.1. A comparison of the reflexes (6.1°, 10.2°, 12.0°, 15.9°, 19.1°, 20.5°, 23.9°) at 2Θ values given in the literature [133] shows that only the characteristic reflexes of zeolite Y are present in all samples. Furthermore, it can be seen that the reflex intensities of $H_{0.99},Na_{0.01}$-Y-7 are lower compared to those of the other samples. This is due to modification of the sample by dealumination of zeolite $H_{0.88},Na_{0.12}$-Y-2.4 which brings about a partial loss of crystallinity. A partial collapse of the zeolite framework during the dealumination with ammonium hexafluorosilicate was found previously by Garralón *et al.* [134], too. They explained the collapse with a too fast extraction of aluminum out of the framework compared to the insertion of silicon which leads to an unstable zeolite structure. A magnification of the [1 1 1] reflex (see Figure 6.2) reveals a shift to higher 2Θ values with increasing n_{Si}/n_{Al} ratio which has also been described by Karge *et al.* [135] for zeolites X and Y. The origin of this shift is seen in slightly longer Al-O bonds compared to Si-O bonds [136] which causes smaller distances of the lattice plains for the dealuminated zeolites Y, and this results in the shift of the reflexes to higher 2Θ values.

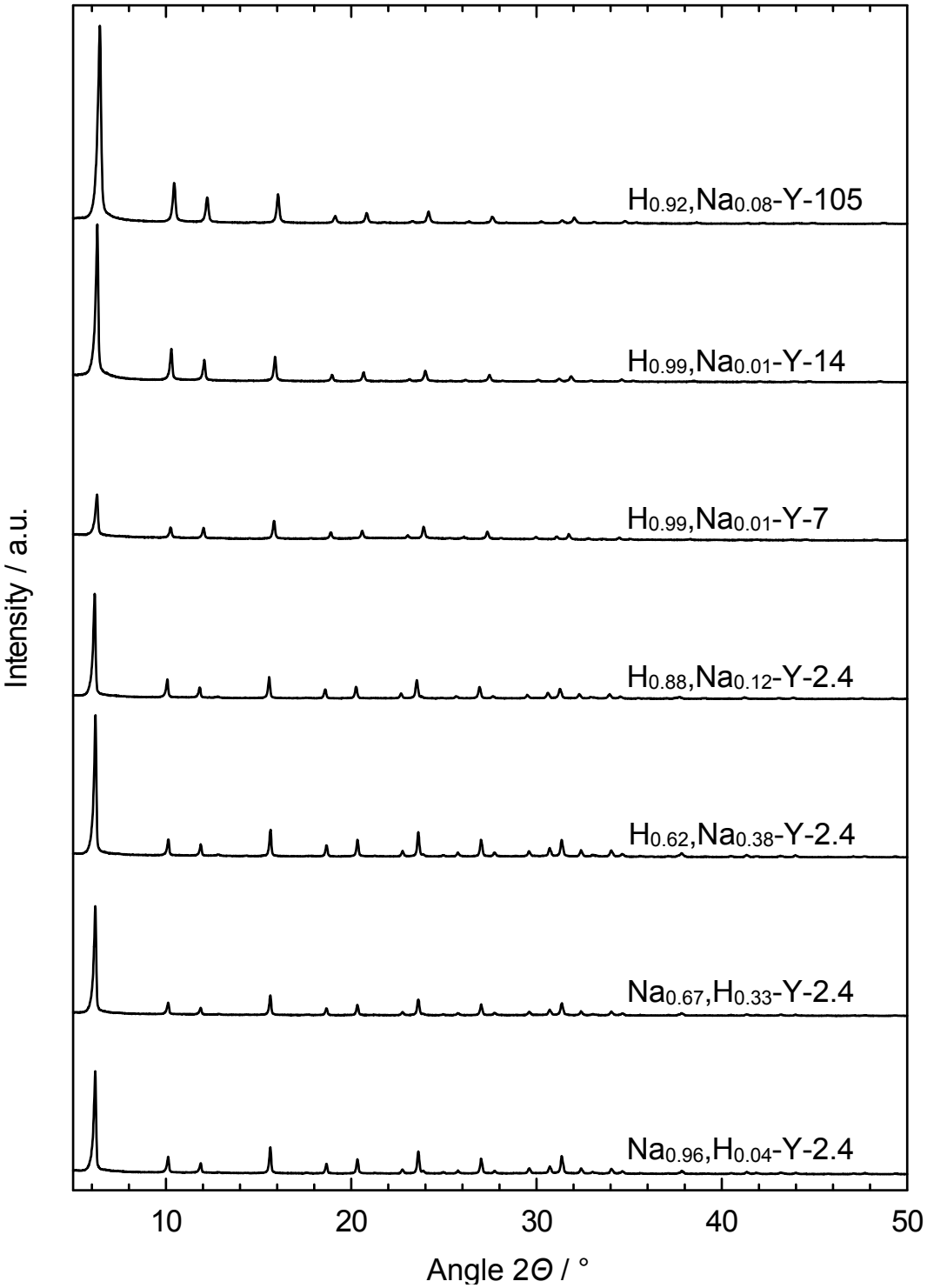

Figure 6.1: X-ray powder diffractograms of all zeolite Y supports of the molybdenum carbide catalysts used within this work.

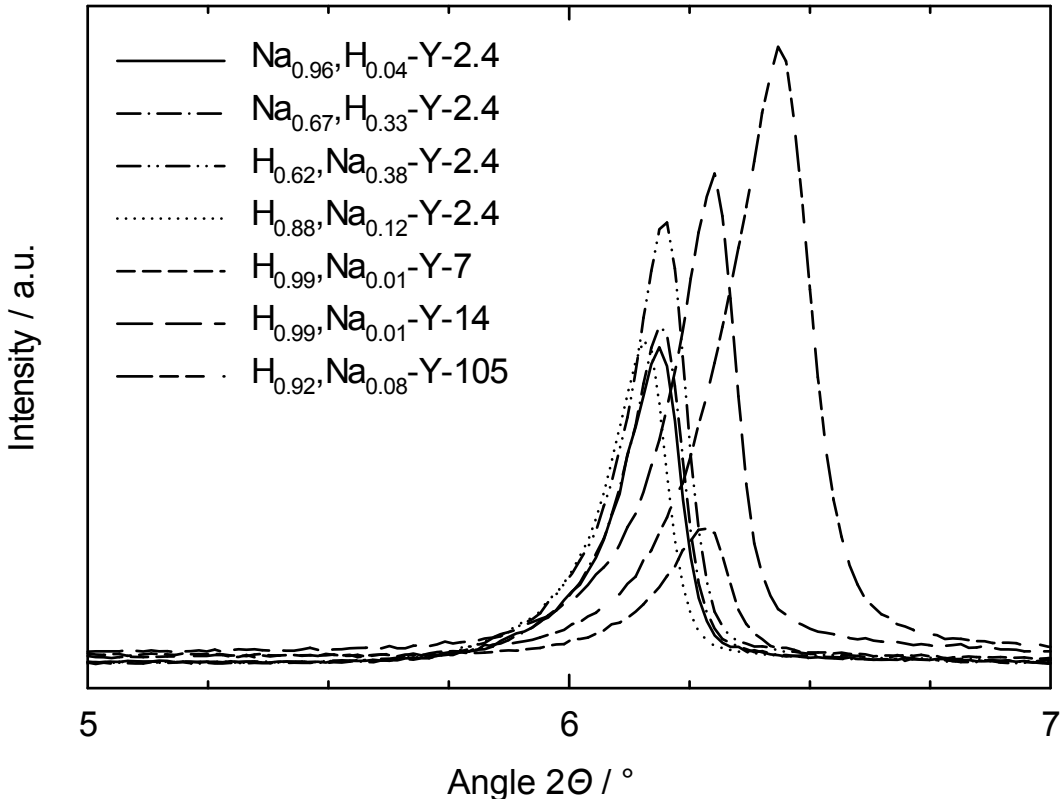

Figure 6.2: Magnification of the [1 1 1] reflex of the powder diffractograms shown in Figure 6.1.

The morphology and crystal size of all supports of the molybdenum carbide catalysts was investigated by SEM. The images are depicted in Figure 6.3. All zeolitic supports consist of crystalline small plates with diameters of *ca.* 1 µm which are agglomerated. The ion exchange of $Na_{0.96}$,$H_{0.04}$-Y-2.4 with NH_4NO_3 and the resulting different concentration of Brønsted acid sites had no influence on the morphology of the crystals (*cf.* Figure 6.3a - d). Nor is the morphology affected by dealumination with ammonium hexafluorosilicate as demonstrated for $H_{0.99}$,$Na_{0.01}$-Y-7 (Figure 6.3e), which is also true for the high-silica zeolites, as shown in Figures 6.3f and g.

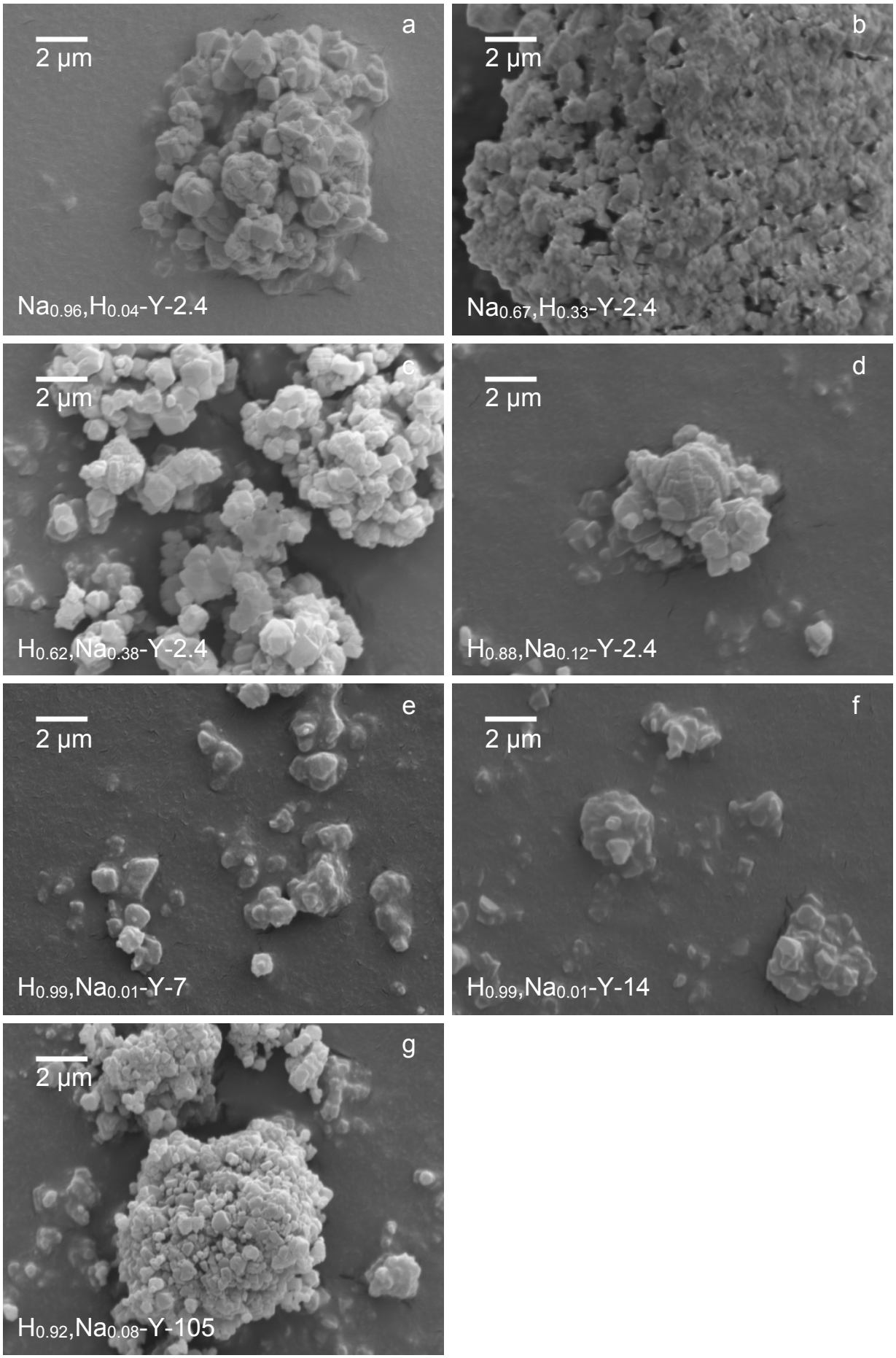

Figure 6.3: SEM images of the zeolite Y supports.

Some information about the aluminum in the samples was obtained by means of ^{27}Al MAS NMR spectroscopy. The spectra in Figure 6.4 show the occurrence of a signal at *ca.* 60 ppm which is attributed to tetrahedrally coordinated aluminum in the zeolite framework [137]. Signals originating from octahedrally coordinated aluminum at 0 ppm occurred for the sample of dealuminated $H_{0.99}$,$Na_{0.01}$-Y-7 and for the high-silica samples $H_{0.99}$,$Na_{0.01}$-Y-14 and $H_{0.92}$,$Na_{0.08}$-Y-105.

It can be concluded from the ^{27}Al MAS NMR spectra that during the ion exchange with ammonium ions, aluminum is kept at tetrahedrally coordinated framework positions. However, the dealumination treatment of the $H_{0.88}$,$Na_{0.12}$-Y-2.4 zeolite with ammonium hexafluorosilicate led to the appearance of a signal at 0 ppm which is attributed to extra-framework aluminum. Thus, aluminum was leached out of the zeolite framework. The high-silica zeolites $H_{0.99}$,$Na_{0.01}$-Y-14 and $H_{0.92}$,$Na_{0.08}$-Y-105 show only very weak signals at 0 ppm which can be a hint that aluminum has been washed out to a larger extent after the dealumination treatment by the manufacturer. Such a treatment is necessary since high-silica zeolite Y cannot be directly synthesized hydrothermally [138].

The ^{29}Si-MAS-NMR spectra of the seven zeolite Y supports are depicted in Figure 6.5. The spectra show peaks in the range from -85 to -112 ppm. Depending on their chemical shift, the peaks were attributed to silicon atoms with a different number of aluminum atoms in their first coordination sphere [139]. The more aluminum resides in the direct neighborhood, the more is the signal of the silicon shifted to positive values. Silicon with four aluminum atoms in its neighborhood can be identified by a chemical shift of -85 ppm whereas silicon without aluminum in its neighborhood is shifted to -106 ppm. Non-zeolitic amorphous silicon has a chemical shift of -112 ppm. Signal intensities and their areas are directly related to the amount of the respective silicon species. Hence, the signal intensities are shifted to lower ppm values with increasing n_{Si}/n_{Al} ratio of the support. The signal areas for each silicon species are obtained by a deconvolution of the spectra (see Table 6.2), which means a simulation of the spectrum by the additive composition of the single signals.

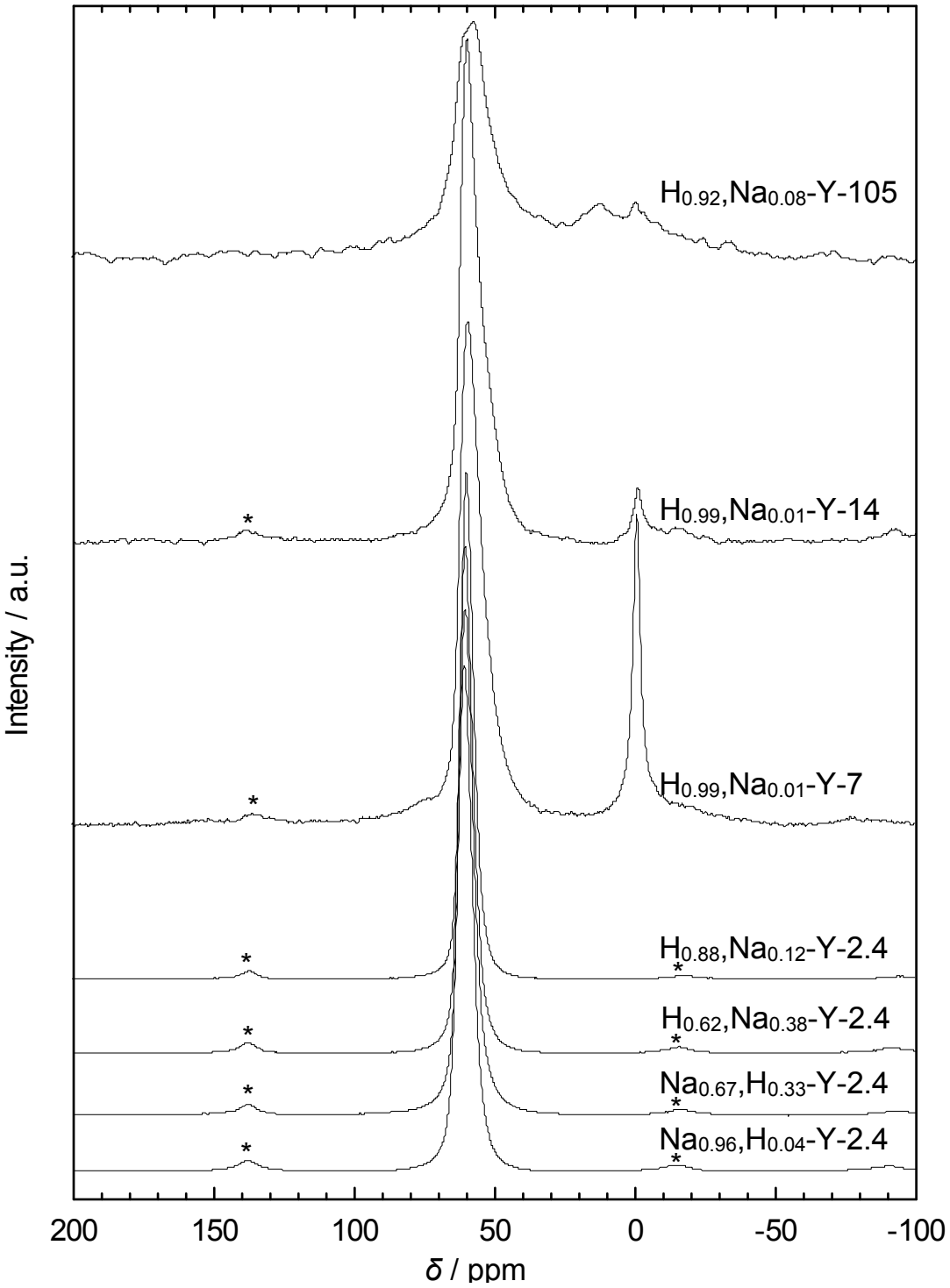

Figure 6.4: ^{27}Al MAS-NMR spectra of the zeolite Y supports of the molybdenum carbide catalysts used within this work. Asterisks denote spinning side bands.

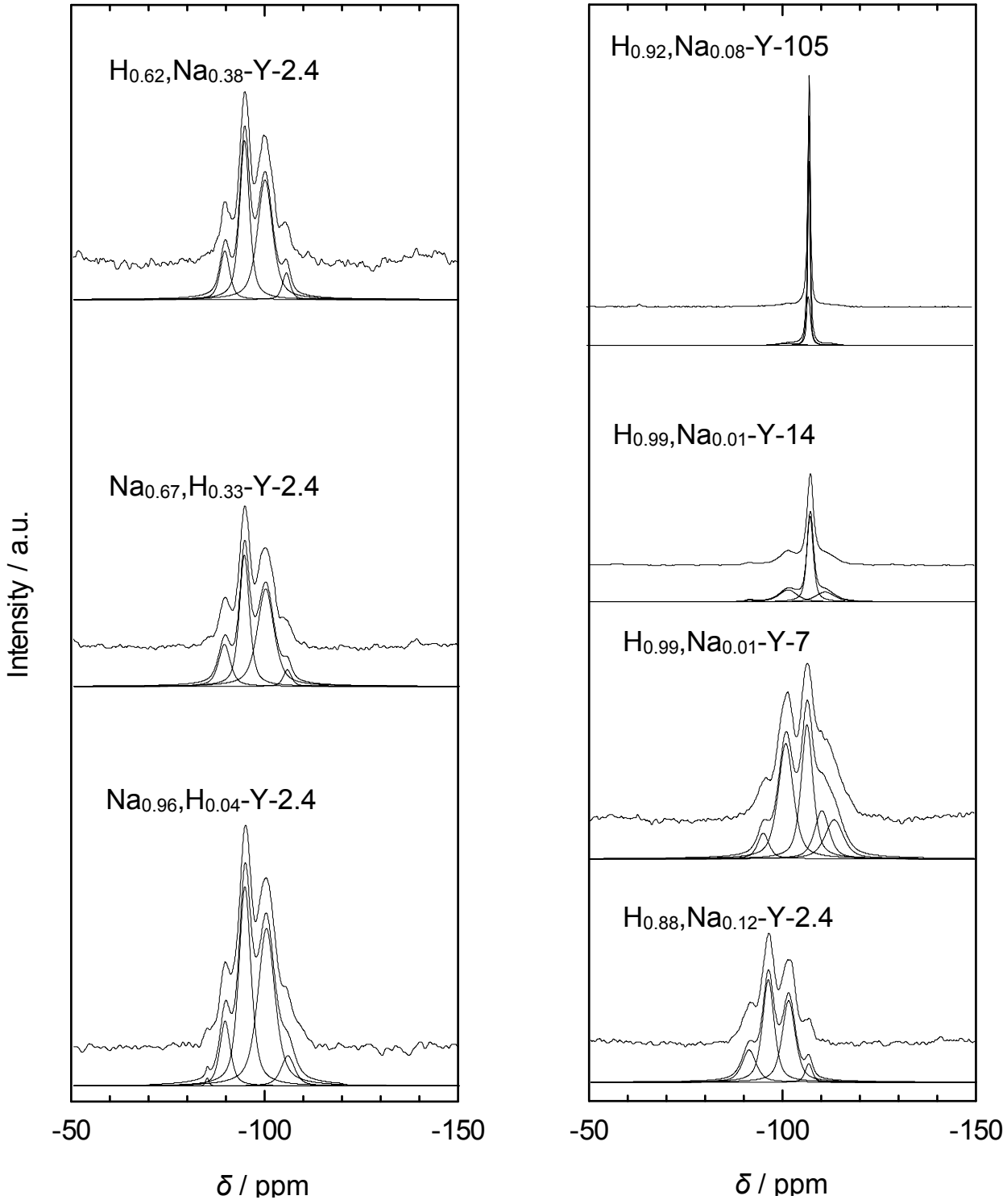

Figure 6.5: ^{29}Si MAS NMR spectra and their deconvolution of the zeolite Y supports of the molybdenum carbide catalysts used within this work.

The relative signal areas from the deconvolution of the ^{29}Si MAS NMR spectra are summarized in Table 6.2. Expectedly, with increasing n_{Si}/n_{Al} ratio of the

support, increasing areas are found for the signals which are attributed to silicon with 1 or 0 aluminum atoms in their direct neighborhood. High amounts of amorphous silicon are found for the dealuminated zeolite $H_{0.99}$,$Na_{0.01}$-Y-7, whereas the other high-silica zeolites $H_{0.99}$,$Na_{0.01}$-Y-14 and $H_{0.92}$,$Na_{0.08}$-Y-105 contain smaller amounts of amorphous silicon. As indicated by the ^{27}Al MAS NMR spectra, the amount of extra-framework aluminum was the highest for $H_{0.99}$,$Na_{0.01}$-Y-7, and the amount of amorphous silicon was the highest on the same catalyst. Hence, one can conclude that the dealumination with ammonium hexafluorosilicate tends to form amorphous silica and alumina, and this goes along with a partial collapse of the zeolite framework.

Table 6.2: Chemical shifts and signal areas of Si species [139,140] occurring in the ^{29}Si MAS NMR spectra of the seven zeolite Y supports.

Zeolite support	**Si(4Al) [ca. -85 ppm]/ %**	**Si(3Al) [ca. -89 ppm]/ %**	**Si(2Al) [ca. -94 ppm]/ %**	**Si(1Al) [ca. -100 ppm]/ %**	**Si(0Al) [ca. -106 ppm]/ %**	**amorph. Si [ca. -112 ppm]/ %**
$Na_{0.96}$,$H_{0.04}$-Y-2.4	0.45	11.12	39.25	42.56	6.62	-
$Na_{0.67}$,$H_{0.33}$-Y-2.4	-	13.98	36.87	45.33	3.82	-
$H_{0.62}$,$Na_{0.38}$-Y-2.4	-	11.61	39.09	44.11	5.18	-
$H_{0.88}$,$Na_{0.12}$-Y-2.4	-	15.82	41.88	37.65	4.65	-
$H_{0.99}$,$Na_{0.01}$-Y-7	-	-	5.80	34.59	31.52	28.08
$H_{0.99}$,$Na_{0.01}$-Y-14	-	-	1.33	22.21	57.52	18.94
$H_{0.92}$,$Na_{0.08}$-Y-105	-	-	-	7.50	89.83	2.67

With the signal areas of the silicon species from Table 6.2, n_{Si}/n_{Al} ratios of the supports are calculated according to Eq. (5.1) in Section 5.2.4, page 69. In Table 6.3, these results are compared to the data obtained from the ICP-OES measurements. While the values obtained by ICP-OES represent the bulk n_{Si}/n_{Al} ratio of the zeolite powder (amorphous and crystalline phase), the n_{Si}/n_{Al} ratio determined by ^{29}Si MAS NMR spectroscopy represents the composition of both elements in the zeolite framework (without the amorphous phase).

Additionally, the specific surface areas of the supports measured by N_2 physisorption are summarized in Table 6.3.

Table 6.3: Comparison of the n_{Si}/n_{Al} ratios determined by ICP-OES and ^{29}Si MAS NMR and the respective specific surface areas of all zeolite Y supports.

Zeolite Y	n_{Si}/n_{Al} **(ICP-OES)**	n_{Si}/n_{Al} **(^{29}Si MAS NMR)**	A_{BET} **/ m²·g⁻¹**
$Na_{0.96},H_{0.04}$-Y-2.4	2.4	2.6	890
$Na_{0.67},H_{0.33}$-Y-2.4	2.4	2.5	470
$H_{0.62},Na_{0.38}$-Y-2.4	2.4	2.6	865
$H_{0.88},Na_{0.12}$-Y-2.4	2.4	2.4	760
$H_{0.99},Na_{0.01}$-Y-7	6.9	6.2	649
$H_{0.99},Na_{0.01}$-Y-14	14.5	14.2	750
$H_{0.92},Na_{0.08}$-Y-105	105.3	51.9	930

The results of the determination of the n_{Si}/n_{Al} ratio of the carriers reveal a very good accordance between the ICP-OES and ^{29}Si MAS NMR method for all supports, except $H_{0.92},Na_{0.08}$-Y-105. This discrepancy might originate from small inaccuracies in the deconvolution of the ^{29}Si spectrum of this support. For high n_{Si}/n_{Al} ratios, small inaccuracies have a great influence on the resulting ratio. When the n_{Si}/n_{Al} ratios obtained from ICP-OES and ^{29}Si MAS NMR are nearly identical one can conclude that the aluminum atoms of zeolitic supports are located mainly on framework positions.

Table 6.4: Concentrations of Brønsted acid sites of the zeolite Y supports as determined by FT-IR spectroscopy.

Catalyst	$n_{pyridine}\cdot m_{catalyst}^{-1}$ **/ µmol·g⁻¹**						
	200 °C	250 °C	300 °C	350 °C	400 °C	450 °C	500 °C
$Na_{0.96},H_{0.04}$-Y-2.4	0	0	2	3	0	0	0
$Na_{0.67},H_{0.33}$-Y-2.4	549	576	583	555	526	448	316
$H_{0.62},Na_{0.38}$-Y-2.4	1052	1058	1031	1019	956	872	685
$H_{0.88},Na_{0.12}$-Y-2.4	1840	1785	1734	1656	1413	1015	625
$H_{0.99},Na_{0.01}$-Y-7	641	618	588	551	495	388	302
$H_{0.99},Na_{0.01}$-Y-14	283	275	250	230	174	156	77
$H_{0.92},Na_{0.08}$-Y-105	18	20	26	22	21	17	15

All zeolite Y supports which are used for the preparation of the molybdenum carbide catalysts were investigated by means of FT-IR spectroscopy and

desorption of pyridine (see Table 6.4). Several trends can be derived for most of the supports: (i) the amount of adsorbed pyridine decreases with increasing desorption temperature at a constant n_{Si}/n_{Al} ratio. (ii) With an increased exchange of sodium by ammonium in the modification of the supports, an increasing initial concentration of Brønsted acid sites at 200 °C is determined. This is due to the formation of protons *via* the decomposition of ammonium ions during the activation treatment. (iii) The amount of adsorbed pyridine at 200 °C decreases with increasing n_{Si}/n_{Al} ratio for those supports that underwent an almost complete exchange of sodium by ammonium. This is not surprising since Brønsted acid sites are clearly related to the amount of aluminum inside the zeolite framework, which is reduced with increasing n_{Si}/n_{Al} ratio.

6.2 Characterization of the Noble Metal Catalysts

6.2.1 Noble Metals Supported on Zeolite Y with Varied Concentrations of Brønsted Acid Sites

In Table 6.5, the chemical compositions of four iridium- and four platinum-containing catalysts are listed. The catalysts consist of *ca.* 3 wt.-% of iridium or platinum supported on zeolite Y and differ in the concentrations of the charge-compensating cations of the support. Within the series of iridium and platinum catalysts, the supports were chosen to obtain noble metal catalysts with low to high concentrations of Brønsted acid sites.

Table 6.5: Chemical compositions of the noble metal catalysts supported on zeolite Y.

Iridium Catalyst	**Platinum Catalyst**
3.0Ir/$Na_{0.96}$,$H_{0.04}$-Y-2.4	3.3Pt/$Na_{0.85}$,$H_{0.15}$-Y-2.4
3.3Ir/$Na_{0.72}$,$H_{0.28}$-Y-2.4	2.8Pt/$Na_{0.59}$,$H_{0.41}$-Y-2.4
2.9Ir/$H_{0.57}$,$Na_{0.43}$-Y-2.4	2.7Pt/$H_{0.63}$,$Na_{0.37}$-Y-2.4
3.1Ir/$H_{0.90}$,$Na_{0.10}$-Y-2.4	2.6Pt/$H_{0.88}$,$Na_{0.12}$-Y-2.4

All noble metal catalysts were prepared by ion exchange. As shown exemplarily in Figure 6.6 for the iridium catalysts, the ion exchange did not result in any structural changes or degradation of the zeolitic frameworks. After the ion exchange with iridium or platinum, all characteristic reflexes for zeolite

Y continue to be present (*cf.* Figure 6.1). The intensities of the reflexes are neither influenced by the noble metal loading which is kept at ca. 3 wt.-% nor by the concentration of Brønsted sites. Their concentration was varied by replacing between 4 and 90 mol-% of the sodium ions of the support by protons.

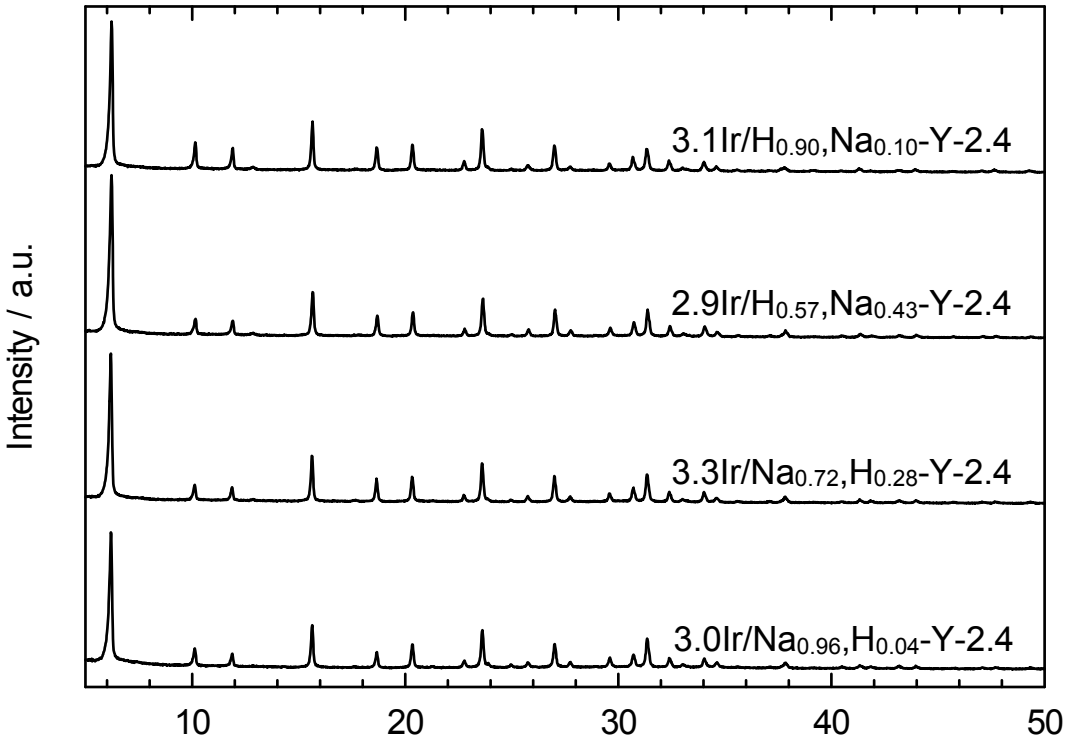

Figure 6.6: X-ray powder diffraction patterns of the iridium-exchanged zeolite Y catalysts.

Metal dispersions of all catalysts were determined by means of H_2 chemisorption. The results of the chemisorption measurements are summarized in Table 6.6. It can be seen that the values of the metal dispersion are generally higher on the iridium than on the platinum catalysts. Since on iridium dispersions of the metal > 1 are found, one can conclude that adsorption stoichiometries of $n_H/n_{Ir} > 1$ occur, in agreement with literature [124,125]. Nevertheless, the dispersion of iridium does not seem to be significantly influenced by the concentration of Brønsted acid sites of the support. This independence of the dispersion from the Brønsted acid site concentration is also found on the platinum catalysts which show dispersion values of ca. 60 %.

Table 6.6: Metal dispersions of the Ir/Na,H-Y-2.4 and Pt/Na,H-Y-2.4 catalysts.

Iridium Catalyst	**Metal Dispersion**	**Platinum Catalyst**	**Metal Dispersion**
3.0Ir/$Na_{0.96}$,$H_{0.04}$-Y-2.4	0.89	3.3Pt/$Na_{0.85}$,$H_{0.15}$-Y-2.4	0.62
3.3Ir/$Na_{0.72}$,$H_{0.28}$-Y-2.4	1.17	2.8Pt/$Na_{0.59}$,$H_{0.41}$-Y-2.4	0.61
2.9Ir/$H_{0.57}$,$Na_{0.43}$-Y-2.4	1.18	2.7Pt/$H_{0.63}$,$Na_{0.37}$-Y-2.4	0.60
3.1Ir/$H_{0.90}$,$Na_{0.10}$-Y-2.4	1.07	2.6Pt/$H_{0.88}$,$Na_{0.12}$-Y-2.4	0.77

Information about the specific surface area of the catalysts was obtained by means of nitrogen physisorption. The results are summarized in Table 6.7. Surface areas between 660 and 840 $m^2 \cdot g^{-1}$ were obtained. This indicates, that the crystallinity of the original zeolite support was neither affected by the ion exchange with ammonium ions or the noble metal complex, nor by the calcination treatments.

Table 6.7: Specific surface areas of the Ir/Na,H-Y-2.4 and Pt/Na,H-Y-2.4 catalysts.

Iridium Catalyst	A_{BET} / $m^2 \cdot g^{-1}$	**Platinum Catalyst**	A_{BET} / $m^2 \cdot g^{-1}$
3.0Ir/$Na_{0.96}$,$H_{0.04}$-Y-2.4	797	3.3Pt/$Na_{0.85}$,$H_{0.15}$-Y-2.4	799
3.3Ir/$Na_{0.72}$,$H_{0.28}$-Y-2.4	832	2.8Pt/$Na_{0.59}$,$H_{0.41}$-Y-2.4	840
2.9Ir/$H_{0.57}$,$Na_{0.43}$-Y-2.4	662	2.7Pt/$H_{0.63}$,$Na_{0.37}$-Y-2.4	790
3.1Ir/$H_{0.90}$,$Na_{0.10}$-Y-2.4	823	2.6Pt/$H_{0.88}$,$Na_{0.12}$-Y-2.4	787

The measured concentrations of Brønsted acid sites of the Ir/Na,H-Y-2.4 and Pt/Na,H-Y-2.4 catalysts are summarized in Table 6.8. The concentration of adsorbed pyridine increases with decreasing concentrations of sodium as determined by ICP-OES. Hence, the assumption that the lacking amount of charge-compensating cations, which cannot be determined by ICP-OES, are protons is confirmed. A comparison of the Brønsted acid site concentrations of 3.0Ir/$Na_{0.96}$,$H_{0.04}$-Y-2.4 and 3.3Pt/$Na_{0.85}$,$H_{0.15}$-Y-2.4 with their support ($Na_{0.96}$,$H_{0.04}$-Y-2.4), reveals an increase of the concentration of Brønsted acid sites when iridium or platinum noble metal is present and reduced. Hence, during the reduction of the noble metals Brønsted acid sites are formed.

Table 6.8: Concentrations of Brønsted acid sites of the Ir/Na,H-Y-2.4 and Pt/Na,H-Y-2.4 catalysts measured by FT-IR spectroscopy.

Catalyst	$n_{pyridine} \cdot m_{catalyst}^{-1}$ / µmol·g^{-1}						
	200 °C	250 °C	300 °C	350 °C	400 °C	450 °C	500 °C
3.0Ir/$Na_{0.96}$,$H_{0.04}$-Y-2.4	125	138	140	115	76	40	9
3.3Ir/$Na_{0.72}$,$H_{0.28}$-Y-2.4	590	635	614	594	537	507	427
2.9Ir/$H_{0.57}$,$Na_{0.43}$-Y-2.4	1036	967	892	853	811	727	590
3.1Ir/$H_{0.90}$,$Na_{0.10}$-Y-2.4	1038	1004	968	923	849	738	592
3.3Pt/$Na_{0.85}$,$H_{0.15}$-Y-2.4	94	114	120	103	72	36	0
2.8Pt/$Na_{0.59}$,$H_{0.41}$-Y-2.4	873	895	882	848	795	699	459
2.7Pt/$H_{0.63}$,$Na_{0.37}$-Y-2.4	565	568	554	528	473	396	256
2.6Pt/$H_{0.88}$,$Na_{0.12}$-Y-2.4	1156	1118	1068	1035	958	773	508

6.2.2 Zeolite Beta, EMC-2, L, MOR, ZSM-5 and Amorphous Silica as Supports

The catalysts summarized in Table 6.9 consist of *ca.* 3 wt.-% of iridium loaded on four large-pore zeolites (12-membered ring pores) and one medium-pore zeolite (ZSM-5) with a significantly lower iridium loading. These catalysts were kindly provided by Dr. Dominic Santi, and the conditions of their preparation *via* ion exchange can be obtained from Ref. [118].

Table 6.9: Chemical compositions of the iridium catalysts as determined by ICP-OES.

Iridium Catalyst
3.5Ir/$Rb_{0.52}$,$H_{0.48}$-Beta-14
3.3Ir/$H_{0.58}$,$Cs_{0.42}$-Beta-14
3.0Ir/$Na_{0.80}$,$H_{0.20}$-EMC-2-4.3
2.9Ir/$K_{0.68}$,$Na_{0.21}$,$H_{0.11}$-L-2.9
2.9Ir/$Na_{0.90}$,$H_{0.10}$-MOR-5.8
0.5Ir/$H_{0.59}$,$Na_{0.41}$-ZSM-5-18

The lower iridium content of zeolite ZSM-5 might be due to a hindered diffusion of the iridium complex during the ion exchange into the 10-membered ring pores of zeolite ZSM-5. This can be supported by the fact that neither molecules like decalin nor tetramethylsilane are adsorbed inside the pores of ZSM-5 [141]. Differences in the pore systems of the zeolitic supports are summarized in Table 4.1, page 17.

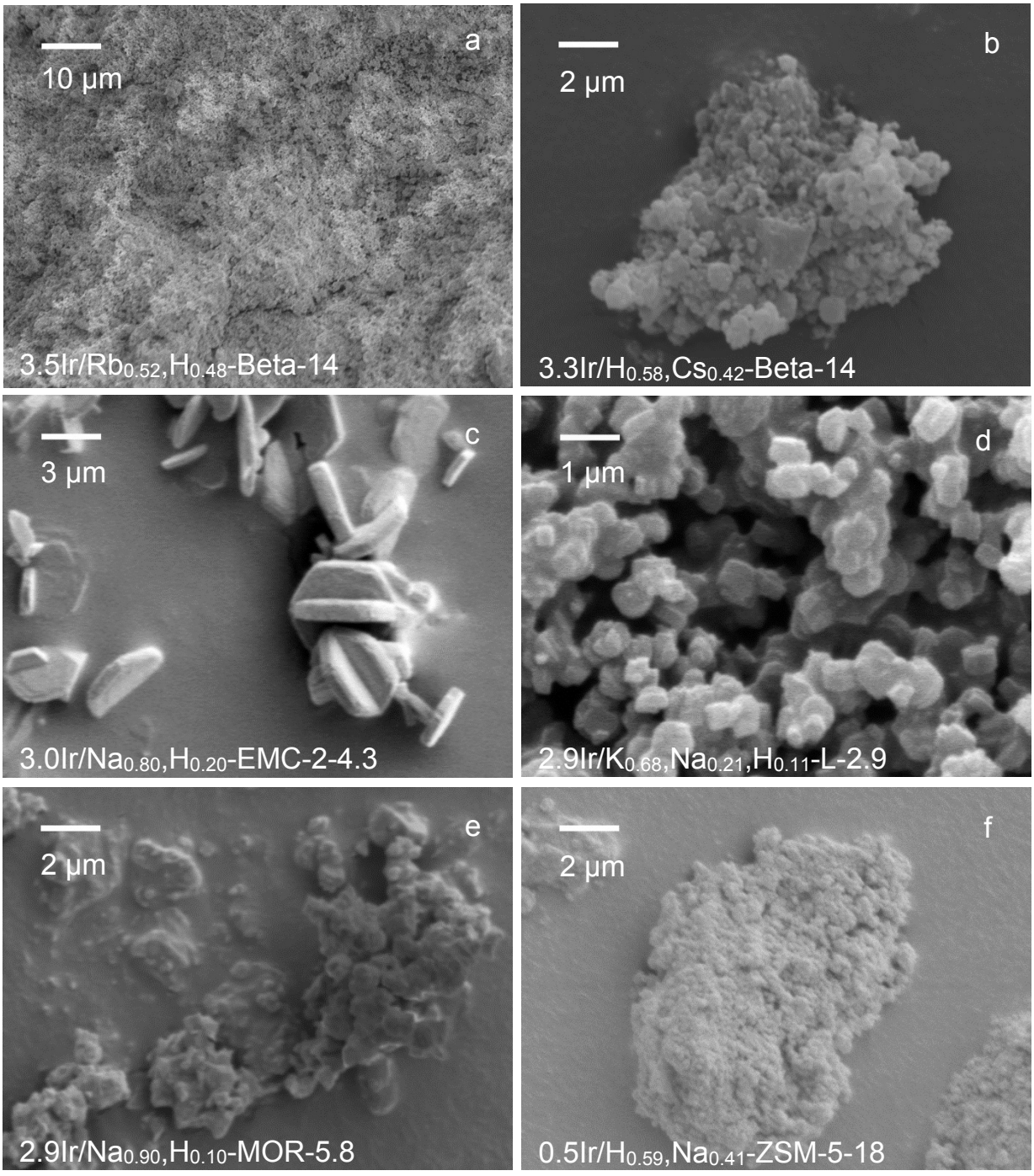

Figure 6.7: SEM pictures of the six catalysts with different pore structures.

All catalysts were characterized by SEM (see Figure 6.7) and XRD (see Figure 6.8) to determine their morphology and phase purity, respectively. The SEM

image of catalyst 3.5Ir/$Rb_{0.52}$,$H_{0.48}$-Beta-14 shows a cutout of a large particle. SEM images of the 3.0Ir/$Na_{0.80}$,$H_{0.20}$-EMC-2-4.3 and 2.9Ir/$K_{0.68}$,$Na_{0.21}$,$H_{0.11}$-L-2. catalysts (Figure 6.7c - d) show that these catalysts are built up by agglomerated particles with 0.5 to 4 µm diameter. A crystalline structure is not visible for both Beta, 2.9Ir/$Na_{0.90}$,$H_{0.10}$-MOR-5.8 and 0.5Ir/$H_{0.59}$,$Na_{0.41}$-ZSM-5-18 catalysts.

X-ray powder diffractograms of the six zeolitic catalysts are depicted in Figure 6.8. A comparison with the simulated XRD powder patterns [133] reveals that the angles, at which the reflexes appear, and their intensities are in good agreement. It is concluded that all zeolites are phase-pure.

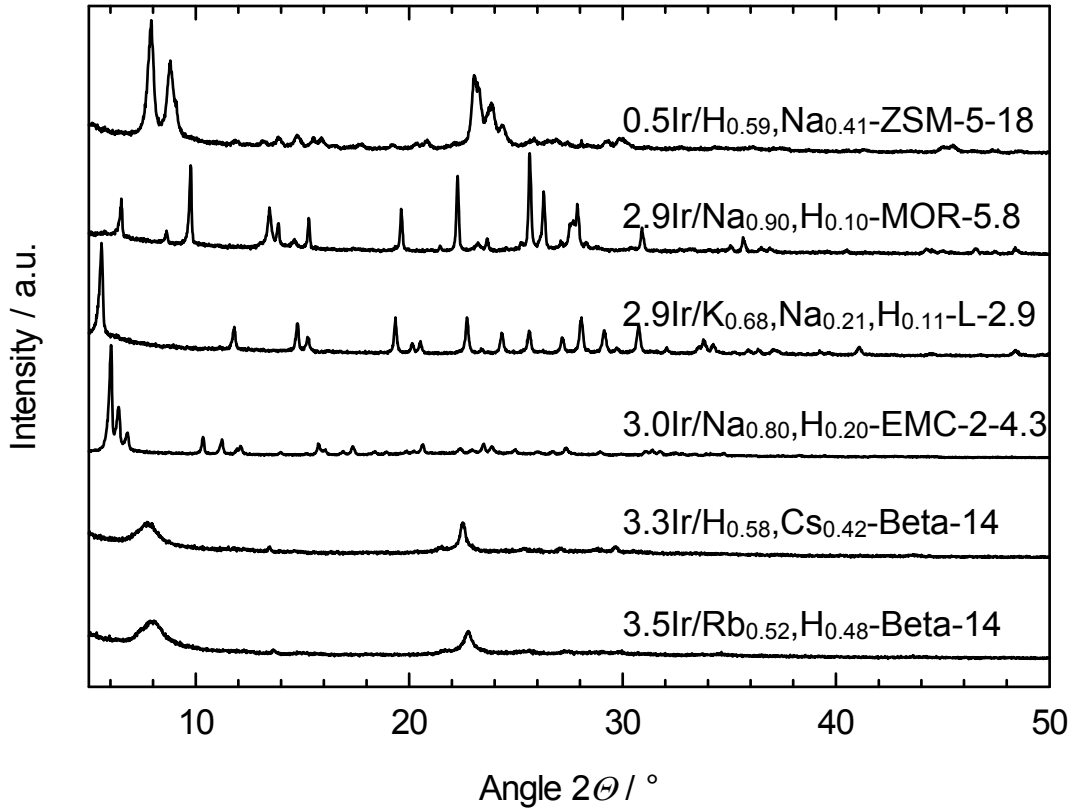

Figure 6.8: X-ray powder diffractograms of the zeolitic catalysts.

In addition to zeolites, amorphous silica loaded with 2.6 wt.-% iridium or 2.7 wt.-% platinum was investigated. The acidic properties of the catalysts and the support were investigated by FT-IR measurements (see Section 5.2.6, page 70). No absorption band at 1545 cm^{-1} was detected with pyridine as probe molecule [142], *i.e.*, these catalysts are free from Brønsted acid sites. By using 2.6Ir/silica and 2.7Pt/silica, the purely metal-catalyzed reactions in the hydroconversion of different hydrocarbons can be investigated.

Table 6.10: Metal dispersions of the supported noble metal catalysts.

Catalyst	**Metal Dispersion**
2.6Ir/silica	1.02
2.7Pt/silica	0.64
3.5Ir/$Rb_{0.52}$,$H_{0.48}$-Beta-14	0.51
3.3Ir/$H_{0.58}$,$Cs_{0.42}$-Beta-14	1.39
3.0Ir/$Na_{0.80}$,$H_{0.20}$-EMC-2-4.3	0.91
2.9Ir/$K_{0.68}$,$Na_{0.21}$,$H_{0.11}$-L-2.9	1.66
2.9Ir/$Na_{0.90}$,$H_{0.10}$-MOR-5.8	1.49
0.5Ir/$H_{0.59}$,$Na_{0.41}$-ZSM-5-18	0.73

The metal dispersions of the eight iridium- or platinum-loaded catalysts are summarized in Table 6.10. Although all catalysts were treated under similar conditions, a broad variety of metal dispersions is obtained. Generally, the dispersion of 2.7Pt/silica is lower than that of the majority of the seven iridium catalysts. A similar trend was found for the catalysts based on zeolite Y (see Section 6.2.1). While the platinum catalyst shows a dispersion of 0.6, the majority of iridium catalysts show dispersions of greater than 1.0. This finding is identical to the results of the dispersion measurements in the previous section and discussed there. As a whole, the metals seem to be well dispersed without a dependence of the dispersion on other factors like the pore structure of the support, its n_{Si}/n_{Al} ratio or the metal loading.

Table 6.11: Specific surface areas of the supported noble metal catalysts measured by N_2 physisorption.

Catalyst	A_{BET} / $m^2 \cdot g^{-1}$
2.6Ir/silica	7.1
2.7Pt/silica	4.3
3.5Ir/$Rb_{0.52}$,$H_{0.48}$-Beta-14	600
3.3Ir/$H_{0.58}$,$Cs_{0.42}$-Beta-14	520
3.0Ir/$Na_{0.80}$,$H_{0.20}$-EMC-2-4.3	330
2.9Ir/$K_{0.68}$,$Na_{0.21}$,$H_{0.11}$-L-2.9	400
2.9Ir/$Na_{0.90}$,$H_{0.10}$-MOR-5.8	320
0.5Ir/$H_{0.59}$,$Na_{0.41}$-ZSM-5-18	420

The measured surface areas of the eight catalysts are summarized in Table 6.11. All specific surface areas of the zeolitic catalysts are in the range of 330 to 600 $m^2 \cdot g^{-1}$. The silica catalysts possess hardly any porosity which is reflected in the very low specific surface areas of 4.3 and 7.1 $m^2 \cdot g^{-1}$.

As summarized in Table 6.12, the measured concentrations of Brønsted acid sites of the six zeolite catalysts at 200 °C are in the range of 73 to 191 $\mu mol \cdot g^{-1}$. By replacing the charge-compensating cations from rubidium to cesium as shown for 3.5Ir/$Rb_{0.52}$,$H_{0.48}$-Beta-14 and 3.3Ir/$H_{0.58}$,$Cs_{0.42}$-Beta-14, the concentration of Brønsted acid sites is lower for the latter one at 200 °C due to a weakening of the sites by the exchange of the charge-compensating cation from rubidium to cesium [26]. Thus, on weakly acid sites, less pyridine is adsorbed and cannot be detected at 200 °C.

Table 6.12: Concentrations of Brønsted acid sites of the supported noble metal catalysts measured by FT-IR spectroscopy.

Catalyst	$n_{pyridine} \cdot m_{catalyst}^{-1}$ / **µmol·g^{-1}**						
	200 °C	250 °C	300 °C	350 °C	400 °C	450 °C	500 °C
3.5Ir/$Rb_{0.52}$,$H_{0.48}$-Beta-14	121	109	93	82	66	48	25
3.3Ir/$H_{0.58}$,$Cs_{0.42}$-Beta-14	73	59	45	31	8	0	0
3.0Ir/$Na_{0.80}$,$H_{0.20}$-EMC-2-4.3	158	154	137	116	98	71	38
2.9Ir/$K_{0.68}$,$Na_{0.21}$,$H_{0.11}$-L-2.9	130	125	123	99	70	42	20
2.9Ir/$Na_{0.90}$,$H_{0.10}$-MOR-5.8	92	88	82	72	62	39	26
0.5Ir/$H_{0.59}$,$Na_{0.41}$-ZSM-5-18	191	182	169	158	151	136	118

6.3 Molydenum Carbide Catalysts

6.3.1 Bulk Molybdenum Carbide

In order to develop a synthesis method for molybdenum carbides, first experiments were conducted with bulk MoO_3. For that purpose, bulk MoO_3 was carburized in a fixed-bed reactor at temperatures between 500 and 1000 °C in a methane/hydrogen or n-octane/hydrogen flow to determine the influence of the carburization temperature and the reagent (carburization conditions can be found in Section 5.1.9, page 67). The carburization temperature, the carburization reagent and the designation of the resulting molybdenum carbide are summarized in Table 6.13.

Table 6.13: Conditions and reagents in the carburization of MoO_3.

Carburization Temperature / °C	Carburization Reagent	Bulk Molybdenum Carbide Designation
700	Methane	β-Mo_2C-700-Me
800	Methane	β-Mo_2C-800-Me
900	Methane	β-Mo_2C-900-Me
1000	Methane	β-Mo_2C-1000-Me
500	n-Octane	β-Mo_2C-500-Oc
600	n-Octane	β-Mo_2C-600-Oc
700	n-Octane	β-Mo_2C-700-Oc
800	n-Octane	β-Mo_2C-800-Oc

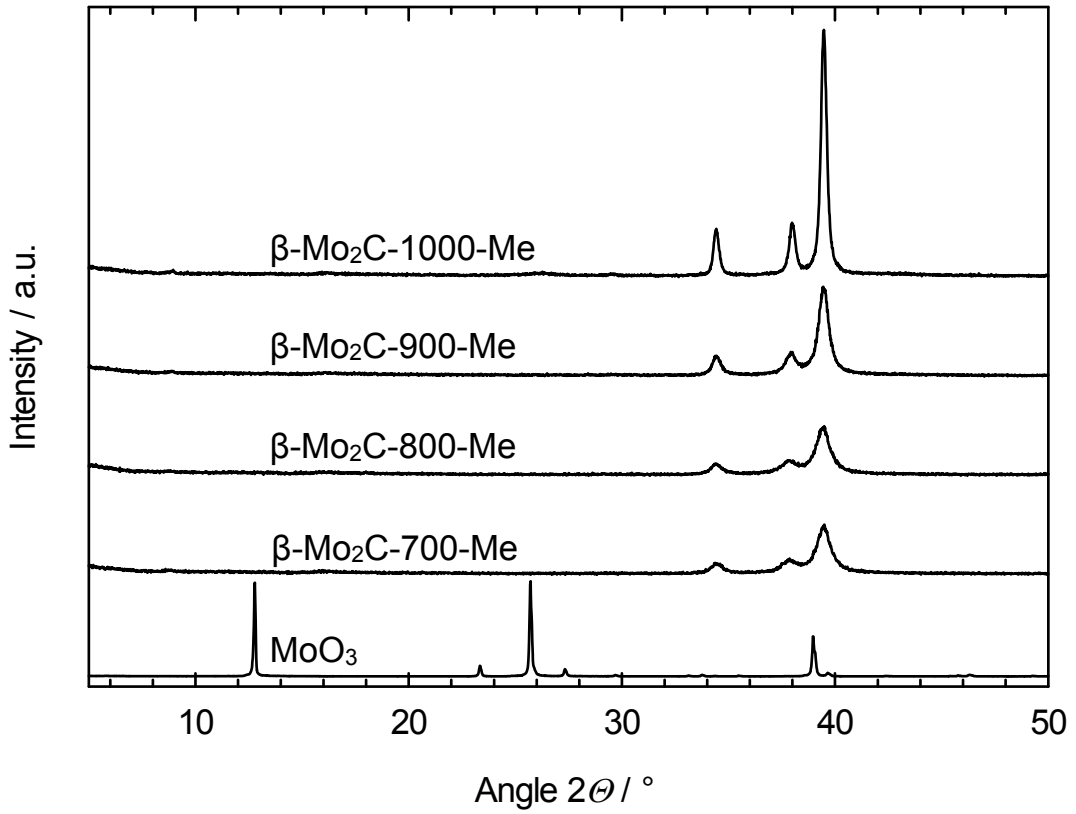

Figure 6.9: X-ray diffractograms of β-Mo_2C made by carburization of MoO_3 with methane at temperatures between 700 and 1000 °C.

The products of the carburization were investigated by X-ray diffraction. The resulting diffractograms are depicted in Figure 6.9 and Figure 6.10. The carburization of MoO_3 with a mixture of methane and hydrogen between 700 and 1000 °C always resulted in a crystalline product with reflexes at 34.5, 37.9 and 39.5° (Figure 6.9). These reflexes can be clearly attributed to pure β-Mo_2C

[107]. With increasing carburization temperature the intensity of the reflexes increases in agreement with the results of Hanif *et al.* [110]. They furthermore found that an increased carburization temperature leads to significant larger particle sizes of β-Mo_2C. In turn, larger particles lead to a reduction of the specific surface areas, which are generally very low for bulk molybdenum carbides, from 38 $m^2 \cdot g^{-1}$ for β-Mo_2C-700-Me to 23 $m^2 \cdot g^{-1}$ for β-Mo_2C-800-Me.

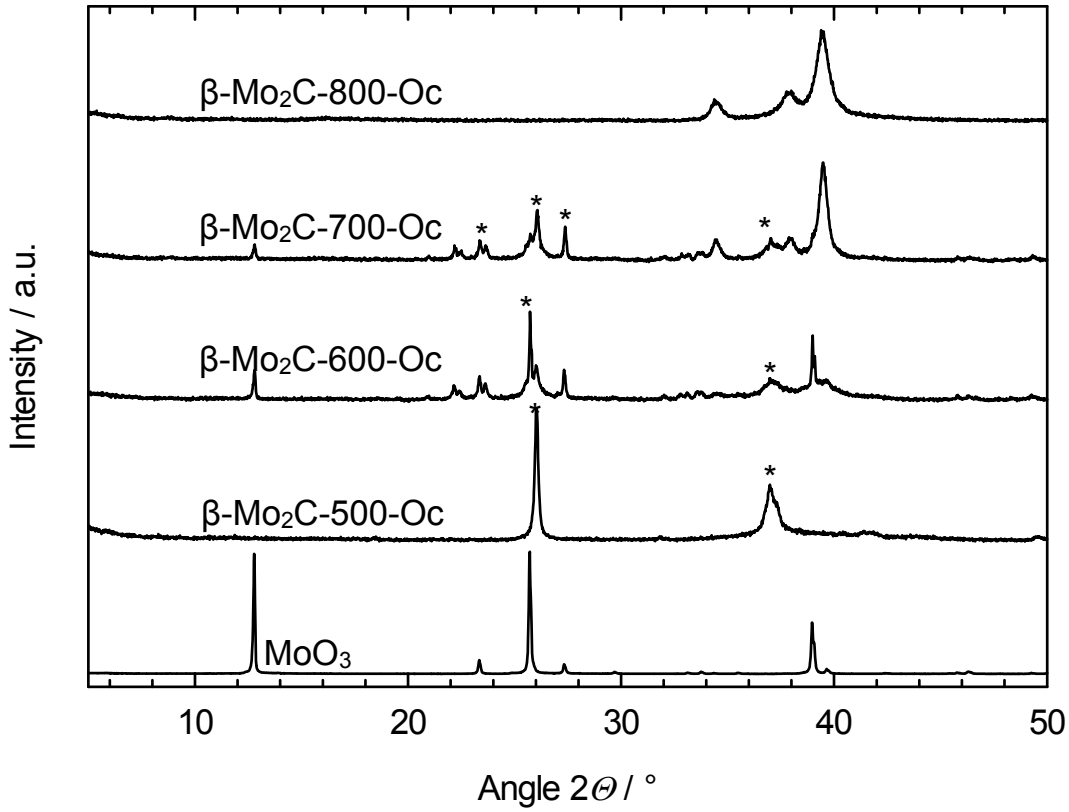

Figure 6.10: X-ray diffractograms of β-Mo_2C made by carburization of MoO_3 with n-octane at temperatures between 500 and 800 °C (asterisks denote reflexes of MoO_3 and MoO_2).

Depicted in Figure 6.10 are the X-ray diffractograms of the products of the carburization of bulk MoO_3 with an n-octane/hydrogen mixture. At temperatures up to 700 °C, reflexes of MoO_3 or MoO_2 are still present. MoO_2 is formed during the carburization by reduction of MoO_3 with hydrogen in a first step [110]. With increasing carburization temperature the intensity of the β-Mo_2C reflexes increases, they evolve at temperatures of about 700 °C.

6.3.2 Supported Molybdenum Carbide Catalysts

One aim of this work was the preparation of beta-molybdenum carbide supported on zeolite Y and the investigation of these catalysts in the hydroconversion of cis-decalin. The detailed characterization of the different zeolite Y supports can be found in Section 6.1, page 96. Among the catalysts listed in Table 6.14, the n_{Si}/n_{Al} ratio of the supports was varied between 2.4 and 105. Additionally, the concentration of Brønsted acid sites was varied on the aluminum-rich Y zeolite. The supports were loaded with different amounts of $(NH_4)_6Mo_7O_{24}$ *via* incipient wetness impregnation (see Section 5.1.8, page 67). The carburized form of the catalyst precursors was made by treatment with a methane/hydrogen mixture at 700 °C (see Section 5.1.9, page 67). Note that, in the nomenclature of the molybdenum carbide catalysts, the number in front of "Mo_2C" denotes the weight percent of molybdenum only referenced to the mass of the dry catalyst. The description of the metal carbide loading by the molybdenum content is due to the fact that carbon cannot be determined by ICP-OES and the analysis for small amounts of carbon by the CHN instrument turned out to be inaccurate.

Molybdenum carbide catalysts with *ca*. 9 wt.-% of molybdenum supported on zeolite Y (n_{Si}/n_{Al} = 2.4) with different concentrations of Brønsted acid sites are summarized in Table 6.15. For the molybdenum loading, the impregnation reagent Na_2MoO_4 was used. n-Octane was used as carburization reagent for all catalysts.

In conclusion, supported molybdenum carbide catalysts were synthesized under variation of the following parameters: (i) n_{Si}/n_{Al} ratio of the faujasite support, (ii) concentration of Brønsted acid sites of the support, (iii) molybdenum carbide loading on the support, (iv) nature of the molybdenum impregnation reagent and (v) nature of the carburization reagent.

Table 6.14: Zeolitic supports which were impregnated by $(NH_4)_6Mo_7O_{24}$ and catalysts obtained by their carburization with a methane/hydrogen mixture.

Zeolitic Support	Molybdenum Carbide Catalyst
$Na_{0.96},H_{0.04}$-Y-2.4	4.2$Mo_2C[NH_4]/Na_{0.96},H_{0.04}$-Y-2.4
$Na_{0.67},H_{0.33}$-Y-2.4	4.6$Mo_2C[NH_4]/Na_{0.67},H_{0.33}$-Y-2.4
$H_{0.62},Na_{0.38}$-Y-2.4	5.0$Mo_2C[NH_4]/H_{0.62},Na_{0.38}$-Y-2.4
$H_{0.88},Na_{0.12}$-Y-2.4	4.5$Mo_2C[NH_4]/H_{0.88},Na_{0.12}$-Y-2.4
$H_{0.99},Na_{0.01}$-Y-7	4.9$Mo_2C[NH_4]/H_{0.99},Na_{0.01}$-Y-7
	7.1$Mo_2C[NH_4]/H_{0.99},Na_{0.01}$-Y-7
	9.8$Mo_2C[NH_4]/H_{0.99},Na_{0.01}$-Y-7
	23.7$Mo_2C[NH_4]/H_{0.99},Na_{0.01}$-Y-7
$H_{0.99},Na_{0.01}$-Y-14	4.3$Mo_2C[NH_4]/H_{0.99},Na_{0.01}$-Y-14
	7.0$Mo_2C[NH_4]/H_{0.99},Na_{0.01}$-Y-14
	10.2$Mo_2C[NH_4]/H_{0.99},Na_{0.01}$-Y-14
	21.6$Mo_2C[NH_4]/H_{0.99},Na_{0.01}$-Y-14
$H_{0.92},Na_{0.08}$-Y-105	4.7$Mo_2C[NH_4]/H_{0.92},Na_{0.08}$-Y-105
	7.2$Mo_2C[NH_4]/H_{0.92},Na_{0.08}$-Y-105
	9.4$Mo_2C[NH_4]/H_{0.92},Na_{0.08}$-Y-105
	23.7$Mo_2C[NH_4]/H_{0.92},Na_{0.08}$-Y-105

Table 6.15: Zeolitic supports which were impregnated by Na_2MoO_4 and catalysts obtained by their carburization with an n-octane/hydrogen mixture.

Zeolitic Support	Molybdenum Carbide Catalyst
$Na_{0.96},H_{0.04}$-Y-2.4	8.2$Mo_2C[Na]/Na_{0.96},H_{0.04}$-Y-2.4
$Na_{0.66},H_{0.34}$-Y-2.4	9.6$Mo_2C[Na]/Na_{0.66},H_{0.34}$-Y-2.4
$H_{0.92},Na_{0.08}$-Y-2.4	8.9$Mo_2C[Na]/H_{0.92},Na_{0.08}$-Y-2.4

The carburized samples were characterized by X-ray diffractometry. Since the results for all carburized samples are similar, the diffractograms of the carburized $Mo_2C/H_{0.89},Na_{0.11}$-Y-105 samples are shown exemplarily in Figure 6.11. After impregnation and carburization all reflexes of the dealuminated Y zeolite support are present, even though the intensities are slightly lower compared to the precursor.

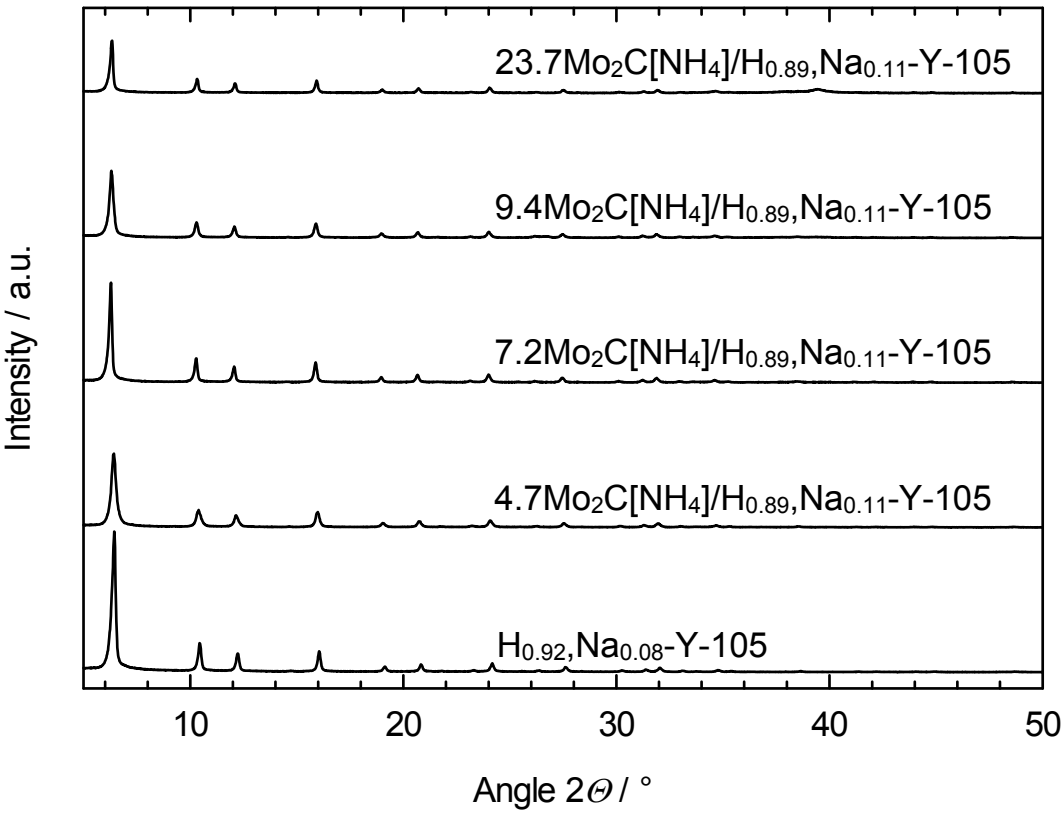

Figure 6.11: X-ray diffractograms of dealuminated zeolite Y loaded with different amounts of molybdenum carbide.

In Figure 6.12, the magnified sections of the diffractograms from Figure 6.11 between 35 and 45° are shown. With increasing molybdenum loading an increasing intensity of the reflex at 39.5° can be identified which is attributed to the (1 0 0) reflex of β-Mo_2C (see Section 6.3.1, page 113). For a detection of the molybdenum carbide reflex a loading of at least 7.2 wt.-% of molybdenum is necessary. The detection of a reflex of the supported molybdenum carbide at loadings > 7.2 wt.-% confirmed the formation of the carbide at the chosen carburization conditions. The lack of reflexes of molybdenum carbide may be due to a very high dispersion of the molybdenum carbide particles, which would result in weak and broad reflexes which disappear in the noise of the measurement. An additional proof for the carbide formation was achieved by means of CHN analysis in combination with ICP-OES. It can be seen in Table 6.16 that the ratio of the detected molar amount of molybdenum to the molar amount of carbon is in the range of 1.7 to 2.0. This finding supports that molybdenum carbide was indeed formed on zeolite Y. Furthermore, also on 4.7Mo_2C/$H_{0.89}$,$Na_{0.11}$-Y-105 with a small amount of molybdenum, the formation of the carbide is indicated by the carbon found by CHN analysis.

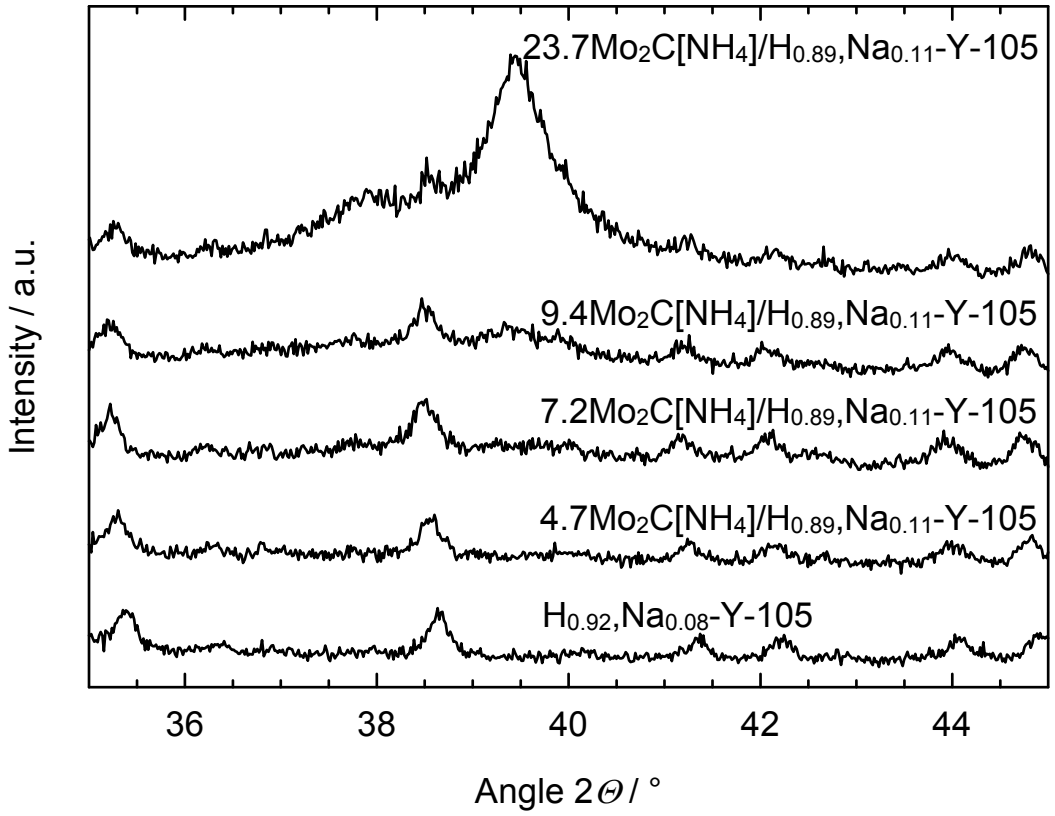

Figure 6.12: Magnification of the X-ray diffractogram of Figure 6.11 in the range of 2Θ = 35 to 45°.

Table 6.16: n_{Mo}/n_C ratio of the supported molybdenum carbide catalysts on H,Na-Y-105.

Catalyst	n_{Mo}/n_C **ratio**
4.7$Mo_2C[NH_4]/H_{0.89},Na_{0.11}$-Y-105	2.0
7.2$Mo_2C[NH_4]/H_{0.89},Na_{0.11}$-Y-105	1.7
9.4$Mo_2C[NH_4]/H_{0.89},Na_{0.11}$-Y-105	1.9
23.7$Mo_2C[NH_4]/H_{0.89},Na_{0.11}$-Y-105	1.8

7 Competitive Hydroconversion of Equimolar Decalin/n-Decane Mixtures

7.1 Preliminary Experiments

7.1.1 Test of the Multi-Component Saturator

The multi-component high-pressure saturator was described in Section 5.3.1.5 (Figure 5.2). Prior to the catalytic experiments, the performance of the saturator was tested over an extended time of 48 h with hydrogen as gas to be saturated with vapors of cis-decalin and n-decane in equimolar amounts. The storage vessel D2 (Figure 5.5) was filled with a liquid mixture of 63.1 mol-% of cis-decalin with small amounts (*cf.* Section 5.3.2.3) of trans-decalin and 36.9 mol-% of n-decane. This liquid mixture was continuously pumped to the head of the saturator column (S1 in Figure 5.5) and trickled down the column into the storage vessel D1. The saturator column was held at T = 137 °C, and the total pressure was 5.0 MPa.

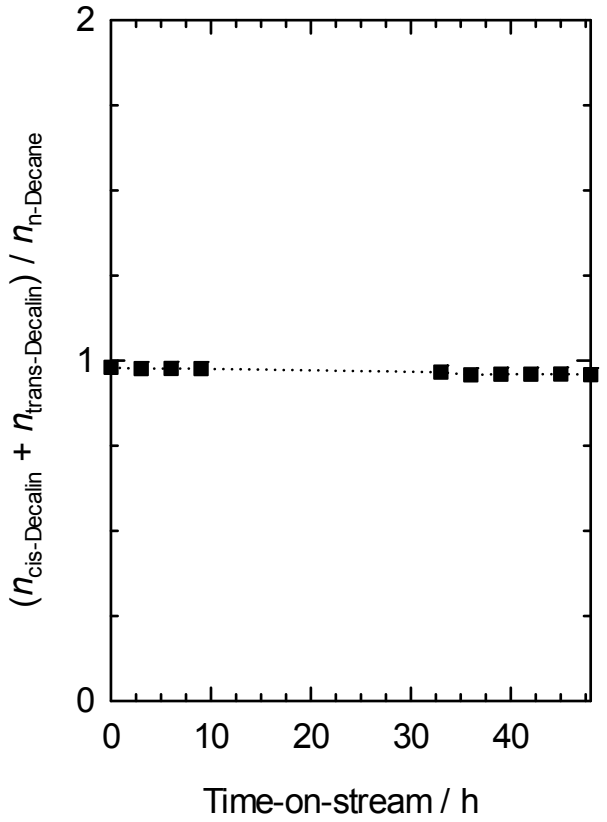

Figure 7.1: Composition of the hydrocarbons in the gas phase leaving the multi-component saturator (Figure 5.2), see text for conditions.

During this test of the saturator, the reactor was empty and held at T = 200 °C. Samples of the gas flowing through the reactor were periodically introduced into the capillary gas chromatograph *via* the gas sampling valve (see Figure 5.5). The result of these analyses is shown in Figure 7.1. The composition of the hydrogen/decalin/n-decane gas mixture generated in the saturator is proved to be fully stationary over the entire duration of the test, and the molar ratio of decalin and n-decane is very close to unity, as desired.

7.1.2 Blank Run – Hydroconversion of the Decalin/n-Decane Mixture in the Empty Reactor

In another set of preliminary experiments, the usual equimolar mixture of decalin and n-decane was passed together with hydrogen through the empty reactor under the conditions of a typical catalytic experiment (Section 5.3.2.3). The reactor temperature was varied from 200 to 400 °C, and the results are depicted in Figure 7.2.

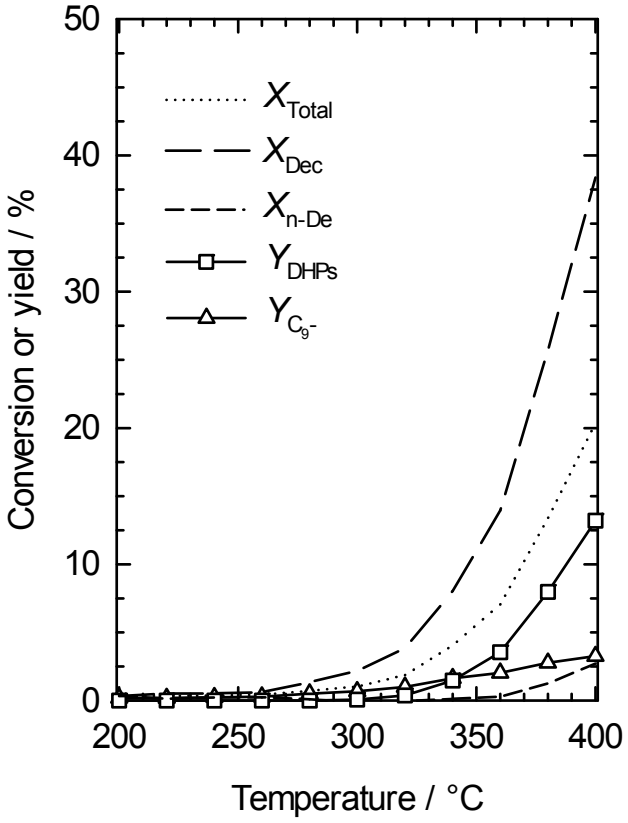

Figure 7.2: Hydroconversion of an equimolar decalin/n-decane mixture at various temperatures in the empty reactor.

It is seen that virtually no conversion of the two feed hydrocarbons occurs below 300 °C. Above this temperature, decalin begins to be dehydrogenated, mainly into tetralin and naphthalene. Besides, some small amounts ($Y_{C_{9-}} \leq 3$ %) of hydrocracked products with less than 10 carbon atoms are formed at severe reaction conditions between 340 and 400 °C. It is noteworthy that skeletal isomers of decalin or n-decane, ring-opening products or open-chain decanes are formed in negligible traces only (with yields < 1 %) throughout, and these reactions are hence not considered in Figure 7.2.

7.1.3 Co-Injection of Decane Isomers

As already pointed out in Sections 5.3.3 and 5.5.2, the co-injection of mixtures of iso-decanes made by catalytic isomerization of n-decane and products from the hydroconversion of decalin turned out to be a very valuable tool for the safe identification of open-chain decanes in the latter reaction [78]. The method was also used in the present work.

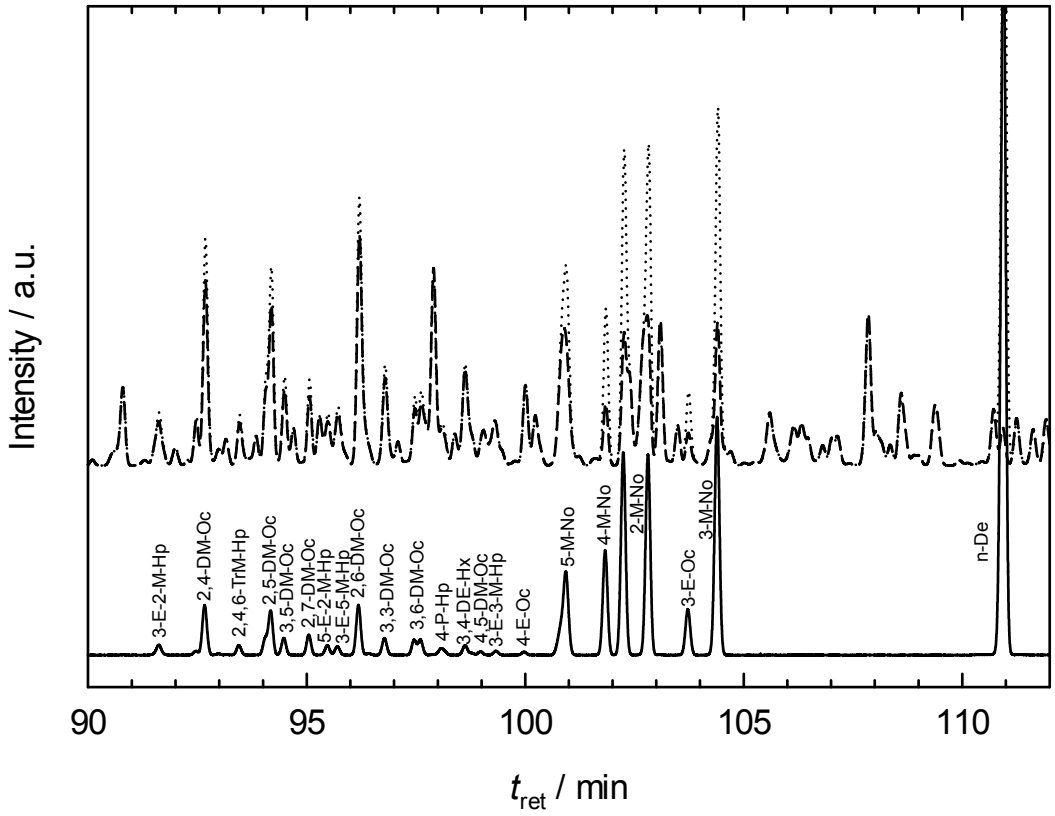

Figure 7.3: Gas chromatogram of the products from (i) n-decane isomerization on zeolite 0.49Pt/$H_{0.55}$,$Na_{0.45}$-Y (bottom, solid line), (ii) the product of decalin hydroconversion on 3.5Ir/$Rb_{0.52}$,$H_{0.48}$-Beta-14 (top, dashed line), and (iii) the co-injection of products (i) and (ii) (top, dotted line).

Shown in the bottom of Figure 7.3 is the relevant section of the gas chromatogram of the mixture of iso-decanes made by catalytic isomerization of n-decane on 0.49Pt/$H_{0.55}$,$Na_{0.45}$-Y zeolite. In the upper part of this figure, the chromatogram of a product from decalin hydroconversion on 3.5Ir/$Rb_{0.52}$,$H_{0.48}$-Beta-14 zeolite is depicted (top, dashed line). Upon co-injection of both hydrocarbon samples (top, dotted line), the intensity of some peaks unambiguously increases, while that of other peaks remains constant. The first category of peaks originates, at least in part, from open-chain decanes, while the second category does not.

7.2 General Aspects

For the experimental investigation of possible ring-opening catalysts, a model naphthene was chosen. Decalin was selected which is the simplest two-ring naphthene which can be obtained by hydrogenation of a polynuclear aromatic hydrocarbon (*viz.* naphthalene) which, in turn, is a typical constituent of LCO. It had been found that decalin is a very suitable model hydrocarbon for testing of ring-opening catalysts [143].

Straight run diesel fuel, as all petroleum fractions, consists of a large number of individual hydrocarbons with different molecular structures, having only the range (200 - 350 °C) of boiling temperatures in common. With this in mind it was decided to conduct, in the present investigation, ring-opening experiments with a suitably selected binary mixture of hydrocarbons. One component in these mixed model feeds was decalin, because a substantial body of information about its catalytic ring opening was already available, *e.g.*, from Refs. [69-71,78-81]. As the second component, n-decane was chosen, because (i) it has the same carbon number as decalin, (ii) it is a typical (and, due to its high cetane number of 77 [74], a desired) constituent of commercial diesel fuels, and (iii) it is a main representative of open-chain decane isomers which are products of decalin hydroconversion on high-performance ring-opening catalysts [78,79,81]. The main objective of the experiments with the mixed decalin/n-decane feed was to find out how the presence of the two hydrocarbons mutually influence their conversions, product yields and product selectivities compared to experiments with the single feeds decalin or n-decane. Throughout the study, in the experiments with the mixed feed, the decalin/n-decane mixture was equimolar.

The selection of the catalysts used in the hydroconversion of the mixed feeds was based on the experience acquired in previous ring-opening studies with the single component decalin as feed [118,119,144]. In a first set of experiments, catalysts consisting of iridium or platinum on non-acidic silica were used (2.6Ir/silica or 2.7Pt/silica) [119]. The results will be described in Section 7.4.

In a second set of experiments bifunctional catalysts with *ca.* 3 wt.-% of iridium or platinum supported on zeolite Y with different concentration of Brønsted acid sites were employed. The results achieved will be discussed in Sections 7.5.1 and 7.5.2, respectively.

Finally, bifunctional catalysts made from iridium (generally 3 wt.-%) on zeolites with pore systems other than zeolite Y were used [118]. The results achieved on these catalysts will be reported in Section 7.5.3.

In addition to the hydroconversion tests with the equimolar decalin/n-decane mixture, experiments with the pure feeds decalin and n-decane were conducted with each catalyst.

7.3 Cis/Trans-Stereoisomerization of Decalin

When cis-decalin is hydroconverted on noble-metal containing catalysts, by far the fastest reaction is the stereoisomerization to trans-decalin. At reaction temperatures between 180 and 440 °C and conversions between 2 and 99 %, mole fractions $n_{\text{tr-Dec}}/(n_{\text{c-Dec}} + n_{\text{tr-Dec}})$ from 74 to 93 % were obtained. Values of around 90 % were calculated by Haas [145] for the cis-/trans-decalin equilibrium previously. However, at temperatures of 100 °C, as they were applied in the present work in the competitive adsorption experiments, only a negligible stereoisomerization was observed. Thus, for the hydroconversion of decalin on noble-metal catalysts, cis- and trans-decalin were lumped together to the pseudo-reactant decalin. Otherwise, high conversions of cis-decalin would be obtained simply by stereoisomerization, resulting in very low selectivities of the interesting reactions, *viz.* ring opening and hydrocracking. Hence, the reactant was simply named decalin when it was hydroconverted on catalysts on which the stereoisomerization of decalin precedes all other reactions.

7.4 Competitive Hydroconversion on the Non-Acidic Catalysts 2.6Ir/silica and 2.7Pt/silica

Pure decalin, pure n-decane and an equimolar mixture of both hydrocarbons were hydroconverted on 2.6Ir/silica and 2.7Pt/silica. The conditions in these experiments can be found in Section 5.3.2, page 81. The conversions attained at different reaction temperatures are depicted in Figure 7.4. Higher activity of a catalyst or reactivity of a hydrocarbon results in lowered reaction temperatures to reach the same conversion.

Figure 7.4 reveals a number of interesting results concerning the hydroconversion of the two C_{10} hydrocarbons on monofunctional metallic catalysts: (i) Generally, iridium is a much more active metal than platinum, it allows one to reach a given conversion (*e.g.*, of pure n-decane) at *ca.* 80 °C lower temperature. (ii) On both catalysts and when hydroconverted alone, n-decane is considerably more reactive than decalin. (iii) The reactivities of the C_{10} hydrocarbons are significantly lower in the mixed-feed experiments compared to the hydroconversion experiments with the pure feeds. This is, in part, expected because, in the mixed-feed experiments, the overall liquid hourly space velocity (*LHSV* ≈ 0.6 to 0.8 h^{-1}) is *ca*. two times as high as in the pure-feed experiments (*LHSV* ≈ 0.3 to 0.4 h^{-1}), *i.e.* the amount of feed hydrocarbons sent over the catalyst per hour is *ca.* two times higher in the mixed-feed experiments than in the pure-feed experiments. However, the particularly remarkable result is that this reduction of the conversions in the mixed feed experiments is much more pronounced for n-decane than for decalin, so that, with a mixed feed, the reactivities of both feed hydrocarbons are virtually equal.

On 2.7Pt/silica the reactivity of n-decane is again strongly diminished, if one goes from the pure-feed to a mixed-feed hydroconversion (Figure 7.4b), while the reactivity of decalin remains practically the same. This pronounced effect of the mode of hydroconversion (pure-feed *versus* mixed-feed) is best interpreted in terms of a competitive adsorption of decalin and n-decane on the metallic catalyst sites: decalin, though intrinsically less reactive, is more strongly adsorbed and hinders the less strongly adsorbed n-decane from getting access to the catalytically active metal sites.

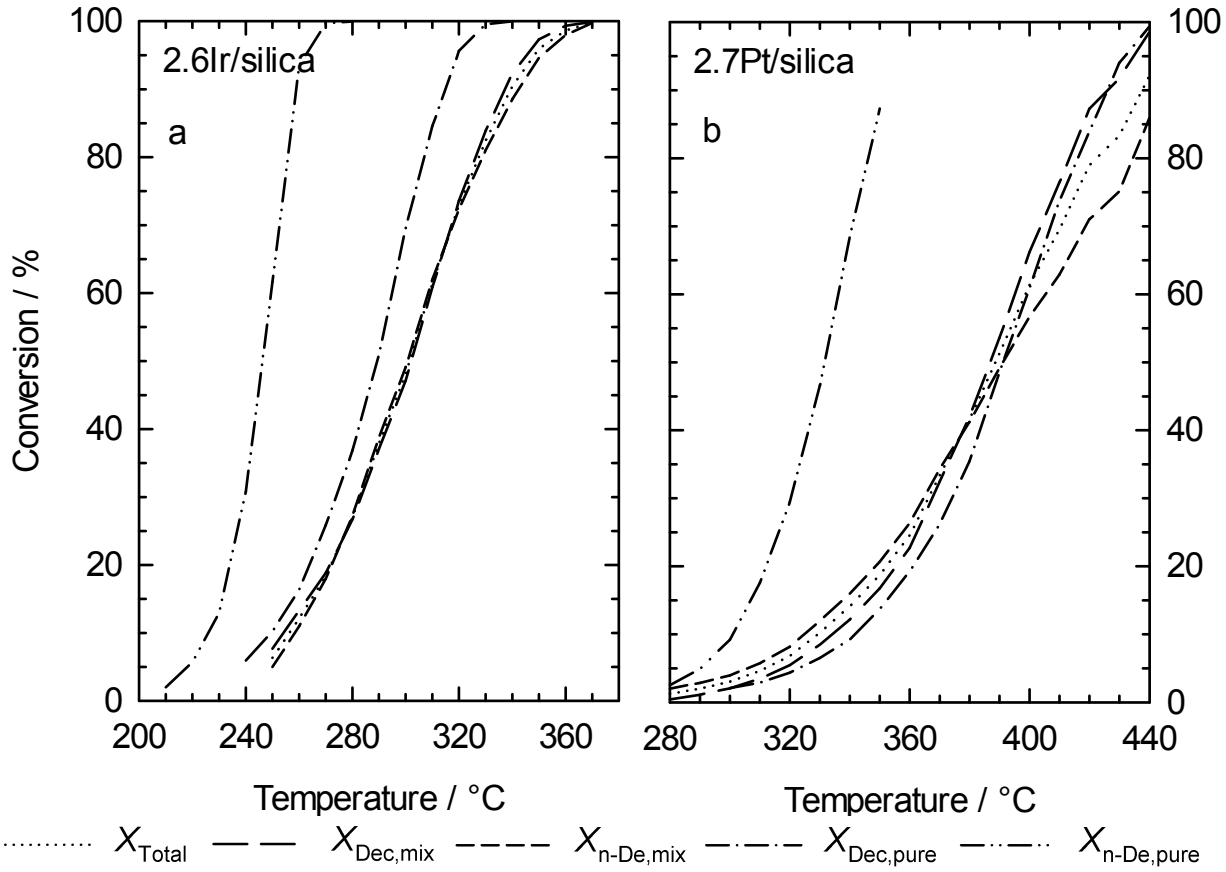

Figure 7.4: Conversions of pure decalin, pure n-decane and of an equimolar decalin/n-decane mixture on a) 2.6Ir/silica and b) 2.7Pt/silica.

Figures 7.5a and b show the product selectivities observed on the 2.6Ir/silica catalyst for the hydroconversion of pure decalin and pure n-decane, respectively. These results agree well with those reported by Haas [119] for Ir/silica catalysts: In the hydroconversion of decalin (Figure 7.5a), ring-opening products (ROPs) are strongly prevailing at low conversion (S_{ROPs} = 80 % at 240 °C) and can be classified as primary products. Upon increasing the reaction temperature and decalin conversion, the selectivity of ROPs strongly decreases, and the selectivities of open-chain decanes (OCDs) and hydrocracked products (C_9-) increase. Figure 7.5a suggests that OCDs and C_9- are formed in consecutive reactions from ROPs. The selectivities of the particularly desired OCDs pass through a maximum of $S_{OCDs,max.}$ = 25 % at T = 300 °C indicating that, at elevated temperatures and conversions, they are themselves consumed by consecutive hydrocracking into C_9- products. It is noteworthy that, on 2.6Ir/silica, hardly any skeletal isomers of decalin are formed at any conversion which unambiguously shows that (i) this catalyst lacks Brønsted acid sites and (ii) iridium metal lacks activity for skeletal isomerization, in agreement with literature reports [70]. No dehydrogenated

products (*i.e.*, tetralin or naphthalene) are formed on 2.6Ir/silica, in-line with a very unfavorable position of the dehydrogenation equilibrium at the relatively low temperatures and high hydrogen partial pressures. It should also be mentioned that, at low to moderate decalin conversions ($X_{Dec} \leq 25$ %), more than 95 % of the ring-opening products consist of a few isomers, *viz.* butylcyclohexane, cis- and trans-1-methyl-2-propylcyclohexane, and cis- and trans-1,2-diethylcyclohexane (the so-called direct ROPs [70]) which one would predict to form from a simple hydrogenolytic cleavage of one of the two six-membered rings in decalin, without skeletal isomerization before or after the ring-opening step.

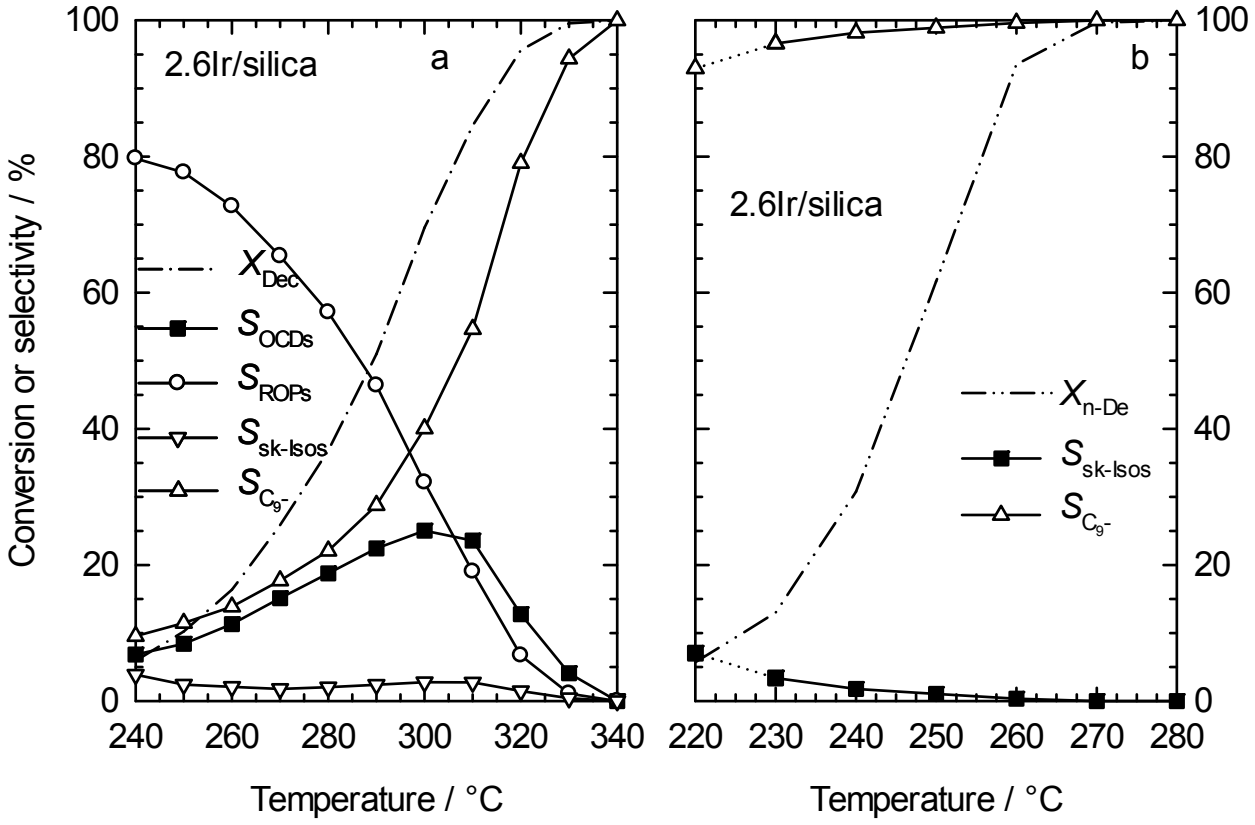

Figure 7.5: Hydroconversion of pure decalin (a) and pure n-decane (b) on catalyst 2.6Ir/silica. Selectivities of different groups of products.

n-Decane (Figure 7.5b) undergoes essentially the same reaction on 2.6Ir/silica as decalin, *viz.* hydrogenolytic cleavage of the carbon-carbon bonds existing in the feed molecule. No skeletal isomerization before or after hydrogenolysis takes place. C_9- hydrocarbons are hence formed almost exclusively over the entire range of n-decane conversions, and as expected, the products consist of n-alkanes to more than 98 %. The slightly elevated selectivities of sk-Isos at low conversions originate from the feed impurity 3-methylnonane and are

hence an artifact. Dotted lines were used between data points of the product selectivities which are considered to be affected by such artifacts.

In Figure 7.6a, the conversions and product selectivities measured in the hydroconversion of the equimolar decalin/n-decane feed on the 2.6Ir/silica catalyst are plotted versus the reaction temperature. The course of the partial and total conversions were already discussed in the context of Figure 7.4a. As expected from the selectivities of the pure-feed experiments (Figures 7.5a and b), three groups of products play a non-negligible role, *viz.* ring-opening products, open-chain decanes and C_9- hydrocarbons. The selectivity of the last-mentioned product group predominates throughout the total range of reaction conditions. This is not surprising in view of the tendency of the feed n-decane to react practically completely to C_9- (Figure 7.5b). An attempt was undertaken to calculate the selectivities of the mixed-feed experiments from the selectivities measured with the pure feeds decalin and n-decane (Figures 7.5a and b). In these calculations the assumption was made that, in the hydroconversion of a given feed hydrocarbon, the product selectivities are primarily determined by the nature of the catalyst and the conversion, but not by the presence or absence of other hydrocarbons.

The product selectivities which were obtained in the mixed-feed experiments at different temperatures are replotted against the total conversion (Figure 7.6b). Subsequently, product selectivities were calculated out of the pure feed results for a virtual mixture of both hydrocarbons. A more detailed description of how this calculation was done can be found in Section 5.5.4. These calculated selectivities are depicted in Figure 7.6c. Calculated selectivities for small conversions were dotted and ignored for the interpretation, because their course is adulterated by feed impurities. For total conversions between 20 and 100 %, there is a rather good agreement between the measured product selectivities (Figure 7.6b) and the calculated ones (Figure 7.6c). The underlying assumption, *i.e.*, on a given catalyst and for a given reactant, the product selectivities are primarily dependent on the conversion, appears to be valid.

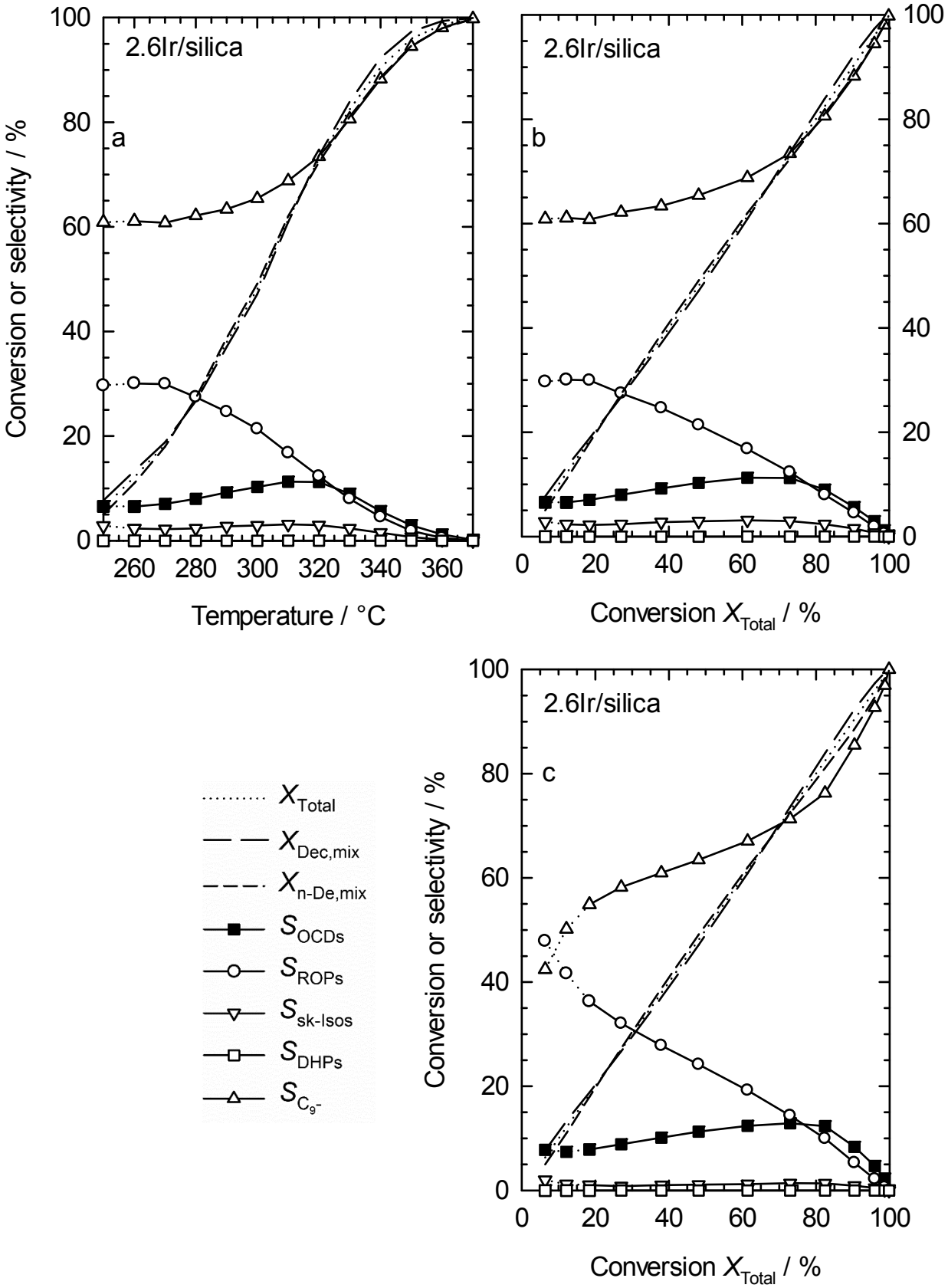

Figure 7.6: Hydroconversion of an equimolar mixture of decalin and n-decane on catalyst 2.6Ir/silica. Measured conversions and product selectivities in dependence of temperature (a); measured product selectivities replotted against the total conversion (b); product selectivities calculated from the selectivities measures with the pure decalin and n-decane feeds (c).

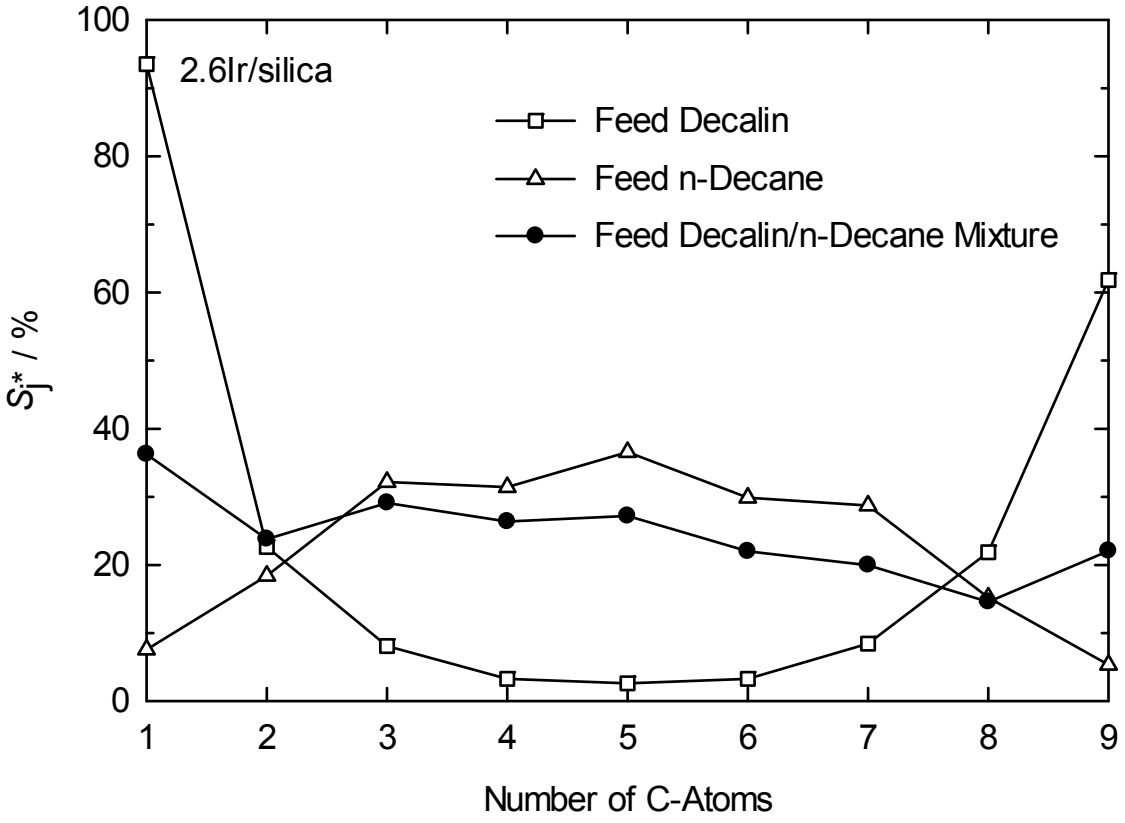

Figure 7.7: Modified hydrocracking selectivities S_j* of decalin, n-decane and an equimolar mixture of both hydrocarbons on catalyst 2.6Ir/silica. The reaction conditions are listed in Table 7.1.

Table 7.1: Reaction conditions for measuring the modified hydrocracking selectivities S_j* plotted in Figure 7.7 (Catalyst: 2.6Ir/silica).

Feed	T_r / °C	X / %	Y_{C_9-} / %	ΣS_j* / %
Pure decalin	300	70	28	226
Pure n-decane	250	31	31	205
Equimolar decalin/n-decane mixture	310	61	43	221

It is also of interest to look at the carbon number distributions of the hydrocracked products C_9- formed on 2.6Ir/silica in the experiments with the pure feeds and the equimolar decalin/n-decane mixture. These distributions in terms of the modified hydrocracking selectivities S_j* (for the definitions see Section 5.5.3, page 89) are shown in Figure 7.7 for conditions of moderate and similar yields of hydrocracked products Y_{C_9-} (see Table 7.1). The results obtained for the experiments with the pure feeds agree well with those reported by Haas [119]: With decalin as feed, a characteristic distribution curve with large amounts of C_1 and C_9, smaller amounts of C_2 and C_8, and very little

C_3 to C_7 was obtained which has been observed previously for decalin hydrogenolysis on iridium metal and referred to as a hammock-type distribution curve [70]. By contrast, the distribution curve obtained for the hydroconversion of n-decane is volcano-shaped and symmetrical around C_5. This symmetry is indicative for a pure primary hydrocracking selectivity, *i.e.*, the n-decane feed molecules undergo hydrogenolysis on the iridium, and the primary moieties of this hydrogenolysis are rapidly desorbed before they can be cleaved again in a secondary hydrogenolysis step. The pure primary hydrogenolysis is also indicated by a sum of modified hydrocracking selectivities (ΣS_j^*) very close to 200 %. The volcano (or bell) shape of the curve for n-decane hydrogenolysis on 2.6Ir/silica reveals that, on this metal, the probability of hydrogenolytic rupture of central bonds in the n-alkane leading to 2 C_5, to C_4 plus C_6, or to C_3 plus C_7 is significantly higher than cleavage of carbon-carbon bonds at the ends of the hydrocarbon chain.

The modified hydrocracking selectivities in Figure 7.7 for the hydroconversion of the equimolar decalin/n-decane mixture are found to be located between those for the experiments with the pure feeds. This finding seems to be consistent with the main conclusion already drawn from the selectivities of the various product groups in Figure 7.6, *i.e.*, the reaction pathways of a given feed hydrocarbon in the hydroconversion on 2.6Ir/silica are not significantly influenced by the presence of another hydrocarbon.

In Figures 7.8a and b, the selectivities of the products made on the 2.7Pt/silica catalyst from, respectively, pure decalin and pure n-decane are shown. The product selectivities differ substantially from the ones observed on 2.6Ir/silica (Figure 7.5). In the hydroconversion of decalin (Figure 7.8a), skeletal isomers of the feed are the most abundant products ($S_{\text{sk-Isos}} \approx 80$ % at 300 °C). Interestingly, a single skeletal isomer, *viz.* spiro[4.5]decane, accounts for more than 30 % of the decalin isomers formed under these conditions, in agreement with results of Haas *et al.* [70] who studied decalin conversion on a non-acidic 2.7Pt/silica catalyst. Another group of products observed at low conversion are ring-opening products, but they occur at low selectivities below 20 %. Open-chain decanes are formed with negligible selectivities throughout the entire range of conversions. Upon increasing the reaction temperature and the decalin conversion, C_9- hydrocarbons are increasingly formed, and the selectivity of dehydrogenated products (tetralin and naphthalene) passes through a maximum of *ca*. 25 % at T = 400 °C. The part of increasing S_{DHPs} is probably due to the dehydrogenation equilibrium getting more and more

favorable, while the decreasing branch of the S_{DHPs} curve is likely to have its origin in the ever faster hydrocracking reaction of decalin into C_9- products. Thus, decalin is hydrocracked before it can be dehydrogenated to tetralin or naphthalene.

The hydroconversion of n-decane on 2.7Pt/silica (Figure 7.8b) leads to the formation of mainly hydrocracked products and, to a lower extent, skeletal isomers. At first glance, these results seem to be very close to the results obtained on 2.6Ir/silica. However, the selectivities of hydrocracked products are somewhat lower and those of skeletal isomers higher on 2.7Pt/silica than the ones obtained on 2.6Ir/silica. Moreover, the hydrocracked products consist to more than 8 % of branched alkanes. All these findings can be explained by a slight isomerization activity of platinum which was reported previously by Haas [119].

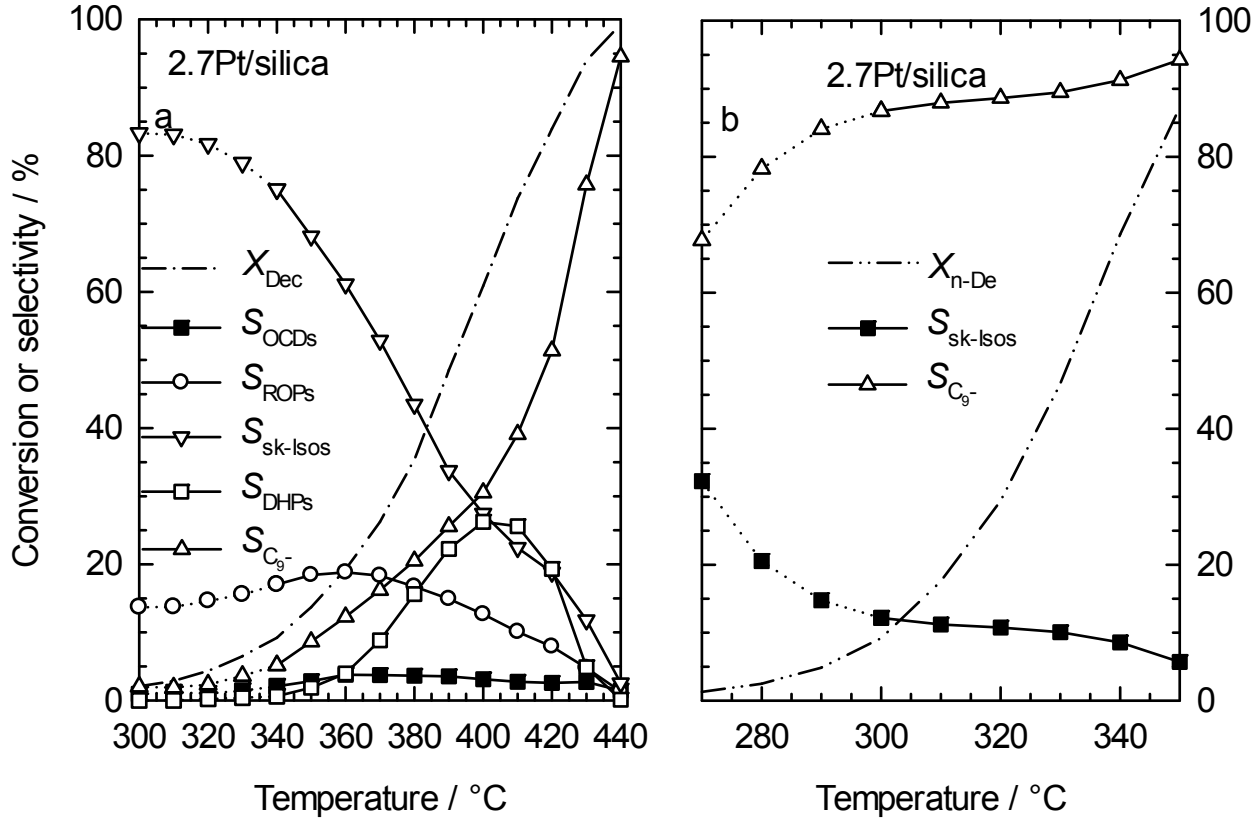

Figure 7.8: Hydroconversion of pure decalin (a) and pure n-decane (b). Selectivities of different groups of products on catalyst 2.7Pt/silica.

The modified hydrocracking selectivities observed on the 2.7Pt/silica catalyst from pure decalin, pure n-decane, and the equimolar mixture of both at moderate yields of hydrocracked products are shown in Figure 7.9. With

n-decane as reactant, a bell-shaped curve is obtained with relatively large amounts of C_3 to C_7 and minor amounts of C_1, C_2, C_8 and C_9 hydrocarbons. Similar curves were previously reported in the literature for the hydrogenolysis of n-decane on 2.0Pt/Al_2O_3 and 2.7Pt/SiO_2 [119,146]. With decalin as feed hydrocarbon, a completely different distribution curve results: its features are low amounts (between 10 and 30 %) of C_2 to C_9 hydrocarbons, but an excessive formation of methane (260 %). Severe secondary hydrocracking all the way down to C_1 occurs on platinum, as indicated by a high value of the sum of all selectivities of C_1 to C_9 amounting to 376 % (see Table 7.2).

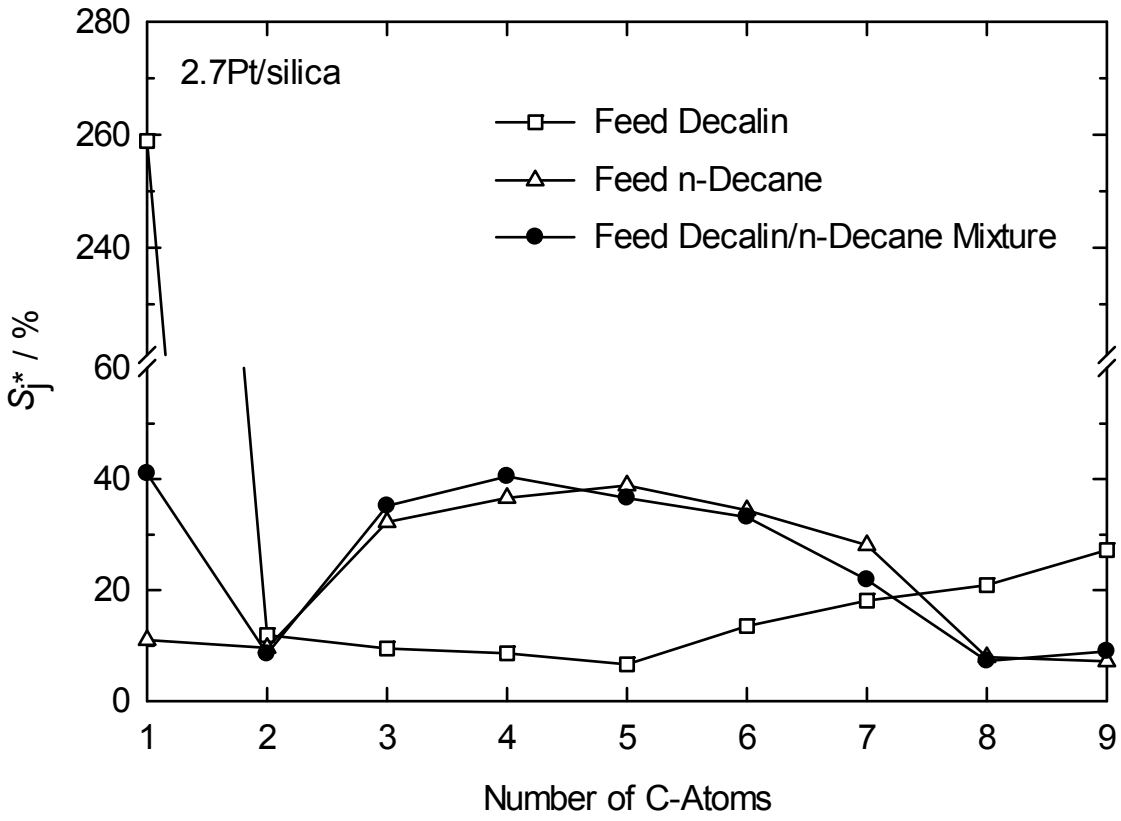

Figure 7.9: Modified hydrocracking selectivities S_j^* of decalin, n-decane and an equimolar mixture of both hydrocarbons on catalyst 2.7Pt/silica. Reaction conditions are given in Table 7.2.

Again, the tendency of non-acidic platinum catalysts to form excessive amounts of methane in the hydrogenolysis of decalin has been reported previously [119]. Figure 7.9 also shows the modified hydrocracking selectivities resulting for the hydroconversion of the equimolar decalin/n-decane mixture. It resembles the one for the hydrogenolysis of pure n-decane. The main difference is a much higher selectivity of methane for the mixed-feed hydroconversion which obviously stems from the reactant decalin.

Table 7.2: Reaction conditions for measuring the modified hydrocracking selectivities S_j* plotted in Figure 7.9 (Catalyst: 2.7Pt/silica).

Feed	T_r / °C	X / %	$Y_{C_{9^-}}$ / %	ΣS_j* / %
Pure decalin	390	49	12	376
Pure n-decane	320	29	26	206
Equimolar decalin/n-decane mixture	360	25	12	233

The results of the hydroconversion of the equimolar decalin/n-decane mixture on the 2.7Pt/silica catalyst are depicted in Figure 7.10. Up to *ca.* 380 °C, the partial conversions of decalin and n-decane are very similar (Figure 7.10a). Above this temperature, the partial conversion of decalin is getting significantly higher than that of n-decane. This effect is due to the onset of decalin dehydrogenation to tetralin and naphthalene which is observed at the same temperature, *cf.* the curve for S_{DHPs} in Figure 7.10a. In Figure 7.10b, the data from Figure 7.10a were re-plotted against the total conversion. Following the same procedure as for the decalin/n-decane mixture on the 2.6Ir/silica catalyst (*cf.* Figure 7.6c) the product selectivities for the mixed-feed experiments on 2.7Pt/silica were now calculated from the selectivities found in the experiments with the pure feeds decalin or n-decane (Figure 7.8). The thus calculated selectivities are plotted *vs.* the total conversion in Figure 7.10c. Again, the measured selectivities (Figure 7.10b) and the calculated ones (Figure 7.10c) generally show a good agreement. This confirms, by and large, the validity of the underlying assumption that the product selectivities are, in the first place, dependent on the nature of the catalyst and the conversion.

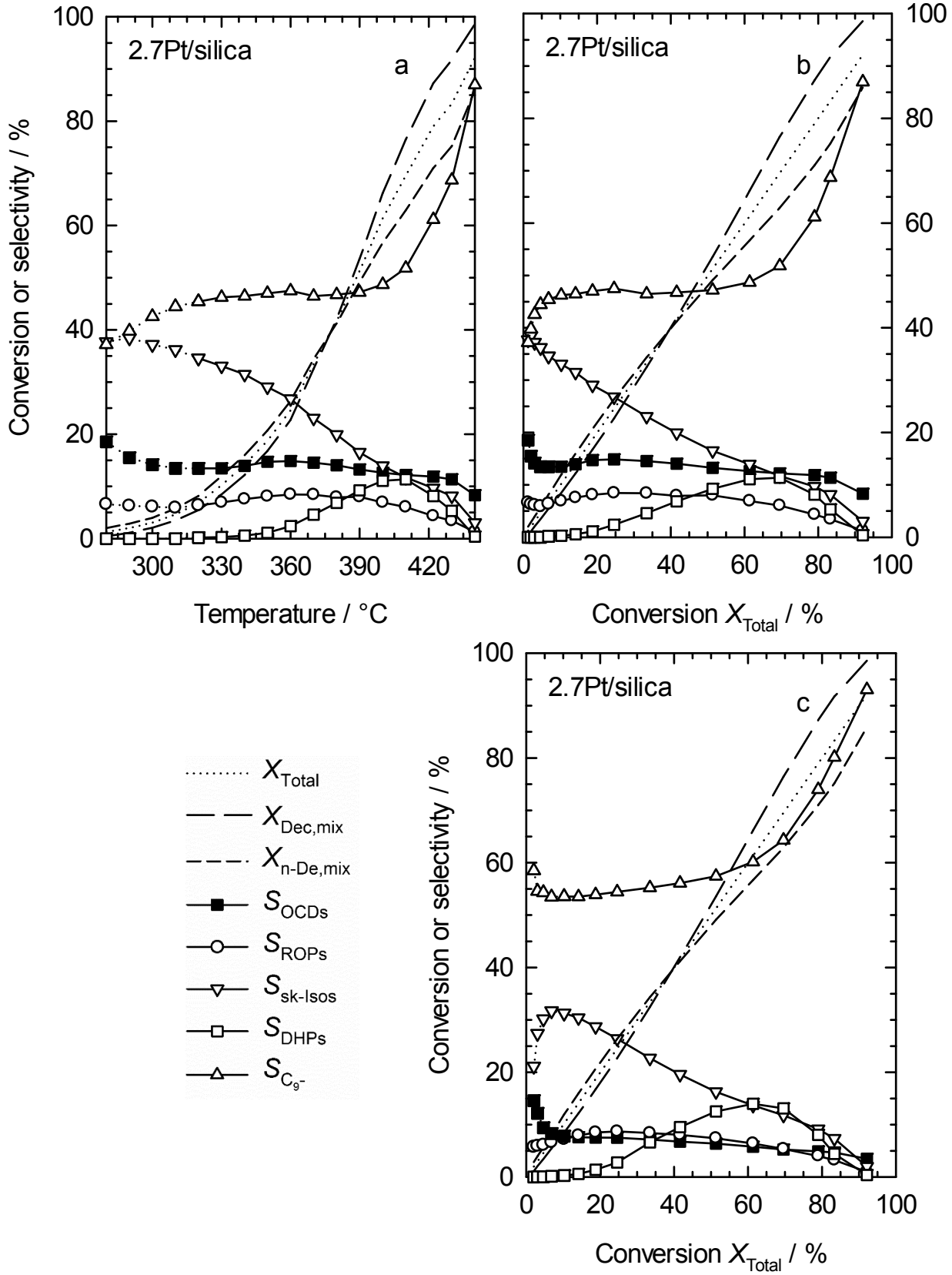

Figure 7.10: Hydroconversion of an equimolar mixture of decalin and n-decane on catalyst 2.7Pt/silica. Measured conversions and product selectivities in dependence of temperature (a); measured product selectivities replotted against the total conversion (b); product selectivities calculated from the selectivities measured with the pure decalin and n-decane feeds (c).

It can be safely stated that two groups of products, namely the skeletal isomers of decalin (sk-Isos) and the ring-opening products (ROPs) still containing one naphthenic ring, can form only from the feed decalin. Figure 7.10 suggests that the selectivities of these products are not affected by the presence of n-decane as the second reactant. On the other hand, in the presence of n-decane, the selectivities of open-chain decanes (OCDs) tend to be higher and those of C_9- hydrocarbons are lower than those predicted by calculation (Figure 7.10c). We attribute the significantly higher selectivities of OCDs in Figure 7.10b as compared with those in Figure 7.10c to a platinum-catalyzed skeletal isomerization of n-decane when it is present in the feed. When iso-decanes are formed from n-decane in the presence of decalin in the mixed-feed experiments, they are displaced from the platinum sites and prevented from a consecutive hydrocracking into C_9- hydrocarbons by competitive adsorption/desorption. The occurrence of such a competitive adsorption on platinum catalysts has been reported in the literature [85]. The larger selectivity of OCDs in the mixed-feed experiments (Figure 7.10b) as compared with the calculated selectivities (Figure 7.10c) compensates nicely the lower selectivities of C_9- hydrocarbons.

Table 7.3: Maximum yields of open-chain decanes obtained with pure decalin as reactant and a decalin/n-decane mixture on 2.6Ir/silica and 2.7Pt/silica.

Catalyst	**Feed**	T_r **/ °C**	X **/ %**	S_{OCDs} **/ %**	$Y_{OCDs,max.}$ **/ %**
2.6Ir/silica	Pure decalin	310	84.6	23.6	19.9
2.6Ir/silica	Equimolar decalin/n-decane mixture	320	73.0	10.3	7.5
2.7Pt/silica	Pure decalin	430	94.0	2.7	2.6
2.7Pt/silica	Equimolar decalin/n-decane mixture	422	79.0	11.4	7.5

Some important facts concerning the formation of open-chain decanes are summarized in Table 7.3 for the catalysts 2.6Ir/silica and 2.7Pt/silica. Iridium is much more active than platinum which is reflected in the lower reaction temperatures for 2.6Ir/silica. The best yields of OCDs are obtained on the iridium catalyst ($Y_{OCDs,max.}$ = 19.9 %). Unfortunately, when converting a mixture consisting of decalin and n-decane on 2.6Ir/silica, the yields of OCDs are lower

than obtained for the pure feed decalin. Hence, OCDs are preferentially hydrocracked, leading to their lower yields.

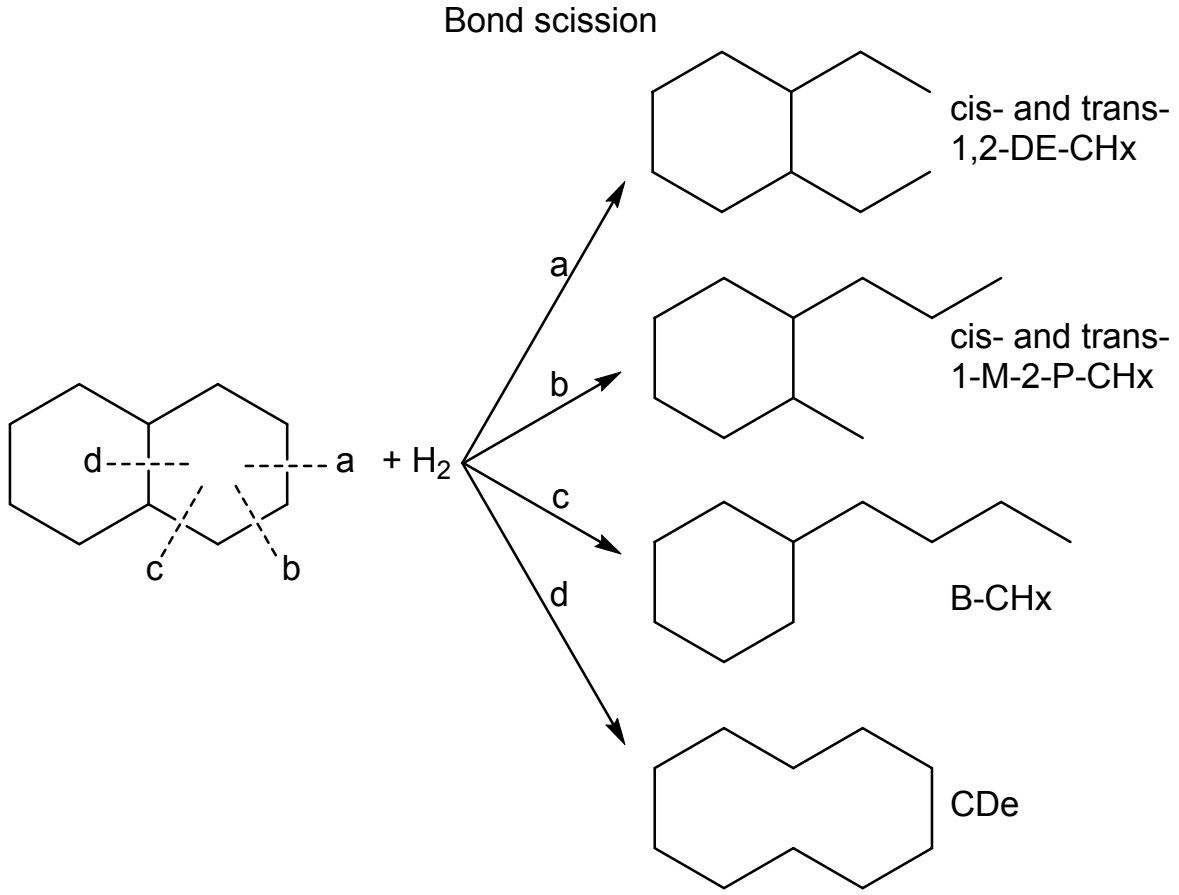

Figure 7.11: Decalin and its direct ring-opening products (direct ROPs) resulting from the cleavage of a single carbon-carbon bond.

In two very recent publications the mechanism of decalin ring opening on the non-acidic iridium catalysts 1.8Ir/Al_2O_3 [69] and 2.6Ir/SiO_2 [70] was discussed in detail. The results of both groups agree well with each other. Neither the noble metal nor the carriers possess any activity for skeletal isomerization, hence the only possible reaction is the direct cleavage of carbon-carbon bonds in a six-membered ring, and the resulting products are referred to as “direct ring-opening products” (direct ROPs or dROPs). As Figure 7.11 shows, the possible direct ROPs are cis- and trans-1-methyl-2-propylcyclohexane, cis- and trans-1,2-diethylcyclohexane, butylcyclohexane, and cyclodecane. No cyclodecane was ever formed from decalin on iridium catalysts [32,67,119]. Of the remaining dROPs, butylcyclohexane is formed by hydrogenolysis of a bond between one substituted and one unsubstituted carbon atom, whereas 1-methyl-2-propylcyclohexane and 1,2-diethylcyclohexane result from cleavage of a bond between two unsubstituted carbon atoms. Figure 7.12a reveals that on iridium, the latter mode of hydrogenolysis, also called the “dicarbene

mechanism", is strongly preferred [32,67]. It is furthermore seen from Figure 7.12a that in the hydroconversion of decalin on non-acidic iridium catalysts, direct ROPs are made almost exclusively, especially at low and moderate conversions. The ring-opening selectivities measured in this work with pure decalin as feed on 2.6Ir/silica (Figure 7.12a) agree very well with those reported in the literature for similar iridium catalysts.

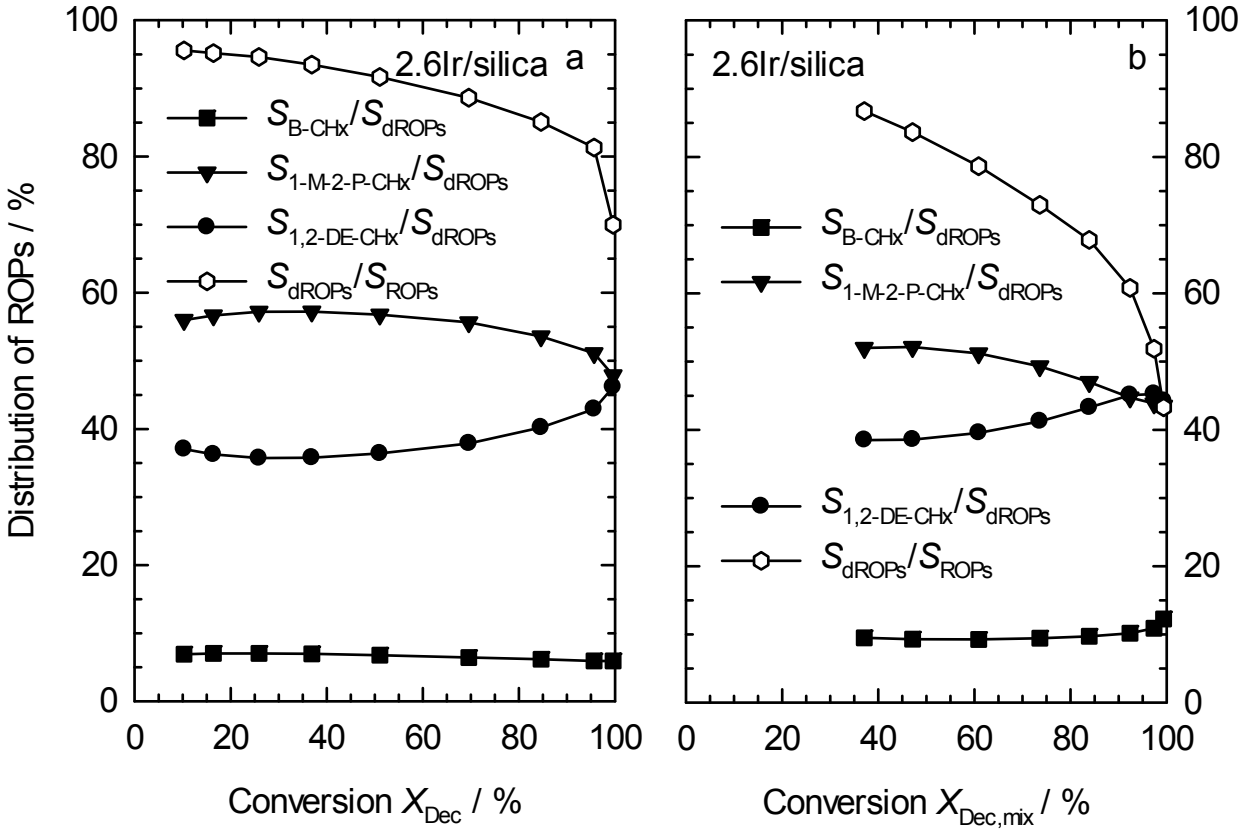

Figure 7.12: Composition of the direct ROPs obtained on 2.6Ir/silica in the hydroconversion of pure decalin as feed (a) and a decalin/n-decane mixture (b).

In Figure 7.12b the selectivities of the direct ROPs formed from decalin in the hydroconversion of the decalin/n-decane mixture on the 2.6Ir/silica catalyst are shown. The curves strongly resemble those obtained with the pure decalin feed (Figure 7.12a). It must be mentioned that, with the mixed feed, the selectivities of the direct ROPs cannot be determined with sufficient accuracy at low decalin conversions with the mixed feed. The reason is that the peak of one stereoisomer of 1-methyl-2-propylcyclohexane in the gas chromatogram overlaps with the large peak of n-decane. The true values for $S_{1\text{-}M\text{-}2\text{-}P\text{-}CHx}/S_{dROPs}$ and S_{dROPs}/S_{ROPs} in Figure 7.12b are therefore higher than shown in the figure.

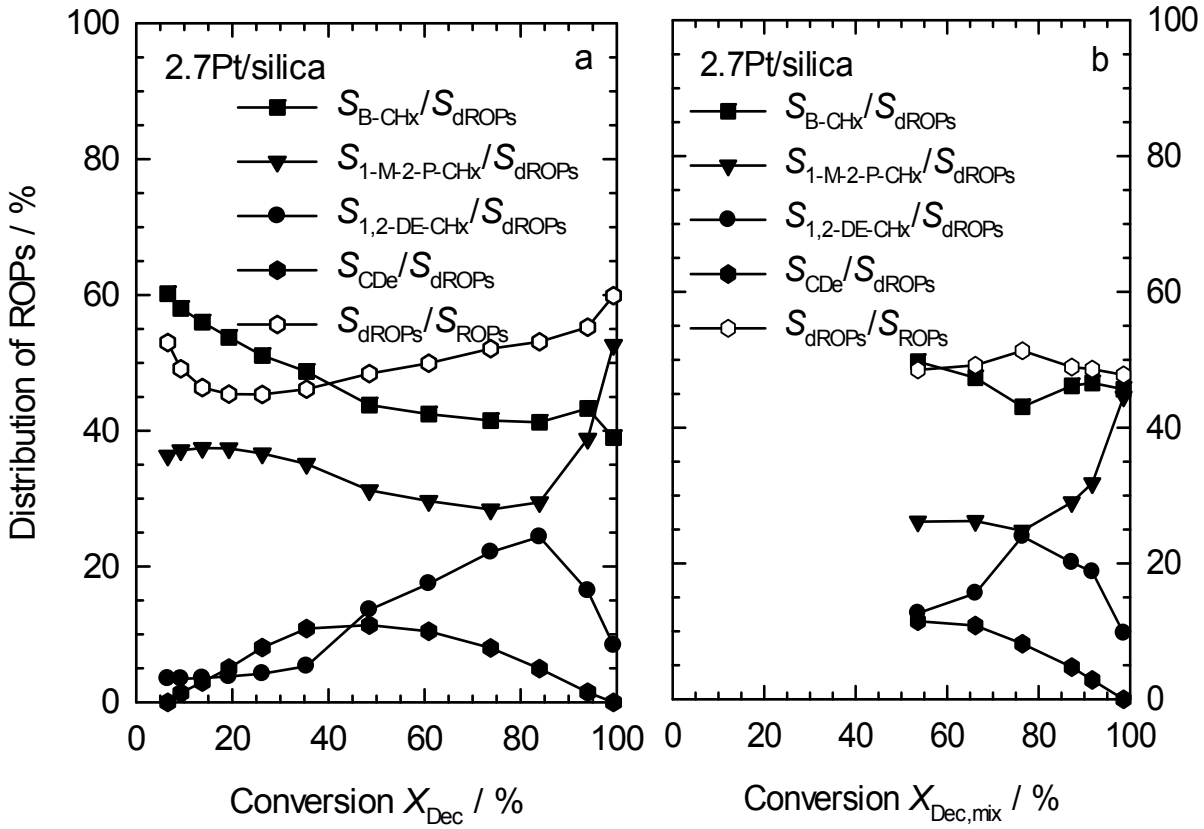

Figure 7.13: Composition of the direct ROPs obtained on 2.7Pt/silica in the hydroconversion of a pure decalin feed (a) and a decalin/n-decane mixture (b).

Figure 7.13a and b show the selectivities of the products formed by ring-opening of decalin on 2.7Pt/silica in the experiments with pure decalin as feed and with the decalin/n-decane mixture, respectively. These selectivities differ strongly from those observed with the 2.6Ir/silica catalyst (Figure 7.12). Using pure decalin as reactant, only *ca.* 50 % of the ROPs produced are direct ROPs. It appears that, on platinum, the direct ring-opening products can undergo a consecutive skeletal isomerization on the metal. Moreover, butylcyclohexane is the most abundant ROP at low conversions followed by 1-methyl-2-propylcyclohexane. This finding is in agreement with literature reports [119] and with the general tendency of platinum to prefer hydrogenolysis of bonds between a tertiary and a secondary carbon atom (*cf.* Figure 7.11). Another difference between platinum and iridium, which is noteworthy, is the formation of cyclodecane on the former metal, though the maximum selectivity of cyclodecane is around 10 %. The formation of CDe from decalin is readily interpreted in terms of hydrogenolysis of the bond between the two tertiary carbon atoms in decalin (*cf.* Figure 7.11). Overall, the ring-opening selectivities found on 2.7Pt/silica are better accounted for by a flat adsorption of the decalin molecules and the multiplet mechanism than by a dicarbene mechanism.

7.5 Competitive Hydroconversion on Bifunctional Catalysts

7.5.1 Ir/Na,H-Y-2.4 Catalysts with Varied Concentrations of Brønsted Acid Sites

A series of four catalysts was prepared which all contained approximately 3 wt.-% of iridium supported on Y-zeolites with different concentrations of Brønsted acid sites (see Table 6.5, page 106). Between 4 and 90 % of the charge-compensating framework cations of the zeolites were replaced by protons. All four catalysts were tested in the hydroconversion of pure decalin, pure n-decane and an equimolar mixture of decalin and n-decane.

The conversions of the pure compounds and their partial conversions in the experiments with the mixture are depicted in Figure 7.14. On all four catalysts n-decane is the more reactive compound when converted alone. The reactivity of pure decalin is lower, this hydrocarbon needs significantly higher reaction temperatures than pure n-decane to reach the same conversion. With increasing concentration of Brønsted acid sites in the catalysts (Figures 7.14a - d), the reactivity difference between both pure hydrocarbons shrinks.

When converted in an equimolar mixture, the reactivities of decalin and n-decane are inverted. Throughout the series of the four catalysts (Figures 7.14a - d), decalin shows higher conversions at the same reaction temperature than n-decane. At a given reaction temperature, the conversion of decalin is virtually the same and independent of the presence or absence of n-decane. On the other hand, a considerable decrease in the reactivity of n-decane can be seen when decalin is present, and significantly higher reaction temperatures are necessary to reach the same conversion.

These findings are again best interpreted in terms of a stronger adsorption of decalin on the active sites of the catalysts. The adsorbed decalin prevents n-decane from being converted on these sites and therefore reduces the measured reactivity of n-decane. Since decalin is readily adsorbed on the active sites, its reactivity is hardly affected by the presence of n-decane and depends on the reactor temperature only.

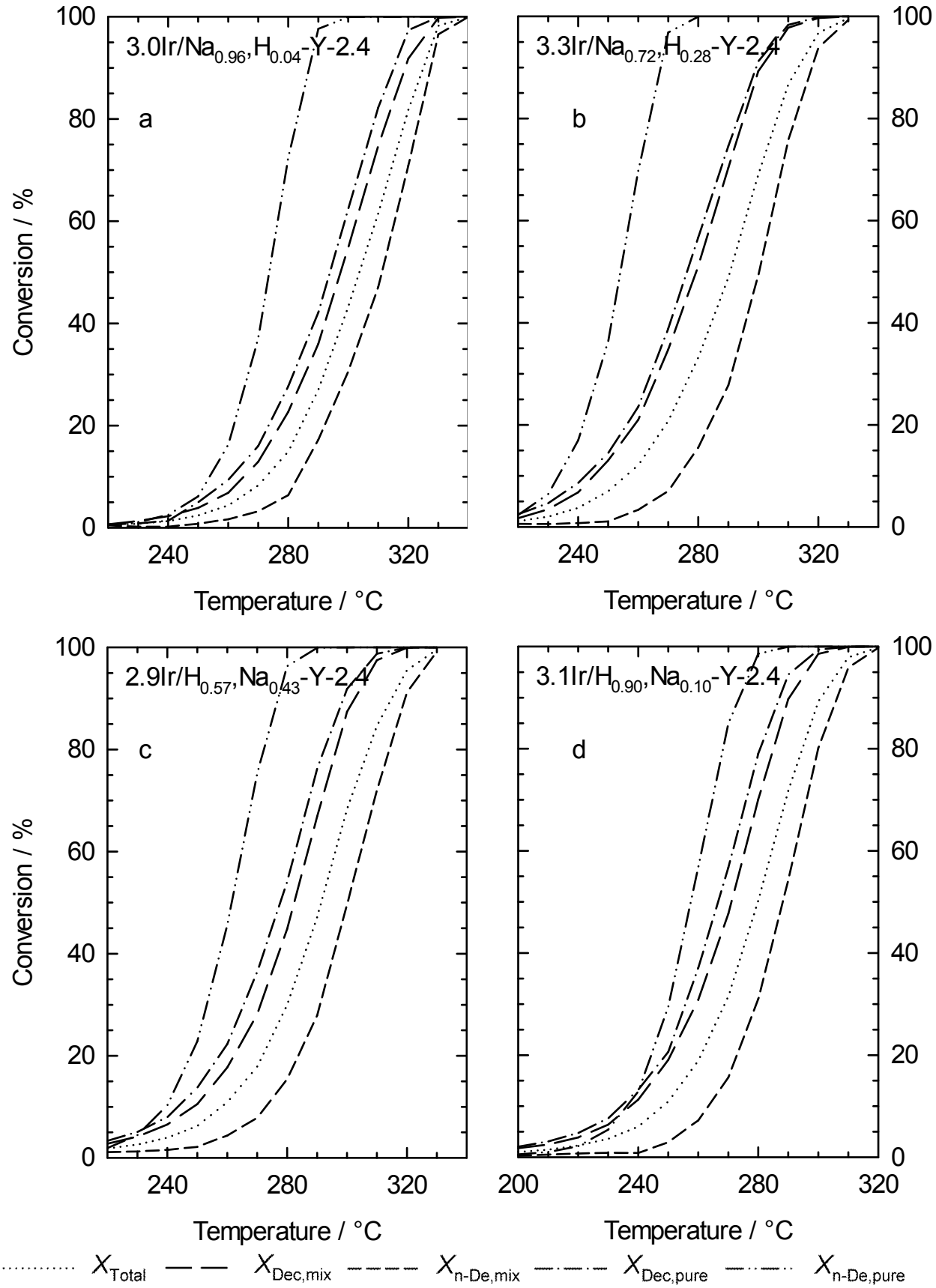

Figure 7.14: Comparison of the conversions measured with pure decalin and pure n-decane and of the same feed hydrocarbons measured with an equimolar decalin/n-decane mixture on Ir/Na,H-Y-2.4 zeolites.

The adsorption properties of cis-decalin and n-decane on catalysts 3.0Ir/$Na_{0.96}$,$H_{0.04}$-Y-2.4, 3.3Ir/$Na_{0.72}$,$H_{0.28}$-Y-2.4 and 3.1/$H_{0.90}$,$Na_{0.10}$-Y-2.4 were tested in the competitive adsorption of an equimolar mixture of both hydrocarbons at 100 °C. The measured breakthrough curves are depicted in Figure 7.15 and compared with the corresponding curves for sea sand. The experimental conditions for the adsorption may be found in Section 5.3.2.4 on page 82.

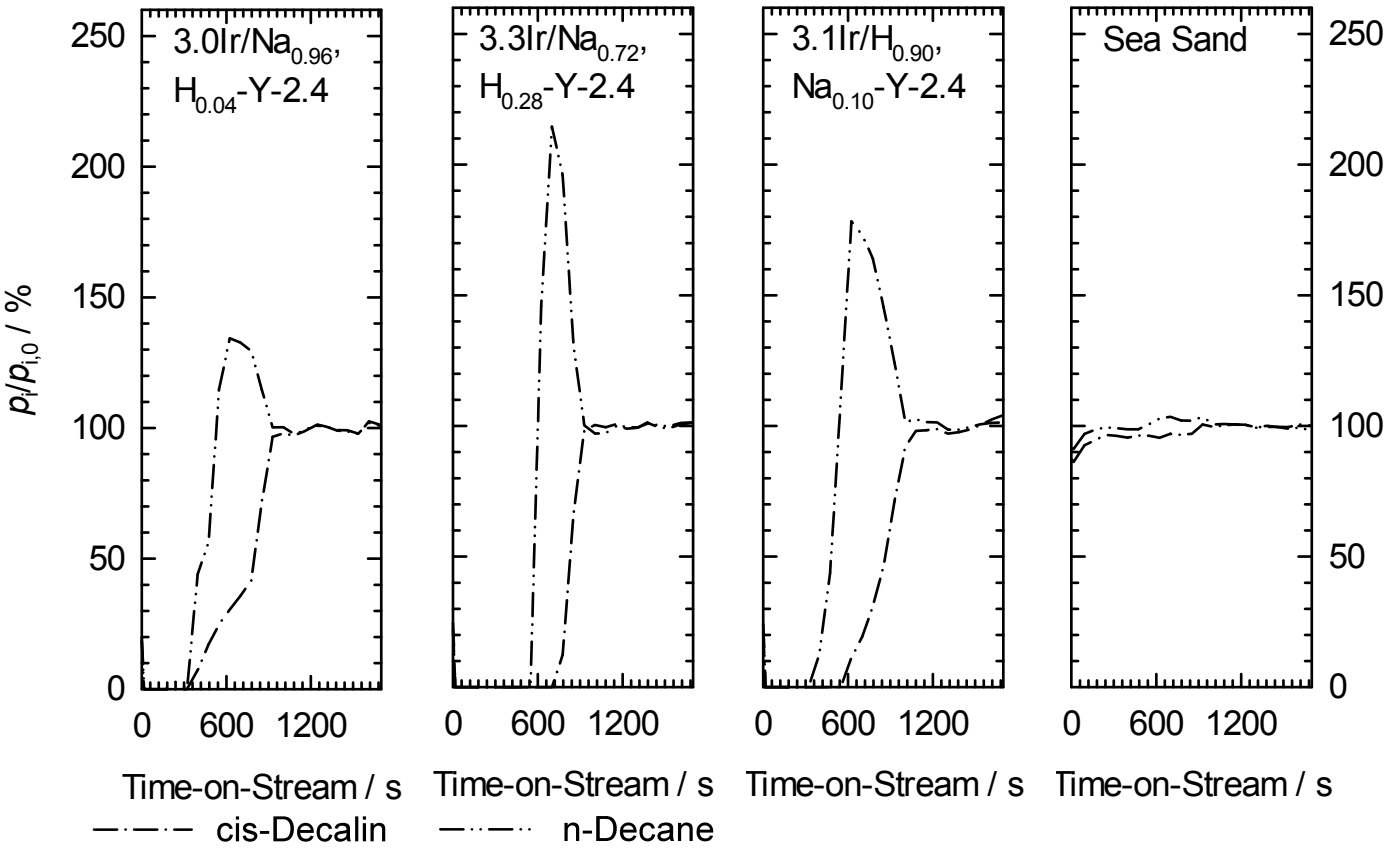

Figure 7.15: Breakthrough curves obtained in the competitive adsorption of an equimolar cis-decalin/n-decane mixture at 100 °C. i stands for cis-decalin or n-decane. $p_{i,0}$ is the partial pressure at the adsorber entrance, $p_{cis\text{-}decalin} = p_{n\text{-}decane} = 0.60$ kPa. p_i is the respective partial pressure at the adsorber exit.

Under these conditions, practically no adsorption of cis-decalin or n-decane occurs on sea sand, both hydrocarbons break through almost immediately at the onset of the experiment. A different situation is encountered with the zeolitic adsorbents: For at least 5 min, none of the hydrocarbons can be detected at the adsorber exit, *i.e.*, both cis-decalin and n-decane are completely adsorbed. Breakthrough of the hydrocarbons is observed after 5 to 10 min. In all cases, n-decane is the first hydrocarbon to break through.

Moreover, $p_{\text{n-decane}}/p_{\text{n-decane,0}}$ even exceeds unity for some time-on-stream, it then passes through a maximum (which can reach a value higher than 200 %), before if falls down to unity, *i.e.*, both adsorptives appear at the adsorber exit in concentrations that equal those at the adsorber entrance.

These curves unambiguously show that cis-decalin is preferentially adsorbed over n-decane on the zeolitic materials used as adsorbents. During the period when $p_{\text{n-decane}} > p_{\text{n-decane,0}}$ ("overshoot" of the curves), n-decane that was initially adsorbed is displaced from the zeolite surface to the gas phase by the more strongly adsorbed decalin.

Table 7.4: Relative Masses of adsorbed cis-decalin and n-decane calculated from the breakthrough curves.

Adsorbent	$m_{\text{c-Dec}}/m_{\text{adsorbent}}$ / mg·g^{-1}	$m_{\text{n-De}}/m_{\text{adsorbent}}$ / mg·g^{-1}
3.0Ir/$Na_{0.96}$,$H_{0.04}$-Y-2.4	305	133
3.3Ir/$Na_{0.72}$,$H_{0.28}$-Y-2.4	347	151
3.1Ir/$H_{0.90}$,$Na_{0.10}$-Y-2.4	353	102

A quantitative evaluation of the adsorbed mass of cis-decalin (see Table 7.4) reveals values of 305, 347 and 353 mg per gram of 3.0Ir/$Na_{0.96}$,$H_{0.04}$-Y-2.4, 3.3Ir/$Na_{0.72}$,$H_{0.28}$-Y-2.4 and 3.1Ir/$H_{0.90}$,$Na_{0.10}$-Y-2.4, respectively. Although identical concentrations in the gas phase of cis-decalin and n-decane are offered to the adsorbents, the amount of adsorbed cis-decalin was two to three times higher compared to n-decane. Usually, the adsorption of the reactant on a catalyst precedes its conversion in heterogeneous catalysis. In this respect, the strongly preferred adsorption of cis-decalin over n-decane on all three catalysts is very advantageous in terms of a wanted hydroconversion of decalin, while keeping open-chain decanes away from being hydrocracked.

An interesting observation was made during the above-described investigation of the competitive adsorption of the cis-decalin/n-decane mixture: Previous work in the group [81] and by others [53,61] had shown that by far the fastest reaction of cis-decalin is its stereoisomerization into trans-decalin which is catalyzed by noble metals long before reactions like skeletal isomerization, ring opening *etc.* take place. In fact, at temperatures above *ca.* 200 °C, where these latter reactions are usually studied, the noble metal-catalyzed stereoisomerization is at equilibrium, *i.e.*, the whole catalytic ring-opening

chemistry inevitably starts from the equilibrium mixture of cis- (*ca.* 10 %) and trans-decalin (*ca.* 90 %), regardless of which stereoisomer is used as reactant. It was found that the stereoisomerization occurs to a negligible extent only at 100 °C, but equilibrium is reached from *ca.* 180 °C onwards.

The results of the hydroconversion of pure decalin on the four Ir/Na,H-Y-2.4 zeolites are depicted in Figure 7.16. The activity of the catalysts and selectivities of the products depend on the concentration of Brønsted acid sites. Especially, the least active catalyst in this series is 3.0Ir/$Na_{0.96}$,$H_{0.04}$-Y-2.4. Upon increasing the concentration of Brønsted acid sites, the catalyst activity increases as well, again as expected. Skeletal isomers of decalin are primary products obtained on all four catalysts. With increasing reaction temperature, the selectivities of skeletal isomers decrease, whereas the selectivities of ring-opening products go through maxima. Appreciable amounts of open-chain decanes are formed on all four Ir/Na,H-Y-2.4 zeolite catalysts. Their selectivities pass through maxima, for the catalyst 3.3Ir/$Na_{0.72}$,$H_{0.28}$-Y-2.4 this maximum is as high as 37.2 %. As usually, the selectivities of hydrocracked products increases with increasing reaction temperature, these undesired products become predominant near full conversion of decalin.

Two effects can be seen from Figure 7.16: Firstly, the temperature at which maximum selectivities of OCDs are reached decreases with increasing concentration of Brønsted acid sites. Secondly, the highest maximum in the selectivities of OCDs occurs on catalyst 3.3Ir/$Na_{0.72}$,$H_{0.28}$-Y-2.4, *i.e.* an intermediate concentration of Brønsted acid sites is favorable for the formation of OCDs [79,81].

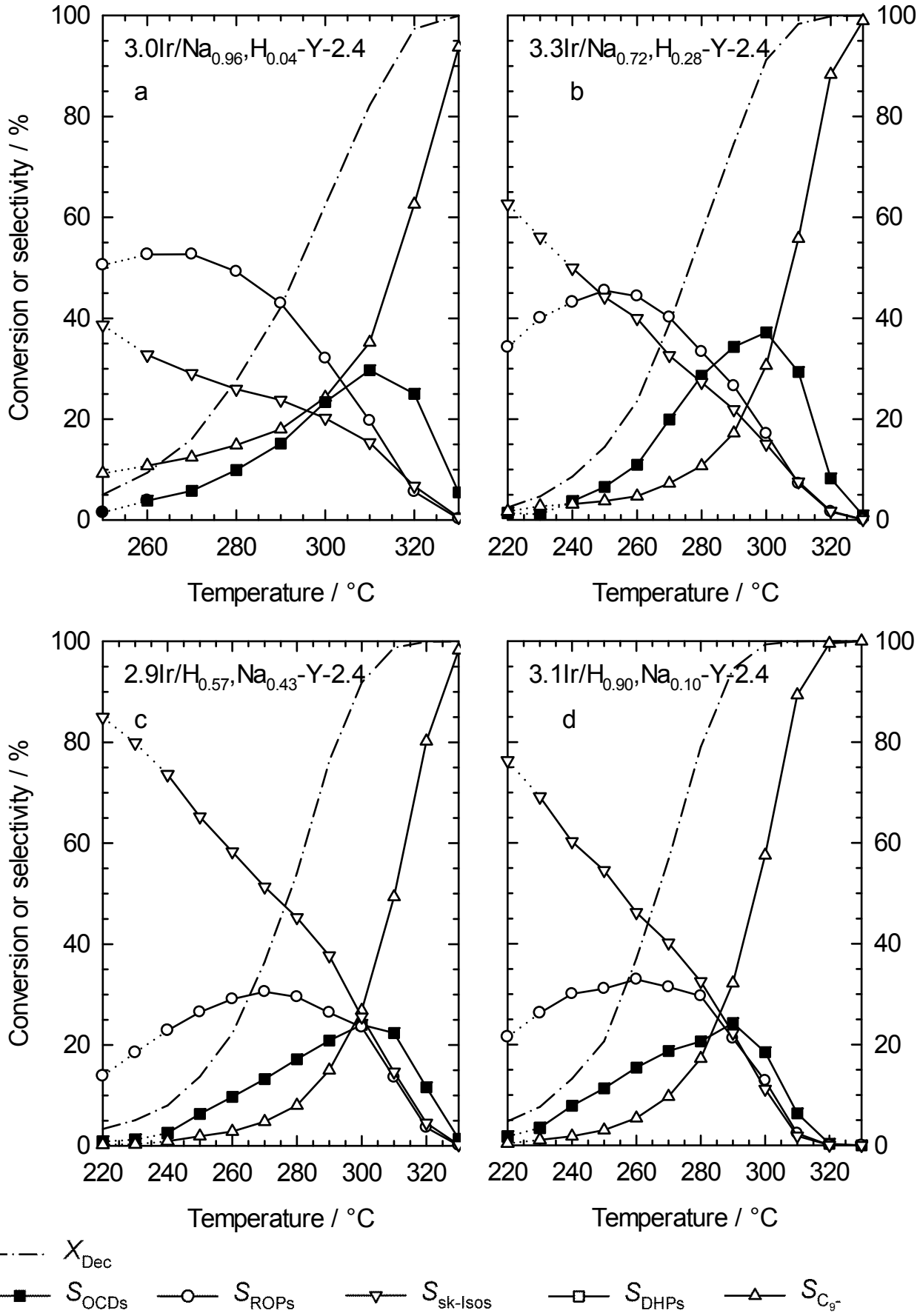

Figure 7.16: Conversions and product selectivities in the hydroconversion of pure decalin on the Ir/Na,H-Y-2.4 catalysts.

In Table 7.5, the conditions at which the highest yields of OCDs on the Ir/Na,H-Y-2.4 catalysts were obtained are summarized. It can be seen that only one catalyst fulfills the requirements of a HIPEROC (Y_{OCDs} > 25 %). The term HIPEROC was coined by Haas *et al.* [70] and later defined more precisely by Santi *et al.* [79] for catalysts which give particularly good yields of OCDs in the ring opening of decalin.

Table 7.5: Maximum yields of open-chain decanes obtained on Ir/Na,H-Y-2.4 catalysts in the hydroconversion of pure decalin.

Catalyst	T_r / °C	X / %	S_{OCDs} / %	$Y_{OCDs,max.}$ / %
3.0Ir/$Na_{0.96}$,$H_{0.04}$-Y-2.4	320	97.4	25.0	24.4
3.3Ir/$Na_{0.72}$,$H_{0.28}$-Y-2.4	300	91.2	37.2	**33.9**
2.9Ir/$H_{0.57}$,$Na_{0.43}$-Y-2.4	310	98.8	22.3	22.1
3.1Ir/$H_{0.90}$,$Na_{0.10}$-Y-2.4	290	94.5	24.3	22.9

The conversions and selectivities of the products in the hydroconversion of pure n-decane on the Ir/Na,H-Y-2.4 catalysts are depicted in Figure 7.17. It appears that, on catalyst 3.0Ir/$Na_{0.96}$,$H_{0.04}$-Y-2.4 with the lowest concentration of Brønsted acid sites, the selectivities of hydrocracked products exceed more than 80 % even at conversions < 10 %. With an increased concentration of Brønsted acid sites of the catalysts, the selectivities of hydrocracked products are lowered, while the selectivities of skeletal isomers are raised for the same conversion. An explanation for this behavior is the need of Brønsted acid sites for the skeletal isomerization of n-decane.

It should also be noted that as larger amounts of n-decane are isomerized at $X_{n\text{-De}} \approx 50$ %, the selectivity of C_9- products is reduced. It seems that the presence of iso-decanes prevents n-decane from being hydrocracked. This effect can also be observed when comparing the selectivities obtained from the n-decane conversion on 2.6Ir/silica and 2.7Pt/silica (*cf.* Figure 7.5b and Figure 7.8b). The reduction of selectivities of C_9- products around conversions of 50 % is also obtained on the isomerization-active 2.7Pt/silica catalyst. One can get the impression, that the isomerization to branched molecules prevents these molecules from undergoing hydrogenolysis. Hence, methyl and ethyl side-chains act as “protection groups” against carbon-carbon bond cleavage.

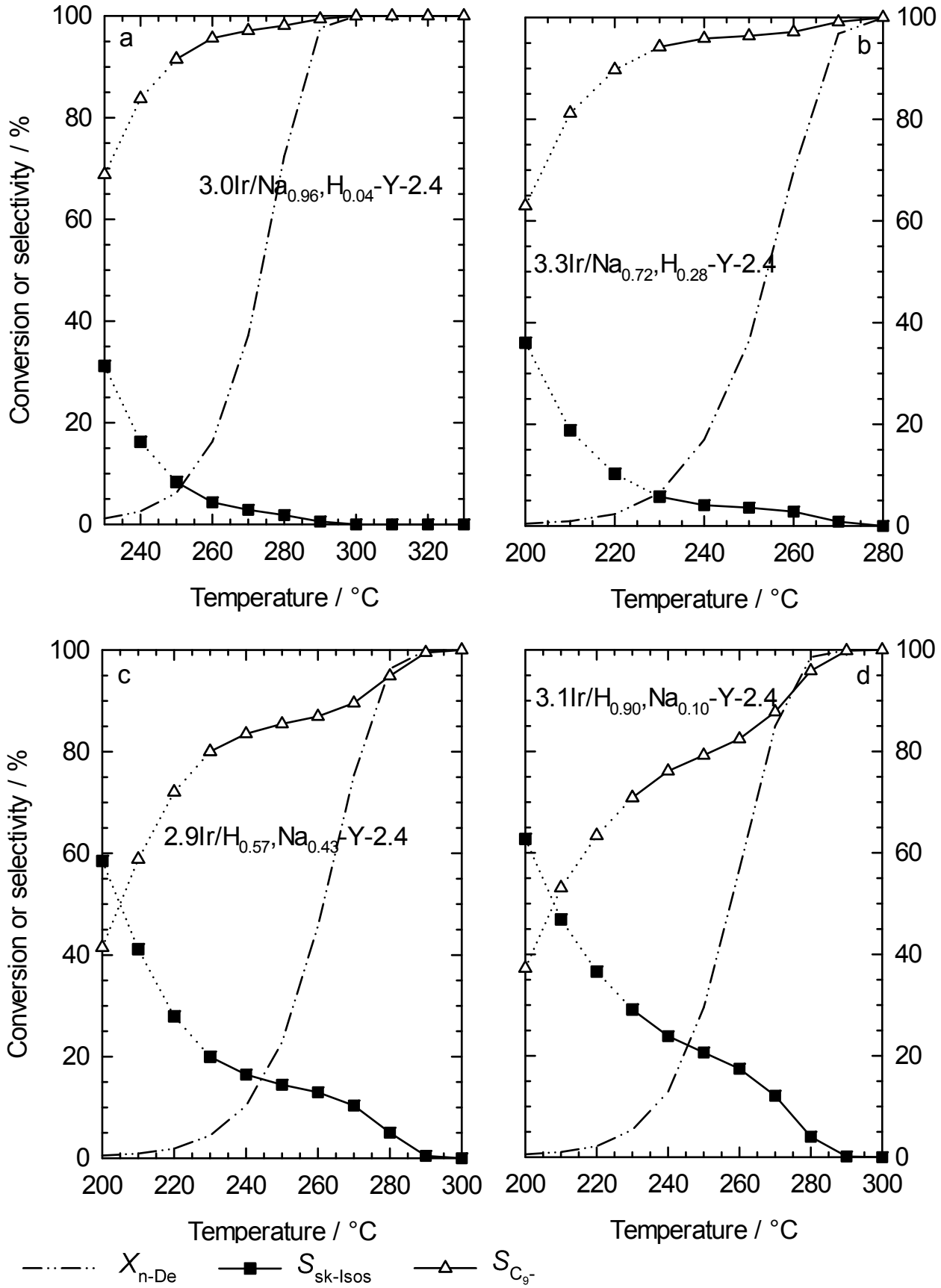

Figure 7.17: Conversions and product selectivities of pure n-decane on the Ir/Na,H-Y-2.4 catalysts.

This concept might be supported by a detailed look at the C_9- hydrocarbons. It is striking that the C_9- products between C_4 and C_7 are almost exclusively n-alkanes (*cf.* Appendix 10.1, Figure 10.1, page 199), even at n-decane conversions between 23 and 37 %. There is only a slightly increased tendency for the formation of branched hydrocracked products with increasing concentration of Brønsted acid sites. This is best explained by (i) carbon-carbon bond scission *via* hydrogenolysis on iridium and (ii) even if significant amounts of n-decane are isomerized, as it is the case on 2.9Ir/$H_{0.57}$,$Na_{0.43}$-Y-2.4 and 3.1Ir/$H_{0.90}$,$Na_{0.10}$-Y-2.4, this is not reflected in the degree of branching of the C_9- products. Hence, branched iso-decanes are hardly hydrocracked on the four Ir/Na,H-Y-2.4 catalysts.

For the conversion of mixtures of decalin and n-decane on the Ir/Na,H-Y-2.4 catalysts the same partial pressures for each feed hydrocarbon compared to the experiments with the pure feed hydrocarbons were again used. The conversions and selectivities observed in the mixed-feed experiments are depicted in Figure 7.18. Primary products are sk-Isos, similar to the experiments with pure decalin as feed. With increasing conversions the selectivities of sk-Isos decrease, while the selectivities of ROPs pass through maxima.

The catalyst with the lowest concentration of acid sites, *viz*. 3.0Ir/$Na_{0.96}$,$H_{0.04}$-Y-2.4, shows high selectivities of hydrocracked products even at very low conversions. With increasing temperature, the selectivity of ROPs passes through a maximum. It is conspicuous that, on this catalyst, the selectivity of OCDs remains on a low level and increases slightly as the selectivity of ROPs decreases.

An increase of the concentration of Brønsted acid sites in this series of catalysts reduces the maximum selectivity of ROPs. At the same time, the selectivity of OCDs increases to 45 % on 2.9Ir/$H_{0.57}$,$Na_{0.43}$-Y-2.4. Similarly high S_{OCDs} are also obtained on 3.1Ir/$H_{0.90}$,$Na_{0.10}$-Y-2.4. An explanation could be the isomerization of n-decane to its branched isomers on the catalysts with higher concentrations of acid sites, since the same selectivities of OCDs were obtained in the pure decalin hydroconversion on both 3.0Ir/$Na_{0.96}$,$H_{0.04}$-Y-2.4 and 3.1Ir/$H_{0.90}$,$Na_{0.10}$-Y-2.4. At the same time, the selectivities of hydrocracked products is remarkably low for X_{Total} below 50 % on the two catalysts containing the highest concentrations of Brønsted acid sites.

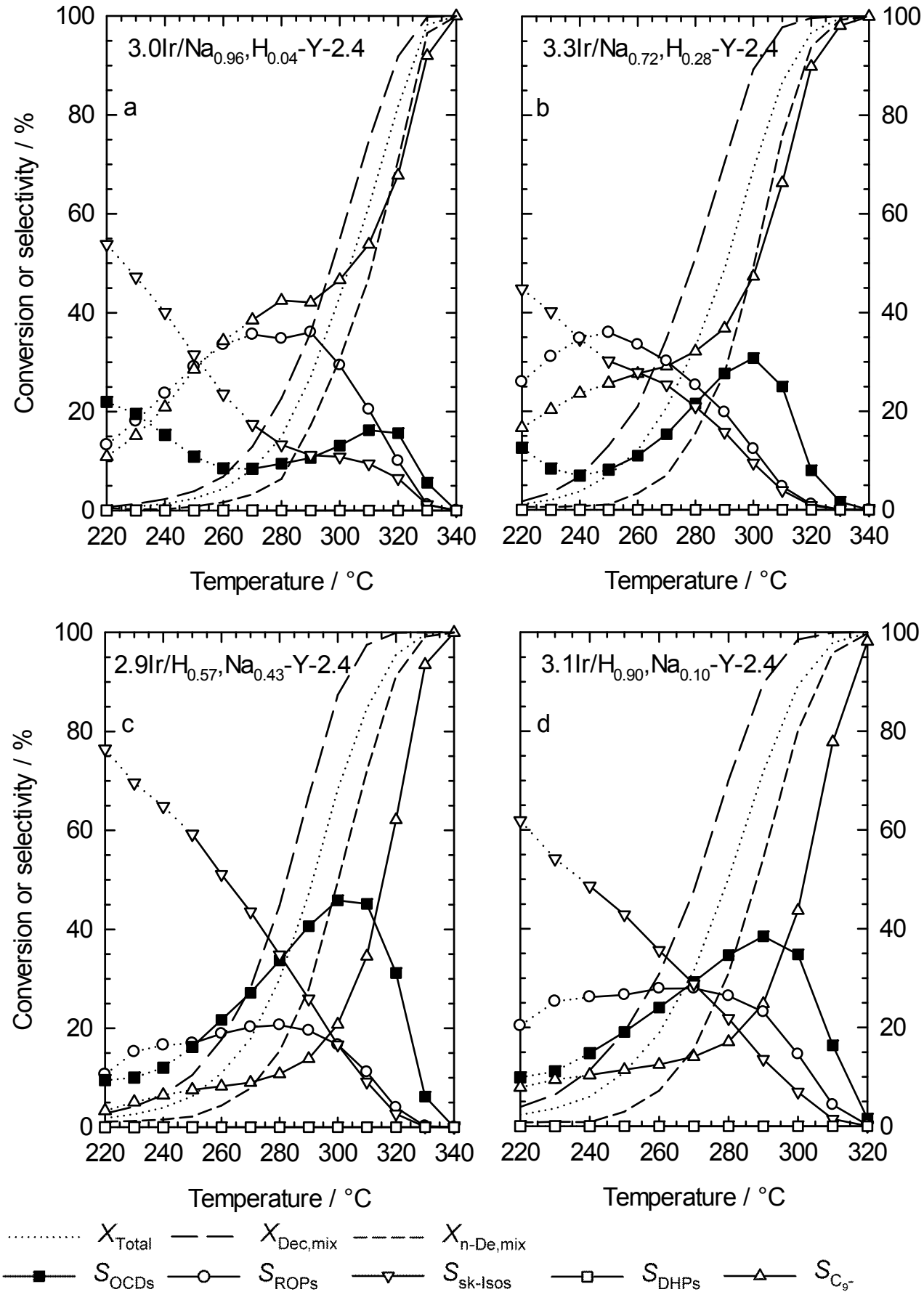

Figure 7.18: Conversions of an equimolar decalin/n-decane mixture and selectivities of different groups of products on the Ir/Na,H-Y-2.4 catalysts.

By and large, the product selectivities for the hydroconversion of the equimolar decalin/n-decane mixtures can be calculated out of the results of the pure feed experiments (*cf.* Appendix 10.1, Figure 10.4, page 202). However, with increasing concentration of Brønsted acid sites of the catalysts higher selectivities of OCDs and lower selectivities of C_9- were measured than predicted by the calculation. This might be explained by an isomerization of n-decane on the Brønsted acid sites of the catalyst. These iso-decanes become noticeable as higher measured selectivities of OCDs.

Table 7.6: Reaction conditions for the experiments that led to the modified hydrocracking selectivities S_j* shown in Figure 7.19 and the content of branched isomers from n-decane shown in Figure 10.1.

Catalyst	**Feed**	T_r / °C	X / %	Y_{C_9-} / %	ΣS_j* / %
3.0Ir/$Na_{0.96}$,$H_{0.04}$-Y-2.4	Pure decalin	310	82	29	215
	Pure n-decane	270	37	36	206
	Equimolar decalin/n-decane mixture	310	62	33	215
3.3Ir/$Na_{0.72}$,$H_{0.28}$-Y-2.4	Pure decalin	300	91	28	201
	Pure n-decane	250	36	35	204
	Equimolar decalin/n-decane mixture	300	69	33	209
2.9Ir/$H_{0.57}$,$Na_{0.43}$-Y-2.4	Pure decalin	300	92	25	185
	Pure n-decane	250	23	20	204
	Equimolar decalin/n-decane mixture	300	68	14	193
3.1Ir/$H_{0.90}$,$Na_{0.10}$-Y-2.4	Pure decalin	290	95	30	186
	Pure n-decane	250	30	23	204
	Equimolar decalin/n-decane mixture	290	72	18	191

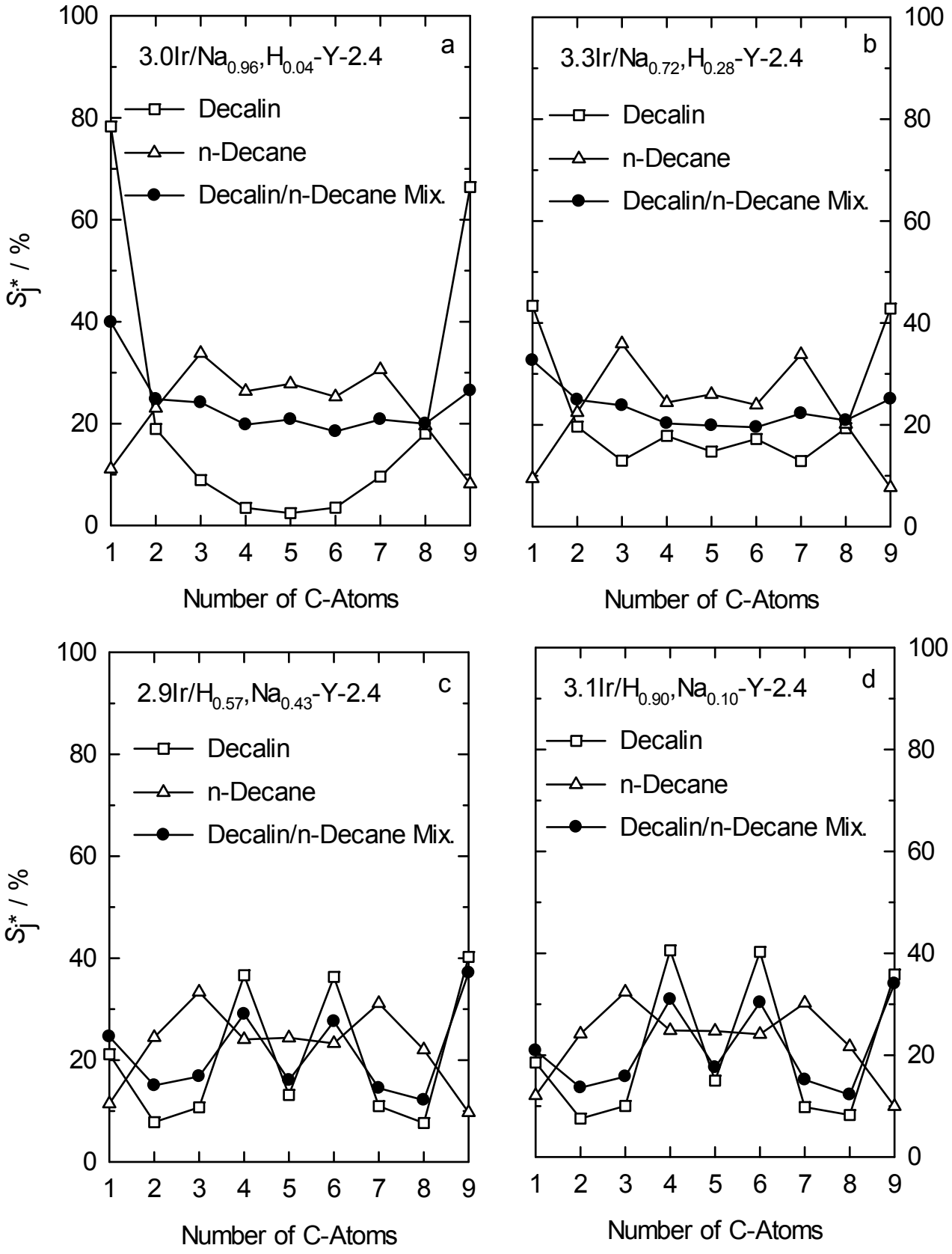

Figure 7.19: Modified hydrocracking selectivities S_j* of decalin, n-decane and an equimolar mixture of both hydrocarbons on the Ir/Na,H-Y-2.4 catalysts. Reaction conditions are depicted in Table 7.6.

Figure 7.19 provides the modified hydrocracking selectivities S_j^* for the experiments with the Ir/Na,H-Y-2.4 catalysts. With increasing concentration of Brønsted acid sites, the shape of the curves for the conversion of pure decalin changes from hammock-shaped to M-shaped. In other words, the behavior of the catalysts changes from a hydrogenolytic to a carbocationic hydrocracking of decalin. The latter favors the paring reaction with its characteristic products iso-butane (C_4) and methylcyclopentane (C_6).

The modified hydrocracking selectivities measured with pure n-decane (see Figure 7.19) exhibit all the shape of flattened bell-type curves. Hence, the different concentrations of Brønsted acid sites on the catalysts seem to have no influence on the carbon number distribution of the hydrocracked products. An intermediate S_j^* curve between the one of pure decalin and n-decane hydroconversion was obtained for the hydroconversion of an equimolar mixture of these two hydrocarbons.

In an attempt to get additional insight into the influence of n-decane on the conversion of decalin, the selectivities of two distinct products (*viz.* butylcyclohexane and methylcyclohexane) were investigated in more detail. Generally, it was found that the selectivity of B-CHx increased with decreasing concentration of Brønsted acid sites of the catalyst at decalin conversions of *ca.* 30 % (*cf.* Appendix 10.1, Figure 10.2, page 200), indicating the formation of B-CHx mainly by hydrogenolysis. For the two catalysts 3.0Ir/$Na_{0.96}$,$H_{0.04}$-Y-2.4, 3.3Ir/$Na_{0.72}$,$H_{0.28}$-Y-2.4 with the least concentration of Brønsted acid sites an increased selectivity of B-CHx was found when an equimolar mixture of decalin and n-decane was hydroconverted. Hence, the presence of n-decane favors the hydrogenolytic carbon-carbon bond scission on these catalysts.

The selectivities of methylcyclohexane are interesting due to the fact that this product can be formed from decalin only by β-scissions of type B or hydrogenolysis. In contrast to butylcyclohexane only small amounts of methylcyclohexane are formed at low decalin conversions. This is not surprising, since M-CHx cannot be a primary product from decalin. Like for B-CHx, the selectivities of M-CHx are increased at decalin conversions of *ca.* 80 % with decreasing concentration of Brønsted acid sites of the catalyst. In other words, the more hydrogenolytically active a catalyst is, the higher are the obtained selectivities of M-CHx on the respective catalyst (*cf.* Appendix 10.1, Figure 10.3, page 201).

7.5.2 Pt/Na,H-Y-2.4 Catalysts with Varied Concentrations of Brønsted Acid Sites

As for the iridium catalysts in Section 7.5.1, the influence of different concentrations of Brønsted acid sites in Pt/Na,H-Y-2.4 catalysts on the hydroconversion of decalin, n-decane and an equimolar mixture of both hydrocarbons was studied. The platinum content of the catalysts was kept constant at approximately 3 wt.-%, whereas between 15 and 88 % of the charge-compensating framework sodium cations in the zeolite were replaced by protons.

In Figure 7.20, the conversions attained on the four Pt/Na,H-Y-2.4 catalysts with pure decalin or pure n-decane are compared with the partial conversions of both hydrocarbons in their competitive hydroconversion. Pure decalin is slightly more reactive than pure n-decane on the Pt/Na,H-Y-2.4 catalysts, which is at variance with the results obtained on Ir/Na,H-Y-2.4 (see Section 7.5.1). With increasing concentration of Brønsted acid sites in the catalysts, the difference in the reactivity of both hydrocarbons becomes more pronounced. In general, the activity of the platinum catalysts is lower throughout the whole series compared to their iridium counterparts.

In the mixed feed, the reactivity of both hydrocarbons is reduced, especially that of n-decane. This is the more pronounced, the fewer Brønsted acid sites the catalyst possesses. As with the Ir/Na,H-Y-2.4 catalysts (see Section 7.5.1), the most straightforward interpretation of the reduction of the reactivity of n-decane in a combined hydroconversion is a competitive adsorption of both hydrocarbons with a preference for decalin.

The product selectivities of the catalytic hydroconversion of pure decalin on the Pt/Na,H-Y-2.4 catalysts are depicted in Figure 7.21. Skeletal isomers of decalin are strongly prevailing, especially at low decalin conversions, on all four catalysts, regardless of their concentration of Brønsted acid sites. With increasing reaction temperature, the selectivities of skeletal isomers drop, and those of ring-opening products and, slightly shifted to higher temperatures, those of open-chain decanes first increase and then pass through maxima. At the highest temperatures, the selectivities of C_9- hydrocarbons strongly increase, as usually.

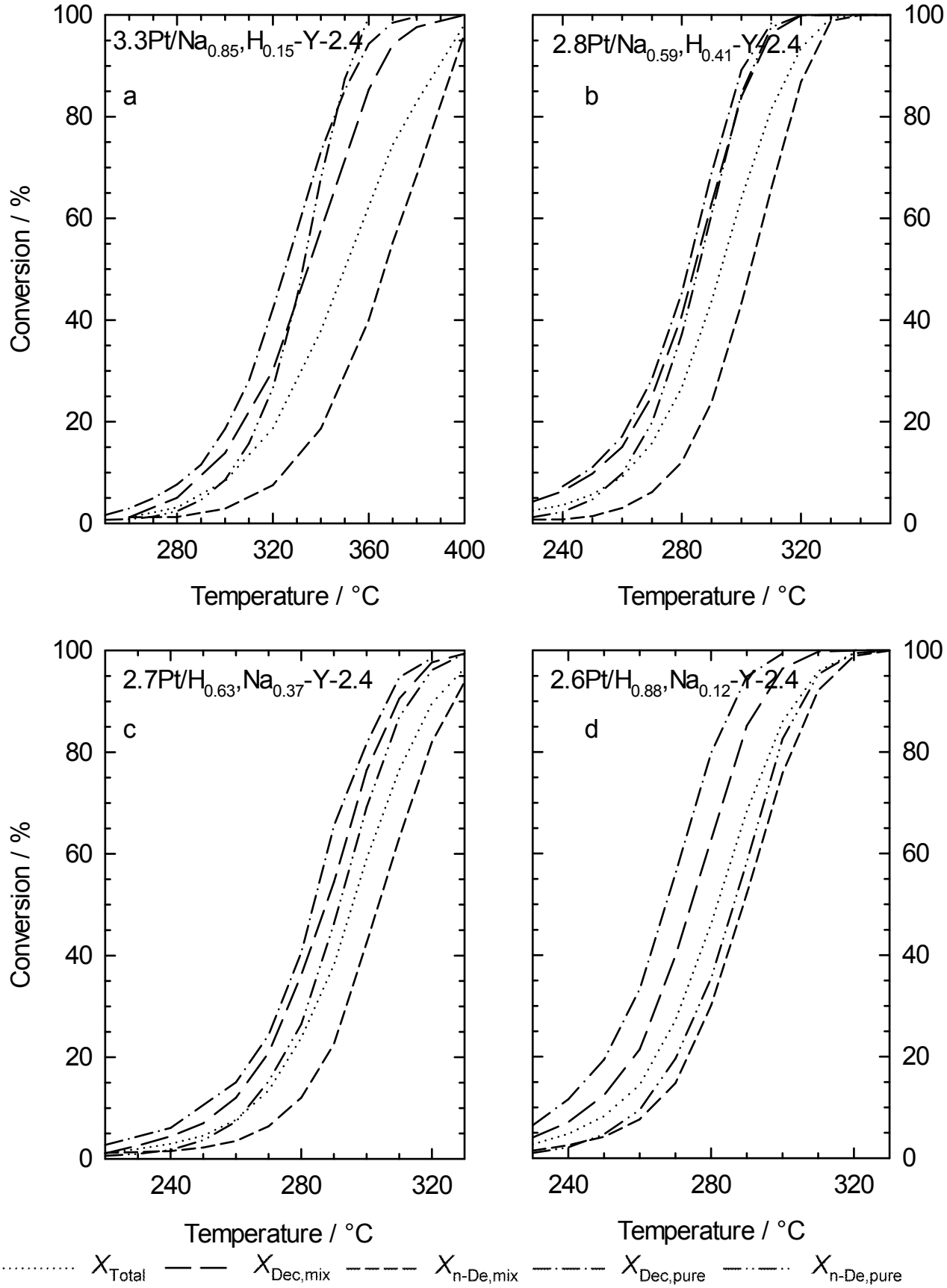

Figure 7.20: Comparison of the conversions measured with pure decalin and with pure n-decane and of the same feed hydrocarbons measured with an equimolar decalin/n-decane mixture on Pt/Na,H-Y-2.4 zeolites.

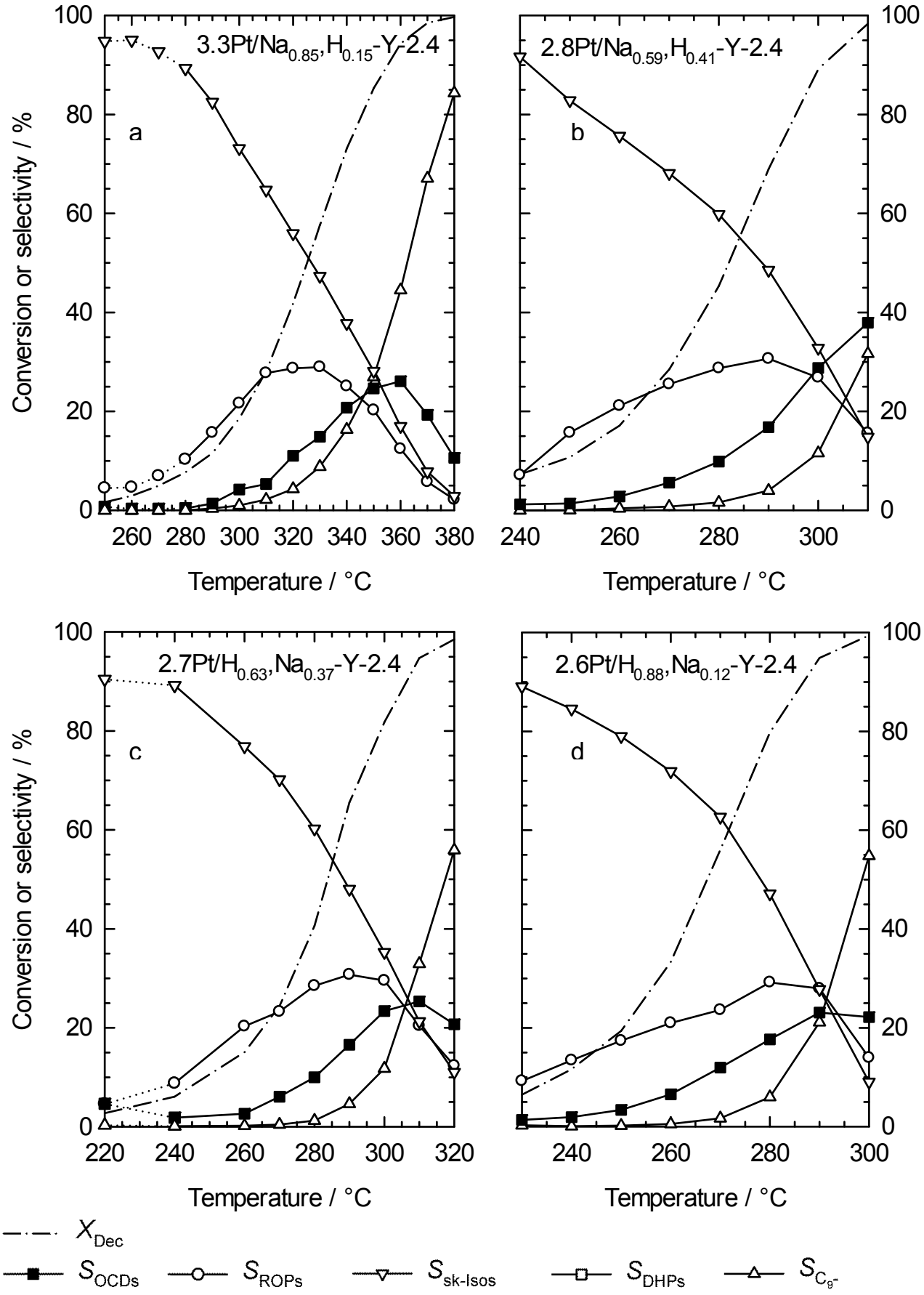

Figure 7.21: Conversions and product selectivities in the hydroconversion of pure decalin on Pt/Na,H-Y-2.4 catalysts.

In contrast to 3.3Pt/$Na_{0.85}$,$H_{0.15}$-Y-2.4, the increased concentration of Brønsted acid sites of the other three catalysts leads to a lowered selectivity of C_9- products at given conversions. This might be interpreted in terms of an increased isomerization activity of the catalysts, leading to a contraction of one decalin ring. The five-membered rings are more easily opened on platinum under less harsh reaction conditions, which in turn leads to a reduced "overcracking" of the ring-opening products to C_9- products.

A look at Table 7.7 shows some relevant trends in the catalytic conversion of decalin on the platinum catalysts. As on the Ir/Na,H-Y-2.4 catalysts, an increase of the concentration of Brønsted acid sites results in an increased activity of the Pt/Na,H-Y-2.4 catalyst. This can be seen from the lowered reaction temperature which is required to reach the same conversion in the series from 3.3Pt/$Na_{0.85}$,$H_{0.15}$-Y-2.4 to 2.6Pt/$H_{0.88}$,$Na_{0.12}$-Y-2.4. In the same order, the yields of OCDs go through a maximum on catalyst 2.8Pt/$Na_{0.59}$,$H_{0.41}$-Y-2.4 which is the only HIPEROC in this series. Hence, too low or too high concentrations of Brønsted acid sites limit the maximum obtainable yields of OCDs from decalin on a catalyst.

Table 7.7: Maximum yields of open-chain decanes obtained on the Pt/Na,H-Y-2.4 catalysts in the hydroconversion of pure decalin.

Catalyst	**Feed**	T_r / °C	X / %	S_{OCDs} / %	$Y_{OCDs,max.}$ / %
3.3Pt/$Na_{0.85}$,$H_{0.15}$-Y-2.4	Decalin	360	94.3	26.1	24.6
2.8Pt/$Na_{0.59}$,$H_{0.41}$-Y-2.4	Decalin	310	98.4	37.9	**37.3**
2.7Pt/$H_{0.63}$,$Na_{0.37}$-Y-2.4	Decalin	310	94.7	25.4	24.0
2.6Pt/$H_{0.88}$,$Na_{0.12}$-Y-2.4	Decalin	300	99.4	22.2	22.0

The results of the hydroconversion of pure n-decane on the Pt/Na,H-Y-2.4 catalysts are depicted in Figure 7.22. As one can see, primary products are skeletal isomers, *viz.* branched decanes in all cases. There are clear differences between the four catalysts. 3.3Pt/$Na_{0.85}$,$H_{0.15}$-Y-2.4 with the lowest concentration of Brønsted acid sites shows the lowest activity in the hydroconversion of n-decane. Similar to the results obtained with decalin, the selectivity of sk-Isos is lower and the selectivity of C_9- is higher than on the other three catalysts.

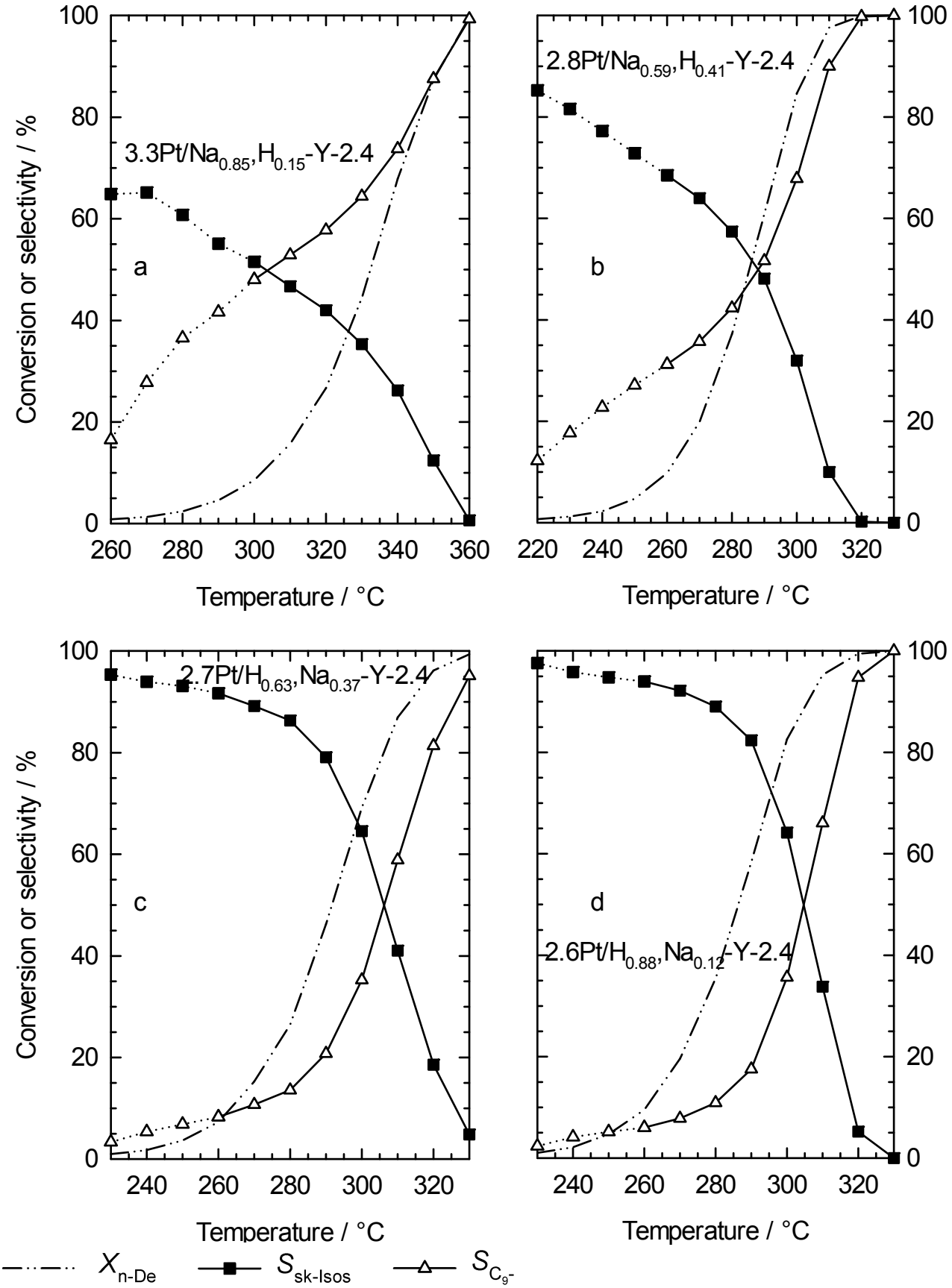

Figure 7.22: Conversions and product selectivities in the hydroconversion of pure n-decane on Pt/Na,H-Y-2.4 catalysts.

In Figure 7.23, the product selectivities observed in the mixed decalin/n-decane conversion are depicted. Primary products on all four catalysts are skeletal isomers of decalin. As in the pure decalin hydroconversion experiments, with increasing conversion the selectivities of OCDs and ROPs pass through maxima. The maximum in the selectivity of OCDs is the highest on the HIPEROC 2.8Pt/$Na_{0.59}$,$H_{0.41}$-Y-2.4. The relatively high selectivities of OCDs on catalysts 2.7Pt/$H_{0.63}$,$Na_{0.37}$-Y-2.4 and 2.6Pt/$H_{0.88}$,$Na_{0.12}$-Y-2.4, in contrast to the pure decalin experiments, are attributed to the isomerization of n-decane on the Brønsted acid sites. A substantial increase of the C_9- product selectivities was found on all four catalysts above total conversions of approximately 50 %.

A comparison of the product selectivities obtained with the mixed feed with those calculated from the selectivities of the pure feed components decalin and n-decane and the respective conversions show by and large a reasonable agreement (see Appendix 10.1, Figure 10.6, page 205). However, generally higher selectivities of the most wanted products, *viz*. open-chain decanes, are obtained in the real mixtures than calculated from the pure-feed measurements. Moreover, the formation of unwanted hydrocracked products is lowered significantly.

The modified selectivities of the hydrocracked products are depicted in Figure 7.24. All four curves of the hydrocracking of pure decalin are M-shaped. With increasing concentration of Brønsted acid sites of the catalysts, the M-shape becomes more pronounced. The M-shape is typical for carbocationic hydrocracking of decalin on bifunctional catalysts. High amounts of C_4 and C_6 are due to the formation of iso-butane and methylcyclopentane, the main products of the acid-catalyzed paring reaction. The modified hydrocracking selectivity of methane, an indicator of hydrogenolytic carbon-carbon bond scission, is the highest on catalyst 3.3Pt/$Na_{0.85}$,$H_{0.15}$-Y-2.4 which contains the lowest concentration of Brønsted acid sites.

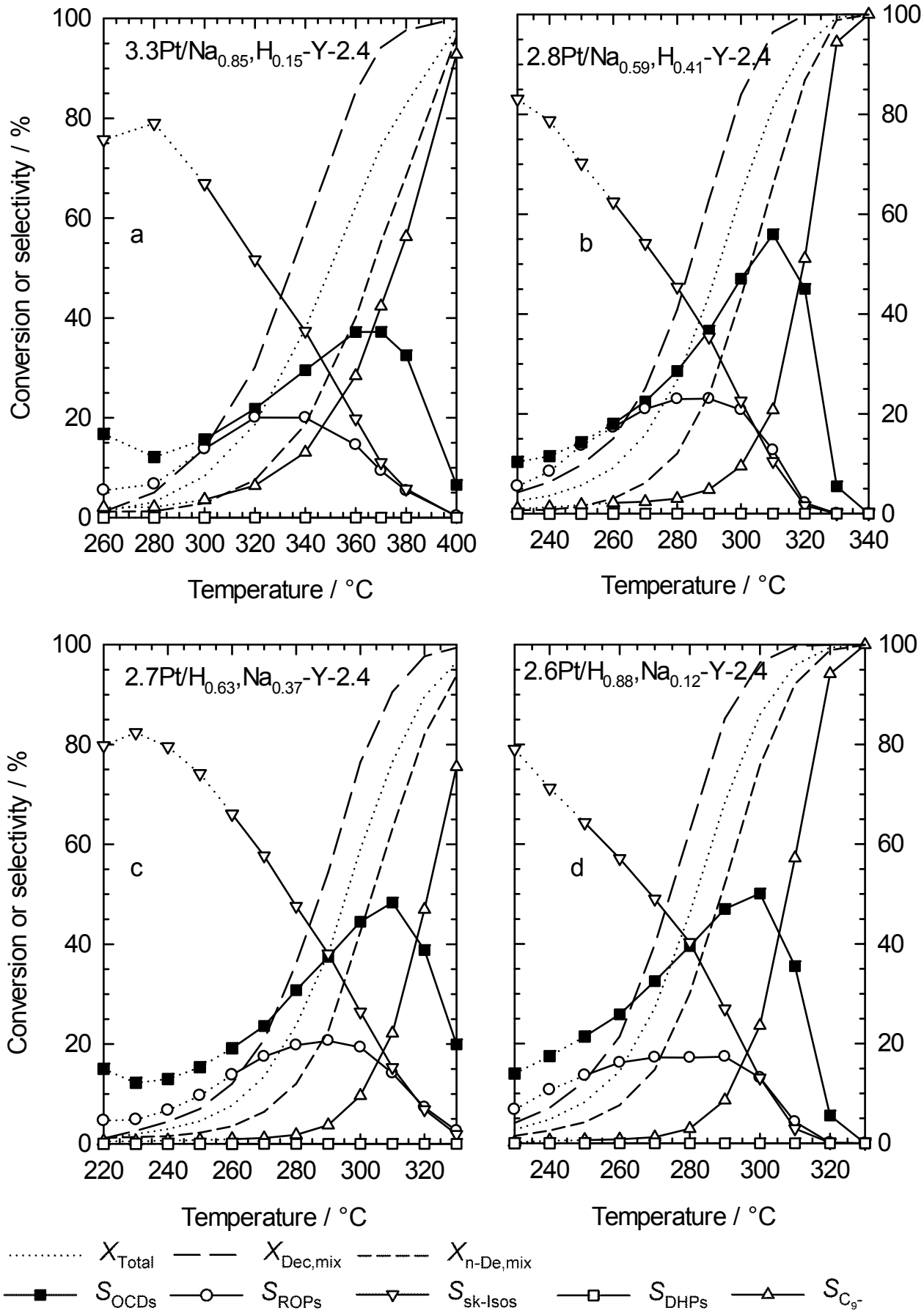

Figure 7.23: Conversion of an equimolar decalin/n-decane mixture and selectivities of different groups of products on Pt/Na,H-Y-2.4 catalysts.

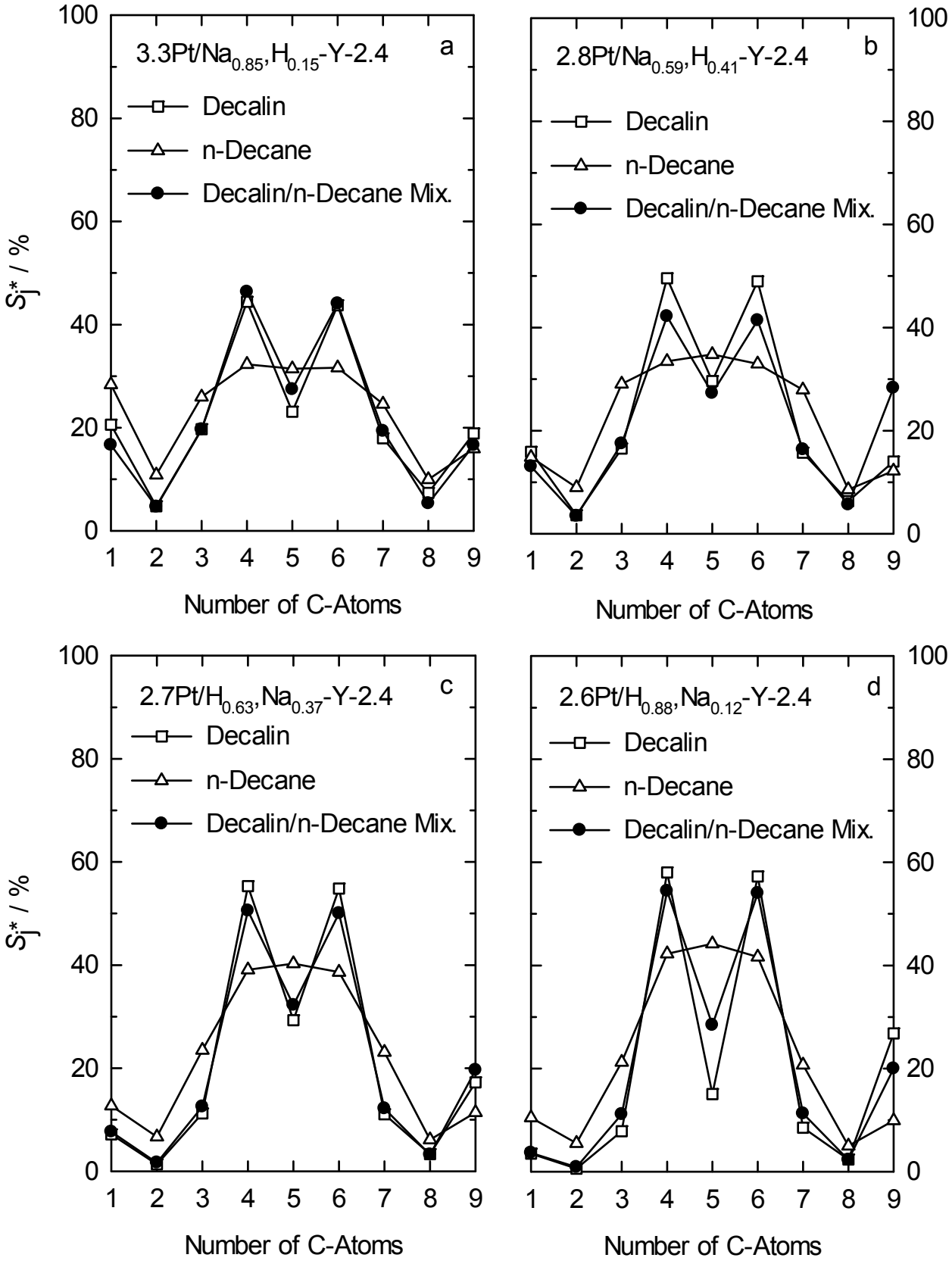

Figure 7.24: Modified hydrocracking selectivities S_j* of decalin, n-decane and an equimolar mixture of both hydrocarbons on the Pt/Na,H-Y-2.4 catalysts. Reaction conditions are depicted in Table 7.8.

Table 7.8: Reaction conditions for the experiments leading to the modified hydrocracking selectivities S_j* in Figure 7.24 and branched isomers from n-decane in Figure 7.25.

Catalyst	**Feed**	T_r / °C	X / %	Y_{C_9-} / %	ΣS_j* / %
3.3Pt/$Na_{0.85}$,$H_{0.15}$-Y-2.4	Decalin	360	94	44	201
	n-Decane	330	44	29	211
	Equimolar decalin/n-decane mixture	360	62	18	200
2.8Pt/$Na_{0.59}$,$H_{0.41}$-Y-2.4	Decalin	310	98	31	200
	n-Decane	290	61	32	203
	Equimolar decalin/n-decane mixture	310	81	17	195
2.7Pt/$H_{0.63}$,$Na_{0.37}$-Y-2.4	Decalin	310	95	33	191
	n-Decane	300	69	24	202
	Equimolar decalin/n-decane mixture	310	77	17	190
2.6Pt/$H_{0.88}$,$Na_{0.12}$-Y-2.4	Decalin	290	95	23	180
	n-Decane	300	83	29	201
	Equimolar decalin/n-decane mixture	300	86	20	186

The carbon number distributions of the hydrocracked products from pure n-decane on the Pt/Na,H-Y-2.4 catalysts in Figure 7.24 are all of the bell-type with minima at C_2 and C_8 and high values of C_4 to C_6. These curves seem to indicate a superposition of bifunctional hydrocracking [35] and hydrogenolysis on platinum. In fact, the curves obtained on 3.3Pt/$Na_{0.85}$,$H_{0.15}$-Y-2.4 and 2.8Pt/$Na_{0.59}$,$H_{0.41}$-Y-2.4 with similar modified hydrocracking selectivities from C_3 to C_7 resemble the curves reported for the hydrogenolysis of n-decane on 2.0Pt/Al_2O_3 [146].

The two other catalysts, 2.7Pt/$H_{0.63}$,$Na_{0.37}$-Y-2.4 and 2.6Pt/$H_{0.88}$,$Na_{0.12}$-Y-2.4 show a lowered formation of C_3 and C_7 and a higher formation of C_4 to C_6 compared to the S_j* curves obtained on 3.3Pt/$Na_{0.85}$,$H_{0.15}$-Y-2.4 and 2.8Pt/$Na_{0.59}$,$H_{0.41}$-Y-2.4. Besides hydrogenolysis, the formation of C_3 and C_7 proceeds *via* an isomerization of n-decane followed by a slower β-scission of Type B compared to the C_4 to C_6 products which can be formed *via* fast β-scissions of Type A [30]. Hence, when the differences in the modified

hydrocracking selectivities between C_3 and C_4 are large, this is an indicator for the classical bifunctional hydrocracking mechanism.

The S_j* curves of the equimolar decalin/n-decane mixtures in Figure 7.24 are all of the M-shape. When comparing the series of the iridium (see Figure 7.19, page 151) with the platinum catalysts it is found that the carbon number distributions obtained from the equimolar mixture differ. In the hydrocracking of the equimolar mixture using an iridium catalyst the selectivity resembles a hybrid between the distributions obtained in the hydroconversion of pure n-decane and decalin (see Figure 7.19). On platinum, the product distributions from the reaction of the mixture follow the selectivity curve obtained from pure decalin.

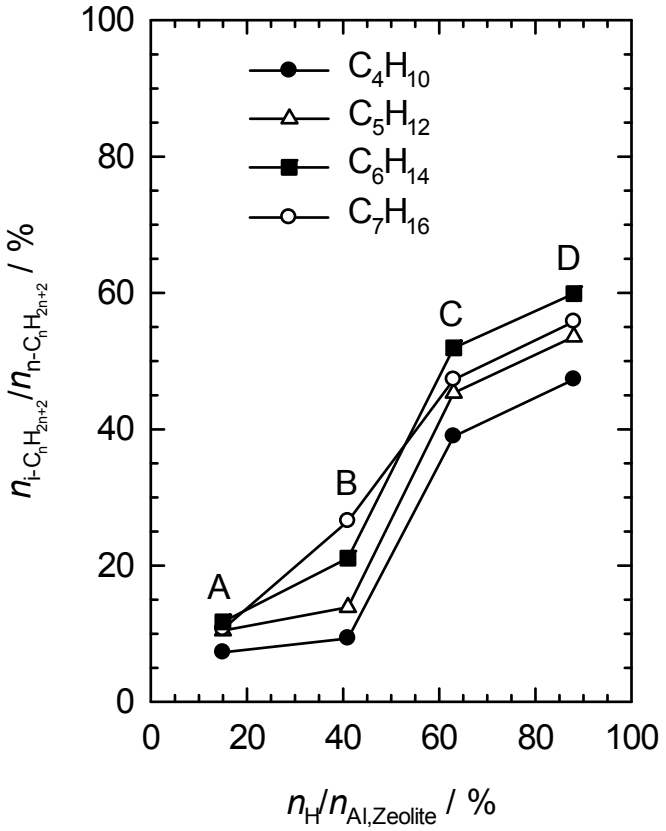

Figure 7.25: Content of branched isomers in the fractions of hydrocracked products from n-decane. The reaction conditions are given in Table 7.8. A: 3.3Pt/$Na_{0.85}$,$H_{0.15}$-Y-2.4; B: 2.8Pt/$Na_{0.59}$,$H_{0.41}$-Y-2.4; C: 2.7Pt/$H_{0.63}$,$Na_{0.37}$-Y-2.4; D: 2.6Pt/$H_{0.88}$,$Na_{0.12}$-Y-2.4.

Further mechanistic information is available from the degree of branching of the hydrocracked products. Depicted in Figure 7.25 is the content of branched

alkanes within the fractions of hydrocracked products. The products obtained on the catalysts 3.3Pt/$Na_{0.85}$,$H_{0.15}$-Y-2.4 and 2.8Pt/$Na_{0.59}$,$H_{0.41}$-Y-2.4 have a low degree of branching compared to the other two catalysts 2.7Pt/$H_{0.63}$,$Na_{0.37}$-Y-2.4 and 2.6Pt/$H_{0.88}$,$Na_{0.12}$-Y-2.4 with higher concentrations of Brønsted acid sites. So there seems to be a clear relationship between the degree of branching of the hydrocracked products from n-decane and the concentration of Brønsted acid sites of the catalyst.

One can conclude, that on catalysts with 3 wt.-% of platinum there is a competition between the hydrogenolytic carbon-carbon bond scission on the metal leading to more non-branched hydrocracked products and bifunctional hydrocracking leading predominantly to branched products. By increasing the concentration of Brønsted acid sites of the catalysts, the participation of hydrogenolysis in the hydrocracking reaction can be lowered and *vice versa*.

For 2.7Pt/silica, the composition of the direct ROPs from decalin was investigated (see Figure 7.13, page 139). In contrast to 2.7Pt/silica only the direct ROPs B-CHx, 1,2-DE-CHx and 1-M-2-P-CHx, but no cyclodecane, were formed on the Pt/Na,H-Y-2.4 catalysts (*cf.* Appendix 10.1, Figure 10.5, page 204). The main direct ROP was B-CHx for the two catalysts with low and 1,2-DE-CHx for the two catalysts with high concentrations of Brønsted acid sites. It is striking that the formation of B-CHx is nearly constant throughout the conversion range, whereas the part of 1,2-DE-CHx decreases and that of 1-M-2-P-CHx increases with increasing decalin conversion. However, the selectivities of the dROPs obtained from pure decalin and an equimolar mixture of decalin and n-decane show the same curve for each dROP. As a result, the admixture of n-decane has no influence on the selectivities of the direct ROPs.

7.5.3 Iridium-Containing Zeolite Catalysts with Different Pore Structures

A series of six zeolite catalysts with five different pore structures was prepared (see Table 6.9 on page 109). All catalysts were loaded with *ca.* 3 wt.-% of iridium with the exception of 0.5Ir/$H_{0.59}$,$Na_{0.41}$-ZSM-5-18. Catalyst 3.3Ir/$H_{0.58}$,$Cs_{0.42}$-Beta-14 is the HIPEROC on which the highest yields of OCDs were obtained so far [79]. All six catalysts were tested, in much the same way as the catalysts described previously, in the hydroconversion of pure decalin, pure n-decane and an equimolar mixture of decalin and n-decane.

The conversions attained in the hydroconversion of pure decalin, pure n-decane and their equimolar mixture are depicted in Figure 7.26. It can be seen that all catalysts showed a high activity, particularly in the hydroconversion of pure n-decane. When converted alone, n-decane begins to react at temperatures which are lower than those needed for the conversion of decalin.

The competitive hydroconversion of the equimolar mixture of decalin and n-decane leads to very different results concerning the reactivities of both feed hydrocarbons. On the catalysts 3.5Ir/$Rb_{0.52}$,$H_{0.48}$-Beta-14, 3.3Ir/$H_{0.58}$,$Cs_{0.42}$-Beta-14 and 3.0Ir/$Na_{0.80}$,$H_{0.20}$-EMC-2-4.3 an inverted reactivity of both feed hydrocarbons is obtained, *viz.* decalin is more reactive than n-decane in the mixed-feed when compared to pure-feed experiments. This effect was previously found for the Ir/Na,H-Y-2.4 catalysts (*cf.* Section 7.5.1, Figure 7.14, page 141) and interpreted as a favored competitive adsorption of decalin. All these catalysts have in common that they are based on 12-ring zeolites with a three-dimensional pore system and Spaciousness Indices (*SI*) of 18 and 21 [46], respectively.

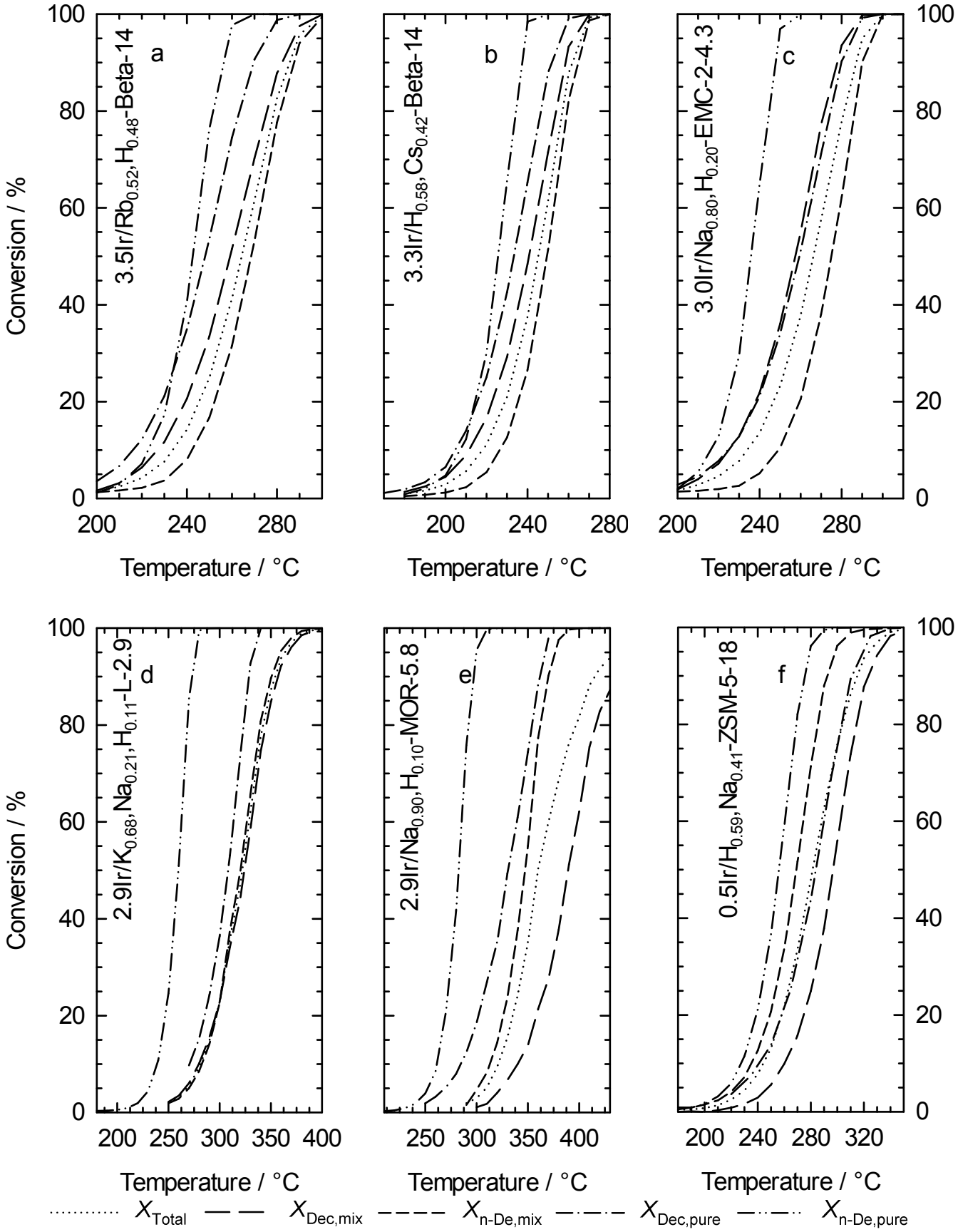

Figure 7.26: Conversions measured with pure decalin, pure n-decane and an equimolar mixture of the same hydrocarbons on the iridium catalysts with different pore structures.

As Figures 7.26d and e reveal, the two catalysts 2.9Ir/$K_{0.68}$,$Na_{0.21}$,$H_{0.11}$-L-2.9 and 2.9Ir/$Na_{0.90}$,$H_{0.10}$-MOR-5.8 show a performance that differs from the ones of the Beta and EMC-2 zeolites (Figures 7.26a, b and c). This is particularly true for the hydroconversion of the decalin/n-decane mixtures: Both for the L-type (Figure 7.26d) and the mordenite (Figure 7.26e) catalyst, significantly higher reaction temperatures are needed. Moreover, the preferential conversion of decalin compared to that of n-decane is no longer given. On 2.9Ir/$K_{0.68}$,$Na_{0.21}$,$H_{0.11}$-L-2.9, the conversion curves for the two hydrocarbons in the mixture fall together (Figure 7.26d), whereas on 2.9Ir/$Na_{0.90}$,$H_{0.10}$-MOR-5.8, n-decane reacts much faster than decalin when both are fed as mixed reactants (Figure 7.26e). These findings are best interpreted as being due to the one-dimensional 12-ring pores of zeolites L and mordenite which manifest themselves in reduced Spaciousness Indices of 16 and 7, respectively [46-48]. It appears that in such 12-ring zeolites with a reduced pore width, the C_{10} feed and/or product hydrocarbons experience hindrances in their diffusion, and this is particularly so for the bulkier decalin molecules compared to the slim n-decane.

Still narrower pores exist in the 10-ring zeolite ZSM-5 for which a Spaciousness Index of 1 has been reported [46]. It is expected that, of the two reactants, n-decane is hydroconverted much faster than decalin (Figure 7.26f) when these two hydrocarbons are offered to the catalyst as an equimolar mixture. One could even have expected that the bulky reactant decalin is not converted at all on 0.5Ir/$H_{0.59}$,$Na_{0.41}$-ZSM-5-18 (shape-selective catalysis). To account for the finding that some conversion of decalin does take place, iridium clusters and/or Brønsted acid sited on the external surface of the ZSM-5 catalyst are invoked.

The selectivities of the products obtained in the hydroconversion of pure decalin on the six iridium-loaded zeolitic catalysts are depicted in Figure 7.27. Skeletal isomers of decalin are primary products, their selectivities decrease with increasing reaction temperature and decalin conversion. The selectivities of ring-opening products pass through maxima at low temperatures, but in some instances, only the descending part of the curves for the ROPs are conspicuous. At elevated reaction temperatures, the selectivity curves for open-chain decanes, the most desired products, pass through maxima, and at high conversions near 100 %, hydrocracking occurs on all catalysts down to the very undesired hydrocarbons with less than ten carbon atoms.

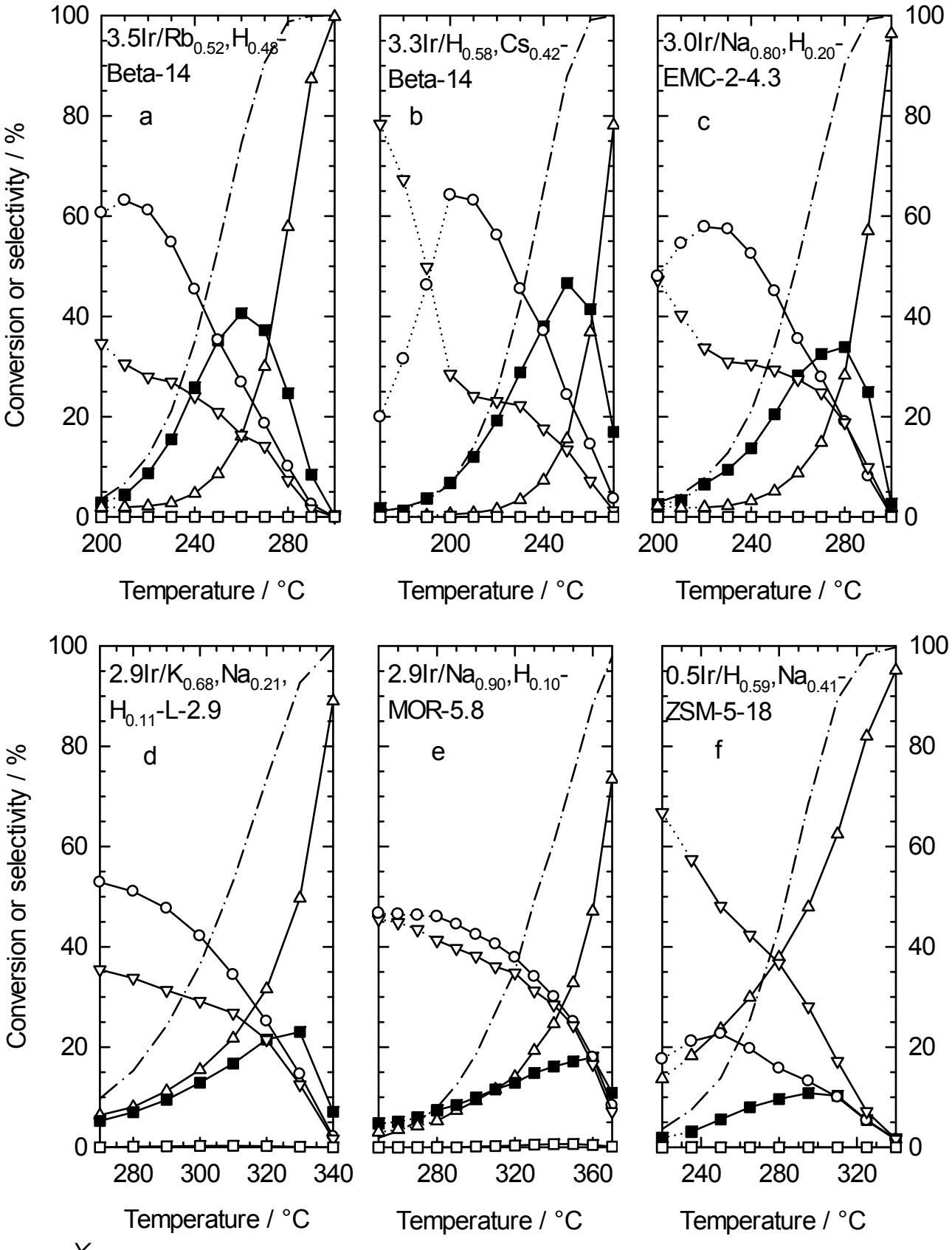

Figure 7.27: Conversions and product selectivities in the hydroconversion of pure decalin on iridium catalysts with different pore structures.

Overall, the figures are consistent with the view that skeletal isomerization of decalin, opening of one ring to ROPs, opening of the second ring to OCDs, and hydrocracking down to C_9- are consecutive reactions on high-performance ring-opening catalysts (see Figure 7.27 and Ref. [79]). As Figure 7.27 shows, high maxima in the selectivities of OCDs are only attained on zeolite catalysts which give high yields of ROPs as well. It should be mentioned that the Beta HIPEROCs show a distribution of direct ROPs which resembles qualitatively the one of 2.6Ir/silica (*cf.* Appendix 10.1, Figure 10.8, page 208). Furthermore, Figure 7.27 reveals that high yields of OCDs are only attained on zeolite catalysts (referred to as HIPEROCs) with a three-dimensional system of large (12-ring) pores, such as zeolites Beta and EMC-2. It has been shown previously that HIPEROCs can also be made from zeolite Y which possesses three-dimensional large pore, as well (see Table 7.5, page 146 and Ref. [81]). The conditions under which maximum yields of OCDs were achieved with the iridium-containing zeolites Beta and EMC-2 are given in Table 7.9.

Table 7.9: Maximum yields of open-chain decanes obtained on iridium-containing zeolite catalysts with different pore systems in the hydroconversion of pure decalin.

Catalyst	T_r / °C	X / %	S_{OCDs} / %	$Y_{OCDs,max.}$ / %
3.5Ir/$Rb_{0.52}$,$H_{0.48}$-Beta-14	270	90.7	37.3	**33.8**
3.3Ir/$H_{0.58}$,$Cs_{0.42}$-Beta-14	260	99.1	41.5	**41.1**
3.0Ir/$Na_{0.80}$,$H_{0.20}$-EMC-2-4.3	280	90.3	33.9	**30.6**
2.9Ir/$K_{0.68}$,$Na_{0.21}$,$H_{0.11}$-L-2.9	330	92.7	23.0	21.4
2.9Ir/$Na_{0.90}$,$H_{0.10}$-MOR-5.8	360	88.4	17.9	15.8
0.5Ir/$H_{0.59}$,$Na_{0.41}$-ZSM-5-18	310	89.4	10.3	9.2

Figure 7.28 shows the selectivities of the products formed in the hydroconversion of pure n-decane on the six iridium-loaded zeolite catalysts in dependence of the reaction temperature. These plots are relatively simple, since two groups of products can be formed from n-decane only, *viz.* skeletal isomers (sk-Isos) and hydrocracked products (C_9-). Of particular relevance for the mechanism of ring opening on HIPEROCs are the data in Figures 7.28a to c. The subsequent discussion will be conducted for catalyst 3.3Ir/$H_{0.58}$,$Cs_{0.42}$-Beta-14 (Figure 7.28b), because it enabled the highest yield of open-chain decanes in the hydroconversion of decalin ($Y_{OCDs,max.}$ = 41.1 %, see Figure 7.27b and Table 7.9), but this discussion equally pertains to the two other HIPEROCs (Figures 7.28a and c).

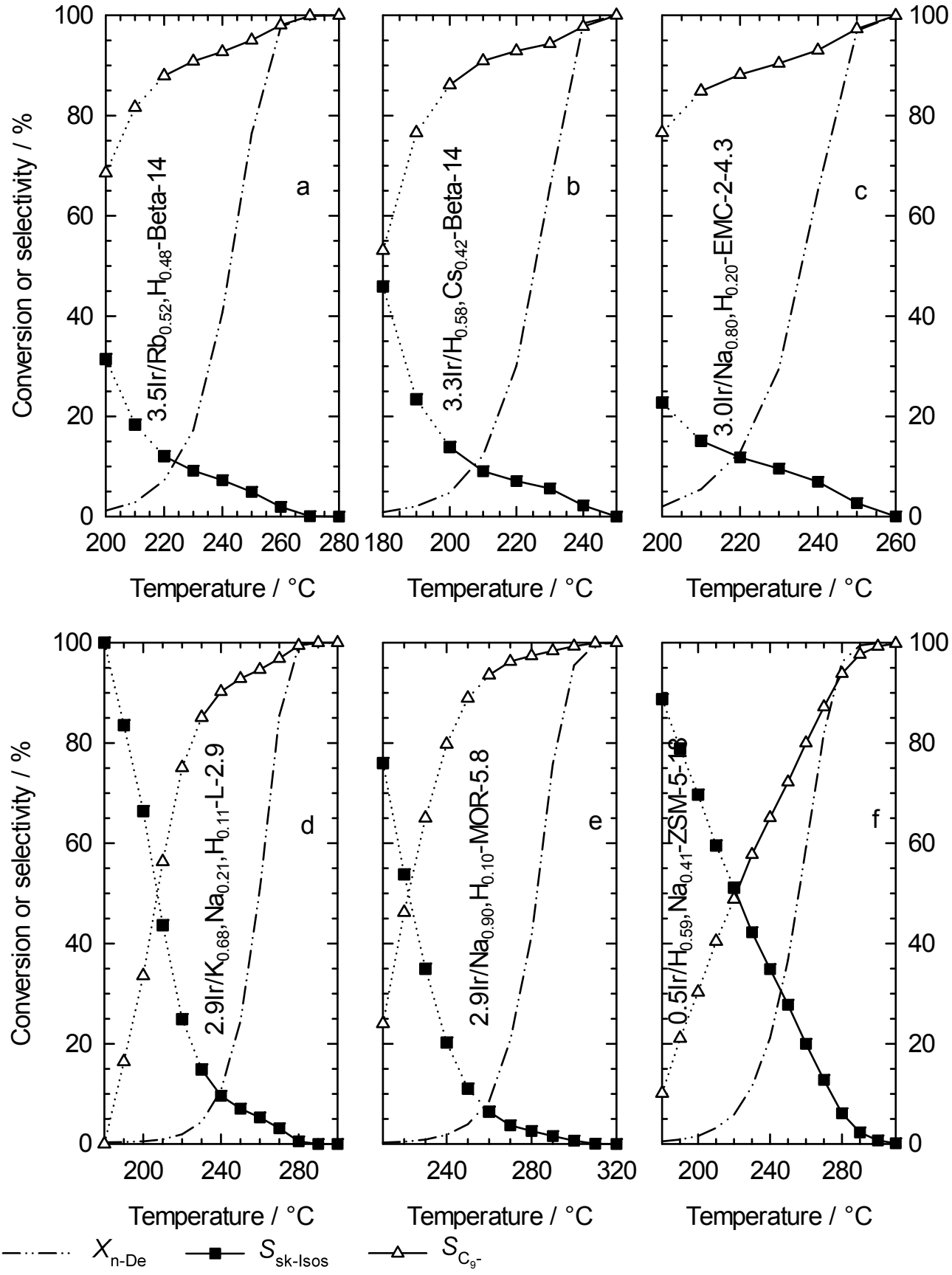

Figure 7.28: Conversions and product selectivities in the hydroconversion of pure n-decane on iridium catalysts with different pore structures.

At a reaction temperature of 210 °C, the n-decane conversion on 3.3Ir/$H_{0.58}$,$Cs_{0.42}$-Beta-14 (Figure 7.28b) is 12.2 %, and the selectivities of hydrocracked products (C_9-) and iso-decanes (sk-Isos) amount to 90.9 % and 9.1 %, respectively. A closer look at the nature of the C_9- products reveals that they consist of C_1 to C_9 alkanes exclusively, with a carbon-number distribution depicted in Figure 7.30b (*vide infra*). Most importantly, C_1 + C_9 and C_2 + C_8 moieties are formed in appreciable amounts, and the C_4 to C_9 fragments consist of n-alkanes exclusively (*cf.* Appendix 10.1, Figure 10.7, page 207). From these findings, it can be doubtlessly concluded that the C_9- products are exclusively formed by hydrogenolysis of n-decane on iridium, rather than on the acid sites of the catalyst *via* carbocations as intermediates.

Table 7.10: Distribution of the monobranched iso-decanes (in mol-%) from n-decane on the HIPEROC 3.3Ir/$H_{0.58}$,$Cs_{0.42}$-Beta-14 and, for comparison, on a conventional bifunctional 0.5Pt/Ca-Y zeolite catalyst (the data for 0.5Pt/Ca-Y are from Ref. [29]).

Catalyst	**3.3Ir/$H_{0.58}$,$Cs_{0.42}$-Beta-14**	**0.5Pt/Ca-Y**
Feed	Pure n-decane	Pure n-decane
T_r / °C	210	220
$X_{n\text{-}De}$ / %	12.2	2.2
2-M-No / %	18.0	15.8
3-M-No / %	29.4	27.1
4-M-No / %	30.1	30.5
5-M-No / %	14.4	15.7
3-E-Oc / %	4.1	4.5
4-E-Oc / %	4.0	6.4

The second reaction occurring in the hydroconversion of n-decane on 3.3Ir/$H_{0.58}$,$Cs_{0.42}$-Beta-14 is skeletal isomerization to iso-decanes. It is very unlikely that this reaction happens on the metal, since iridium has repeatedly been reported to lack activity for skeletal isomerization of hydrocarbons [67,69,70]. A detailed look at the skeletal isomers formed furnishes valuable insight into the isomerization mechanism. It is seen from Table 7.10 that, at the reaction conditions chosen, the isomers from n-decane consist of monobranched iso-decanes. Methylnonanes are dominating, but ethyloctanes are formed as well in smaller amounts. Among the methylnonanes branching in the 3- and 4-position is clearly favored over branching in the 2- and 5-positions. Precisely these features were previously shown to hold for

isomerization of n-decane on conventional bifunctional catalysts, for example on 0.5Pt/Ca-Y zeolite, and rationalized in terms of carbocation chemistry *via* protonated cyclopropanes [29]. Thus, the striking similarities between the product distributions in isomerization of n-decane on the HIPEROC and a conventional bifunctional catalyst are, in our opinion, strong evidence for isomerization of n-decane occurring, on both types of catalysts, on the acid sites.

In conclusion, the results obtained in the hydroconversion of n-decane on the HIPEROCs (Figures 7.28a to c) support and give independent evidence for a mechanism advanced recently for the hydroconversion of decalin on HIPEROCs [79]. In this mechanism (see Figure 4.18, page 49), the main role of the weakly acid sites is to isomerize six-membered naphthenic rings into five-membered ones, while cleavage of endocyclic carbon-carbon bonds occurs by hydrogenolysis on the noble metal.

The results of the competitive hydroconversion of the equimolar decalin/n-decane mixture on the six zeolite catalysts are displayed in Figure 7.29. The results obtained with the zeolite Beta and EMC-2 catalysts will be discussed first and separately from those on the zeolites L, MOR and ZSM-5.

On the two zeolites Beta and on zeolite EMC-2 (Figures 7.29a to c), decalin is more reactive than n-decane, at variance with the experiments in which the pure hydrocarbons were used as reactants (Figures 7.26a to c). This is again attributed to a preferred adsorption of decalin on the zeolitic catalysts. In-line with the preferred conversion of decalin, the product selectivities resemble the ones obtained from pure decalin as feed, *i.e.*, skeletal isomers of decalin are preferentially formed at low conversions, next ring-opening products and open-chain decanes appear, and their selectivities pass through maxima. At high conversions, the selectivities of hydrocracked products (C_9-) rapidly approach 100 %. Surprisingly high selectivities of open-chain decanes are observed, but this may be misleading because iso-decanes are probably not only formed by double ring opening from decalin, but also by skeletal isomerization of n-decane. Another peculiarity, which is particularly conspicuous on 3.3Ir/$H_{0.58}$,$Cs_{0.42}$-Beta-14, is the relatively high selectivity of C_9- at moderate conversions, This is probably due to the formation of C_9- from both feed hydrocarbons in this region.

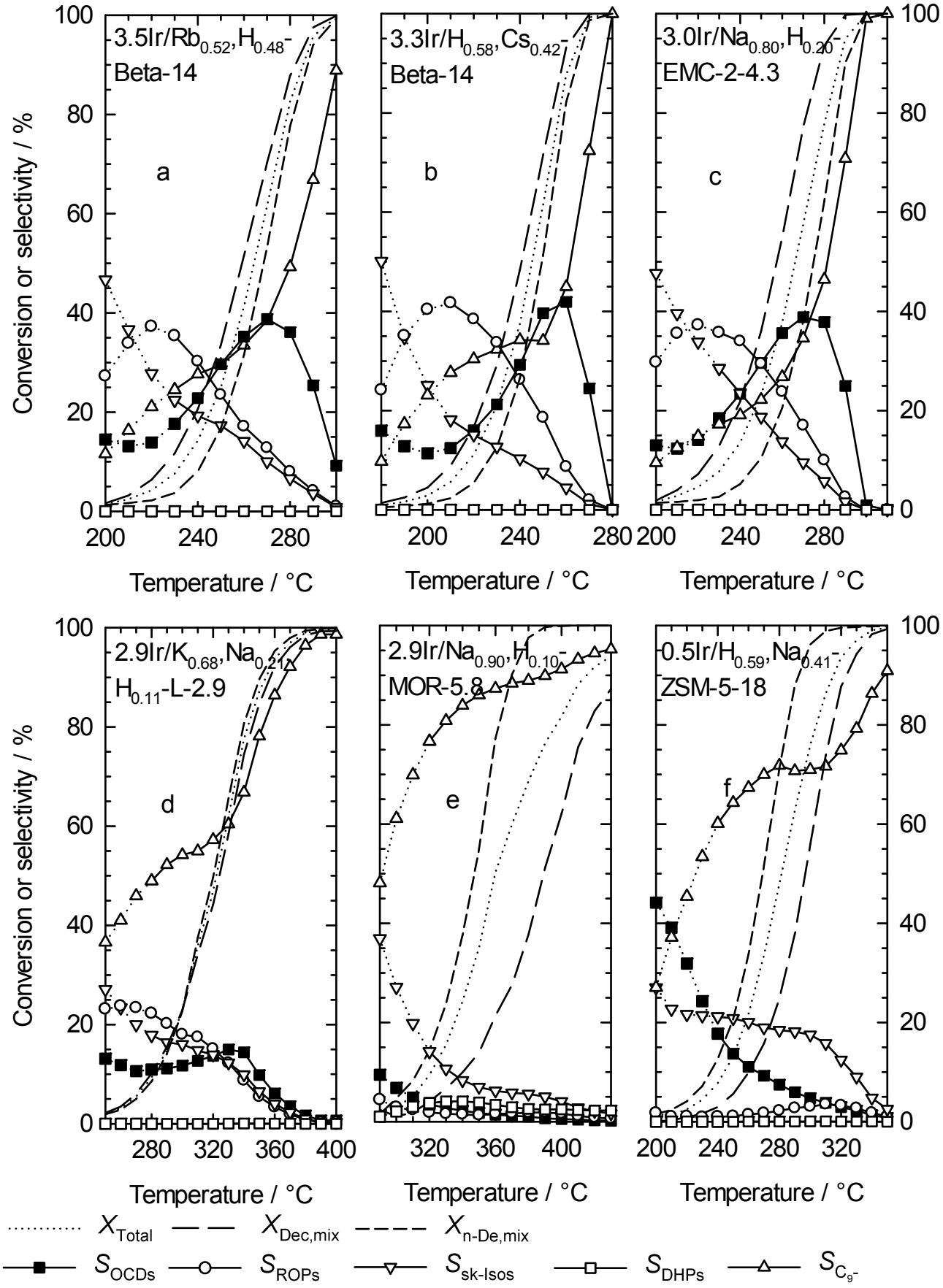

Figure 7.29: Conversion of an equimolar decalin/n-decane mixture and selectivities of different groups of products on zeolitic iridium catalysts with different pore structures.

As the Spaciousness Indices of zeolites L, mordenite and ZSM-5 indicate (*SI* = 16, 7 and 1, respectively [46-48]), their pores are getting narrower in the above order. This has strong repercussions on the relative reactivities of decalin and n-decane offered to the catalysts as an equimolar mixture (Figures 7.29d to f) which was interpreted in terms of diffusion hindrances in connection with the reactant conversions in Figures 7.26d to e. In a complex reaction network, the occurrence of diffusional hindrances inside the catalyst pores is detrimental for making intermediates and rather favors the formation of the end products of the reaction network (in the present case of hydrocracked products C_9-). Indeed, the selectivities of skeletal isomers of decalin, of ring-opening products, and of open-chain decanes are small throughout, especially on the mordenite catalyst, whereas C_9- hydrocarbons are produced with high selectivities even at moderate conversions. Finally, the relatively low activity of 2.9Ir/$Na_{0.90}$,$H_{0.10}$-MOR-5.8 requires high reaction temperatures around 350 to 400 °C, and at these high temperatures noticeable amounts of dehydrogenated products (tetralin and naphthalene) are formed.

The product selectivities of the hydroconversion of an equimolar decalin/n-decane mixture was calculated out of the pure feed experiments for the six iridium catalysts. It was found that the calculated selectivities revealed a good agreement with the measured ones (*cf.* Appendix 10.1, Figure 10.9, page 209). As for the Ir/Na,H-Y-2.4 catalysts, higher measured selectivities of OCDs and lower ones of hydrocracked products were found than expected from the calculation on the three HIPEROCs. This positive effect for an increasing formation of OCDs is turned in its opposite on the catalysts based on zeolite L, mordenite and ZSM-5. Hence, a too narrow pore system is deleterious for the formation of open-chain decanes.

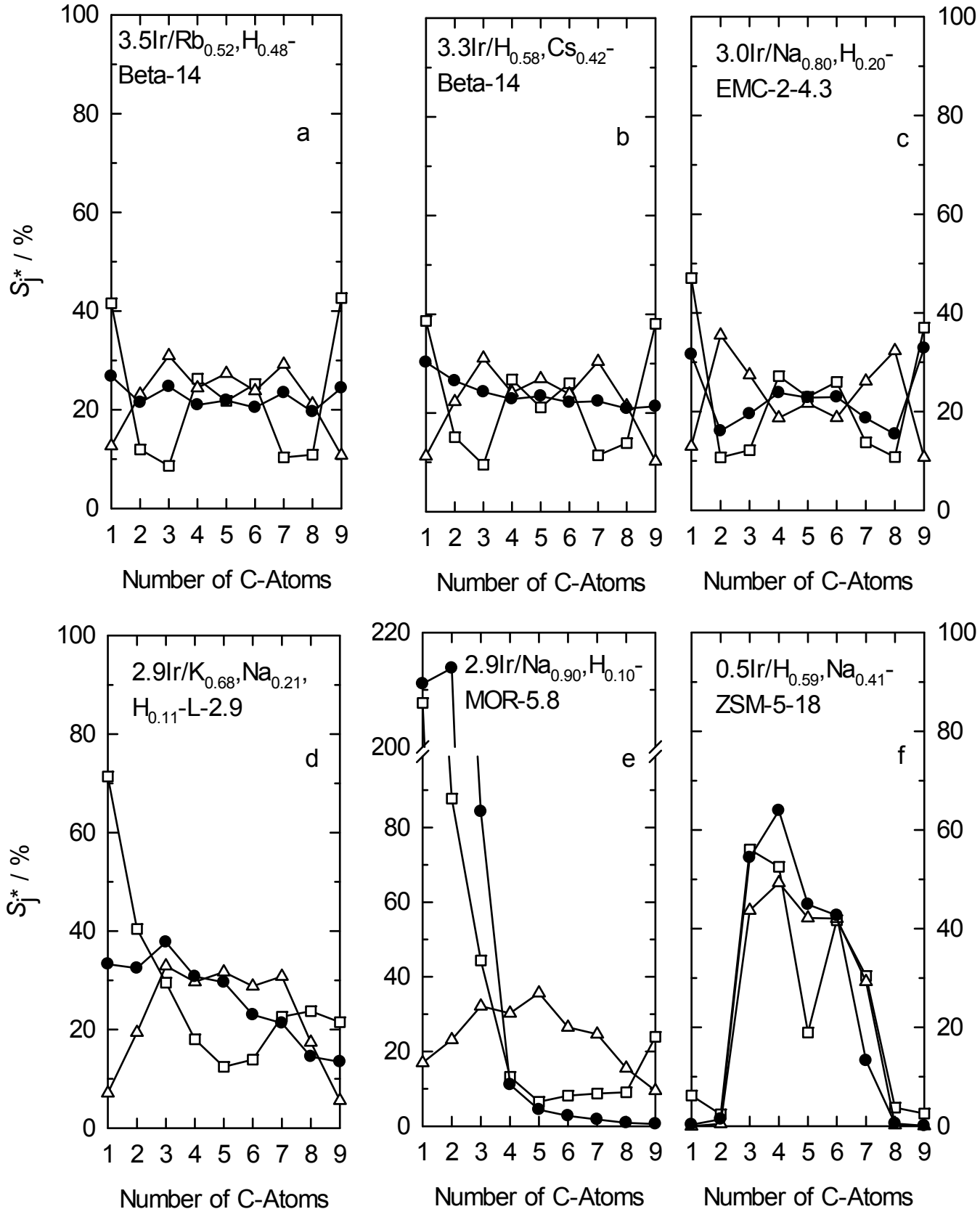

Figure 7.30: Modified hydrocracking selectivities S_j* in the hydroconversion of decalin, n-decane and an equimolar mixture of both hydrocarbons on the iridium catalysts with different pore structures. The reaction conditions are listed in Table 7.11.

Table 7.11: Reaction conditions for the experiments for which the modified hydrocracking selectivities S_j* are shown in Figure 7.30.

Catalyst	**Feed**	T_r / °C	X / %	Y_{C_9-} / %	ΣS_j* / %
3.5Ir/$Rb_{0.52}$,$H_{0.48}$-Beta-14	Decalin	260	74.5	12.0	199.0
	n-Decane	230	17.3	15.7	203.5
	Equimolar decalin/n-decane mixture	270	61.6	23.7	205.0
3.3Ir/$H_{0.58}$,$Cs_{0.42}$-Beta-14	Decalin	250	88.0	13.7	200.6
	n-Decane	210	12.2	11.1	201.7
	Equimolar decalin/n-decane mixture	260	87.8	39.5	214.0
3.0Ir/$Na_{0.80}$,$H_{0.20}$-EMC-2-4.3	Decalin	280	90.3	25.5	207.6
	n-Decane	230	29.6	26.7	204.2
	Equimolar decalin/n-decane mixture	270	57.7	20.0	203.7
2.9Ir/$K_{0.68}$,$Na_{0.21}$, $H_{0.11}$-L-2.9	Decalin	330	92.7	46.1	253.5
	n-Decane	250	24.6	22.9	203.5
	Equimolar decalin/n-decane mixture	330	62.1	37.5	236.1
2.9Ir/$Na_{0.90}$,$H_{0.10}$-MOR-5.8	Decalin	360	88.4	41.7	409.5
	n-Decane	280	41.6	40.5	214.3
	Equimolar decalin/n-decane mixture	360	50.3	44.0	530.8
0.5Ir/$H_{0.59}$,$Na_{0.41}$-ZSM-5-18	Decalin	295	68.6	32.9	214.5
	n-Decane	250	36.7	26.5	207.3
	Equimolar decalin/n-decane mixture	280	48.1	34.5	221.5

The modified selectivities of the hydrocracked products obtained on the six catalysts are depicted in Figure 7.30. The results in the hydroconversion of the pure feeds and the mixed-feed on catalysts 3.5Ir/$Rb_{0.52}$,$H_{0.48}$-Beta-14, 3.3Ir/$H_{0.58}$,$Cs_{0.42}$-Beta-14 and 3.0Ir/$Na_{0.80}$,$H_{0.20}$-EMC-2-4.3 are found to be very similar. When comparing the three curves in Figures 7.30a to c, the course of each curve shows great similarities among the three catalysts. The distribution of the hydrocracked products of the n-decane conversion shows maxima at C_3 and C_7 on the Beta catalysts. These curves are very similar to the ones for the 3.3Ir/$Na_{0.72}$,$H_{0.28}$-Y-2.4 catalyst (*cf.* Figure 7.19, page 151) and seem to be typical for hydrogenolytic conversion of n-decane.

Although, the selectivities of the C_3 and C_7 fractions are very high on 3.0Ir/$Na_{0.80}$,$H_{0.20}$-EMC-2-4.3, this catalyst shows pronounced maxima at C_2 and C_8 in the hydroconversion of n-decane. Nothing similar was obtained on all other catalysts (whether large-pore zeolites or not) and seems to be typical for EMC-2. It is not understood why these high amounts of C_2 and C_8 are formed on this catalyst, since the dimensions of its pore system are very close to that of zeolite Y. It is speculated that the favored formation of C_2 + C_8 is due to a peculiarity of the shape of the cages in the EMC-2 framework.

The distributions of the hydrocracked products from decalin on the three HIPEROCs show high amounts of methane and C_4, C_5, C_6 and C_9 (see Figures 7.30a to c). These curves seem to be a hybrid of a hammock-type curve and some kind of a bell-type curve. A comparison with the results obtained on 3.3Ir/$Na_{0.72}$,$H_{0.28}$-Y-2.4 (*cf.* Figure 7.19b, page 151) reveals, that also on this catalyst the selectivities of the C_4 to C_6 fractions are elevated. What these four catalysts have in common is their preferred formation of OCDs, indicating that this shape of S_j* curves obtained from decalin hydroconversion seems to be typical for HIPEROCs [79].

The modified hydrocracking selectivities from the hydroconversion of an equimolar mixture of decalin and n-decane in Figures 7.30a to c are intermediates of the ones obtained from the conversion of the pure hydrocarbons. The product selectivities of the C_9- products do not seem to be influenced by the presence of the respective other hydrocarbon.

The reduction of the pore system in the catalysts 2.9Ir/$K_{0.68}$,$Na_{0.21}$,$H_{0.11}$-L-2.9, 2.9Ir/$Na_{0.90}$,$H_{0.10}$-MOR-5.8 and 0.5Ir/$H_{0.59}$,$Na_{0.41}$-ZSM-5-18 leads to modified hydrocracking selectivities (Figures 7.30d - e) which differ from all others and whose interpretation need further investigation. However, it is noticeable that the catalysts based on zeolites L and MOR show a high formation of methane in the hydroconversion of decalin, whereas on 0.5Ir/$H_{0.59}$,$Na_{0.41}$-ZSM-5-18 practically no C_1 + C_9 and C_2 + C_8 was formed as typical for conventional bifunctional catalysts.

8 Molybdenum Carbide Catalysts in the Hydroconversion of cis-Decalin

The characterization of the molybdenum carbides described in Section 6.3, page 113, revealed that the synthesis of bulk and supported molybdenum carbide was successful. Bulk molybdenum carbide could be prepared by carburization of MoO_3 with methane/hydrogen or n-octane/hydrogen mixtures. In addition, the molybdenum-loaded zeolite samples were carburized with the same reactants under identical reaction conditions. Supported molybdenum carbide catalysts were synthesized by impregnation of zeolite Y using aqueous solutions of either Na_2MoO_4 or $(NH_4)_6Mo_7O_{24}$ as molybdenum sources. Certain parameters of the catalysts, such as the n_{Si}/n_{Al} ratio of the zeolite or the concentration of Brønsted acid sites or the loading with molybdenum were varied. The catalytic properties of these materials in the hydroconversion of cis-decalin are discussed in the following sections.

8.1 Bulk Molybdenum Carbide Catalysts in the Hydroconversion of cis-Decalin

Bulk β-Mo_2C-900 was tested in the hydroconversion of cis-decalin. The reaction conditions are given in Section 5.3.2.1 on page 81 and the characterization of the catalyst in Section 6.3.1 on page 113. The conversion of decalin and the product selectivities are depicted in Figure 8.1a. A conversion of decalin of 45 % was obtained at a reaction temperature of 390 °C on catalyst β-Mo_2C-900. Such a low conversion at the relatively high reaction temperature reveals a low activity of β-Mo_2C-900 in the hydroconversion of decalin. The stereoisomerization of cis-decalin into trans-decalin occurred on bulk molybdenum carbide, as also observed on the noble-metal catalysts. A ratio of $n_{trans\text{-}decalin}/(n_{cis\text{-}decalin} + n_{trans\text{-}decalin})$ of 88.4 % is obtained at 350 °C, which represents the thermodynamic equilibrium between both stereoisomers [145].

By far the most abundant products at low decalin conversions are the skeletal isomers of decalin. The most abundant skeletal isomer of decalin at low conversion is spiro[4.5]decane with selectivities of more than 30 %. Hence, spiro[4.5]decane is a primary product on bulk β-Mo_2C, as also on 2.7Pt/silica. The selectivities of ring-opening products of decalin and open-chain decanes are low with less than 10 or 5 %, respectively, throughout the whole

conversion range measured. As the conversion of decalin increases, the selectivity of hydrocracked products increases as well. The catalytic behavior of bulk β-Mo_2C resembles qualitatively the one of 2.7Pt/silica (see Figure 7.8a, page 132). However, S_{ROPs} and S_{DHPs} are lower than found on 2.7Pt/silica.

The carbon number distribution of the hydrocracked products from decalin on β-Mo_2C-900 are depicted in Figure 8.1b. The modified selectivities of the C_3 to C_9 products reach values between 9 to 21 % with a minimum at C_5. Slightly increased selectivities are obtained for C_2 with 33 %. Methane is by far the most abundant hydrocracked product with a modified hydrocracking selectivity of 284 %. A comparison with the modified hydrocracking selectivities obtained on 2.7Pt/silica reveals a close similarity. This indicates that the hydrocracking properties of bulk molybdenum carbide resemble the one of noble metals, especially of platinum.

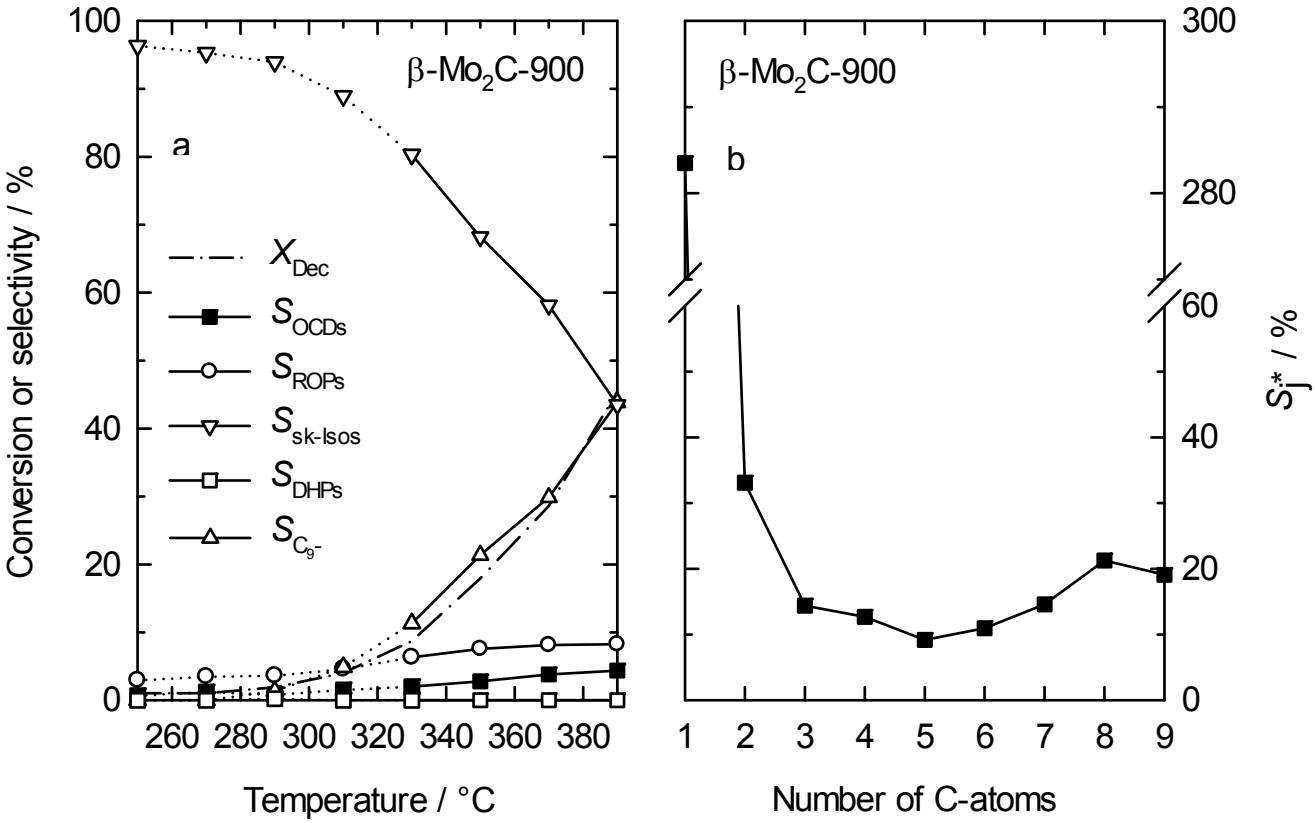

Figure 8.1: a) Conversion and product selectivities of decalin on β-Mo_2C-900 and b) modified hydrocracking selectivities S_j* of decalin. S_j* obtained at: T_r = 390 °C; X_{Dec} = 45 %; $Y_{C_{9-}}$ = 20 %; Σ S_j* = 419 %.

8.2 Supported Molybdenum Carbide Catalysts in the Hydroconversion of cis-Decalin

8.2.1 Variation of the Concentration of Brønsted Acid Sites of the Support

Bulk molybdenum carbide possesses a low activity in the hydroconversion of decalin, as shown in the previous Section 8.1. Hence, four catalysts containing *ca.* 5 wt.-% of molybdenum carbide supported on zeolite Y with different concentrations of Brønsted acid sites were prepared. Their preparation and the results of their characterization are described in Sections 5.1.8 to 5.1.9 on page 67 and Section 6.3.2 on page 116, respectively. The conversions of decalin and the product selectivities obtained on the four catalysts are depicted in Figure 8.2.

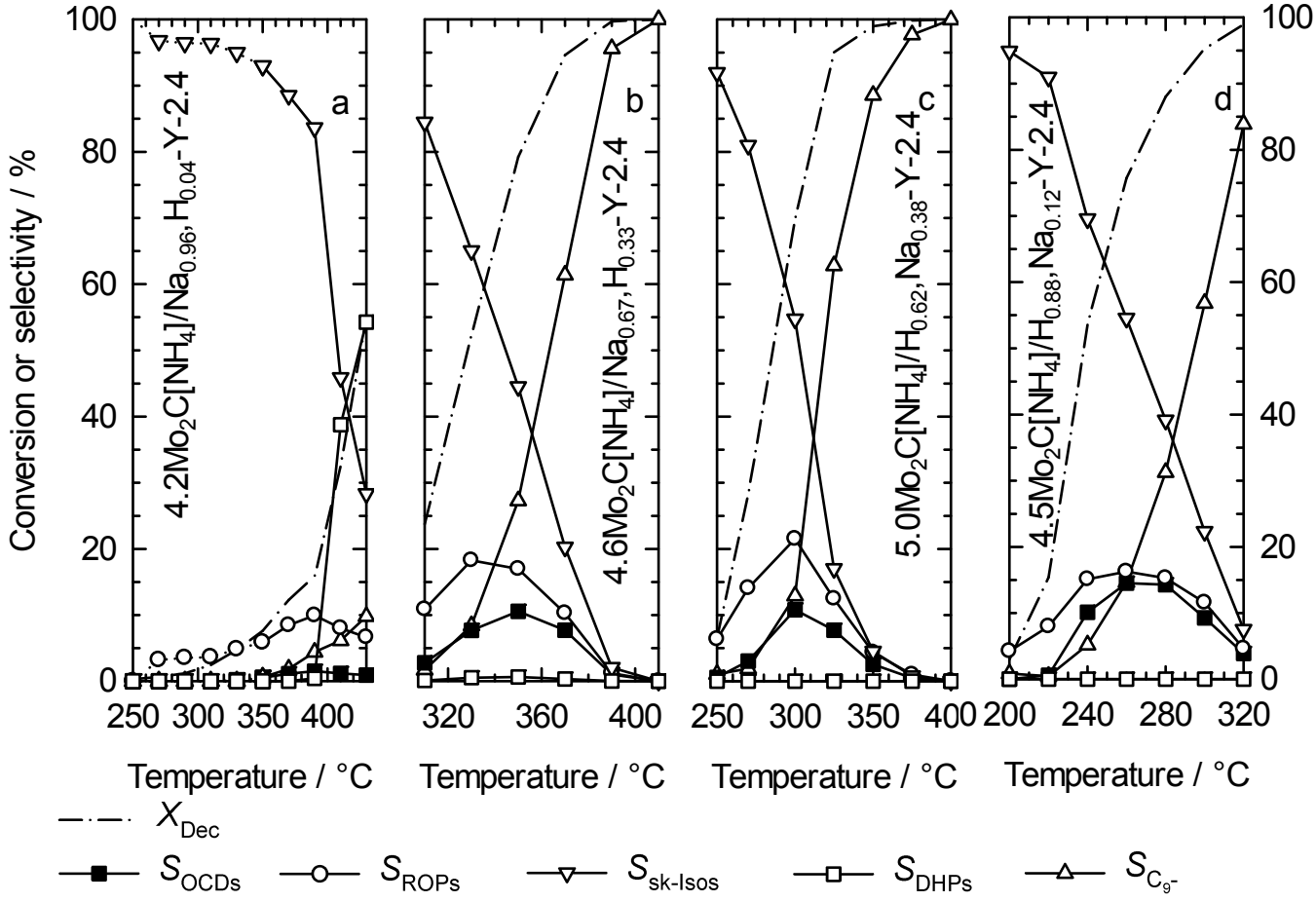

Figure 8.2: Conversion and product selectivities in the hydroconversion of decalin on supported molybdenum carbide catalysts with different concentrations of Brønsted acid sites.

An increasing catalytic activity is obtained on the four catalysts with increasing concentration of Brønsted acid sites (see Figures 8.2a to d), as reflected in the higher conversions for identical reaction temperatures. In addition, the four catalysts can be ranked according to their activity in the stereoisomerization of cis- to trans-decalin. At T_r = 350 °C the following ratios of $n_{trans\text{-}decalin}/(n_{cis\text{-}decalin} + n_{trans\text{-}decalin})$ are reached: 81.7, 89.5, 89.6 and 91.8 % for the catalysts dealt with in Figures 8.2a to d. Thermodynamic equilibrium is reached faster on the catalysts containing higher concentrations of Brønsted acid sites. Primary products on all catalysts are skeletal isomers of decalin, which is reflected by their very high selectivities at low decalin conversions.

On catalyst 4.2$Mo_2C[NH_4]/Na_{0.96},H_{0.04}$-Y-2.4, which possesses the lowest concentration of Brønsted acid sites among the four catalysts, very small selectivities of ring-opening products of decalin, open-chain decanes and hydrocracked products are obtained at elevated temperatures. Beyond 400 °C, the selectivity of dehydrogenated products increases strongly.

The product selectivities obtained on the other three catalysts (Figures 8.2b - d) show the same course. Skeletal isomers are predominant at low conversions. With increasing temperatures, the selectivity of sk-Isos decreases, whereas those of ROPs and OCDs pass through maxima. The maxima in the selectivities of ROPs and OCDs are reached at lower reaction temperatures with higher concentration of Brønsted acid sites of the catalyst (see Table 8.1). Selectivities of OCDs of 15 % were obtained on catalyst 4.5$Mo_2C[NH_4]/H_{0.88},Na_{0.12}$-Y-2.4 which is the highest value among the four catalysts.

Table 8.1: Maximum selectivities of OCDs and reaction conditions for the obtained modified hydrocracking selectivities S_j* in Figure 8.3.

Catalyst	T_r / °C	X_{Dec} / %	$S_{OCDs,max.}$ / %	Y_{C_9-} / %	ΣS_j* / %
4.2$Mo_2C[NH_4]/Na_{0.96},H_{0.04}$-Y-2.4	390	16	1.6	1	280
4.6$Mo_2C[NH_4]/Na_{0.67},H_{0.33}$-Y-2.4	350	79	11	22	232
5.0$Mo_2C[NH_4]/H_{0.62},Na_{0.38}$-Y-2.4	300	70	11	9	190
4.5$Mo_2C[NH_4]/H_{0.88},Na_{0.12}$-Y-2.4	260	76	15	11	175

In contrast to 4.2$Mo_2C[NH_4]/Na_{0.96},H_{0.04}$-Y-2.4, the other three catalysts containing Brønsted acid sites show very low selectivities of dehydrogenated

products, even at reaction temperatures of 400 °C. However, the formation of hydrocracked products becomes more and more prevailing at decalin conversions > 50 %.

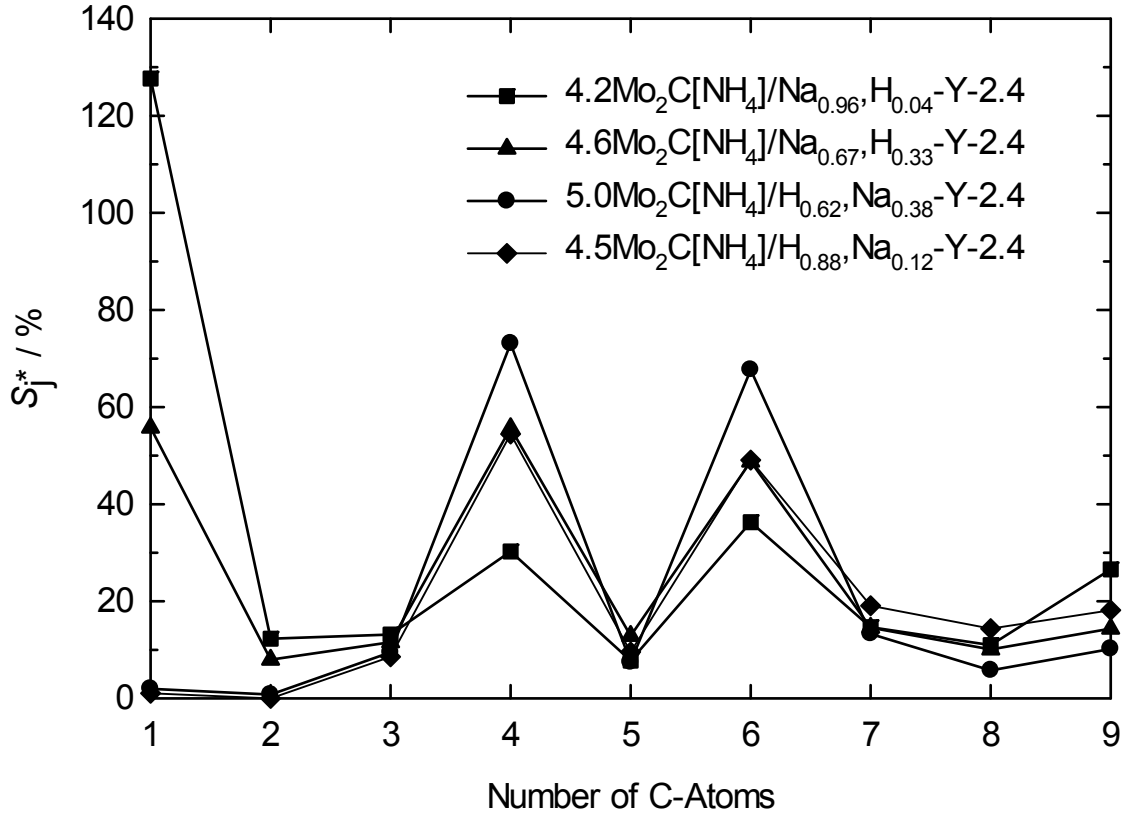

Figure 8.3: Modified hydrocracking selectivities S_j^* of the C_9- products obtained in the hydroconversion of decalin on supported molybdenum carbide catalysts with different concentrations of Brønsted acid sites. Reaction conditions are given in Table 8.1.

It has been shown in the previous sections, that the distribution of the hydrocracked products can give valuable information about the mechanism of ring opening of decalin. The S_j^* curves for all four catalysts are depicted in Figure 8.3. All curves show maxima at C_4 and C_6 due to a strong formation of iso-butane and methylcyclopentane, the products of the paring reaction. Between 77 and 93 % of all C_4-products and 58 to 88 % of all C_6-products are iso-butane and methylcyclopentane, respectively. Usually, for conventional bifunctional or monofuncional acidic catalysts M-shaped curves were obtained in the hydroconversion of decalin [78]. However, usual M-shape curves are only obtained for the two catalysts with the highest concentrations of Brønsted acid sites. The other two catalysts, *i.e.*, 4.2Mo$_2$C[NH$_4$]/Na$_{0.96}$,H$_{0.04}$-Y-2.4 and 4.6Mo$_2$C[NH$_4$]/Na$_{0.67}$,H$_{0.33}$-Y-2.4, showed a pronounced formation of methane,

especially the former one. Hence, some of the carbon-carbon bonds seem to be broken by hydrogenolysis. As the sum of the modified hydrocracking selectivities exceeds by far 200 %, secondary hydrocracking takes place on both catalysts. Therefore, exocyclic hydrogenolytic bond cleavage of alkyl side chains of ROPs is the preferred reaction on molybdenum carbide which leads to the high selectivities of C_1 in Figure 8.3.

8.2.2 Variation of the Molybdenum Carbide Loading and the n_{Si}/n_{Al} ratio of the Support

It is found, that the maximum selectivities of OCDs, the most valuable products, and ROPs in the hydroconversion of decalin are obtained on the supported molybdenum carbide catalysts with the highest concentration of Brønsted acid sites (see Section 8.2.1). Hence, zeolite Y was used in its H-form as carrier on which the influence of the molybdenum carbide loading and of the n_{Si}/n_{Al} ratio of the support was investigated. The product selectivities obtained in the conversion of decalin on molybdenum carbide catalysts with *ca.* 5 wt.-% of molybdenum and n_{Si}/n_{Al} ratios between 2.4 and 105 are depicted in Figure 8.4.

The product selectivities obtained in the hydroconversion of decalin on the catalysts with different n_{Si}/n_{Al} ratios of the zeolites (Figure 8.4) show similar trends as the selectivities on catalysts with different concentrations of Brønsted acid sites (Figure 8.2). Primary products are skeletal isomers of decalin, of which spiro[4.5]decane is again the most abundant at low conversions. At conversions of about 50 %, spiro[4.5]decane is formed with selectivities around 4 % for the catalysts with n_{Si}/n_{Al} ratios between 2.4 and 14. On the catalyst with the highest n_{Si}/n_{Al} ratio $4.7Mo_2C[NH_4]/H_{0.92},Na_{0.08}$-Y-105 and at similar conversion, $S_{spiro[4.5]decane}$ is slightly higher with a value of 7 %.

The selectivities obtained for the formation of OCDs and ROPs pass through maxima at conversions > 50 %, whereas the selectivity of hydrocracked products increases strongly in the region of $S_{ROPs,max.}$. Dehydrogenated products, like tetralin and naphthalene, where not formed on any of these four catalysts.

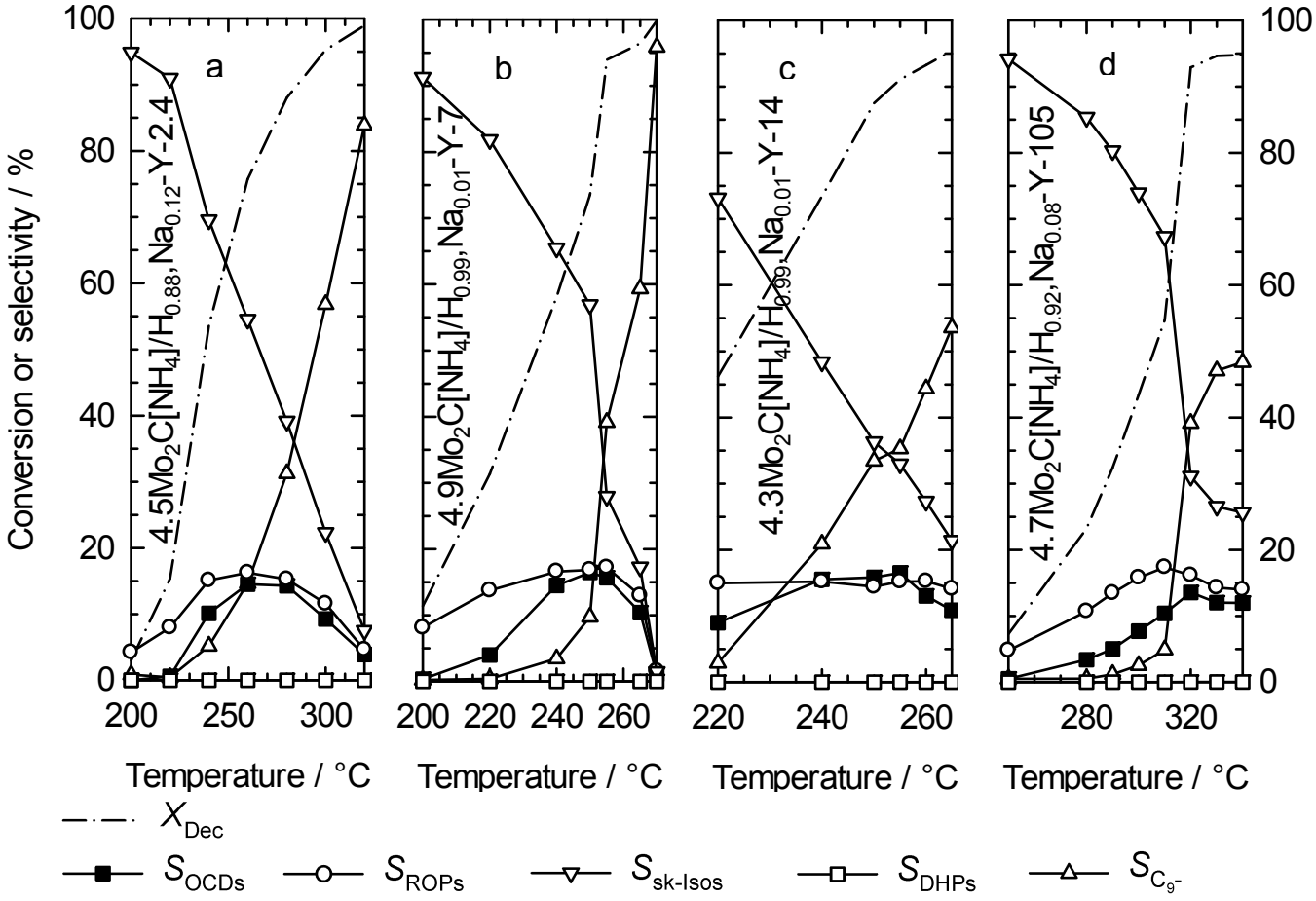

Figure 8.4: Conversion and product selectivities in the hydroconversion of decalin on supported molybdenum carbide catalysts with different n_{Si}/n_{Al} ratios of the zeolitic carriers.

A look at the distribution of the hydrocracked products clearly reveals an M-shaped curve for all four catalysts. It is noticeable, that on catalyst $4.7Mo_2C[NH_4]/H_{0.92},Na_{0.08}$-Y-105 modified hydrocracking selectivities of ca. 10 % of methane are found. Methane cannot be formed by β-scissions, but only by hydrogenolysis. Hence, if the number of Brønsted acid sites is reduced, as it is the case for an n_{Si}/n_{Al} ratio of 105, the hydrogenolytic activity of molybdenum carbide becomes conspicuous.

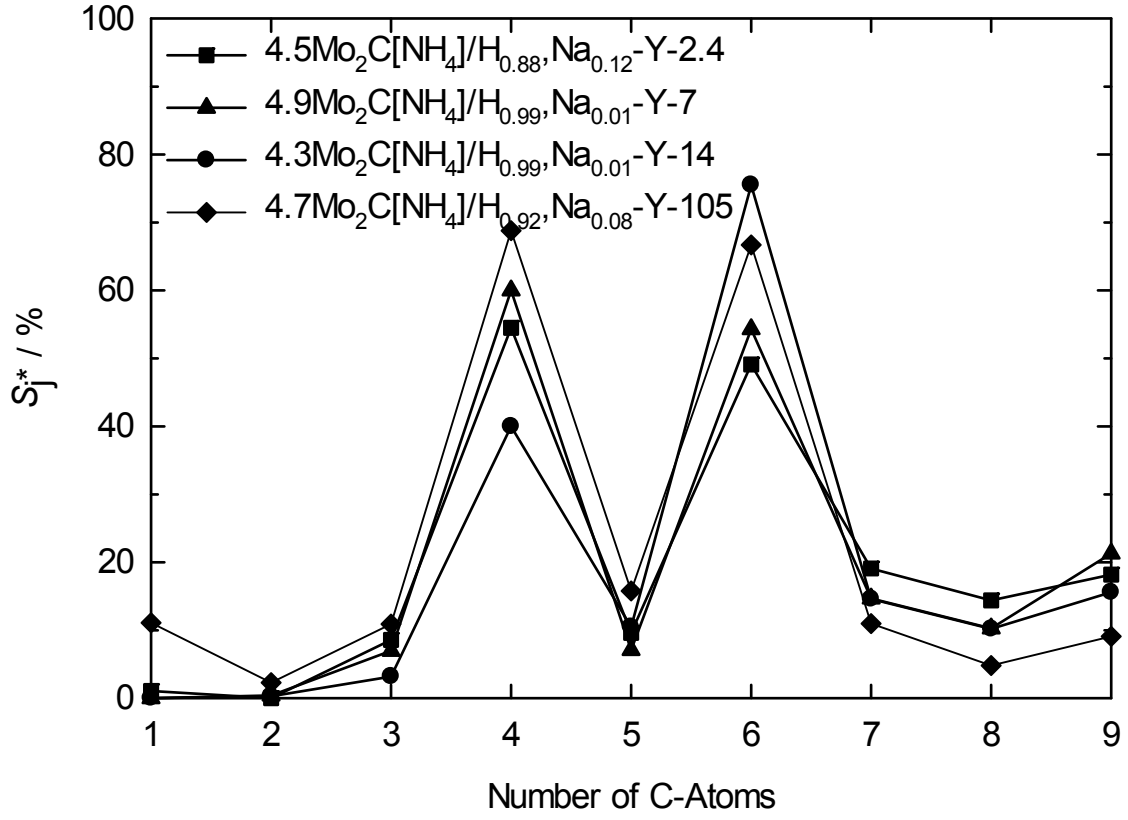

Figure 8.5: Modified hydrocracking selectivities S_j* in the hydroconversion of decalin obtained on supported molybdenum carbide catalysts with different n_{Si}/n_{Al} ratios of the carriers. Reaction conditions are given in Table 8.2.

The superposition of hydrocracking *via* carbocations on the acidic zeolite and hydrogenolysis on molybdenum carbide becomes even more convincing when the results of decalin hydroconversion on zeolite $H_{0.92}$,$Na_{0.08}$-Y-105 loaded with different amounts of molybdenum are compared. In Figure 8.6, the carbon-number distributions of the hydrocracked products observed on these catalysts with 4.7 to 23.7 wt.-% molybdenum are compared. The curve for the catalyst with the lowest molybdenum content, *i.e.*, 4.7$Mo_2C[NH_4]/H_{0.92}$,$Na_{0.08}$-Y-105 was already shown in Figure 8.5. As the content of molybdenum in increased from 4.7 to 23.7 wt.-% two characteristic changes in the S_j* curves occur: (i) The M-shape in the region C_3 to C_7 becomes less pronounced and eventually disappears (indicating a decreasing contribution of the paring reaction and hydrocracking *via* carbocations) and (ii) the selectivities of C_1 and C_9 increase markedly (indicating a strongly increasing contribution of hydrocracking by hydrogenolysis on Mo_2C). In fact, the modified hydrocracking selectivity on 23.7$Mo_2C[NH_4]/H_{0.92}$,$Na_{0.08}$-Y-105 (Figure 8.6) resembles the one obtained for the hydroconversion of decalin on bulk molybdenum carbide (see Section 8.1, Figure 8.1b, page 178).

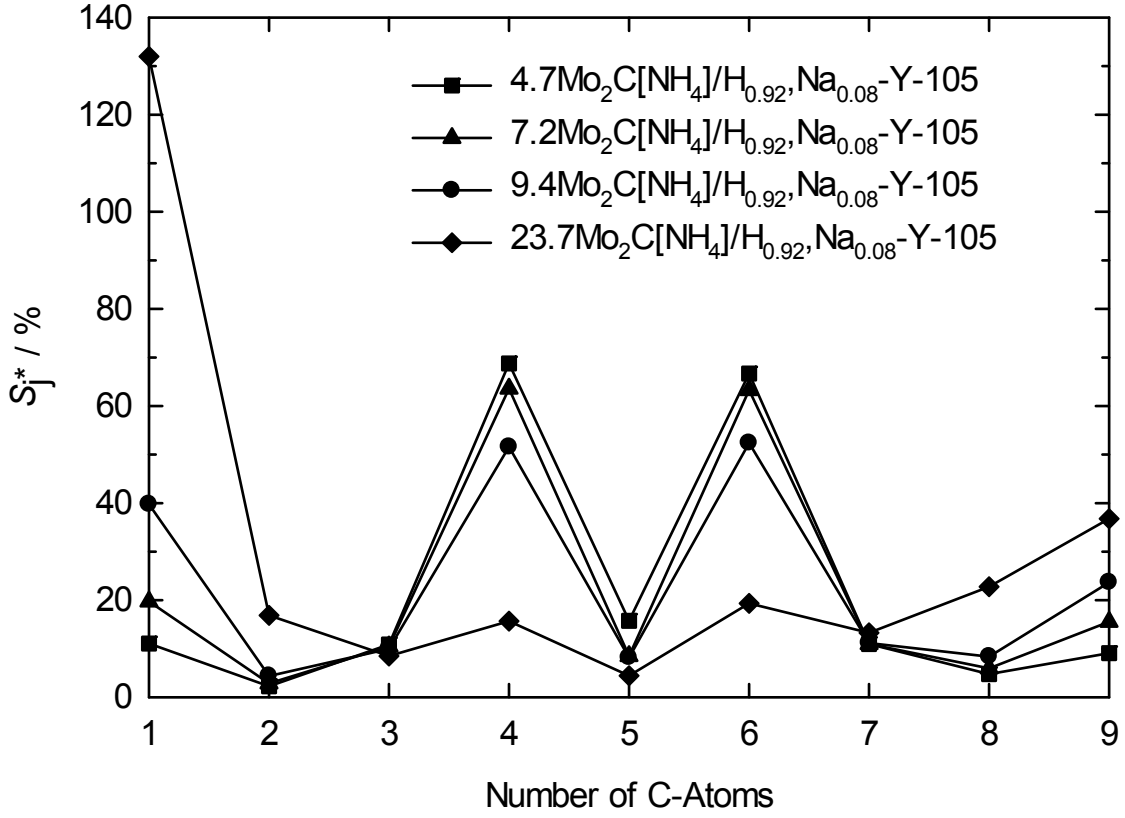

Figure 8.6: Modified hydrocracking selectivities S_j* in the hydroconversion of decalin obtained on supported molybdenum carbide catalysts with different amounts of carburized molybdenum supported on $H_{0.92}$,$Na_{0.08}$-Y-105. Reaction conditions are given in Table 8.2.

Table 8.2: Maximum selectivities of OCDs and reaction conditions for measuring the modified hydrocracking selectivities S_j* in Figures 8.5 and 8.6.

Catalyst	T_r / °C	X_{Dec} / %	$S_{OCDs,max.}$ / %	Y_{C_9-} / %	ΣS_j* / %
4.5$Mo_2C[NH_4]/H_{0.88}$,$Na_{0.12}$-Y-2.4	260	76	15	11	175
4.9$Mo_2C[NH_4]/H_{0.99}$,$Na_{0.01}$-Y-7	250	74	16	7	175
4.3$Mo_2C[NH_4]/H_{0.99}$,$Na_{0.01}$-Y-14	255	91	17	32	170
4.7$Mo_2C[NH_4]/H_{0.92}$,$Na_{0.08}$-Y-105	320	93	14	36	200
7.2$Mo_2C[NH_4]/H_{0.92}$,$Na_{0.08}$-Y-105	330	80	15	13	201
9.4$Mo_2C[NH_4]/H_{0.92}$,$Na_{0.08}$-Y-105	320	66	13	9	210
23.7$Mo_2C[NH_4]/H_{0.92}$,$Na_{0.08}$-Y-105	320	66	12	13	270

As open-chain decanes are the most desired products, their selectivities obtained on molybdenum carbide catalysts were investigated in more detail.

An overview on the maximum selectivities of OCDs obtained on H-Y catalysts with different n_{Si}/n_{Al} ratios and loadings of molybdenum carbide are given in Figure 8.7. The following trends can be deduced from Figure 8.7: (i) as the molybdenum loading is kept constant, the maximum selectivities of OCDs pass through a maximum as the n_{Si}/n_{Al} ratio of the support increases from 2.4 to 105; (ii) at a constant n_{Si}/n_{Al} ratio, the selectivity of OCDs passes through a maximum with increasing molybdenum loading.

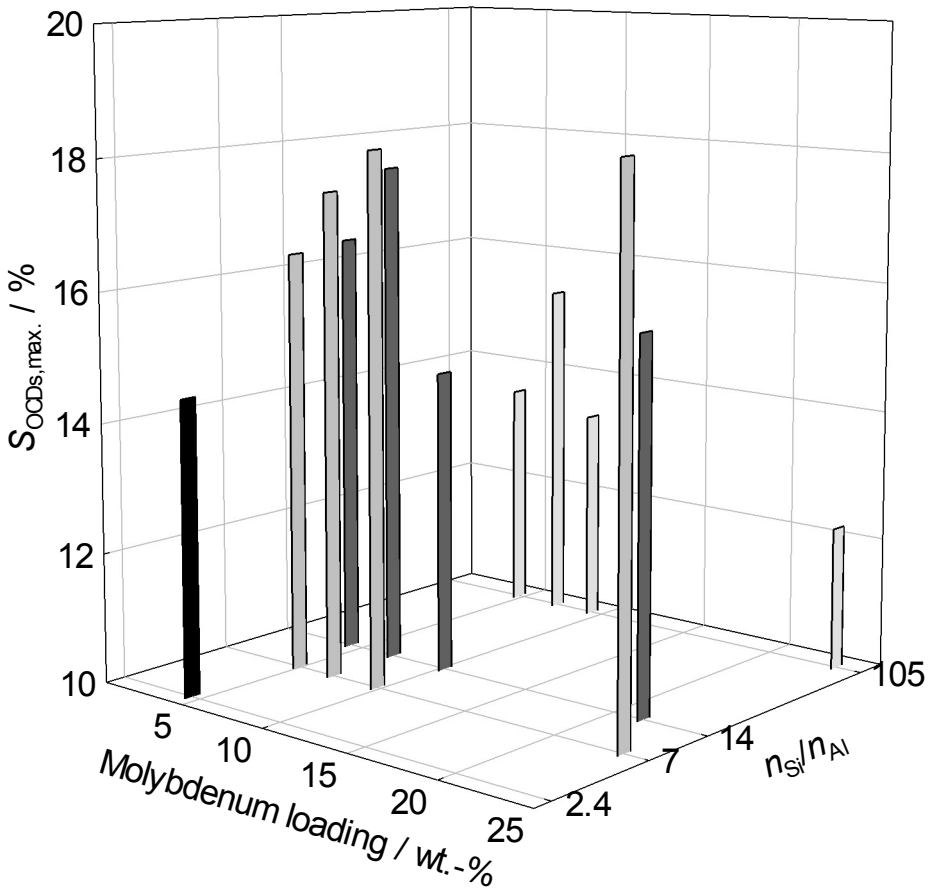

Figure 8.7: Maximum selectivities of OCDs obtained in the hydroconversion of decalin on molybdenum carbide supported on zeolite H-Y in dependence of the molybdenum loading and the n_{Si}/n_{Al} ratio of the support.

The highest $S_{OCDs,max.}$ of 18 % are obtained on catalysts 9.8$Mo_2C[NH_4]/H_{0.99},Na_{0.01}$-Y-7 and 23.7$Mo_2C[NH_4]/H_{0.99},Na_{0.01}$-Y-7 with an intermediate n_{Si}/n_{Al} ratio and medium to high molybdenum loadings. Since the selectitivities of OCDs do not exceed 18 % also the maximal yields of OCDs remain on a low level of $Y_{OCDs,max.} < 16$ %. Hence, supported molybdenum carbide catalysts are far away from being HIPEROCs in the ring opening of decalin.

In the same manner, as for the maximum selectivities of OCDs, the maximum ROPs selectivities which are obtained on the catalysts with varied molybdenum loading and modified support are depicted in Figure 8.8. In general, the maximum ROPs selectivities follow two trends: (i) at the same molybdenum loading the obtained ROPs selectivities pass through a maximum with increased n_{Si}/n_{Al} ratio of the support. (ii) The same is found for an increasing molybdenum loading on the same carrier.

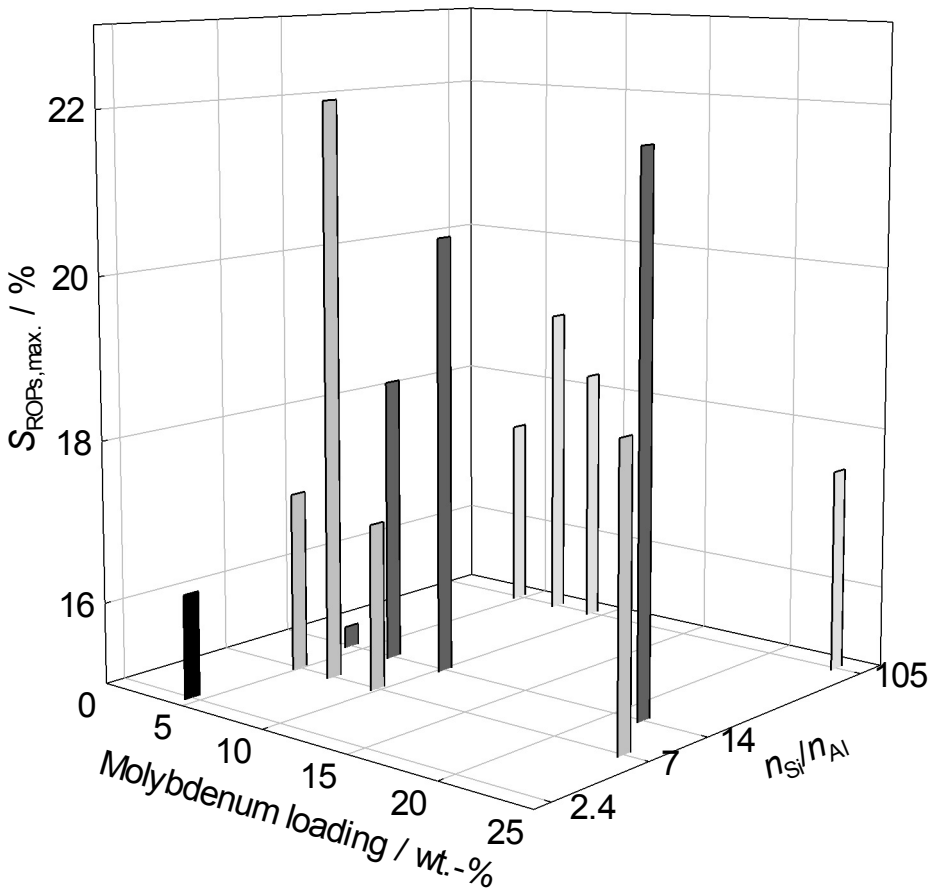

Figure 8.8: Maximum selectivities of ROPs obtained in the hydroconversion of decalin on molybdenum carbide supported on zeolite H-Y in dependence of the molybdenum loading and the n_{Si}/n_{Al} ratio of the support.

The supported molybdenum carbide catalysts with the highest selectivities and yields of OCDs and ROPs from the hydroconversion of decalin were described within this section. At first glance, a comparison of these values with these reported in the literature for the same class of catalysts might be disappointing [116]. Maximum yields of ROPs of 60 to 70 % are far beyond the yields attained for supported molybdenum carbide catalysts in this work. However,

there is (i) no discrimination between ROPs and OCDs in the literature due to incomplete product analyses and (ii) ROPs are not only restricted to C_{10} one-ring naphthenes. These two reasons led to high ROPs selectivities in the literature. If the combined yields of OCDs and ROPs were taken into account more than 33 % of $Y_{OCDs+ROPs}$ were found for catalyst 7.1$Mo_2C[NH_4]/H_{0.99},Na_{0.01}$-Y-7 which is at least half of the reported values.

8.2.3 Variation of the Molybdenum Carbide Precursors

For the preparation of all catalysts that have been discussed in the previous sections $(NH_4)_6Mo_7O_{24}$ was used as impregnation reagent. Now, the results obtained on catalysts made from a different molybdenum carbide precursor, *viz.* Na_2MoO_4, will be discussed. Around 9 wt.-% of molybdenum were loaded onto zeolite Y with an n_{Si}/n_{Al} ratio of 2.4 and different concentrations of Brønsted acid sites. The results of the hydroconversion of decalin on those catalysts are depicted in Figure 8.9.

The activity of the three catalysts is low, high reaction temperatures are required to reach the usual conversions, especially for the catalysts 8.2$Mo_2C[Na]/Na_{0.96},H_{0.04}$-Y-2.4 and 9.6$Mo_2C[Na]/Na_{0.66},H_{0.34}$-Y-2.4. Both catalysts contain low concentrations of Brønsted acid sites. Open-chain decanes and ring-opening products are formed to a negligible extent on both catalysts. Main products at low conversions are skeletal isomers, followed by dehydrogenated products (DHPs). The selectivities of DHPs pass through maxima with increasing reaction temperature before the formation of hydrocracked products becomes predominant.

The situation is slightly different for catalyst 8.9$Mo_2C[Na]/H_{0.92},Na_{0.08}$-Y-2.4 with the highest concentration of Brønsted acid sites. On this catalyst skeletal isomers of decalin are the primary products at low decalin conversions. DHPs are found at low conversion but as the reaction temperatures increase, DHPs are formed with decreasing selectivity. The selectivities of ROPs are higher than those of OCDs and both curves pass through maxima in the region of 50 % decalin conversion. As usually, main products at high conversion are C_9-hydrocarbons.

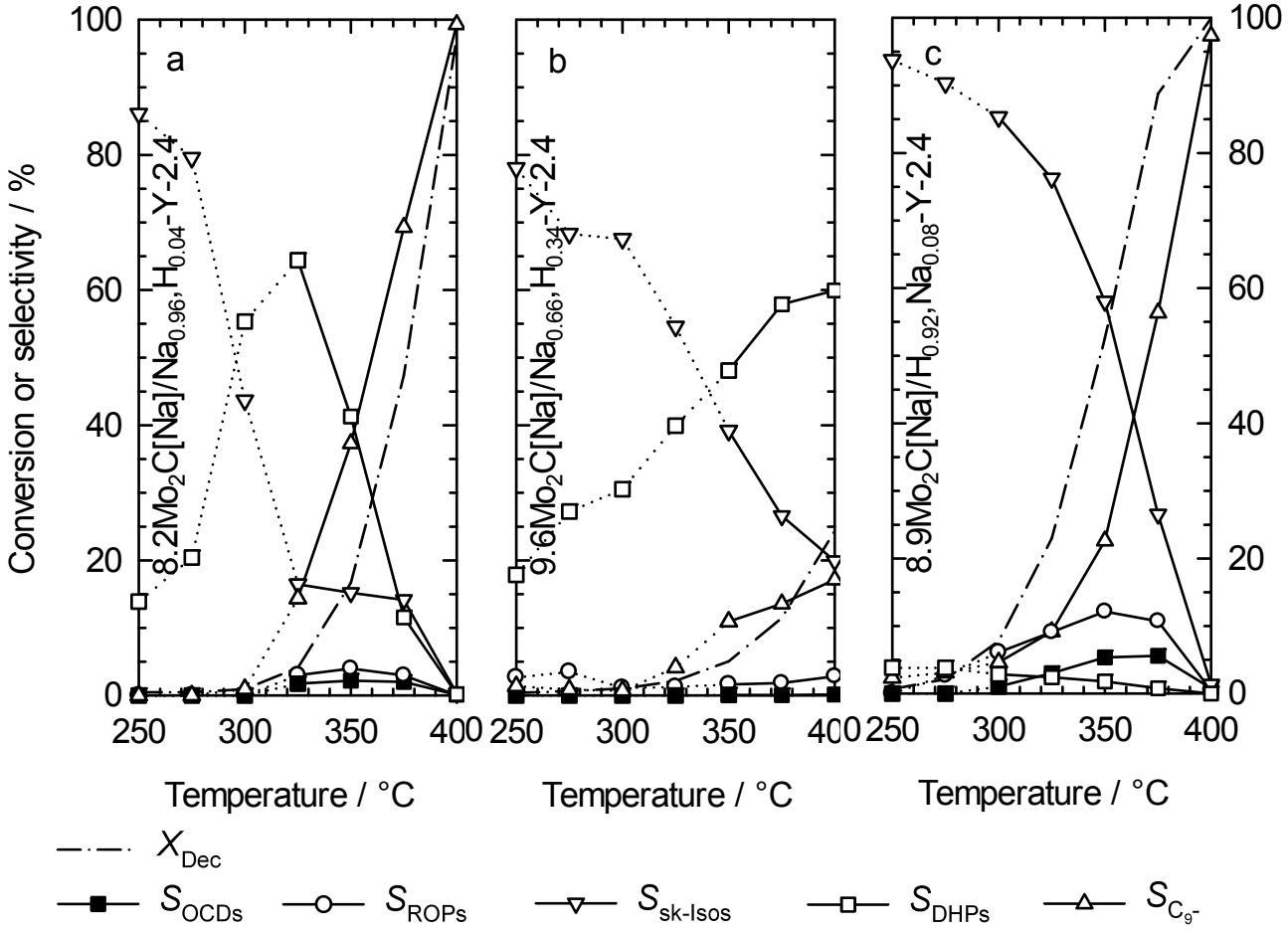

Figure 8.9: Conversion and product selectivities of decalin in the hydroconversion of decalin on supported molybdenum carbide catalysts with different concentrations of Brønsted acid sites.

Table 8.3: Maximum selectivities of OCDs and reaction conditions for the modified hydrocracking selectivities S_j* presented in Figure 8.10.

Catalyst	T_r / °C	X_{Dec} / %	$S_{OCDs,max.}$ / %	Y_{C_9-} / %	ΣS_j* / %
8.2Mo_2C[Na]/$Na_{0.96}$,$H_{0.04}$-Y-2.4	350	16.7	2.2	6.2	366
9.6Mo_2C[Na]/$Na_{0.66}$,$H_{0.34}$-Y-2.4	350	5.1	0.1	0.6	492
8.9Mo_2C[Na]/$H_{0.92}$,$Na_{0.08}$-Y-2.4	375	88.8	5.6	50.0	220

Methane is dominating the hydrocracked products on the first two catalysts as shown in Figure 8.10. The shapes of the S_j* curves obtained for these catalysts resembles the one of bulk molybdenum carbide. Also the low activity of the catalysts seems to be the same as that of bulk molybdenum carbide. However, bulk molybdenum carbide does not lead to the formation of DHPs from decalin, as the two catalysts do.

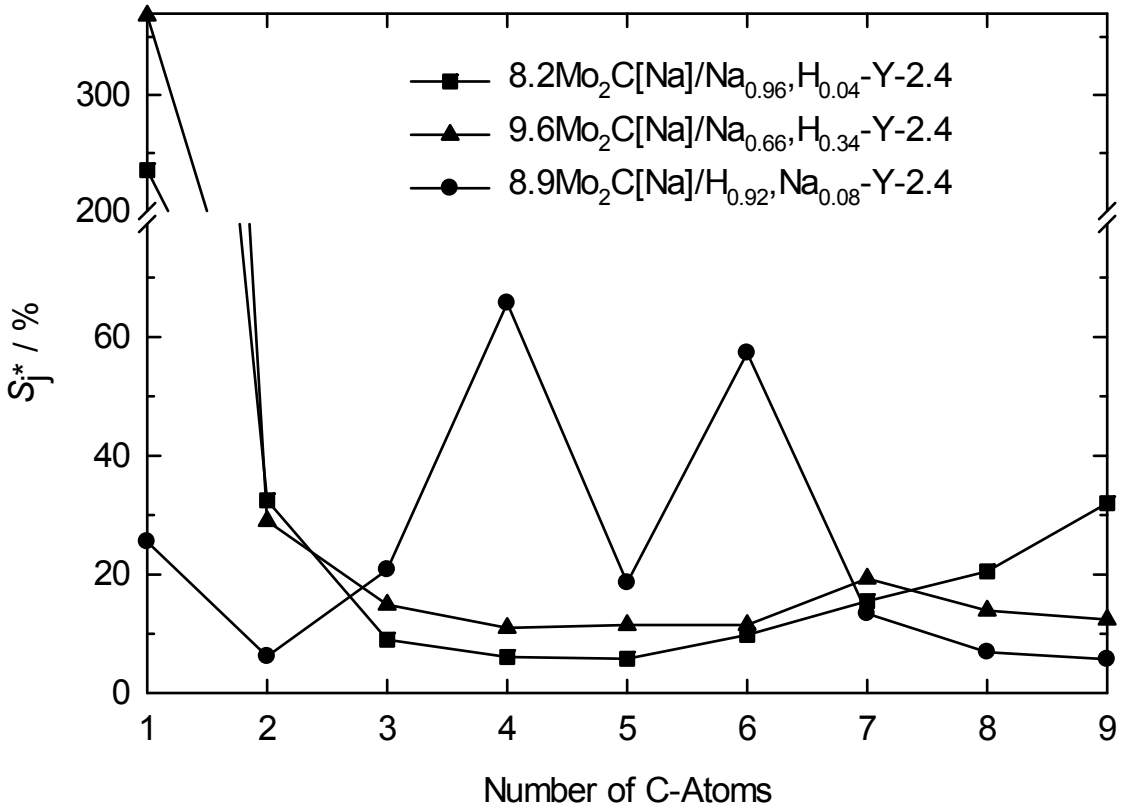

Figure 8.10: Modified hydrocracking selectivities S_j* in the hydroconversion of decalin obtained on supported molybdenum carbide catalysts with different concentrations of Brønsted acid sites. Reaction conditions are given in Table 8.3.

For the catalyst which contains the highest concentration of Brønsted acid sites, the carbon number distribution of the hydrocracked products resembles an M-shaped curve with maxima at C_4 and C_6 due to the formation of iso-butane and methylcyclopentane. Hydrogenolysis occurs to a minor extent, as methane is found among the hydrocracked products and which cannot be formed *via* the classical bimolecular hydrocracking.

Thus, a substitution of $(NH_4)_6Mo_7O_{24}$ by Na_2MoO_4 as impregnation reagent for the formation of the precursors of supported molybdenum carbide catalysts leads to a reduced catalyst activity and large amounts of dehydrogenated products. Moreover, the formation of ROPs and OCDs is reduced significantly.

9 References

[1] S. Brunauer, P.H. Emmett, E. Teller, J. Am. Chem. Soc. 60 (1938) 309-319.

[2] CONCAWE Report No. 01/13., *https://www.concawe.eu/DocShareNoFrame/docs/1/NDDHGAMADFHKNMMGMEMMHDFAVEVCW69YV3PDW69DWYGY/CEnet/docs/DLS/Rpt_13-1R-2013-01142-01-E.pdf* (Access on 31.10.2013).

[3] Amtliche Mineralöldaten, Bundesamt für Wirtschaft und Ausfuhrkontrolle, Germany, *http://www.bafa.de/bafa/de/energie/mineraloel_rohoel/amtliche_mineraloeldaten/index.html* (Access on 31.10.2013).

[4] DIN EN 590:2009+A1:2010, „Kraftstoffe für Kraftfahrzeuge – Dieselkraftstoff – Anforderung und Prüfverfahren“.

[5] J. Weitkamp, in: “Handbook of Heterogeneous Catalysis”, 2nd Edn., G. Ertl, H. Knözinger, F. Schüth, J. Weitkamp (Eds.), Vol. 7, Wiley-VCH, Weinheim, 2008, p. 3133-3152.

[6] G. Bellussi, A. Carati, R. Millini, in: “Zeolites and Catalysis – Synthesis, Reactions and Applications”, J. Čejka, A. Corma, S. Zones (Eds.), Vol. 2, Wiley-VCH, Weinheim, 2010, p. 449-491.

[7] A.F. Cronstedt, Kongl. Svenska Vetenskaps Academiens Handlingar 17 (1756) 120-123.

[8] D.S. Coombs, A. Alberti, T. Armbruster, G. Artioli, C. Colella, E. Galli, J.D. Grice, F. Liebau, J.A. Mandarino, H. Minato, E.H. Nickel, E. Passaglia, D.R. Peacor, S. Quartieri, R. Rinaldi, M. Ross, R.A. Sheppard, E. Tillmanns, G. Vezzalini, Can. Mineral. 35 (1997) 1571-1606.

[9] J.V. Smith, Zeolites 4 (1984) 309-310.

[10] W. Loewenstein, Am. Mineral. 39 (1954) 92-96.

[11] L.B. McCusker, F. Liebau, G. Engelhardt, Pure Appl. Chem. 73 (2001) 381-394.

[12] http://www.iza-structure.org (Access on 31.10.2013).

[13] J. Weitkamp, Solid State Ionics 131 (2000) 175-188.

[14] Ch. Baerlocher, L.B. McCusker, D.H. Olson, “Atlas of Zeolite Framework Types“, 6th Revised Edition, Elsevier, Amsterdam, London, New York, Oxford, Paris, Shannon, Tokyo, 2007, 398 pp.

[15] H. Maas, A. Khatyr, G. Calzaferri, Microporous Mesoporous Mater. 65 (2003) 233-242.

[16] A. Delabie, K. Pierloot, M.H. Groothaert, R.A. Schoonheydt, L.G. Vanquickenborne, Eur. J. Inorg. Chem. (2002) 515-530.
[17] N.Y. Chen, W.E. Garwood, Catal. Rev.-Sci. Eng. 28 (1986) 185-264.
[18] H.A. Szymanski, D.N. Stamires, G.R. Lynch, J. Opt. Soc. Am. 50 (1960) 1323-1328.
[19] H.G. Karge, in: “Catalysis and Adsorption by Zeolites“, G. Öhlmann, H. Pfeifer, R. Fricke (Eds.), Studies in Surface Science and Catalysis, Vol. 65, Elsevier, Amsterdam, Oxford, New York, Tokyo, 1991, p. 133-156.
[20] G.H. Kühl, J. Phys. Chem. Solids 38 (1977) 1259-1263.
[21] P.A. Jacobs, H.K. Beyer, J. Phys. Chem. 83 (1979) 1174-1177.
[22] B.V. Liengme, W.K. Hall, Trans. Faraday Soc. 62 (1966) 3229-3243.
[23] L.A. Pine, P.J. Maher, W.A. Wachter, J. Catal. 85 (1984) 466-476.
[24] P.A. Jacobs, W.J. Mortier, Zeolites 2 (1982) 226-230.
[25] P.A. Jacobs, Catal. Rev.: Sci. Eng. 24 (1982) 415-440.
[26] W.J. Mortier, J. Catal. 55 (1978) 138-145.
[27] G.A. Olah, Á. Molnár, “Hydrocarbon Chemistry“, 2nd Edn., John Wiley & Sons, New Jersey, 2003, p. 45-46.
[28] J. Weitkamp, M. Hunger, in: “Introduction to Zeolite Science and Practice“, J. Čejka, H. van Bekkum, A. Corma, F. Schüth (Eds.), Studies in Surface Science and Catalysis, Vol. 168, Elsevier, Amsterdam, 2007, p. 787-835.
[29] J. Weitkamp, Ind. Eng. Chem. Prod. Res. Dev. 21 (1982) 550-558.
[30] J. Weitkamp, P.A. Jacobs, J.A. Martens, Appl. Catal. 8 (1983), 123-141.
[31] W.O. Haag, R.M. Dessau, in: “Proceedings of the 8th International Congress on Catalysis“, Vol. 2, Verlag Chemie, Weinheim, DECHEMA, Frankfurt am Main, 1984, p. 305-316.
[32] F.G. Gault, in: ”Advances in Catalysis“, D.D. Eley, H. Pines, P.B. Weisz (Eds.), Vol. 30, Academic Press, New York, 1981, p. 1-95.
[33] J.R. Anderson, N.R. Avery, J. Catal. 5 (1966) 446-463.
[34] G. Leclercq, L. Leclercq, R. Maurel, J. Catal. 50 (1977) 87-97.
[35] J. Weitkamp, ChemCatChem 4 (2012) 292-306.
[36] H.L. Coonradt, W.E. Garwood, Ind. Eng. Chem. Proc. Des. Dev. 3 (1964) 38-45.
[37] J. Weitkamp, H. Schulz, J. Catal. 29 (1973) 361-366.
[38] D.M. Brouwer, H. Hogeveen, Recl. Trav. Chim. Pays-Bas 89 (1970) 211-224.

[39] J. Weitkamp, in: “Handbook of Heterogeneous Catalysis”, 2nd Edn., G. Ertl, H. Knözinger, F. Schüth, J. Weitkamp (Eds.), Vol. 4, Wiley-VCH, Weinheim, 2008, p. 3133-3152.
[40] C.J. Egan, G.E. Langlois, R.J. White, J. Am. Chem. Soc. 84 (1962) 1204-1212.
[41] A.E. Hirschler, J. Catal. 2 (1963) 428-439.
[42] P.E. Pickert, J.A. Rabo, E. Dempsey, V. Schomaker, in: “Proceedings of the Third International Congress on Catalysis”, W.M.H. Sachtler, G.C.A. Schuit, P. Zwietering (Eds.), Vol. 1, North-Holland Publishing Company, Amsterdam, 1965, p. 714-728.
[43] J. Weitkamp, S. Ernst, in: “Catalysis“, J.W. Ward (Ed.), Studies in Surface Science and Catalysis, Vol. 38, Elsevier, Amsterdam, 1988, p. 367-382.
[44] S. Ernst, J. Weitkamp, in: “Proceedings of the International Symposium on Zeolite Catalysis“, Siófok, Hungary, May 13-16, 1985, p. 457-466.
[45] J. Weitkamp, S. Ernst, Catal. Today 19 (1994) 107-149.
[46] J. Weitkamp, S. Ernst, R. Kumar, Appl. Catal. 27 (1986) 207-210.
[47] Y. Traa, S. Sealy, J. Weitkamp, in:“Molecular Sieves - Science and Technology, H.G. Karge, J. Weitkamp (Eds.), Vol. 5 Springer, Berlin, Heidelberg, 2007, p. 103-154.
[48] J. Weitkamp, C.Y. Chen, S. Ernst, in: „Successful Design of Catalysts“, T. Inui (Ed.), Studies in Surface Science and Catalysis, Vol. 44, Elsevier, Amsterdam, 1989, p. 343-350.
[49] H.B. Mostad, T.U. Riis, O.H. Ellestad, Appl. Catal. 64 (1990) 119-141.
[50] D. Kubička, N. Kumar, P. Mäki-Arvela, M. Tiitta, V. Niemi, T. Salmi, D.Y. Murzin, J. Catal. 222 (2004) 65-79.
[51] A. Corma, V. González-Alfaro, A.V. Orchillés, J. Catal. 200 (2001) 34-44.
[52] M. Santikunaporn, J.E. Herrera, S. Jongpatiwut, D.E. Resasco, W.E. Alvarez, E.L. Sughrue, J. Catal. 228 (2004) 100-113.
[53] D. Kubička, N. Kumar, P. Mäki-Arvela, M. Tiitta, V. Niemi, H. Karhu, T. Salmi, D.Y. Murzin, J. Catal. 227 (2004) 313-327.
[54] D. Kubička, M. Kangas, N. Kumar, M. Tiitta, M. Lindblad, D.Y. Murzin, Top Catal. 53 (2010) 1438-1445.
[55] K.C. Mouli, V. Sundaramurthy, A.K. Dalai, Z. Ring, Appl. Catal., A 321 (2007) 17-26.
[56] K.C. Mouli, V. Sundaramurthy, A.K. Dalai, J. Mol. Catal., A 304 (2009) 77-84.
[57] A.H. Alzaid, K.J. Smith, Appl. Catal., A 450 (2013) 243-252.

[58] S.J. Ardakani, K.J. Smith, Appl. Catal., A 403 (2011) 36-47.
[59] S.A. D'Ippolito, L.B. Gutierrez, C.L. Pieck, Appl. Catal., A 445-446 (2012) 195-203.
[60] S.A. D'Ippolito, L.B. Gutierrez, C.R. Vera, C.L. Pieck, Appl. Catal., A 452 (2013) 48-56.
[61] R. Moraes, K. Thomas, S. Thomas, S. Van Donk, G. Grasso, J.-P. Gilson, M. Houalla, J. Catal. 299 (2013) 30-43.
[62] S. Samoila, M. Boutzeloit, C. Especel, F. Epron, P. Marécot, Appl. Catal., A 369 (2009) 104-112.
[63] A. Djeddi, I. Fechete, F. Garin, Top. Catal. 55 (2012) 700-709.
[64] R.N. Rao, N. You, S. Yoon, D.P. Upare, Y.-K. Park, C.W. Lee, Catal. Lett. 141 (2011) 1047-1055.
[65] S. Dokjampa, T. Rirksomboon, D.T.M. Phuong, D.E. Resasco, J. Mol. Catal. A: Chem. 274 (2007) 231-240.
[66] P.T. Do, W.E. Alvarez, D.E. Resasco, J. Catal. 238 (2006) 477-488.
[67] G.B. McVicker, M. Daage, M.S. Touvelle, C.W. Hudson, D.P. Klein, W.C. Baird, B.R. Cook, J.G. Chen, S. Hantzer, D.E.W. Vaughan, E.S. Ellis, O.C. Feeley, J. Catal. 210 (2002) 137-148.
[68] G. Bellussi, A. Haas, S. Rabl, D. Santi, M. Ferrari, V. Calemma, J. Weitkamp, Chin. J. Catal. 33 (2012) 70-84.
[69] R. Moraes, K. Thomas, S. Thomas, S. Van Donk, G. Grasso, J.-P. Gilson, M. Houalla, J. Catal. 286 (2012) 62-77.
[70] A. Haas, S. Rabl, M. Ferrari, V. Calemma, J. Weitkamp, Appl. Catal., A 425-426 (2012) 97-109.
[71] J. Weitkamp, S. Rabl, A. Haas, D. Santi, M. Ferrari, V. Calemma, in: „Preprints of the Conference – The Future Role of Hydrogen in Petrochemistry and Energy Supply", S. Ernst, A. Lercher, J. Lichtscheidl, M. Marchionna, F. Nees, E. Santacesaria (Eds.), DGMK Tagungsbericht 2010-3, DGMK, Hamburg, 2010, p. 77-86.
[72] F. Garin, F.G. Gault, J. Am. Chem. Soc. 97 (1975) 4466-4476.
[73] J.R. Anderson, N.R. Avery, J. Catal. 2 (1963) 542-544.
[74] R.C. Santana, P.T. Do, M. Santikunaporn, W.E. Alvarez, J.D. Taylor, E.L. Sughrue, D.E. Resasco, Fuel 85 (2006) 643-656.
[75] J.A.R. van Veen, J.K. Minderhoud, L.G. Huve, W.H.J. Stork, in: "Handbook of Heterogeneous Catalysis", 2nd Edn., G. Ertl, H. Knözinger, F. Schüth, J. Weitkamp (Eds.), Vol. 6, Wiley-VCH, Weinheim, 2008, p. 2778-2808.
[76] M. Rigutto, in: "Zeolites and Catalysis", J. Čejka, A. Corma, S. Zones (Eds.), Vol. 2, Wiley-VCH, Weinheim, 2010, p. 547-584.

[77] S.T. Sie, in: “Handbook of Heterogeneous Catalysis”, 2nd Edn., G. Ertl, H. Knözinger, F. Schüth, J. Weitkamp (Eds.), Vol. 6, Wiley-VCH, Weinheim, 2008, p. 2809-2830.
[78] S. Rabl, A. Haas, D. Santi, C. Flego, M. Ferrari, V. Calemma, J. Weitkamp, Appl. Catal., A 400 (2011) 131-141.
[79] D. Santi, T. Holl, V. Calemma, J. Weitkamp, Appl. Catal., A 455 (2013) 46-57.
[80] J. Weitkamp, S. Rabl, A. Haas, D. Santi, M. Ferrari, V. Calemma, Oil Gas European J. 37 (2) (2011) 94-98.
[81] S. Rabl, D. Santi, A. Haas, M. Ferrari, V. Calemma, G. Bellussi, J. Weitkamp, Microporous Mesoporous Mater. 146 (2011) 190-200.
[82] EP2446962, May 02, 2012, Eni S.p.A., (Inv.: J. Weitkamp, S. Rabl, M.M. Ferrari, V. Calemma).
[83] EP2471596, July 04, 2012, Eni S.p.A., (Inv.: J. Weitkamp, S. Rabl, M.M. Ferrari, V. Calemma).
[84] EP2610005, July 03, 2013, Eni S.p.A., (Inv.: J. Weitkamp, S. Rabl, M.M. Ferrari, V. Calemma).
[85] H. Dauns, J. Weitkamp, Chem. Ing. Tech. 58 (1986) 900-902.
[86] J.F.M. Denayer, R.A. Ocakoglu, W. Huybrechts, B. Dejonckheere, P. Jacobs, S. Calero, R. Krishna, B. Smit, G.V. Baron, J.A. Martens, J. Catal. 220 (2003) 66-73.
[87] J.F.M. Denayer, K. De Meyer, J.A. Martens, G.V. Baron, Angew. Chem. Int. Ed. 42 (2003) 2774-2777.
[88] Z. Yang, Q. Li, R. Hua, M.R. Gray, K.C.Chou, J. Phys. Chem. 113 (2009) 20355-20359.
[89] J.S. Lee, S. Locatelli, S.T. Oyama, M. Boudart, J. Catal. 125 (1990) 157-170.
[90] S.J. Ardakani, X. Liu, K.J. Smith, Appl. Catal., A 324 (2007) 9-19.
[91] E.A. Blekkan, C. Pham-Huu, M.J. Ledoux, J. Guille, Ind. Eng. Chem. Res. 33 (1994) 1657-1664.
[92] P.M. Patterson, T.K. Das, B.H. Davis, Appl. Catal., A 251 (2003) 449-455.
[93] H. Moissan, C. R. Hebd. Seances Acad. Sci. 116 (1893) 1225-1227.
[94] K. Kuo, G. Hägg, Nature 170 (1952) 245-246.
[95] E.V. Clougherty, K.H. Lothrop, J.A. Kafalas, Nature 191 (1961) 1194.
[96] R.P. Elliott, “Constitution of Binary Alloys, First Supplement”, McGraw-Hill Book Company, New York, 1965, p. 220-221.
[97] E. Rudy, S. Windisch, A.J. Stosick, J.R. Hoffman, Trans. Metall. Soc. AIME 239 (1967) 1247-1267.

[98] W.A. Frad, in: “Advances in Inorganic Chemistry and Radiochemistry”, H.J. Emeléus, A.G. Sharpe (Eds.), Vol. 11, Academic Press, New York, London, 1968, p. 177-179.
[99] R. Ferro, R. Marazza, in: “Atomic Energy Review – Molybdenum: Physico-Chemical Properties of its Compounds and Alloys”, L. Brewer (Ed.), International Atomic Energy Agency, Vienna, 1980, pp. 714.
[100] L. Volpe, M. Boudart, J. Solid State Chem. 59 (1985) 348-356.
[101] T.Y. Velikanova, V.Z. Kublii, B.V. Khaenko, Powder Metall. Met. Ceram. 77 (1988) 891-896.
[102] S.T. Oyama, Catal. Today 15 (1992) 179-200.
[103] H.O. Pierson, “Handbook of Refractory Carbides and Nitrides”, William Andrew Publishing, Noyes, 1996, p. 110-112.
[104] D.J. Sajkowski, S.T. Oyama, Appl. Catal., A 134 (1996) 339-349.
[105] E. Furimsky, Appl. Catal., A 240 (2003) 1-28.
[106] B. Predel, in:” Landolt-Börnstein - Group IV Physical Chemistry - Numerical Data and Functional Relationships in Science and Technology – Co-Mo (Carbon-Molybdenum)”, O. Madelung (Ed.), Vol. 5b, SpringerMaterials - The Landolt-Börnstein Database, DOI: 10.1007/10040476_643.
[107] T. Miyao, I. Shishikura, M. Matsuoka, M. Nagai, S.T. Oyama, Appl. Catal., A 165 (1997) 419-428.
[108] L. Volpe, M. Boudart, Catal. Rev.: Sci. Eng. 27 (1985) 515-538.
[109] G.V. Samsonov, I.M. Vinitskii, “Handbook of Refractory Compounds”, IFI/Plenum Data Company, New York, 1980, 555 pp.
[110] A. Hanif, T. Xiao, A.P.E. York, J. Sloan, M.L.H. Green, Chem. Mater. 14 (2002) 1009-1015.
[111] EP 0 396 475 A1, March 26, 1990, Pechiney Electrometallurgie, (Inv.: M.-J. Ledoux, J.-L. Guille, C. Pham-Huu, S. Marin).
[112] X. Liu, K.J. Smith, Appl. Catal., A 335 (2008) 230-240.
[113] P. Da Costa, J.-L. Lemberton, C. Potvin, J.-M. Manoli, G. Perot, M. Breysse, G. Djega-Mariadassou, Catal. Today 65 (2001) 195-200.
[114] W. Ding, S. Li, G.D. Meitzner, E. Iglesia, J. Phys. Chem., B 105 (2001) 506-513.
[115] W. Li, G.D. Meitzner, R.W. Borry, E. Iglesia, J. Catal. 191 (2000) 373-383.
[116] S.J. Ardakani, K.J. Smith, Appl. Catal., A 403 (2011) 36-47.
[117] G.H. Kühl, in: “Catalysis and Zeolites: Fundamentals and Applications”, J. Weitkamp, L. Puppe (Eds.), Springer-Verlag, Berlin, Heidelberg, 1999, p. 151-153.

[118] D. Santi, Ph.D. Thesis, University of Stuttgart, 2012.
[119] A. Haas, Ph.D. Thesis, University of Stuttgart, 2012.
[120] G. Engelhardt, U. Lohse, E. Lippmaa, M. Tarmak, M. Mägi, Z. Anorg. Allg. Chem. 482 (1981) 49-64.
[121] H.G. Karge, M. Hunger, H.K. Beyer, in: “Catalysis and Zeolites: Fundamentals and Applications”, J. Weitkamp, L. Puppe (Eds.), Springer-Verlag, Berlin, Heidelberg, 1999, p. 208-211.
[122] H. Karge, Z. Phys. Chem. 76 (1971) 133-153.
[123] C.A. Emeis, J. Catal. 141 (1993) 347-354.
[124] G.B. McVicker, R.T. Baker, R.L. Garten, E.L. Kugler, J. Catal. 65 (1980) 207-220.
[125] F. Locatelli, B. Didillon, D. Uzio, G. Niccolai, J.P. Candy, J.M. Basset, J. Catal. 193 (2000) 154-160.
[126] T.E. Daubert, R.P. Danner, “Physical and Thermodynamic Properties of Pure Chemicals”, Hemisphere Publishing Corporation, New York, 1989, 2030 pp.
[127] G. Kortüm, H. Lachmann, “Einführung in die chemische Thermodynamik“, 7th Edn., Verlag Chemie, Weinheim and Vandenhoeck & Ruprecht, Göttingen, 1981, pp. 248-251.
[128] J. Weitkamp, H. Dauns, Appl. Catal. 38 (1988) 167-177.
[129] J. Weitkamp, H. Dauns, Chem. Ing. Tech. 56 (1984) 929-930.
[130] J. Weitkamp, R. Gläser, in: “Handbook of Heterogeneous Catalysis”, 2nd Edn., G. Ertl, H. Knözinger, F. Schüth, J. Weitkamp (Eds.), Vol. 4, Wiley-VCH, Weinheim, 2008, p. 2045-2053.
[131] J. Weitkamp, in: “Hydrocracking and Hydrotreating“, J.W. Ward, S.A. Qader (Eds.), ACS Symp. Ser., Vol. 20, Washington, D.C., 1975, p. 1-27.
[132] E. Leibnitz, H.G. Struppe, “Handbuch der Gaschromatographie”, 3rd Edn., Akademische Verlagsgesellschaft Geest & Portig G.-G., Leipzig, 1984, 828 pp.
[133] M.M.J. Treacy, J.B. Higgins, in: “Collection of Simulated XRD Powder Patterns for Zeolites”, 4th Edn., Elsevier, Amsterdam, 2001, p. 586.
[134] G. Garralón, V. Fornés, A. Corma, Zeolites 8 (1988) 268-272.
[135] H.G. Karge, M. Hunger, H.K. Beyer, in: “Catalysis and Zeolites: Fundamentals and Applications”, J. Weitkamp, L. Puppe (Eds.), Springer-Verlag, Berlin, Heidelberg, 1999, p. 310-314.
[136] J.B. Jones, Acta Crystallogr., Sect. B: Struct. Crystallogr. Cryst. Chem., 24 (1968) 355-358.
[137] D. Freude, H.-J. Behrens, Cryst. Res. Technol. 16 (1981) K36-K38.

[138] R. Xu, W. Pang, J. Yu, Q. Huo, J. Chen, “Chemistry of Zeolites and Related Porous Materials“, John Wiley & Sons, Singapore, 2007, p. 4.
[139] E. Lippmaa, M. Mägi, A. Samoson, G. Engelhardt, A.-R. Grimmer, J. Am. Chem. Soc. 102 (1980) 4889-4893.
[140] H.G. Karge, M. Hunger, H.K. Beyer, in: “Catalysis and Zeolites: Fundamentals and Applications”, J. Weitkamp, L. Puppe (Eds.), Springer-Verlag, Berlin, Heidelberg, 1999, p. 250-256.
[141] R.M. Dessau, in: “Adsorption and Ion Exchange with Synthetic Zeolites”, W.H. Flank (Ed.), ACS Symp. Ser., Vol. 135, Washington, D.C., 1980, p. 123-135.
[142] H. Knözinger, in: ”Handbook of Heterogeneous Catalysis”, 2nd Edn., G. Ertl, H. Knözinger, F. Schüth, J. Weitkamp (Eds.), Vol. 2, Wiley-VCH, Weinheim, 2008, p. 1135-1163.
[143] V. Calemma, M. Ferrari, S. Rabl, J. Weitkamp, Fuel 111 (2013) 763-770.
[144] S. Rabl, Ph.D. Thesis, University of Stuttgart, 2011.
[145] A. Haas, Diploma thesis, University of Stuttgart, 2008.
[146] J. Weitkamp, in: ”Actas do 9.° Simpósio Iberoamericano de Catálise - Proceedings of the 9th Iberoamerican Symposium on Catalysis”, M.F. Portela (Ed.), Vol. 2, Technical University, Lisboa, 1984, p. 1332-1341.

10 Appendices

10.1 Additional Information

Content:

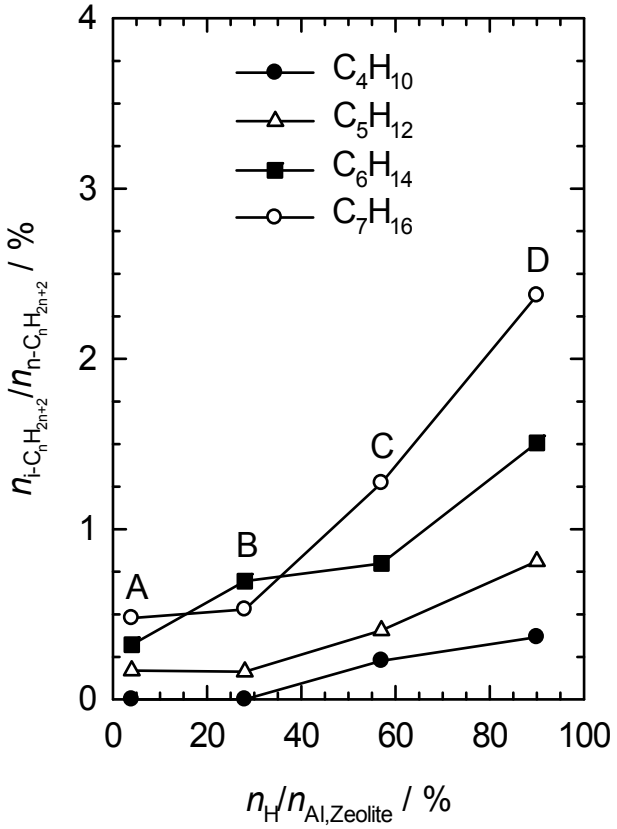

Figure 10.1: Content of branched isomers in the fractions of hydrocracked products from n-decane. The reaction conditions are given in Table 7.6, page 150. A: 3.0Ir/$Na_{0.96}$,$H_{0.04}$-Y-2.4; B: 3.3Ir/$Na_{0.72}$,$H_{0.28}$-Y-2.4; C: 2.9Ir/$H_{0.57}$,$Na_{0.43}$-Y-2.4; D: 3.1Ir/$H_{0.90}$,$Na_{0.10}$-Y-2.4.

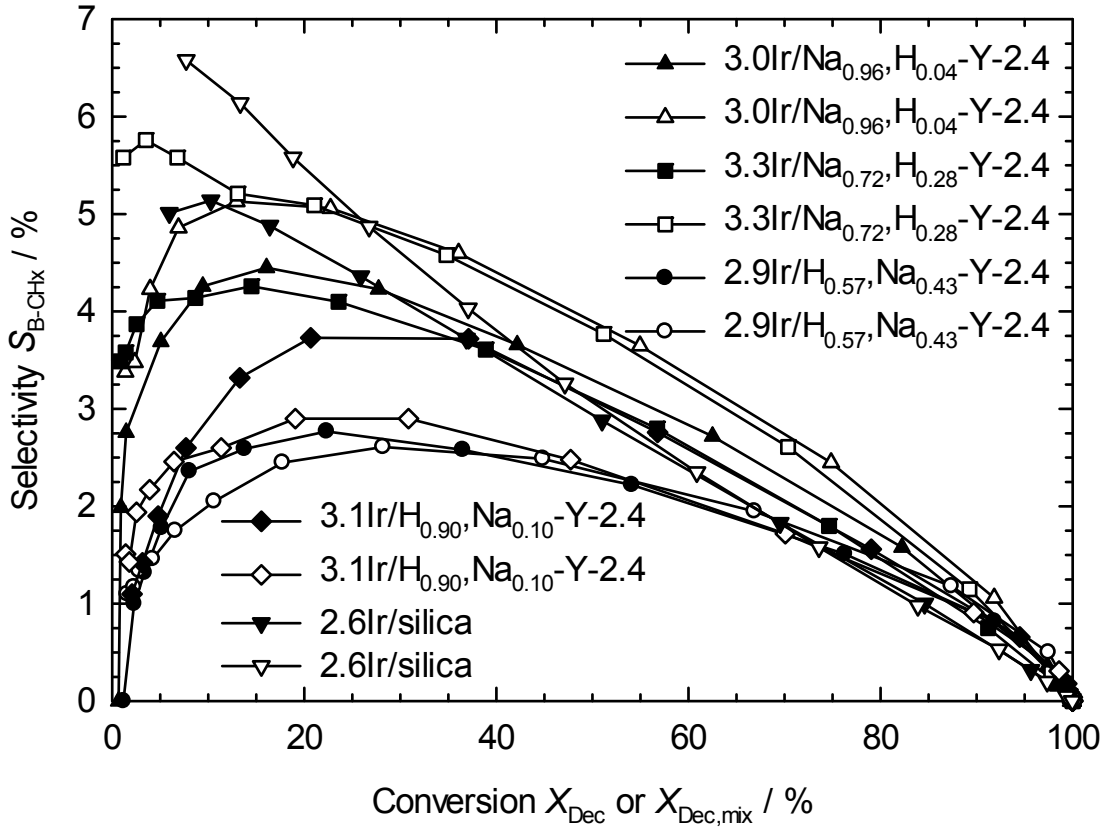

Figure 10.2: Selectivities of butylcyclohexane in dependence of the decalin conversion. The filled symbols designate the selectivities in the experiments with pure decalin as feed, the open symbols stand for the selectivities in the mixed-feed experiments.

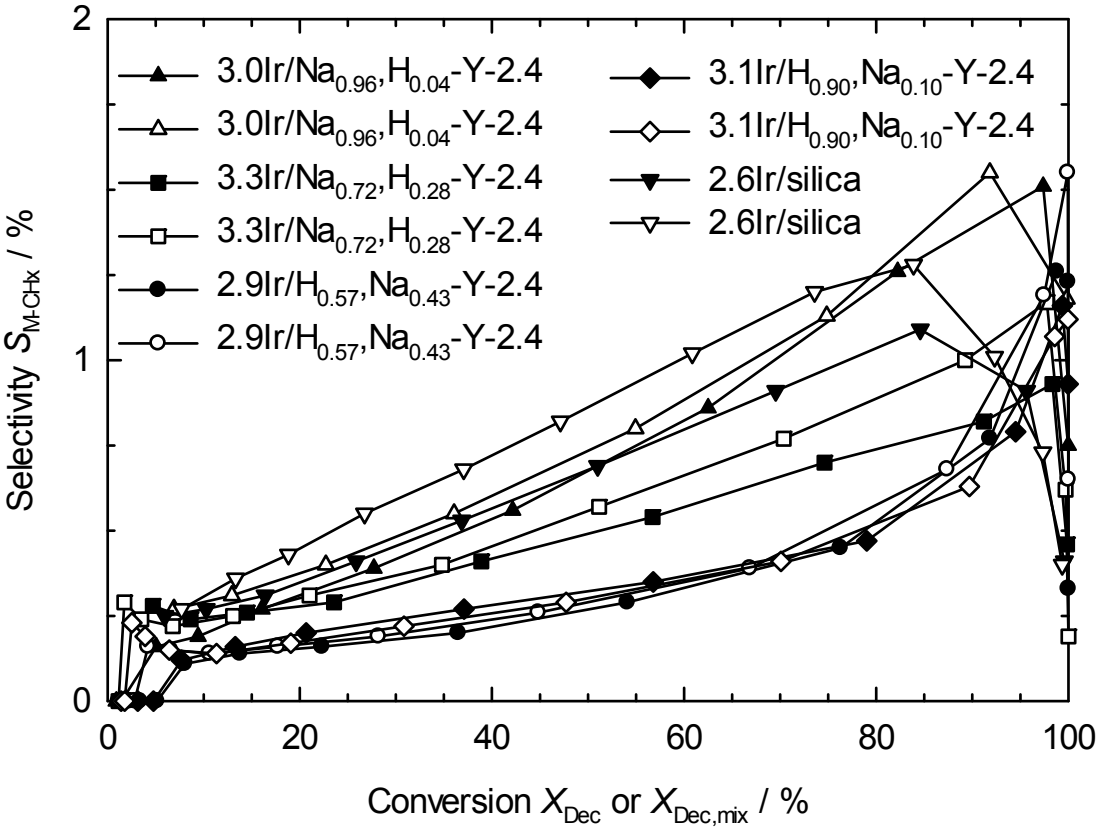

Figure 10.3: Selectivities of methylcyclohexane in dependence of the decalin conversion. The filled symbols represent the selectivities in the experiments with pure decalin as feed, the open symbols represent the selectivities in the mixed-feed experiments.

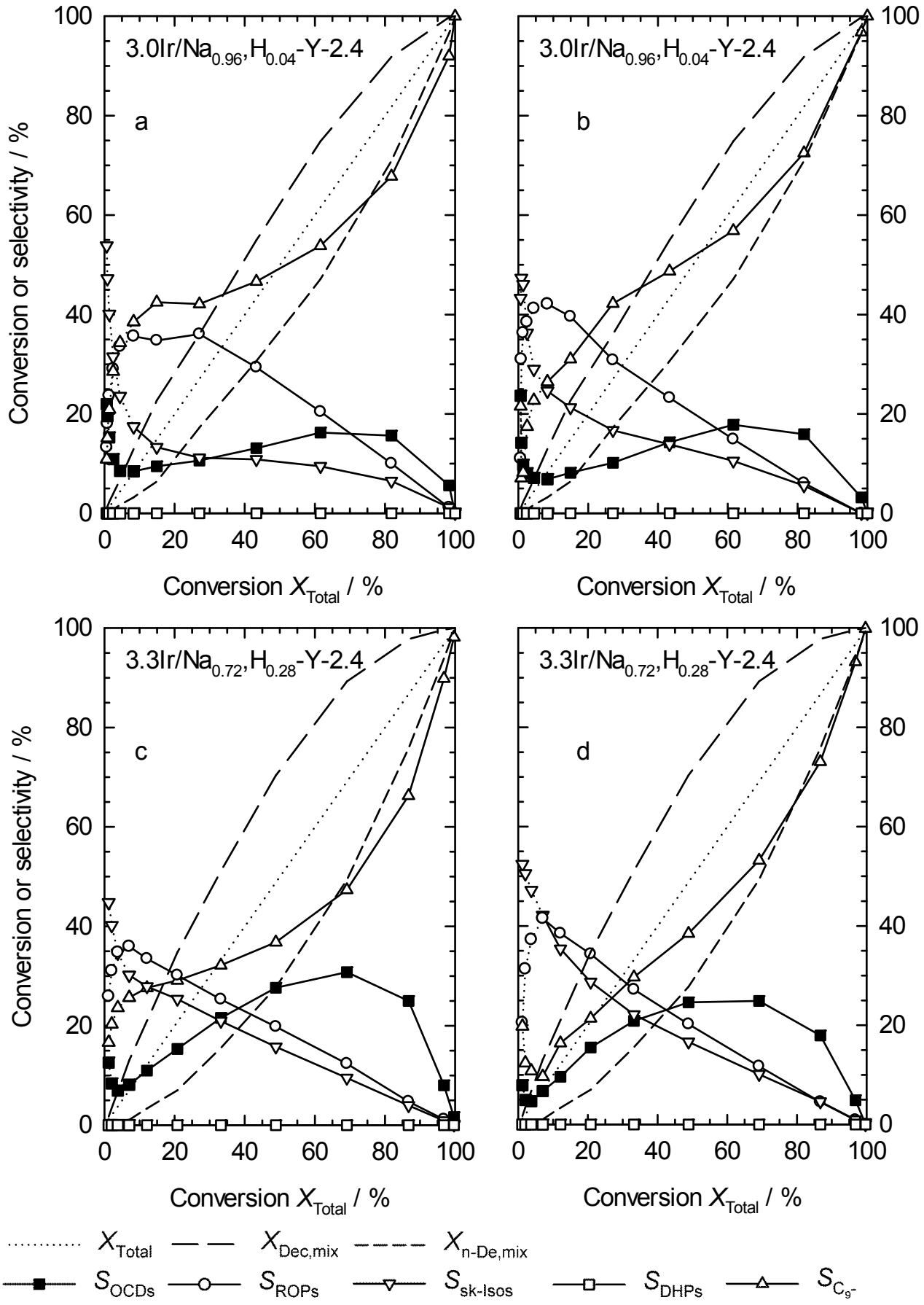

Figure 10.4: Measured (left) and calculated (right) selectivities and conversions of the decalin/n-decane conversion on the Ir/Na,H-Y-2.4 catalysts.

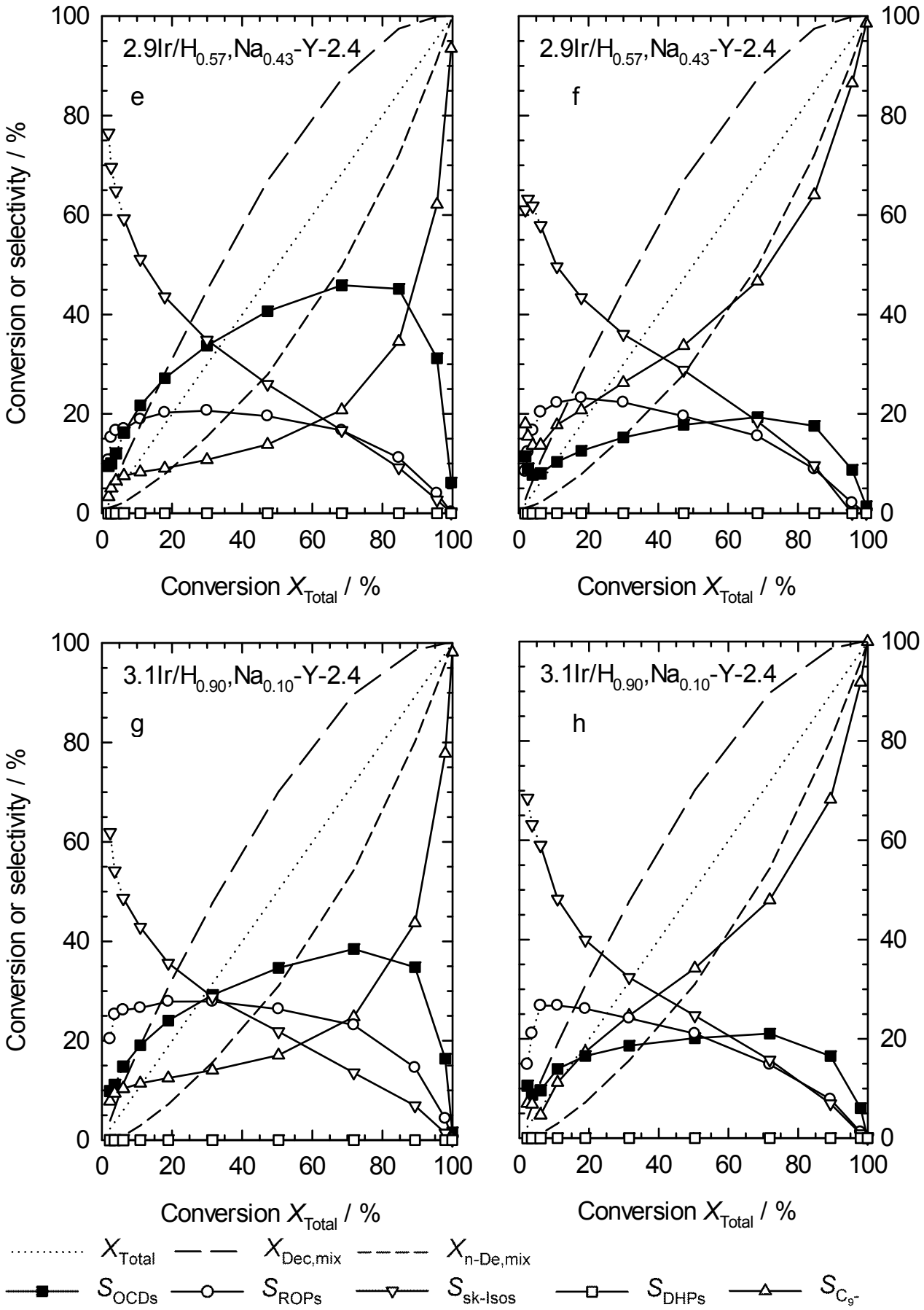

Figure 10.4: continued

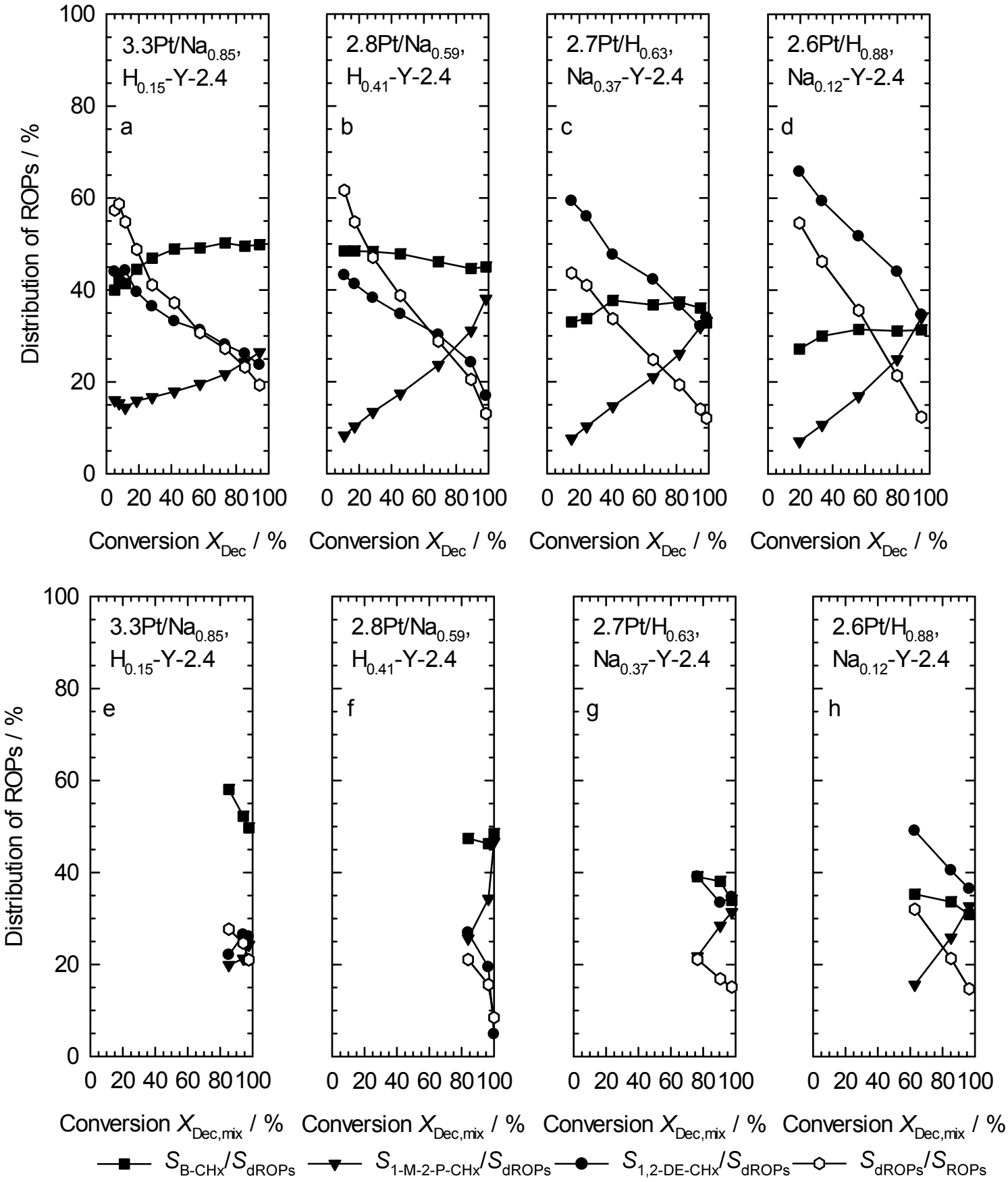

Figure 10.5: Direct ROPs of decalin obtained from pure decalin as reactant (a – d) and the equimolar decalin/n-decane mixture (e – h) on the Pt/Na,H-Y catalysts.

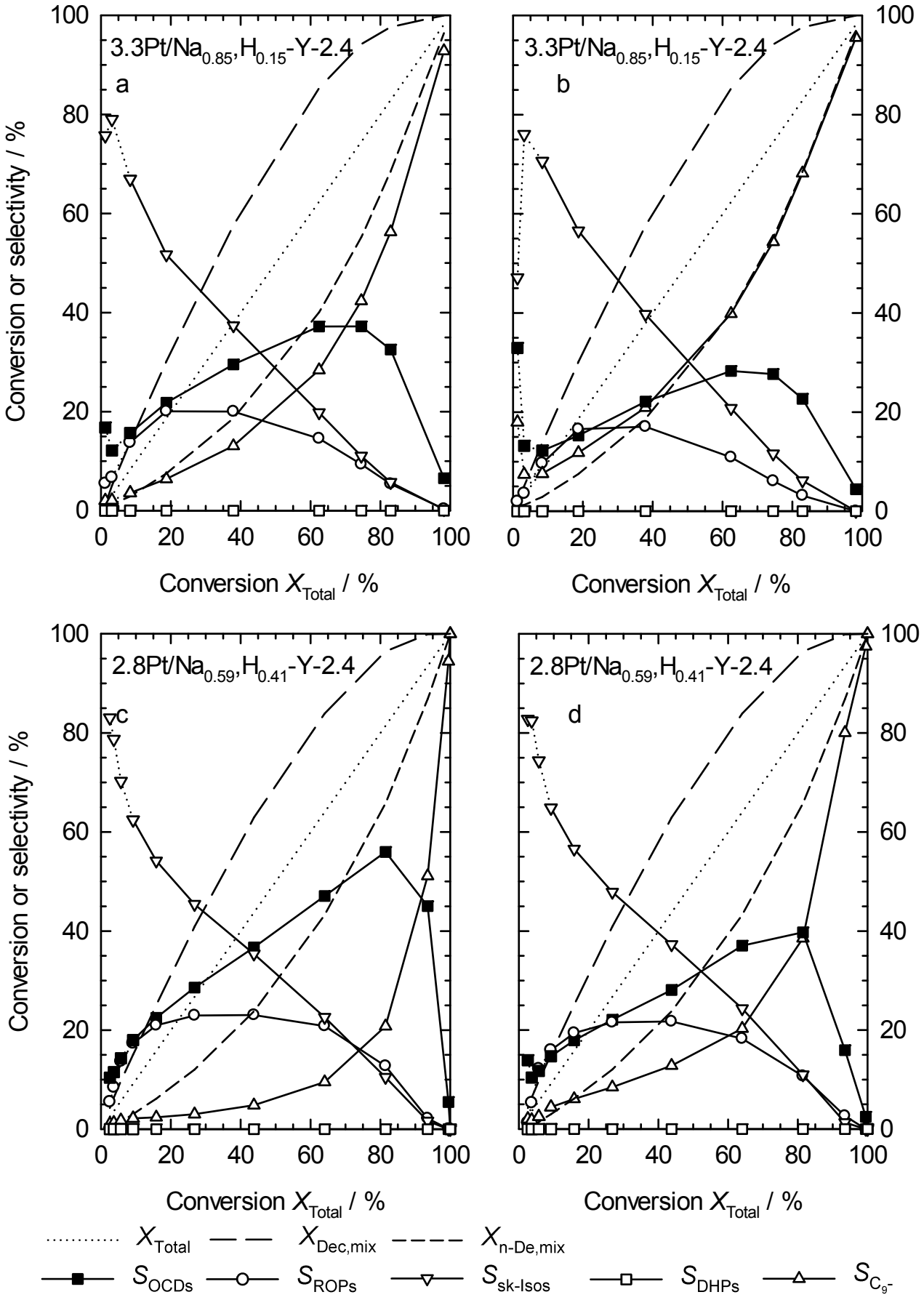

Figure 10.6: Measured (left) and calculated (right) selectivities of the decalin/n-decane conversion on the Pt/Na,H-Y-2.4 catalysts.

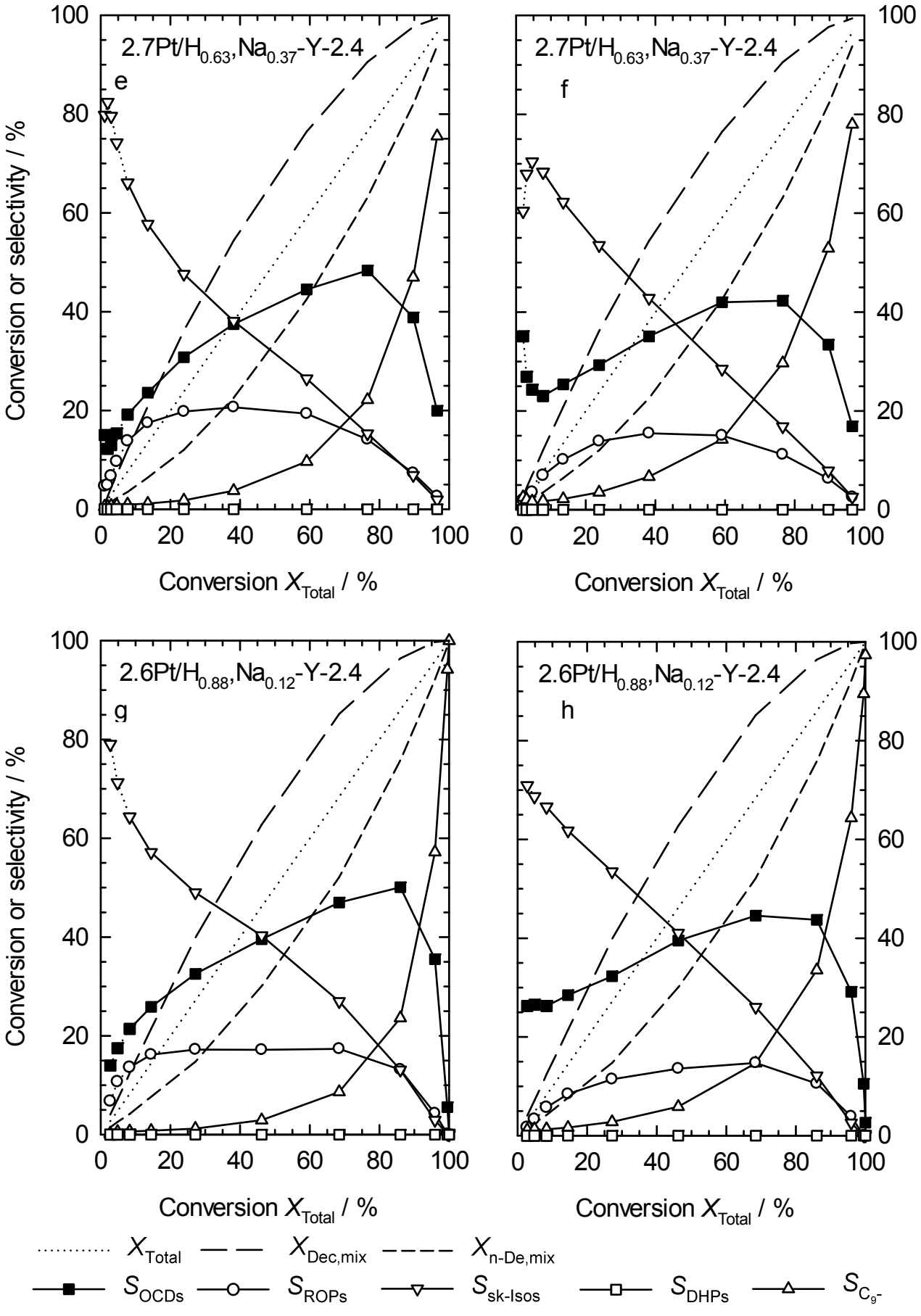

Figure 10.6: continued

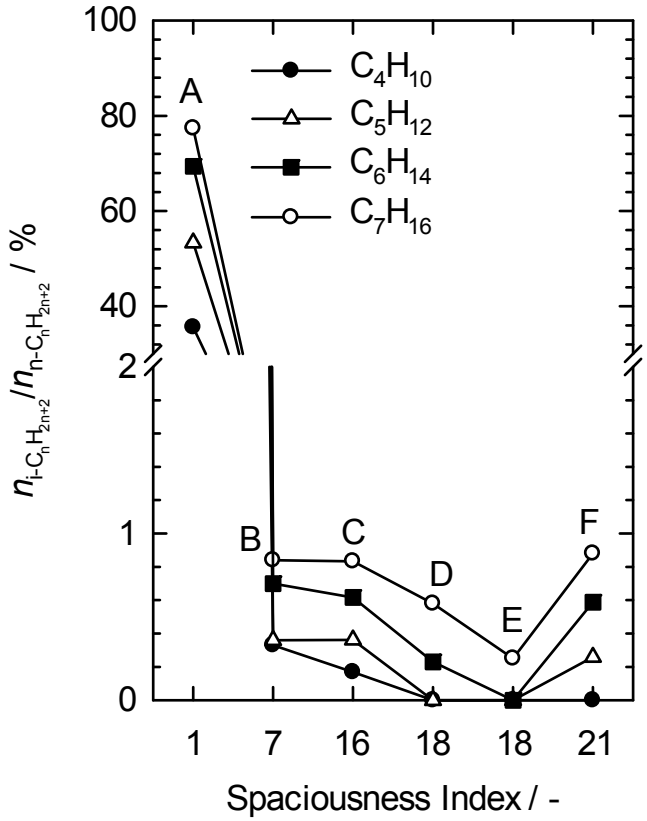

Figure 10.7: Content of branched isomers in the fractions of hydrocracked products from n-decane. The reaction conditions are given in Table 7.11, page 175. A: 0.5Ir/$H_{0.59}$,$Na_{0.41}$-ZSM-5-18; B: 2.9Ir/$Na_{0.90}$,$H_{0.10}$-MOR-5.8; C: 2.9Ir/$K_{0.68}$,$Na_{0.21}$,$H_{0.11}$-L-2.9; D: 3.5Ir/$Rb_{0.52}$,$H_{0.48}$-Beta-14; E: 3.3Ir/$H_{0.58}$,$Cs_{0.42}$-Beta-14; F: 3.0Ir/$Na_{0.80}$,$H_{0.20}$-EMC-2-4.3.

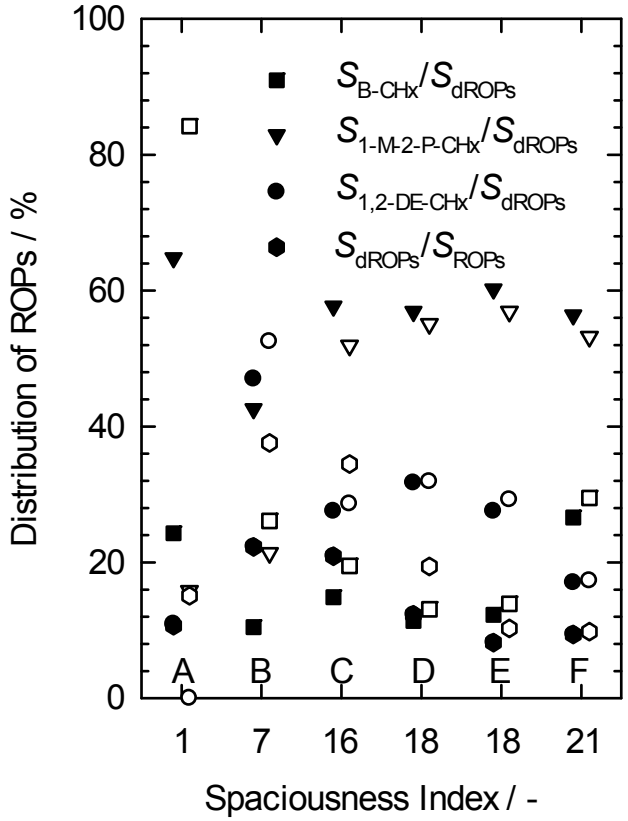

Figure 10.8: Direct ROPs of decalin obtained in the hydroconversion of pure decalin (filled) and of the equimolar decalin/n-decane mixture (open) on the iridium catalysts with different pore structure. The reaction conditions are given in Table 7.11.

A: 0.5Ir/$H_{0.59}$,$Na_{0.41}$-ZSM-5-18; B: 2.9Ir/$Na_{0.90}$,$H_{0.10}$-MOR-5.8;
C: 2.9Ir/$K_{0.68}$,$Na_{0.21}$,$H_{0.11}$-L-2.9; D: 3.5Ir/$Rb_{0.52}$,$H_{0.48}$-Beta-14;
E: 3.3Ir/$H_{0.58}$,$Cs_{0.42}$-Beta-14; F: 3.0Ir/$Na_{0.80}$,$H_{0.20}$-EMC-2-4.3.

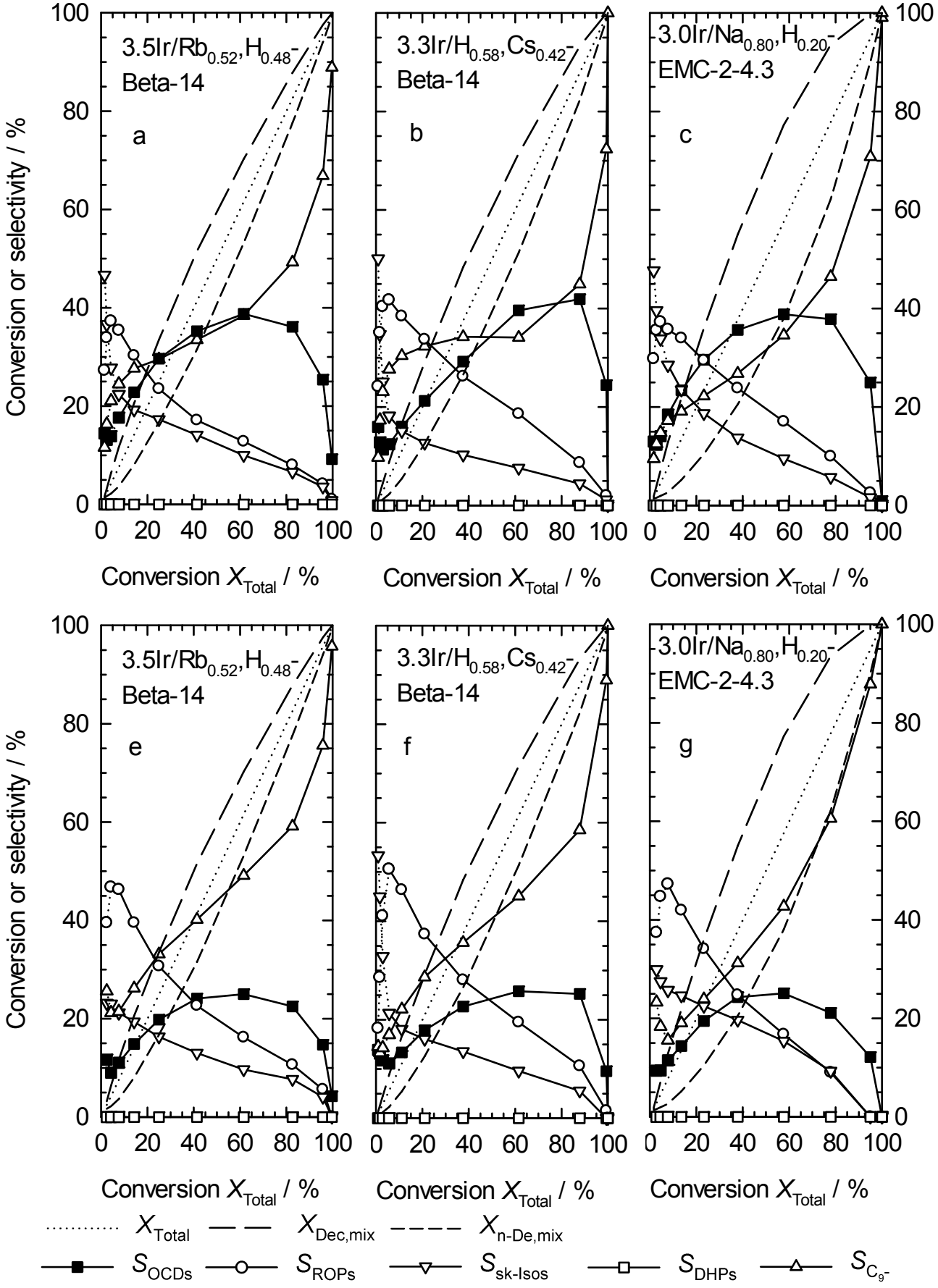

Figure 10.9: Measured (up) and calculated (down) selectivities of the decalin/n-decane conversion on the iridium catalysts with different pore systems.

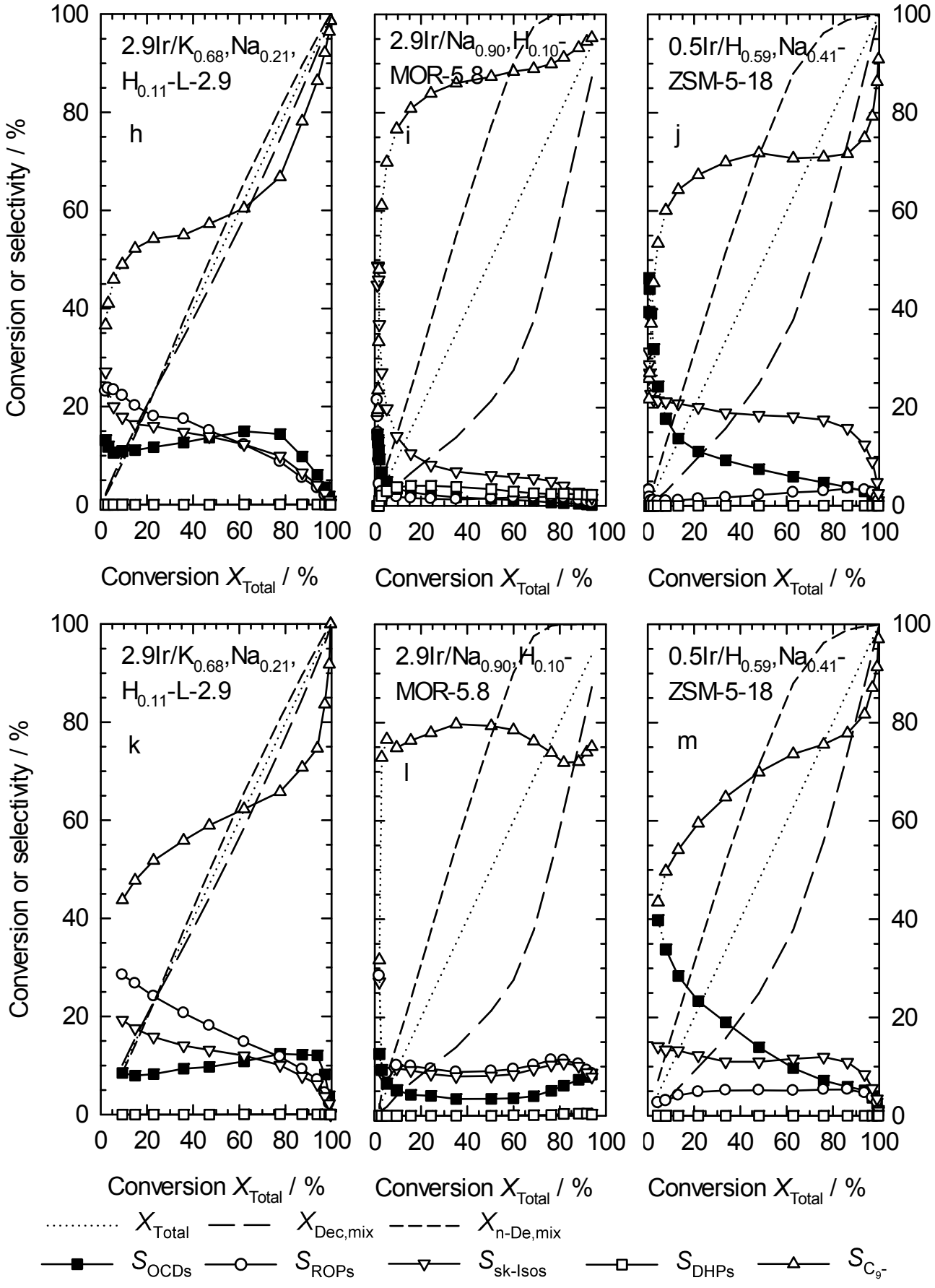

Figure 10.9: continued.

10.2 Retention Times

Table 10.1: Products formed in the hydroconversion of decalin and their retention times (t_{ret}) in the gas chromatographic analyses, as of July 01, 2013.

t_{ret} / min	Product	t_{ret} / min	Product
11.95	methane	55.15	2,5-dimethylhexane
12.30	ethane	55.45	2,4-dimethylhexane
13.20	propane	55.60	ethylcyclopentane
14.55	iso-butane	55.80	C_8
15.70	n-butane	55.90	C_8
16.25	neo-pentane	56.95	1,2,4-trimethylcyclopentane
19.60	2-methylbutane	57.10	C_8
21.55	n-pentane	58.35	1,2,3-trimethylcyclopentane
24.95	2,2-dimethylbutane	58.80	C_8
28.30	cyclopentane	59.80	C_8
28.35	2,3-dimethylbutane	60.60	2,3-dimethylhexane
28.75	2-methylpentane	60.95	3-ethyl-2-methylpentane
30.60	3-methylpentane	61.30	C_8
32.90	n-hexane	61.55	2-methylheptane
36.55	2,2-dimethylpentane	61.85	4-methylheptane
37.10	methylcyclopentane	62.40	3,4-dimethylhexane
37.45	2,4-dimethylpentane	62.70	C_8
38.50	C_7	63.00	3-methylheptane
40.95	C_7	63.25	3-ethylhexane
41.65	3,3-dimethylpentane	63.70	C_8
42.50	cyclohexane	64.00	cis-1,3-dimethylcyclohexane
43.55	2-methylhexane	64.35	1,4-dimethylcyclohexane
44.00	2,3-dimethylpentane	65.10	C_8
44.70	1,1-dimethylcyclopentane	65.60	1,1-dimethylcyclohexane
45.10	3-methylhexane	65.90	1-ethyl-3-methylcyclopentane
46.45	cis-1,3-dimethylcyclopentane	66.30	1-ethyl-3-methylcyclopentane
46.90	trans-1,3-dimethylcyclopentane	66.55	1-ethyl-2-methylcyclopentane
47.45	trans-1,2-dimetylcyclopentane	66.65	C_8
47.60	C_7	67.15	1-ethyl-1-methylcyclopentane
49.25	n-heptane	67.65	n-octane
53.30	cis-1,2-dimethylcyclopentane	67.80	trans-1,2-dimethylcyclohexane
53.50	methylcyclohexane	68.60	1,2,3,4-tetramethylcyclopentane
53.90	1,1,3-trimethylcyclopentane	68.85	C_8

t_{ret} / min	Product
69.05	1,4-dimethylcyclohexane
69.75	C_8
70.35	propylcyclopentane
70.95	C_9
71.20	2,3,5-trimethylhexane
71.40	C_9
71.65	2,2-dimethylheptane
72.20	C_9
72.40	2,4-dimethylheptane
72.80	C_9
73.05	4,4-dimethylheptane
73.30	C_9
73.50	4-ethyl-2-methylhexane
73.60	2,6-dimethylheptane
73.75	C_9
74.00	C_9
74.25	1,3,5-trimethylcyclohexane
74.45	ethylcyclohexane
74.85	2,5-dimethylheptane
75.05	3,5-dimethylheptane
75.20	3,5-dimethylheptane
75.45	3,3-dimethylheptane
75.65	C_9
76.00	1,1,4-trimethylcyclohexane
76.25	C_9
76.55	1,3-diethylcyclopentane
77.20	3-ethyl-2-methylhexane
77.40	C_9
77.60	C_9
77.75	C_9
78.10	C_9
78.40	3-ethyl-3-methylhexane
78.85	2,3-dimethylheptane
79.15	3-ethyl-4-methylhexane
79.30	3,4-dimethylheptane
79.45	3,4-dimethylheptane
79.65	4-ethylheptane
80.15	4-methyloctane
80.30	2-methyloctane
80.60	C_9
80.85	C_9
81.05	C_9
81.50	3-ethylheptane
81.70	3-methyloctane
81.80	C_9
81.95	C_9
82.10	C_9
82.35	C_9
82.60	2,4,6-trimethylheptane
82.95	ROP
83.10	1,1,3,5-tetramethylcyclohexane
83.30	C_9
83.55	C_9
83.70	C_9
83.85	C_9
84.30	C_9
84.50	C_9
84.75	1,2,3-trimethylcyclohexane
85.00	1,1,3,5-tetramethylcyclohexane
85.25	1-ethyl-4-methylcyclohexane
85.75	1,2,3,4,5-pentamethylcyclopentane
86.15	C_9
86.25	1,1,4,4-tetramethylcyclohexane
86.40	C_9
86.65	1,1,3-trimethylcyclohexane
87.20	n-nonane
87.45	3,3,5-trimethylheptane
87.75	3-ethyl-2-methylheptane
87.90	C_9
88.20	sk-Iso
88.55	C_9
88.75	sk-Iso
89.15	ROP
89.35	1-ethyl-2-methylcyclohexane

t_{ret} / min	Product
89.65	C_9
89.80	sk-Iso
89.90	C_9
90.15	OCD
90.25	OCD
90.60	ROP
90.85	sk-Iso
91.00	OCD
91.30	2,4-dimethyloctane
91.40	sk-Iso
91.60	2,3-dimethyloctane
91.80	2-iso-propyl-1,3-dimethylcyclopentane
91.95	sk-Iso
92.10	4,4-dimethyloctane
92.25	sk-Iso
92.40	sk-Iso
92.65	3,5-dimethyloctane
92.80	2,5-dimethyloctane
93.10	3,5-dimethyloctane
93.30	1,2,4,5-tetramethylcyclohexane
93.40	1,5-dimethylbicyclo[3.2.1]octane
93.65	2,7-dimethyloctane
93.85	1-ethyl-2-methylcyclohexane
94.00	OCD
94.15	OCD
94.25	OCD
94.40	sk-Iso
94.75	2,6-dimethyloctane
95.00	4-ethyl-4-methylheptane
95.20	sk-Iso
95.40	3,3-dimethyloctane
95.50	sk-Iso
95.65	sk-Iso
95.80	sk-Iso
96.00	3,6-dimethyloctane
96.25	3,6-dimethyloctane
96.40	ROP
96.55	sk-Iso
96.65	sk-Iso
96.75	3-ethyl-2-methylheptane
96.95	sk-Iso
97.15	sk-Iso
97.25	4-propylheptane
97.35	sk-Iso
97.55	3,4-diethylhexane
97.60	sk-Iso
97.75	sk-Iso
97.95	4,5-dimethyloctane
98.25	sk-Iso
98.55	3-ethyl-3-methylheptane
98.75	1,2,3,5-tetramethylcyclohexane
98.85	sk-Iso
99.15	sk-Iso
99.30	sk-Iso-1-6
99.50	4-ethyloctane
99.65	sk-Iso
99.90	ROP
100.10	3,3-diethylhexane
100.45	5-methylnonane
100.75	4-methylnonane
100.90	ROP
101.15	2-methylnonane
101.30	trans-1,4-diethylcyclohexane
101.55	cis-1,4-diethylcyclohexane
101.65	sk-Iso
101.90	1-ethyl-2,4-dimethylcyclohexane
102.20	3-ethyloctane
102.45	sk-Iso
102.60	sk-Iso
102.70	sk-Iso
102.85	3-methylnonane
103.00	sk-Iso
103.15	sk-Iso
103.45	sk-Iso

t_{ret} / min	Product
103.70	sk-Iso
104.05	cis-1-methyl-4-(methylethyl)cyclohexane
104.15	sk-Iso
104.50	3,7,7-trimethylbicyclo[4.1.0]heptane
104.70	sk-Iso
104.95	sk-Iso
105.25	sk-Iso
105.45	sk-Iso
105.55	sk-Iso
105.85	sk-Iso
106.05	sk-Iso
106.30	1-methyl-3-propylcyclohexane
106.50	sk-Iso
106.75	sk-Iso
107.00	ROP
107.15	tert-butylcyclohexane
107.45	cis-perhydroindane
107.85	sk-Iso
108.30	sk-Iso
108.35	sk-Iso
108.60	sk-Iso
108.90	sk-Iso
109.05	1-methyl-3-(methylethyl)cyclohexane
109.15	sk-Iso
109.35	n-decane
109.65	ROP
109.80	1-methyl-2-propylcyclohexane
110.05	1-methyl-1propylcyclohexane
110.35	sk-Iso
110.55	sk-Iso
110.60	sk-Iso
110.75	ROP
111.00	sk-Iso
111.35	ROP
111.50	sk-Iso
111.80	sk-Iso
112.05	trans-1,4-diethylcyclohexane
112.20	sk-Iso
112.40	sk-Iso
112.55	sk-Iso
112.75	sk-Iso
112.90	sk-Iso
113.15	1,2-diethylcyclohexane
113.25	sk-Iso
113.40	sk-Iso
113.60	sk-Iso
113.90	sk-Iso
114.20	sk-Iso
114.40	sk-Iso
114.65	sk-Iso
114.85	sk-Iso
115.35	1-methyl-2-propylcyclohexane
115.60	sk-Iso
115.80	1,2-diethylcyclohexane
116.35	1-(methylpropyl)cyclohexane
116.70	1,1-diethylcyclohexane
117.00	sk-Iso
117.20	sk-Iso
117.50	sk-Iso
117.80	butylcyclohexane
117.95	sk-Iso
118.10	sk-Iso
118.45	pentylcyclopentane
118.65	sk-Iso
118.85	sk-Iso
119.05	sk-Iso
119.30	sk-Iso
119.70	sk-Iso
120.05	octahydro-5-methyl-1H-indene
120.50	sk-Iso
120.80	sk-Iso
121.00	sk-Iso
121.25	sk-Iso
121.50	sk-Iso

t_{ret} / min	Product
121.90	sk-Iso
122.20	sk-Iso
122.70	sk-Iso
122.95	sk-Iso
123.00	sk-Iso
123.70	bicyclo[4.1.0]heptane
123.85	sk-Iso
124.20	trans-decalin
124.60	spiro[4.5]decane
124.75	sk-Iso
124.90	sk-Iso
125.25	sk-Iso
125.50	sk-Iso
126.10	sk-Iso
126.60	sk-Iso
126.80	sk-Iso
127.05	sk-Iso
127.20	sk-Iso
127.85	sk-Iso
128.10	sk-Iso
128.40	sk-Iso
128.65	sk-Iso
129.60	sk-Iso
129.75	sk-Iso
130.15	bicyclopentyl
130.95	sk-Iso
131.45	sk-Iso
132.10	sk-Iso
132.65	endo-2-methylbicyclo[3.3.1]nonane
133.40	sk-Iso
133.85	bicyclo[5.3.0]decane
134.00	sk-Iso
134.30	sk-Iso
134.70	sk-Iso
135.30	cis-decalin
136.10	sk-Iso

t_{ret} / min	Product
136.60	sk-Iso
137.25	sk-Iso
137.35	sk-Iso
138.65	decahydro-2-methylnaphthalene
140.35	sk-Iso
141.20	sk-Iso
142.00	sk-Iso
142.80	sk-Iso
143.35	sk-Iso
144.70	cyclodecane
145.00	sk-Iso
145.60	sk-Iso
147.50	tetralin
152.60	naphthaline

Erklärung über die Eigenständigkeit der Dissertation

Ich versichere, dass ich die vorliegende Arbeit mit dem Titel
„Competitive Hydroconversion of Decalin and n-Decane on Noble-Metal Catalysts and the Evaluation of Molybdenum Carbide as Ring-Opening Catalyst“
selbständig verfasst und keine anderen als die angegebenen Quellen und Hilfsmittel benutzt habe; aus fremden Quellen entnommene Passagen und Gedanken sind als solche kenntlich gemacht.

Declaration of Authorship

I hereby certify that the dissertation entitled
“Competitive Hydroconversion of Decalin and n-Decane on Noble-Metal Catalysts and the Evaluation of Molybdenum Carbide as Ring-Opening Catalyst”
is entirely my own work except where otherwise indicated. Passages and ideas from other sources have been clearly indicated.

Name/Name: Tobias Holl

Unterschrift/Signed: _____

Datum/Date: 20.01.2014